

Natural radionuclide and stable element studies of rock samples from the Osamu Utsumi mine and Morro do Ferro analogue study sites, Poços de Caldas, Brazil

A B MacKenzie¹, R D Scott¹, P Linsalata², N Miekeley³,
J K Osmond⁴, D B Curtis⁵

¹ Scottish Universities Research and Reactor Centre, Glasgow, UK

² New York, University Medical Center, Institute of Environmental
Medicine, Tuxedo, New York, USA

³ Department of Chemistry, Pontifical Catholic University,
Rio de Janeiro, Brazil

⁴ Geology Department, Florida State University, Tallahassee,
Florida, USA

⁵ Los Alamos National Laboratory, Los Alamos, New Mexico, USA

January 1991

SVENSK KÄRNBRÄNSLEHANTERING AB

SWEDISH NUCLEAR FUEL AND WASTE MANAGEMENT CO

BOX 5864 S-102 48 STOCKHOLM

TEL 08-665 28 00 TELEX 13108 SKB S

TELEFAX 08-661 57 19



NAGRA NTB 90 - 25
SKB TR 90 - 16
UK DOE WR 90 - 047

Poços de Caldas Report No. 7

**Natural radionuclide and stable
element studies of rock samples
from the Osamu Utsumi mine and
Morro do Ferro analogue study
sites, Poços de Caldas, Brazil.**

JANUARY 1991

An international project with the participation of Brazil, Sweden (SKB),
Switzerland (NAGRA), United Kingdom (UK DOE) and USA (US DOE).
The project is managed by SKB, Swedish Nuclear Fuel and
Waste Management Co.

NATURAL RADIONUCLIDE AND STABLE ELEMENT STUDIES OF
ROCK SAMPLES FROM THE OSAMU UTSUMI MINE AND MORRO DO
FERRO ANALOGUE STUDY SITES, POÇOS DE CALDAS, BRAZIL

A B MacKenzie¹, R D Scott¹, P Linsalata², N Miekeley³,
J K Osmond⁴, D B Curtis⁵

- 1 Scottish Universities Research and Reactor Centre,
Glasgow, UK
- 2 New York University Medical Center, Institute of
Environmental Medicine, Tuxedo, New York, USA
- 3 Department of Chemistry, Pontifical Catholic
University, Rio de Janeiro, Brazil
- 4 Geology Department, Florida State University,
Tallahassee, Florida, USA
- 5 Los Alamos National Laboratory, Los Alamos, New
Mexico, USA

January 1991

This report concerns a study which was conducted
for SKB. The conclusions and viewpoints presented
in the report are those of the author(s) and do not
necessarily coincide with those of the client.

Information on SKB technical reports from
1977-1978 (TR 121), 1979 (TR 79-28), 1980 (TR 80-26),
1981 (TR 81-17), 1982 (TR 82-28), 1983 (TR 83-77),
1984 (TR 85-01), 1985 (TR 85-20), 1986 (TR 86-31),
1987 (TR 87-33), 1988 (TR 88-32), 1989 (TR 89-40)
and 1990 (TR 90-46) is available through SKB.

Natural radionuclide and stable element studies of rock samples from the Osamu Utsumi mine and Morro do Ferro analogue study sites, Poços de Caldas, Brazil.

A.B. MacKENZIE¹, R.D. SCOTT¹, P. LINSALATA², N. MIEKELEY³,

J.K. OSMOND⁴ and D.B. CURTIS⁵.

¹Scottish Universities Research and Reactor Centre, East Kilbride, Glasgow G75 0QU (U.K.).

²New York University Medical Center, Institute of Environmental Medicine, Tuxedo, New York 109 87 (USA).

³Department of Chemistry, Pontifical Catholic University, Rua Marquês de São Vicente 225, 22453 Rio de Janeiro (Brazil).

⁴Geology Department, Florida State University, Tallahassee, Florida 32306 (USA).

⁵Los Alamos National Laboratory, Los Alamos, New Mexico 87545 (USA).

Abstract

This report describes a study of the distribution and behaviour of natural radionuclides and selected stable elements at the Poços de Caldas natural analogue study sites. At the Osamu Utsumi mine, the study was focussed upon investigation of the behaviour of natural decay series radionuclides and stable elements at the redox fronts which exist in the mine. Uranium nodules from the mine were also analyzed for natural decay series radionuclides in order to characterize their ages and growth rates, and for natural plutonium. At Morro do Ferro, the objective was to provide additional information on the geochemical behaviour of thorium, uranium and the light rare-earth elements and to relate this to the groundwater flow pattern in an attempt to evaluate the degree of mobilization of these species.

A summary review of those aspects of the geochemistry of natural decay series radionuclides relevant to the interpretation of radioactive disequilibrium is provided along with a detailed treatment of mathematical modelling of natural decay series disequilibria in rock-water interactions. The overall study comprised a number of discrete subprojects carried out in five different laboratories and each of these is described in detail. In addition to constituting a self-contained study, the results and conclusions of this work were also used as an input for modelling studies and other aspects of this integrated research programme.

The natural decay series studies at the Osamu Utsumi mine confirmed the generally greater mobility of U(VI) and Ra than of U(IV), Th and Pa in groundwater. The results further confirmed that, at the position of the drillcore studied, the long-term direction of groundwater flow had been downwards along the line of the main fissure system, rather than upwards as is presently observed.

Dissolution of uranium and other elements at the redox fronts followed by diffusive movement into both the oxidized and the reduced rock is identified as the mechanism giving rise to the observed concentration profiles about the redox fronts. Deposition of uranium, either as thin, dispersed coatings on other minerals or as discrete nodules, occurs in the reduced rock as a consequence of the reduction of U(VI) to U(IV). Deposition of uranium, almost certainly by uptake on iron oxides, is also identified as a significant retardation process in the oxidized rock. Some of the uranium nodules are young (on a $10^5 - 10^6$ year timescale) and exhibit growth rates of 1.8 – 2.6 cm in 10^6 a, whereas others are old on this timescale and exhibit equilibrium within the natural decay series. The time required for growth of nodules in the reduced rock is estimated to be of the order of 10^5 a at least, while a time of the order of $10^4 - 10^5$ a is required for dissolution of micronodules stranded in the oxidized rock following the passage of the redox front.

The natural ^{239}Pu content of a nodule from the reduced rock was measured as $2.3 \pm 0.7 \times 10^8$ atoms per gram, consistent with a state of secular equilibrium between ^{238}U and ^{239}Pu . The study thus reveals that uranium (plus daughters) and plutonium are chemically stable in the form of nodules in the reduced rock for a time of at least 10^5 years.

One of the redox fronts studied was concluded to have been effectively static (on a cm scale) for a period of at least 7×10^5 a, while the natural decay series data for the other fronts were consistent with rates of movement in the range 2 – 20 m in 10^6 a, in good general agreement with the estimated rate of regional erosion.

Redistribution of thorium was observed at the redox fronts, with preferential deposition on the reduced sides of the fronts. The degree of this redistribution of thorium is estimated to be at least two orders of magnitude less than the corresponding redistribution of uranium. Separation of uranium from thorium is observed as the redox fronts move downwards and the degree of separation increases with increased length of flow path of the groundwater.

Summary data are provided for a range of stable elements, including the rare-earths, which support the observations made above for uranium and indicate that the zone around the redox fronts contains generally elevated concentrations of most elements in conjunction with active dissolution at the front. This results in a variety of distributions of

different elements about the redox fronts. The redox fronts thus represent an initial zone of retardation which would be a positive factor in far-field radionuclide migration considerations. However, a negative aspect of this situation is that the zone of enhanced concentrations moves in response to movement of the redox front and, given a sufficient distance of travel, could result in a breakthrough of high concentrations of radionuclides into the near-surface environment.

Zusammenfassung

Dieser Bericht behandelt die Verteilung und das Verhalten natürlicher Radionuklide und ausgewählter stabiler Elemente in den zwei Untersuchungsgebieten für Analog-Studien von Poços de Caldas. In der Osamu Utsumi Uranmine galt das Interesse vor allem dem Verhalten von Radionukliden der natürlichen Zerfallsreihen und von ausgewählten stabilen Elementen im Bereich von Redox-Fronten, wie sie in der Mine auftreten. An den knollenartigen Uran-Ausscheidungen wurden ferner Analysen von Zerfallsreihen-Nukliden im Hinblick auf die Bestimmung von Alter und Wachstumsgeschwindigkeit durchgeführt sowie auch der Gehalt an natürlichem Plutonium bestimmt. Am Morro do Ferro sollten zusätzliche Einblicke in das geochemische Verhalten von Thorium, Uran und der leichten Seltenen Erden-Elemente gewonnen werden. Unter Einbezug des Grundwasserfließnetzes ergab sich ferner die Möglichkeit, das Ausmass der Mobilisierung dieser Elemente zu ermitteln.

Es wird ein zusammenfassender Ueberblick über das geochemische Verhalten der Zerfallsreihen-Nuklide gegeben, soweit es für die Interpretation der radioaktiven Ungleichgewichte von Bedeutung ist. Die mathematische Modellierung dieser Ungleichgewichte, wie sie bei der Gesteins/Wasser-Wechselwirkung auftreten, wird eingehend behandelt. Die Gesamtstudie enthält eine Reihe von Teilprojekten, die in fünf verschiedenen Laboratorien bearbeitet wurden und die hier im Detail dargestellt werden. Im Hinblick auf eine in sich geschlossene Gesamtstudie wurden Ergebnisse und Schlüsse dieser Untersuchungen auch als Eingabe für Modellierungen und andere Aspekte des Gesamtprogramms verwendet.

Die Zerfallsreihen-Untersuchung in der Osamu Utsumi Mine bestätigte die allgemein höhere Mobilität von U(VI) und Ra gegenüber U(IV), Th und Pa im Grundwasser. Die Ergebnisse zeigten ferner, dass das Grundwasser am Ort des untersuchten Bohrkerns langfristig im Spaltensystem nach unten floss und nicht nach oben, wie das z.Z. der Fall ist.

Konzentrationsprofile über die Redoxfront zeigen die Auflösung von Uran und anderer Elemente und ihre diffusive Verteilung beidseits der Redoxfront. Die Abscheidung von Uran entweder als dünne und feinverteilte Ueberzüge auf anderen Mineralien oder als knollige Ausscheidungen erfolgt im reduzierenden Bereich als Folge der Reduktion von U(VI) zu U(IV). Auch im oxidierenden Bereich scheidet sich Uran vor allem durch Sorption an Eisenoxiden ab, ein Mechanismus der zu einer ausgeprägten Retardation des Urans auch im oxidierenden Bereich führt.

Einige der UO₂-Knollen erwiesen sich als jung (im Bereich von 10⁵-10⁶ a) mit Wachstumsraten von 1.8-2.6 cm in 10⁶ a, während andere älter sind (>10⁶ a) und säkulares radioaktives Gleichgewicht in den Zerfallsreihen aufweisen. Der Zeitbedarf zur Bildung von UO₂-Knollen wird auf mindestens ~10⁵ a geschätzt, während für die Auflösung von Mikroknollen auf der oxidierenden Seite der fortschreitenden Front etwa 10⁴-10⁵ a erforderlich sind.

Der natürliche ²³⁹Pu-Gehalt eines UO₂-Knollens wurde zu 2.3±0.7x10⁸ Atome/g bestimmt, entsprechend einem säkularen Gleichgewicht zwischen ²³⁸U und ²³⁹Pu. Die Untersuchung zeigte, dass Uran (plus Tochterelemente) sowie Plutonium in den Knollen der reduzierenden Zone chemisch stabil sind über eine Zeit von mindestens 10⁵ a.

Eine der Redoxfronten erwies sich als praktisch ruhend (im cm-Bereich) über eine Zeitspanne von mindestens 7x10⁵ a, während die Zerfallsreihen-Analyse anderer Fronten zu Geschwindigkeiten im Bereich von 2-20 cm in 10⁶ a führte, in allgemein guter Uebereinstimmung mit der geschätzten regionalen Erosionsrate.

Auch für Thorium wurde eine Umverteilung an der Redoxfront mit einer Anreicherung auf der reduzierenden Seite festgestellt. Der Grad dieser Umverteilung ist aber mindestens um zwei Grössenordnungen kleiner als beim Uran. Das Ausmass der Trennung zwischen Uran und Thorium vergrössert sich mit dem Fortschreiten der Redoxfront nach unten.

Für eine Reihe stabiler Elemente einschliesslich der Seltenen Erden werden summarische Daten gegeben, die im allgemeinen, wie beim Uran, auf eine Anreicherung um die Redoxfront hinweisen, die mit Lösungsvorgängen an der Front verbunden sind. So resultiert eine Vielfalt von Konzentrationsprofilen um die Redoxfront und diese bildet eine erste Retardationszone, wie sie für die Radionuklidwanderung im Fernfeld erwünscht ist. Ein negativer Aspekt dieser Situation ist allerdings die Wanderung der Redoxfront und damit der Anreicherungszone und die Möglichkeit ihres Einbruchs in die oberflächennahe Umgebung.

Résumé

Le présent rapport décrit une étude de la distribution et du comportement de radionucléides naturels et de quelques éléments stables des sites d'analogues naturels de Poços de Caldas. A Osamu Utsumi, on a focalisé l'étude sur le comportement des séries de radionucléides à désintégration naturelle et d'éléments stables aux fronts redox rencontrés dans la mine. Sur des nodules d'uranium prélevés dans la mine, on a également analysé les séries de radionucléides à désintégration naturelle pour caractériser leur âge et leur vitesse de croissance, et pour leur teneur en plutonium naturel. A Morro do Ferro, on a cherché à obtenir un complément d'informations sur le comportement géochimique du thorium, de l'uranium et des terres rares légères, et à relier ce comportement aux systèmes d'écoulement des eaux souterraines dans le but d'évaluer le degré de mobilisation de ces espèces.

On présente un survol succinct des aspects de la géochimie des séries de radionucléides à désintégration naturelle qui ont une importance pour l'interprétation du déséquilibre radioactif, ainsi qu'un compte rendu détaillé du traitement par modèle mathématique des déséquilibres des séries de désintégration naturelle dans les interactions eau-roche. L'étude décrit en outre en détail un certain nombre de sous-projets réalisés par cinq laboratoires différents. Enfin, pour boucler le travail sur lui-même, les résultats et conclusions de la présente étude ont été utilisés comme input pour des modélisations et autres traitements de ce programme de recherche intégré.

Les études des séries de désintégration naturelle des roches de la mine de Osamu Utsumi ont confirmé la mobilité généralement plus grande de U(VI) et de Ra que de U(IV), Th et Pa dans les eaux souterraines. Les résultats confirment en outre que sur le lieu de prélèvement des carottes, les écoulements souterrains à long terme se font vers le bas le long du système de fissures principal, et non vers le haut comme on peut l'observer actuellement.

La dissolution de l'uranium et d'autres éléments sur le front redox, suivi par un mouvement diffusif de part et d'autre de ce front, dans la roche oxydée et la roche réduite, est identifiée comme le mécanisme provoquant les profils de concentration observés autour des fronts redox. Dans la roche réduite, les dépôts d'uranium, que ce soit sous forme de minces pellicules déposées sur les autres minéraux ou sous forme de nodules individuels, sont la conséquence de la réduction de U(VI) en U(IV). Dans la roche oxydée, le dépôt d'uranium, presque certainement dû à la capture d'oxydes du fer,

est identifié comme un processus de retardation significatif. Certains nodules d'uranium sont jeunes (pour une échelle de temps de 0.1 à 1 million d'années) et révèlent des vitesses de croissance de 1.8 à 2.6 cm par million d'années, tandis que d'autres, considérés comme anciens à cette échelle de temps, montrent un équilibre des séries désintégration naturelle. Dans la roche réduite, le temps nécessaire à la croissance des nodules est estimé à au moins cent mille ans, alors que le temps nécessaire pour la dissolution de micronodules pris dans la roche oxydée après le passage du front redox est estimé à environ dix mille à cent mille ans. La teneur en ^{239}Pu naturel d'un nodule dans la roche réduite a été mesurée à $2.3 \times 0.7 \times 10^8$ atomes par gramme. Cette teneur est en accord avec l'état d'équilibre séculaire entre ^{238}U et ^{239}Pu . Ces résultats montrent que l'uranium (avec ses descendants) et le plutonium sont, sous forme de nodules dans la roche réduite, stables pour une période d'au moins cent mille ans.

L'un des fronts redox étudiés s'est révélé effectivement statique (à l'échelle centimétrique) sur une période d'au moins sept cent mille ans. Les données des séries de désintégration naturelle des autres fronts correspondent à des vitesses de migration de l'ordre de 2 à 20 m par million d'années, ce qui est en bon accord avec la valeur estimée de la vitesse d'érosion régionale.

On a observé une redistribution du thorium sur les fronts redox, avec une tendance préférentielle au dépôt du côté réduit des fronts. Le taux de redistribution du thorium est estimé à au moins deux ordres de grandeur inférieur à celui de l'uranium. Une séparation de l'uranium et du thorium est observée quand les fronts redox se déplacent vers le bas, et le taux de séparation augmente parallèlement avec la longueur des voies d'écoulement de l'eau souterraine.

Les données succinctes qui sont fournies pour une série d'éléments stables, y compris des terres rares, confirment les observations décrites ci-dessus pour l'uranium. Elles indiquent que les zones voisines des fronts redox contiennent en général des concentrations élevées de la plupart de ces éléments, ce qui est à mettre en relation avec la dissolution active sur les fronts. Il en résulte une palette de distributions variée des différents éléments autour des fronts redox. Les fronts redox représentent ainsi une zone primaire de retardation, considérée comme un facteur favorable dans le cadre des considérations sur la migration de radionucléides sur de longues distances. Toutefois, cette situation présente également un aspect défavorable, à savoir que la zone de concentrations accrues se déplace en réponse au déplacement du front redox, et que, si la distance de migration est suffisante, on pourrait avoir une émergence de radionucléides en concentration élevée dans l'environnement proche de la surface.

Preface

The Poços de Caldas Project was designed to study processes occurring in a natural environment which contains many features of relevance for the safety assessment of radioactive waste disposal. The study area, in the State of Minas Gerais, Brazil, is a region of high natural radioactivity associated with volcanic rocks, geothermal springs and uranium ore deposits. It contains two sites of particular interest on which the project work was focussed: the Osamu Utsumi uranium mine and the Morro do Ferro thorium/rare-earth ore body. The first site is notable in particular for the prominent redox fronts contained in the rock, while Morro do Ferro was already well-known as one of the most naturally radioactive locations on the surface of the Earth, owing to the high thorium ore grade and the shallow, localised nature of the deposit.

The features displayed by these two sites presented the opportunity to study a number of issues of concern in repository performance assessment. The four objectives set after the first-year feasibility study were:

1. Testing of equilibrium thermodynamic codes and their associated databases used to evaluate rock/water interactions and solubility/speciation of elements.
2. Determining interactions of natural groundwater colloids with radionuclides and mineral surfaces, with emphasis on their role in radionuclide transport processes.
3. Producing a model of the evolution and movement of redox fronts, with the additional aim of understanding long-term, large-scale movements of trace elements and rare-earths over the front (including, if possible, natural Pu and Tc).
4. Modelling migration of rare-earths (REE) and U-Th series radionuclides during hydrothermal activity similar to that anticipated in the very near-field of some spent-fuel repositories.

The project ran for three and a half years from June 1986 until December 1989 under the joint sponsorship of SKB (Sweden), NAGRA (Switzerland), the Department of the Environment (UK) and the Department of Energy (USA), with considerable support from a number of organisations in Brazil, notably Nuclebrás (now Urânio do Brasil). The first-year feasibility study was followed by two and a half years of data collection and interpretation, focussed on the four objectives above.

This report is one of a series of 15, summarising the technical aspects of the work and presenting the background data. A complete list of reports is given below. Those in series A present data and interpretations of the sites, while those in series B present the results of modelling the data with performance assessment objectives in mind. The main findings of the project are presented in a separate summary (no. 15).

The work presented in this report is a detailed description of the geochemistry of natural decay series radionuclides and natural plutonium in rock samples from the Osamu Utsumi mine and Morro do Ferro environments, with particular reference to redox front evolution and genesis (objective 3).

Poços de Caldas Project Report Series

Series A: Data, Descriptive, Interpretation

Report No.	Topic	Authors (Lead in Capitals)
1.	The regional geology, mineralogy and geochemistry of the Poços de Caldas alkaline caldera complex, Minas Gerais, Brazil.	SCHORSCHER, Shea.
2.	Mineralogy, petrology and geochemistry of the Poços de Caldas analogue study sites, Minas Gerais, Brazil. I: Osamu Utsumi uranium mine.	WABER, Schorscher, Peters.
3.	Mineralogy, petrology and geochemistry of the Poços de Caldas analogue study sites, Minas Gerais, Brazil. II: Morro do Ferro.	WABER.
4.	Isotopic geochemical characterization of selected nepheline syenites and phonolites from the Poços de Caldas alkaline complex, Minas Gerais, Brazil.	SHEA.
5.	Geomorphological and hydrogeological features of the Poços de Caldas caldera and the Osamu Utsumi mine and Morro do Ferro analogue study sites, Brazil.	HOLMES, Pitty, Noy.
6.	Chemical and isotopic composition of groundwaters and their seasonal variability at the Osamu Utsumi and Morro do Ferro analogue study sites, Poços de Caldas, Brazil.	NORDSTROM, Smellie, Wolf.
7.	Natural radionuclide and stable element studies of rock samples from the Osamu Utsumi mine and Morro do Ferro analogue study sites, Poços de Caldas, Brazil.	MacKENZIE, Scott, Linsalata, Miekeley, Osmond, Curtis.
8.	Natural series radionuclide and rare-earth element geochemistry of waters from the Osamu Utsumi mine and Morro do Ferro analogue study sites, Poços de Caldas, Brazil.	MIEKELEY, Coutinho de Jesus, Porto da Silveira, Linsalata, Morse, Osmond.

Report No.	Topic	Authors (Lead in Capitals)
9.	Chemical and physical characterisation of suspended particles and colloids in waters from the Osamu Utsumi mine and Morro do Ferro analogue study sites, Poços de Caldas, Brazil.	MIEKELEY, Coutinho de Jesus, Porto da Silveira, Degueldre.
10.	Microbiological analysis at the Osamu Utsumi mine and Morro do Ferro analogue study sites, Poços de Caldas, Brazil.	WEST, Vialta, McKinley.

Series B: Predictive Modelling and Performance Assessment

11.	Testing of geochemical models in the Poços de Caldas analogue study.	BRUNO, Cross, Eikenberg, McKinley, Read, Sandino, Sellin.
12.	Testing models of redox front migration and geochemistry at the Osamu Utsumi mine and Morro do Ferro analogue study sites, Poços de Caldas, Brazil.	Ed: McKINLEY, Cross, Haworth, Lichtner, MacKenzie, Moreno, Neretnieks, Nordstrom, Read, Romero, Scott, Sharland, Tweed.
13.	Near-field high-temperature transport: Evidence from the genesis of the Osamu Utsumi uranium mine, Poços de Caldas alkaline complex, Brazil.	CATHLES, Shea.
14.	Geochemical modelling of water-rock interactions at the Osamu Utsumi mine and Morro do Ferro analogue study sites, Poços de Caldas, Brazil.	NORDSTROM, Puigdomènech, McNutt.

Summary Report

15.	The Poços de Caldas Project: Summary and implications for radioactive waste management.	CHAPMAN, McKinley, Shea, Smellie.
-----	---	-----------------------------------

Contents

	page
Abstract	i
Preface	ix
1. Introduction	1
1.1. Natural decay series radionuclides: summary of geochemical properties and use in natural analogue studies	1
1.2. Mathematical modelling of natural decay series disequilibria in rock-water interactions	7
1.2.1. Continuous removal	12
1.2.2. Continuous deposition	15
1.2.3. Timescales in continuous processes	17
1.2.4. The behaviour of ^{226}Ra	18
1.3. Natural radionuclide studies of rock samples at the Osamu Utsumi mine and Morro do Ferro: background and objectives	20
2. Osamu Utsumi uranium mine	23
2.1. F1 drillcore studies	23
2.1.1. Natural decay series studies	23
2.1.2. Stable element studies	67
2.2. Other redox front studies	104
2.2.1. Redox front 71ZE23	104
2.2.2. Redox front II	109
2.2.3. Redox front NM	113
2.2.4. Redox front IV	119
2.3. Studies of uranium nodules from the Osamu Utsumi mine	125
2.3.1. Growth rates of two pitchblende nodules	125
2.3.2. Uranium decay series characteristics of an old pitchblende nodule	129
2.3.3. Uranium/thorium disequilibria in uranium-bearing micronodules near a redox front	131
2.4. Natural plutonium geochemistry in a redox front	135
3. Morro do Ferro	137
3.1. Objectives	139
3.2. Results of core sample analyses	140
3.2.1. Borehole MF10	140
3.2.2. Borehole MF12	151
3.3. Discussion	156
4. Conclusions	156
5. Acknowledgements	159
6. References	160
Appendix 1: Interlaboratory comparison of analytical methods	165

1. Introduction

1.1. Natural decay series radionuclides: summary of geochemical properties and use in natural analogue studies

Investigation of the radioactive disequilibrium which can develop between parent and daughter radionuclides in the natural radioactive decay series (Fig. 1) during rock-water interactions has, for some time, been recognized as a useful technique in the study of the mechanisms and rates of geochemical reactions and physical processes in the environment (Ivanovich and Harmon, 1982). In the development of concepts for the disposal of radioactive waste, natural analogue studies (Chapman *et al.*, 1984) involving the use of natural decay series radionuclides have been applied in the investigation of numerous processes considered to be of importance in the context of far-field migration of waste radionuclides following the eventual failure of the engineered near-field barriers. Some of the topics which have been studied in this way include: the relative mobility of uranium, thorium and radium in groundwaters (Latham and Schwarcz, 1987a); the stability and radionuclide retention capacity of minerals over geological timescales (Gascoyne, 1986); transport and retardation processes affecting radionuclides in water-bearing fissures in crystalline rocks (Smellie *et al.*, 1986; Alexander *et al.*, 1988, 1989a); radionuclide dispersion within consolidated sediments (Thiel *et al.*, 1983) and within crystalline rocks (Schwarcz *et al.*, 1982; Gascoyne and Schwarcz, 1986); the rate of dissolution of uranium from crystalline rocks (Latham and Schwarcz, 1987b, c); the dissolution and dispersion of radionuclides from pitchblende (Scott *et al.*, 1990).

The basis for the use of the natural decay series radionuclides in such studies depends primarily upon differences in solubility between the various members of the decay chains. Uranium, thorium and radium provide isotopes with half-lives appropriate for use in natural analogue studies and the solubility characteristics of these elements can be summarized as follows.

Uranium in the 6+ oxidation state is relatively soluble, existing in solution predominantly as anionic complexes of the uranyl ion (e.g. $[\text{UO}_2(\text{CO}_3)_2]^{2-}$), whereas uranium in the 4+ oxidation state exhibits a much lower solubility. The U(IV)/U(VI) transition is readily effected as a result of varying environmental redox conditions (Wedepohl, 1978) and the uranium concentration in rocks and sediments can show marked variations depending upon prevailing redox conditions. Thus, oxidized rocks and sediments often show much lower uranium concentrations than reduced systems and

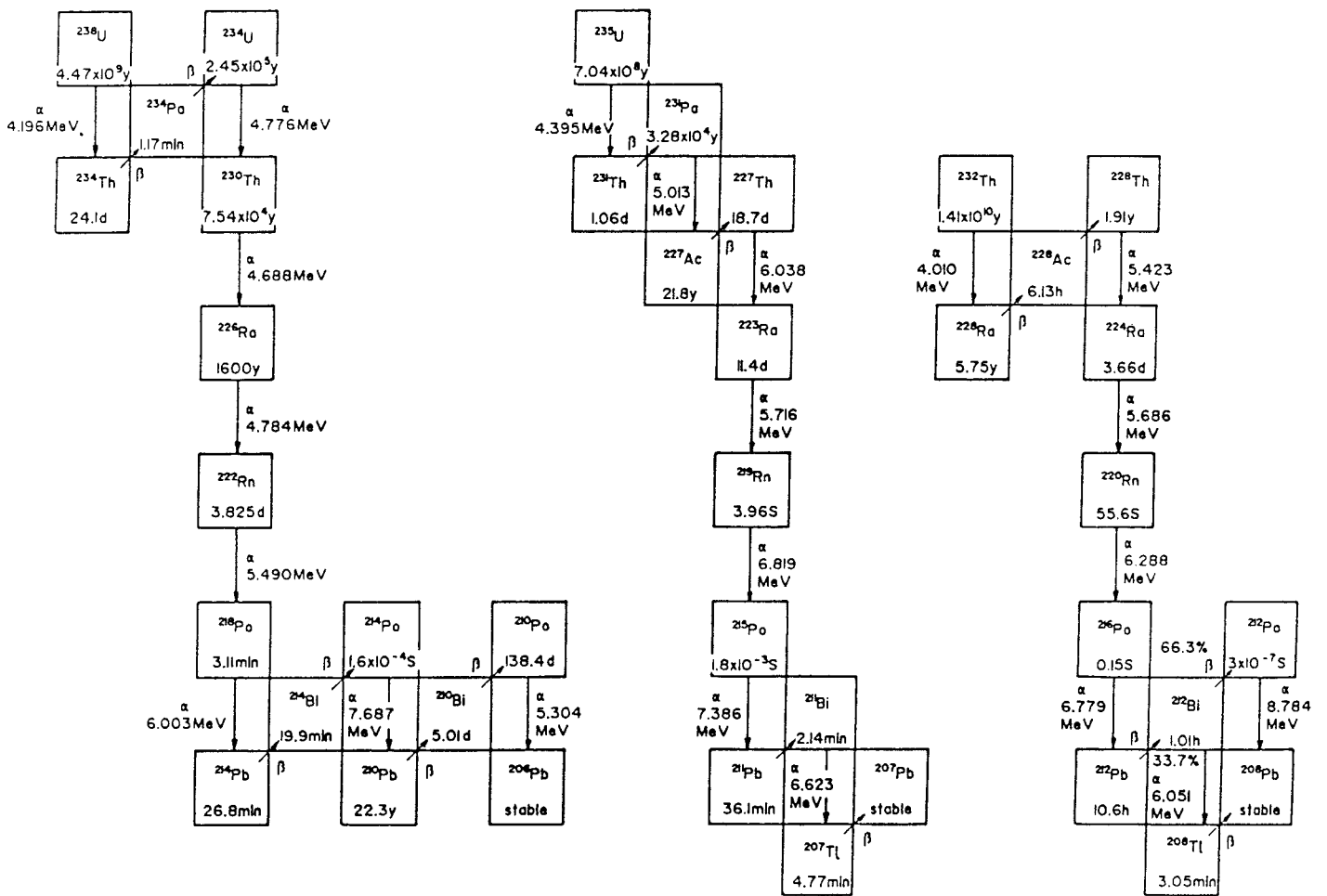


Figure 1. The natural radioactive decay series.

abrupt discontinuities in uranium concentration can develop at redox fronts, with such concentration patterns persisting over geological timescales in some cases (Wedepohl, 1978; Ivanovich and Harmon 1982; Colley *et al.*, 1984, 1989; Das, 1985; Scott *et al.*, 1990). The converse situation applies to groundwaters, in which high uranium concentrations are observed under oxidizing conditions and low concentrations under reducing conditions (Kaufman *et al.*, 1969; Osmond *et al.*, 1983, Cowart, 1980; Andrews and Kay, 1982).

In addition to these intrinsic solubility controls over uranium distributions, a further feature which can be of importance in certain circumstances is the uptake of uranium in authigenic minerals such as iron and manganese oxyhydroxides and carbonates (Smellie *et al.*, 1986; Scott *et al.*, 1990; MacKenzie *et al.*, 1989).

Thorium exists naturally only in the 4+ oxidation state and exhibits an extremely low solubility in the aquatic environment under conditions of low temperature and pressure (Ivanovich and Harmon, 1982). Thorium is highly susceptible to removal from solution by hydrolysis and by uptake on solid surfaces and its highly insoluble character is evidenced by its average seawater concentration of about $5 \times 10^{-5} \mu\text{gl}^{-1}$ relative to the corresponding uranium concentration of $3.4 \mu\text{gl}^{-1}$. Particulate scavenging is often the dominant process controlling thorium concentrations in solution, leading to undersaturation of thorium in conjunction with residence times in solution of less than a day in water with a high particulate content (Broecker *et al.*, 1973; Anderson *et al.*, 1983a, 1983b; McKee *et al.*, 1984). The chemistry of uranium and thorium is further detailed by Bruno *et al.* (this report series; Rep. 11).

Radium exists only in the 2+ oxidation state and is the most electropositive of the group IIa metals, resulting in a generally lower solubility of radium salts than those of the other metals in the group (Cotton and Wilkinson, 1968; Greenwood and Earnshaw, 1984). Nevertheless, radium exhibits a much higher solubility than thorium in natural waters and, since all naturally occurring isotopes of radium are produced by the decay of thorium isotopes (Fig. 1), the geochemistry of radium is dominated by its dissolution from thorium-containing rocks and sediments (Kaufman *et al.*, 1973; Moore, 1969a, b, 1972; Latham and Schwarcz 1987a). In solution, radium exhibits similar biogeochemical behaviour to barium and is subject to removal from solution by incorporation in authigenic silicates, carbonates and iron and manganese oxides (Wolgemuth, 1970; Wolgemuth and Broecker, 1970; Ku *et al.*, 1970; Edmond, 1970; Li *et al.*, 1973; Moore and Reid, 1973; MacKenzie *et al.*, 1989).

The pronounced insolubility of thorium relative to radium and uranium generates the characteristic deviations from unity observed for the $^{230}\text{Th}/^{234}\text{U}$ and $^{226}\text{Ra}/^{230}\text{Th}$ activity

ratios in many natural waters, rocks and sediments. In addition to these solubility-induced disequilibria between different elements, natural decay series geochemistry is also characterized by isotopic fractionation of uranium, with ^{234}U being preferentially removed from minerals to the aqueous phase relative to ^{238}U . This effect is considered to be the result of a number of processes including recoil ejection and possible oxidation of the product nucleus during alpha decay of ^{238}U , and lattice destabilization and damage induced by alpha decay leading to preferential leaching along the alpha track by groundwater (Fleischer, 1980). Groundwaters thus have typical $^{234}\text{U}/^{238}\text{U}$ activity ratios greater than unity while residual rocks which have been subject to leaching have $^{234}\text{U}/^{238}\text{U}$ activity ratios of less than unity. In addition, uptake of uranium by recently ($<10^6\text{a}$) forming minerals often imparts a $^{234}\text{U}/^{238}\text{U}$ activity ratio of greater than unity to such species.

Dissolution of uranium must, therefore, be considered as a two component system involving both bulk dissolution of the total mineral and preferential recoil loss of ^{234}U from the mineral surface. The faster the rate of bulk dissolution relative to recoil loss of ^{234}U , the closer to unity will be the $^{234}\text{U}/^{238}\text{U}$ activity ratios of both the groundwater and the residual rock. Conversely, a very slow rate of bulk dissolution will generate much larger deviations from unity in the $^{234}\text{U}/^{238}\text{U}$ activity ratio, particularly in the groundwater. The rate of bulk dissolution will depend upon the mineral involved and the physical and chemical properties of the water in contact with it. The rate of recoil loss of ^{234}U will be determined by the specific activity of ^{238}U in the outermost layer (of depth $\sim 100\ \mu\text{m}$) of the mineral since the process is ineffective at greater depths.

In conventional approaches to the interpretation of natural decay series data in studies of rock-water interactions, thorium is assumed to be essentially insoluble, while uranium and radium are assumed to be soluble and, on the basis of this approximation, the following qualitative observations can be made:

- (1) If the solid phase $^{234}\text{U}/^{238}\text{U}$ activity ratio is less than unity then recoil loss of ^{234}U to solution has occurred within the last 10^6a and the ^{234}U has remained in solution for a sufficiently long time to be removed from the section of rock being studied. The greater the deviation of the $^{234}\text{U}/^{238}\text{U}$ activity ratio from unity, the slower is the rate of bulk dissolution of the mineral relative to the rate of recoil loss of ^{234}U .
- (2) If the $^{234}\text{U}/^{238}\text{U}$ activity ratio of the solid phase is greater than unity then the rock has experienced, within the last 10^6a , deposition of uranium from groundwater.

- (3) If the $^{230}\text{Th}/^{234}\text{U}$ activity ratio is less than unity in the rock then it has experienced deposition of uranium within the last $\sim 3 \times 10^5$ a.
- (4) If the $^{230}\text{Th}/^{234}\text{U}$ activity ratio of the rock is greater than unity, dissolution and removal of uranium within the last $\sim 3 \times 10^5$ a is implied. A complicating factor can, however, apply in this case in that if a sudden (relative to the ^{230}Th half-life of 7.5×10^4 a) deposition of uranium occurs in which the $^{234}\text{U}/^{238}\text{U}$ activity ratio is greater than unity, then ^{230}Th can grow in to a state of transient equilibrium with the excess ^{234}U to give a $^{230}\text{Th}/^{234}\text{U}$ activity ratio of greater than one (Friedlander *et al.*, 1981; Alexander *et al.*, 1989b).
- (5) If the $^{226}\text{Ra}/^{230}\text{Th}$ activity ratio of the solid phase is greater than unity then deposition of ^{226}Ra within the last $\sim 10^4$ a is implied.
- (6) If the $^{226}\text{Ra}/^{230}\text{Th}$ activity ratio is less than unity then dissolution and removal of ^{226}Ra has occurred within the last $\sim 10^4$ a, with alpha recoil effects as described above for ^{234}U possibly contributing to the removal process.

A highly convenient method of presentation of natural decay series analytical data for rock samples is in the form of a graph plotting one radionuclide activity ratio against another. For example, Latham and Schwarcz (1987a, b, c) have utilized plots of $^{234}\text{U}/^{238}\text{U}$ against $^{230}\text{Th}/^{234}\text{U}$ and $^{226}\text{Ra}/^{230}\text{Th}$ against $^{230}\text{Th}/^{234}\text{U}$ to illustrate the effects of various removal and deposition processes affecting uranium and radium in rocks. In the present work, we have adopted and extended the approach of Thiel *et al.* (1983) in which plots of $^{234}\text{U}/^{238}\text{U}$ against $^{230}\text{Th}/^{238}\text{U}$ are used. By making the assumption that the rock initially exists with the natural decay series radionuclides in a state of secular equilibrium, which is at some time disturbed by the addition of uranium from the groundwater, or removal of uranium to the groundwater, either in a single rapid event or in a continuous process, the $^{234}\text{U}/^{238}\text{U}$ versus $^{230}\text{Th}/^{238}\text{U}$ plot can be divided into various sectors representing the effects of different processes as shown in Figure 2. The different sectors of the graph correspond to a uranium removal area (A) involving either a continuous or sudden removal of uranium, a uranium removal area (A') which can only be attained by samples which have undergone removal of uranium in a single rapid event and cannot be attained by samples subject to continuous removal of uranium, a uranium deposition sector (B) involving either continuous or sudden deposition of uranium, a uranium deposition area (B') which can only be attained by samples which have undergone deposition of uranium in a single rapid event and cannot be attained by samples subject to continuous removal

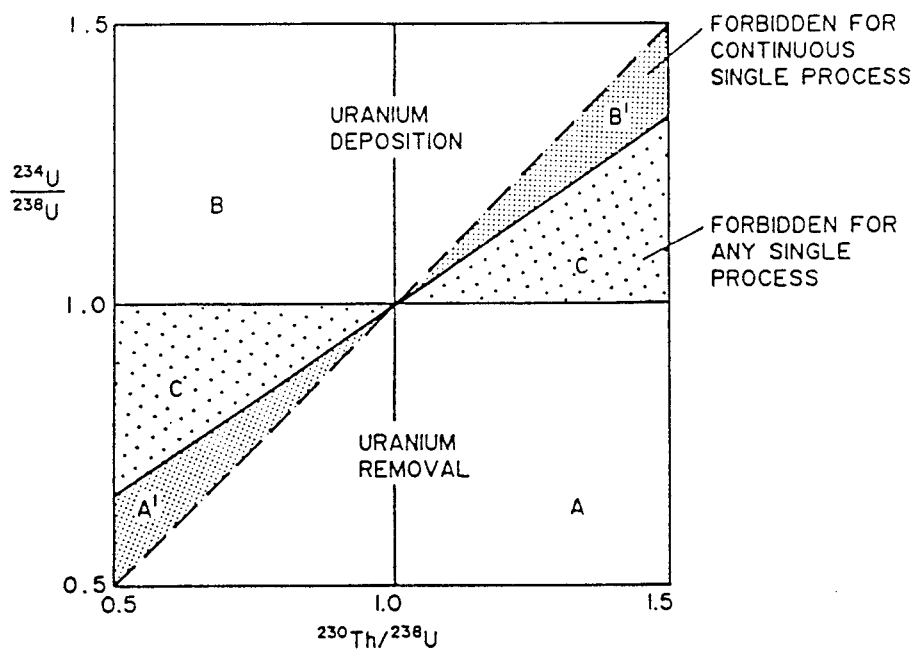


Figure 2. Regions of uranium deposition and removal in a plot of $^{234}\text{U}/^{238}\text{U}$ versus $^{230}\text{Th}/^{238}\text{U}$ for whole-rock samples based upon Thiel et al. (1983) and Alexander et al. (1989b).

of uranium, and two areas (C) which correspond to combinations of the $^{234}\text{U}/^{238}\text{U}$ and $^{230}\text{Th}/^{238}\text{U}$ activity ratios which cannot be produced in the rock by any single uranium addition or removal process, whether continuous or a single rapid event; these sectors are consequently classed as “forbidden” or “complex process” areas.

The underlying basis for division of the activity ratio plot into these sectors involves the quantitative mathematical treatment of the radioactive disequilibrium induced between uranium and thorium during rock-water interactions. This topic is discussed in Alexander *et al.* (1989b) and is dealt with in more detail in the following section.

1.2. Mathematical modelling of natural decay series disequilibria in rock-water interactions

As discussed above, departures from secular equilibrium in the ^{238}U - ^{234}U - ^{230}Th decay chain can be used qualitatively to indicate disturbance of the system as a result of rock-water interactions. However, there is a fundamental difficulty in the interpretation of the activity ratios if quantitative information is being sought: three measurements are made, but these are outnumbered by unknown quantities. Thus, even if it is assumed that the rock initially contains ^{238}U and its descendants in secular equilibrium, the initial activity of the rock, parameters describing the addition or removal of uranium and thorium and the time which has elapsed since the disturbance are all unknown. Also, the system might have been perturbed suddenly (that is to say, over a time very much shorter than any of the half-lives involved) or have been subject to a continuous process over a longer time, perhaps extending up to the present; it is therefore important to try to distinguish between these alternatives. Under certain circumstances it is possible to calculate an “age” from U-Th activities (Ivanovich and Harmon, 1982) but such a deduction obviously requires assumptions about the initial conditions and the degree of closure of the system which would have to be otherwise justified. There is considerable literature on these matters (see, for instance, Latham and Schwarcz (1989) and references therein), but a systematic presentation of the basis of the present analysis is in order since some quite general interesting points emerge from the mathematical results of the models, many of which do not seem to have been made explicitly before.

The following assumptions are made in setting up and solving the equations for the chain members:

- (a) The decay of ^{238}U may be neglected over the timescales of interest, say up to 2Ma.
- (b) At time zero, the rock contains ^{238}U and its daughters in secular equilibrium.
- (c) At time zero, the secular equilibrium is disturbed by a sudden deposition or removal of uranium, or by the onset of a continuous process of deposition or removal, and in either case the $^{234}\text{U}/^{238}\text{U}$ activity ratio may or may not be unity.
- (d) ^{230}Th is very much less mobile than uranium in so far as it is much less likely to be removed from rock by the action of groundwater and then transported. Thorium mobility is, however, easily incorporated in the formalism.

The simplest case to treat is the sudden addition of uranium to, or removal from, a rock which is initially in secular equilibrium at time zero. Then at time t :

$$A_1 = R + P_1$$

$$A_2 = R + P_1(1 - \exp(-\lambda_2 t)) + P_2 \exp(-\lambda_2 t)$$

$$A_3 = R + P_1[1 - \exp(-\lambda_3 t)] + (P_2 - P_1) [\exp(-\lambda_2 t) - \exp(-\lambda_3 t)] \lambda_3 / (\lambda_3 - \lambda_2)$$

The notation, used consistently throughout, employs subscripts 1, 2, 3 for ^{238}U , ^{234}U and ^{230}Th respectively; A represents activity, R the initial activity in the rock, and P the sudden input. Sudden removal is accommodated by negative values of P . The rock returns to secular equilibrium with a new value of $R + P_1$ and, as already mentioned, a plot of A_2/A_1 against A_3/A_1 (Thiel *et al.*, 1983) provides a convenient method of visualizing the evolution of the system in time. It is evident that, in such a plot (Fig. 2), a sudden perturbation is capable of moving the system from its initial position at the origin into the upper left or the lower right quadrant for the cases of sudden addition or sudden removal of uranium respectively, since ^{234}U is liable to be more mobile than ^{238}U . The paths traced out by the system as secular equilibrium is restored are shown for two representative cases in Figure 3. If, however, uranium is added or removed in equilibrium, then the new state of the system will be represented by a point on the abscissa, either to the left or right of the origin, and the system will return to equilibrium along the abscissa at a rate determined by the ^{230}Th half-life. The two lines marked A and B on Figure 3 are important because they delineate regions in the plane which may or may not be reached during the evolution of the system, depending upon the type of disturbance which it has undergone. A is a locus for which $A_2 = A_3$ and B is an asymptotic line of slope $(\lambda_3 - \lambda_2)/\lambda_3$ defining two regions of the plane which can never be reached

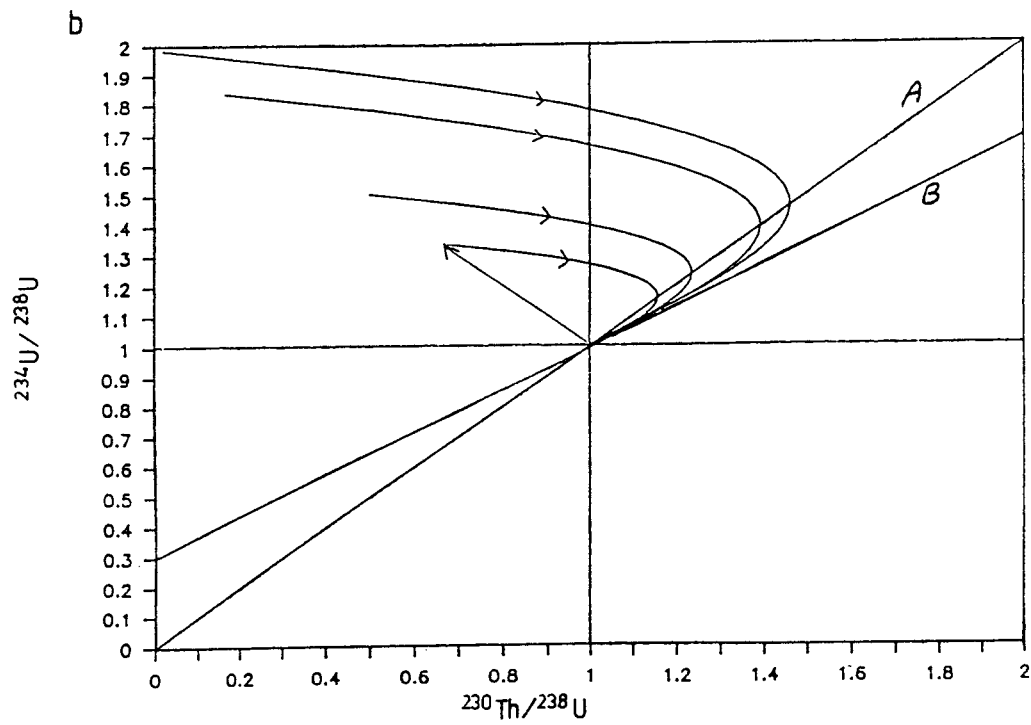
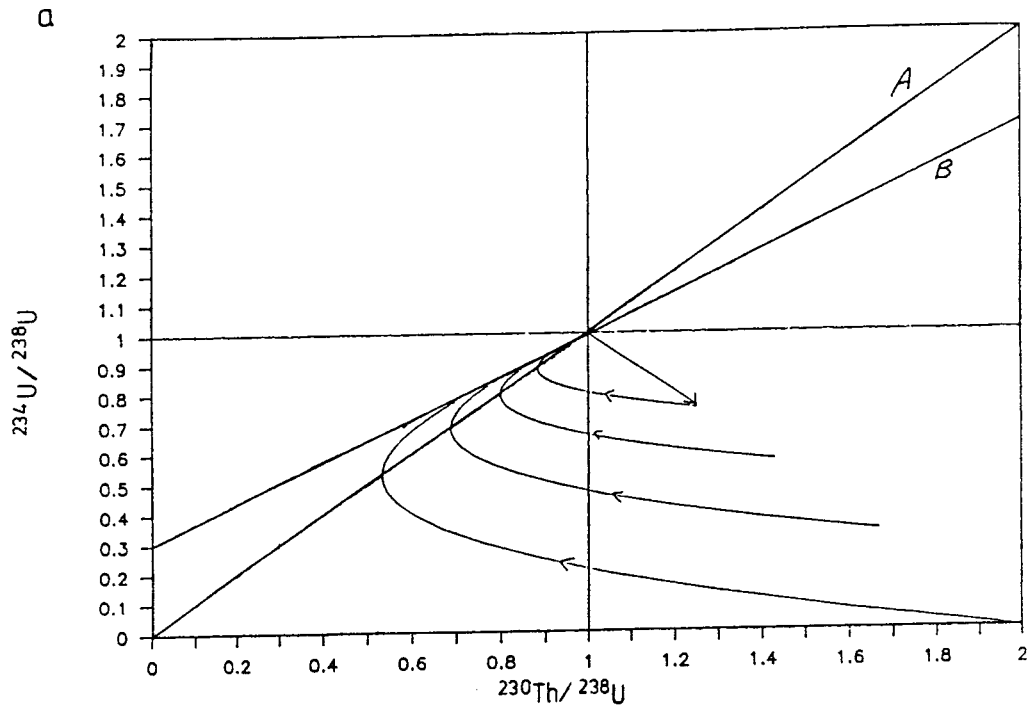


Figure 3. Return to equilibrium of the activity ratios after (a) sudden removal of uranium and (b) sudden addition.

during the return to equilibrium as long as the system has been subjected only to a single disturbance, whether sudden or continuous. The triangular regions between the lines cannot in fact be reached by continuous deposition or removal, as will become clear from the solutions of the equations governing these cases.

Some general points about timescales emerge from the above. First of all, consider the behaviour of ^{234}U and ^{230}Th after a sudden input of uranium ($P_2 > P_1$): the excess ^{234}U decays towards the (new) ^{238}U activity value and ^{230}Th grows in towards this value. The ^{230}Th , however, overshoots both the ^{238}U and ^{234}U activities and there are therefore times, call them T_{13} and T_{23} ($T_{23} > T_{13}$), when the ^{230}Th activity is equal to that of ^{238}U and ^{234}U respectively. Thus the ^{230}Th activity approaches secular equilibrium with ^{238}U from above, and at times $> T_{23}$ we have $A_3 > A_2 > A_1$. A sudden loss of uranium (again with $P_2 > P_1$) produces similar effects except that ^{230}Th approaches equilibrium from beneath and $A_3 < A_2 < A_1$ at times $> T_{23}$. From the expressions for A_1 , A_2 and A_3 we obtain

$$T_{13} = \ln[(P_2\lambda_3 - P_1\lambda_2) / \lambda_3(P_2 - P_1)] / (\lambda_3 - \lambda_2)$$

$$T_{23} = \ln[(P_2\lambda_3 - P_1\lambda_2) / \lambda_2(P_2 - P_1)] / (\lambda_3 - \lambda_2)$$

which are independent of R . Also,

$$T_{23} - T_{13} = \ln(\lambda_3 / \lambda_2) / (\lambda_3 - \lambda_2)$$

as it must, because after time T_{13} the system may be considered to consist of a part in secular equilibrium at the new A_1 value plus an excess of ^{234}U alone. ^{230}Th will grow into transient equilibrium with this excess ^{234}U and it is well known that the ^{230}Th activity attains its maximum value and is equal to the ^{234}U activity at a time equal to $T_{23} - T_{13}$ above. Of course, T_{23} has its minimum value of 0.18 Ma, and $T_{13} = 0$, when $P_1 = 0$. T_{13} has a minimum value of 0 and a maximum value of ∞ , corresponding to the extreme cases of a sudden input of ^{234}U alone and an equilibrium input respectively. It is clear, however, that in this latter case secular equilibrium will be re-established to within the experimental uncertainties within a few ^{230}Th half-lives, say 0.5 Ma. It is interesting to note that the system spends 0.18 Ma traversing the region between the ordinate and the line defining T_{23} , irrespective of its initial position in the deposition or removal quadrants, and that points lying in the restricted triangular region therefore could indicate a sudden disturbance which took place at least that long ago. There is another possibility arising from the observation that the operation of a continuous process will cause the system to trace out a curve in the plane. If this process stops, then the system

will return to equilibrium along the same path as it would have done if it had been “suddenly” moved there from the origin, i.e. the system could have entered the triangular region between lines A and B (Fig. 3) as a result of the stopping of a continuous process at least 0.18 Ma ago. It is clear that the nature of a disturbance cannot be deduced from a single point on an activity ratio plot except in the rather limited and negative sense that certain continuously acting processes are incapable of generating a certain range of activity ratios, but a suitable selection of samples throughout the region under investigation coupled with hydrogeological, mineralogical and geochemical data might enable a convincing history to be constructed. Also, any point on the plot can be reached by postulating an appropriate sequence of events, but it will not necessarily be possible to construct a unique sequence from the information which is available.

Further difficulties are encountered when processes of continuous deposition of uranium onto, or removal from, a rock are considered because it is necessary to set up an explicit mathematical model of the interaction. This is to be contrasted with the situation above where all that is really involved is the evolution of the system back to secular equilibrium, and the sequence of events leading to the starting point of such evolution does not influence the further development of the system. Consider, first, the removal of uranium from a rock by the action of groundwater. This can be considered to arise in two obvious ways: by bulk dissolution of the matrix or by a leaching process which removes the uranium but leaves the rock largely intact. Mathematically these processes are described as zero order or first order processes respectively, and expressions may readily be written down and solved to give the time dependence of the activity ratios. Similarly, accumulation can be considered to arise from a non-depleting source in flowing groundwater, in which case a zero order process is being postulated, or (see the discussion by Latham and Schwarcz, 1989) a first order effect, where the deposition is proportional to the amount of uranium already present, can be advanced. The various possibilities must eventually be graded on the grounds of physical, chemical or geological reality, but it can be argued that the most reasonable cases to consider are removal and deposition of uranium taken as first and zero order processes respectively.

1.2.1. Continuous removal

With the notation as before, for ^{238}U :

$$\frac{dN_1}{dt} = -\lambda'_1 N_1$$

where λ'_1 represents the probability per unit time of removal of a ^{238}U atom (by means other than decay, which is neglected) and so

$$A_1 = R \exp(-\lambda'_1 t) \text{ assuming } A_1 = R \text{ at } t = 0.$$

For ^{234}U , the decay chain may be contracted to omit the two short-lived β -decays intervening between ^{238}U and ^{234}U and hence

$$\frac{dN_2}{dt} = f_1 A_1 - \lambda_2 N_2 - \lambda'_2 N_2$$

Here, the factor f_1 ($f_1 \geq 0.5$) represents the fraction of decays of ^{238}U which result in ^{234}U atoms remaining in the rock after the occurrence of an α -decay and two β -decays. That is to say, it takes account of the fact that the ^{234}Th daughter ($T_{1/2} = 24.1$ days) may physically recoil into solution during the process of α -decay by modification of the source term. Since ^{234}Th and ^{234}Pa are both insoluble, it may be that recoil and ionization following β -decay supplies the removal mechanism but, in any case, it is the source term which is affected and the possibility is included for the sake of generality. The result is

$$A_2 = R[\exp(-(\lambda_2 + \lambda'_2)t) + \{\exp(-\lambda'_1 t) - \exp(-(\lambda_2 + \lambda'_2)t)\} f_1 \lambda_2 / (\lambda_2 + \lambda'_2 - \lambda'_1)]$$

For ^{230}Th :

$$\frac{dN_3}{dt} = f_2 A_2 - \lambda_3 N_3 - \lambda'_3 N_3$$

Here, thorium mobility has been allowed since f_2 accounts for α -decay recoil losses and λ'_3 describes leaching. In low-temperature fluid-rock interactions it would be expected that $f_2 \approx 1$, that $\lambda'_3 \ll \lambda'_1$ or λ'_2 and that $\lambda'_2 \geq \lambda'_1$.

The solution is:

$$A_3 = R[a \exp(-\lambda'_1 t) + b \exp(-(\lambda_2 + \lambda'_2)t) + c \exp(-(\lambda_3 + \lambda'_3)t)]$$

where

$$a = f_1 f_2 \lambda_2 \lambda_3 / \{(\lambda_2 + \lambda'_2 - \lambda'_1) / (\lambda_3 + \lambda'_3 - \lambda'_1)\}$$

$$b = [f_2 \lambda_3 (\lambda_2 + \lambda'_2 - \lambda'_1) - f_1 f_2 \lambda_2 \lambda_3] / \{(\lambda_2 + \lambda'_2 - \lambda'_1) (\lambda_3 + \lambda'_3 - (\lambda_2 + \lambda'_2))\}$$

and $c = 1 - a - b$

These relations reduce to the simpler ones given by Alexander *et al.* (1989b) for the case of no recoil loss ($f_1 = f_2 = 1$) and immobile thorium ($\lambda'_3 = 0$). The interesting feature here is the long-term behaviour of the activity ratios A_2/A_1 and A_3/A_1 which are plotted on the Thiel diagram. Evidently, at times such that exponential terms are negligible,

$$A_2/A_1 \rightarrow f_1 \lambda_2 / (\lambda_2 + \lambda'_2 - \lambda'_1)$$

$$A_3/A_1 \rightarrow f_1 f_2 \lambda_2 \lambda_3 / \{(\lambda_2 + \lambda'_2 - \lambda'_1)(\lambda_3 + \lambda'_3 - \lambda'_1)\}$$

so that values of λ'_1 and λ'_2 can be determined if there is reason to believe that a steady state has been reached and that recoil loss and thorium movement can be neglected. A steady state can only be reached, however, if $\lambda_2 + \lambda'_2 > \lambda'_1$, which is automatic since $\lambda'_2 \geq \lambda'_1$, and if $\lambda_3 + \lambda'_3 > \lambda'_1$. If uranium is removed in equilibrium, then $A_2/A_1 \rightarrow f_1$ and $A_3/A_1 \rightarrow f_1 f_2 \lambda_3 / (\lambda_3 + \lambda'_3 - \lambda'_1)$, which implies that the system will evolve to a point in the third or fourth quadrant on the Thiel plot, even although ^{234}U is not being preferentially leached, since λ'_1 will always be greater than λ'_3 . The ratio $A_3/A_2 \rightarrow f_2 \lambda_3 / (\lambda_3 + \lambda'_3 - \lambda'_1)$ and, on the assumption that f_2 is close to unity, that is if an atom of ^{230}Th ejected into the fluid immediately returns to the surface of the rock (thorium being insoluble), it is clear that A_3/A_2 will always be greater than unity. Thus, if recoil loss of ^{230}Th can be neglected, the system evolves to a steady state end-point in either the third or the fourth quadrant, but cannot cross the line A in Figure 3. Some representative paths are shown in Figure 4 where the effect of a chemically reasonable (small) amount of thorium mobility is illustrated: it is evidently negligible. If conditions were such that thorium and uranium had roughly equal values for λ' , then movement into "forbidden" areas of the plot becomes possible. It is clear that appreciable shifts from

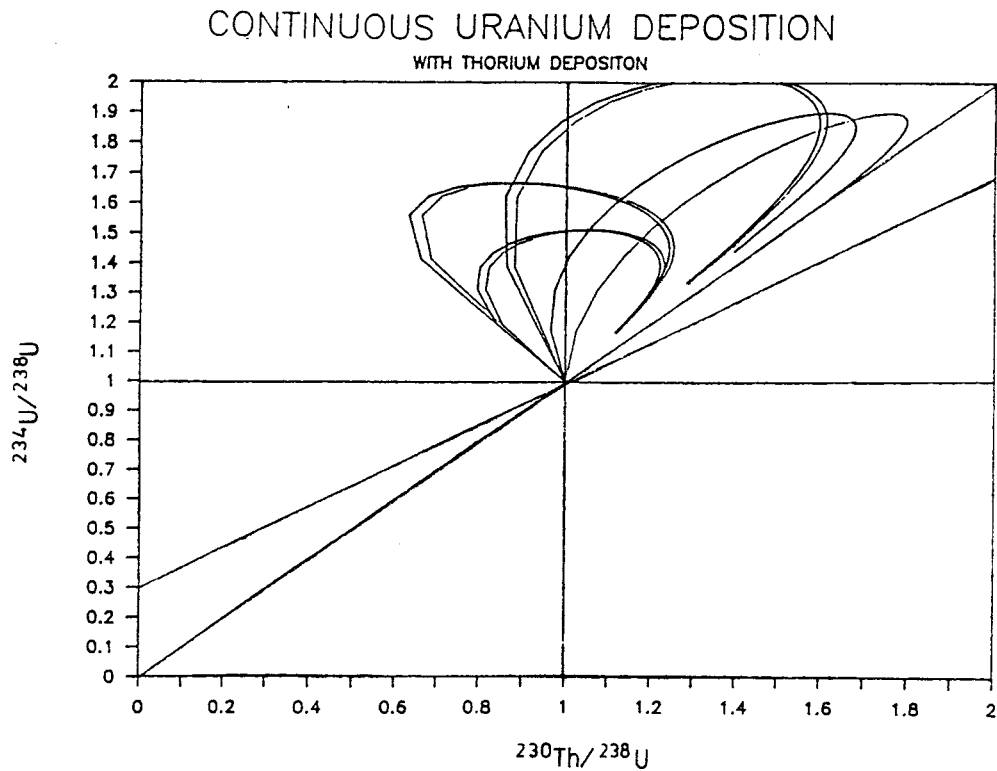
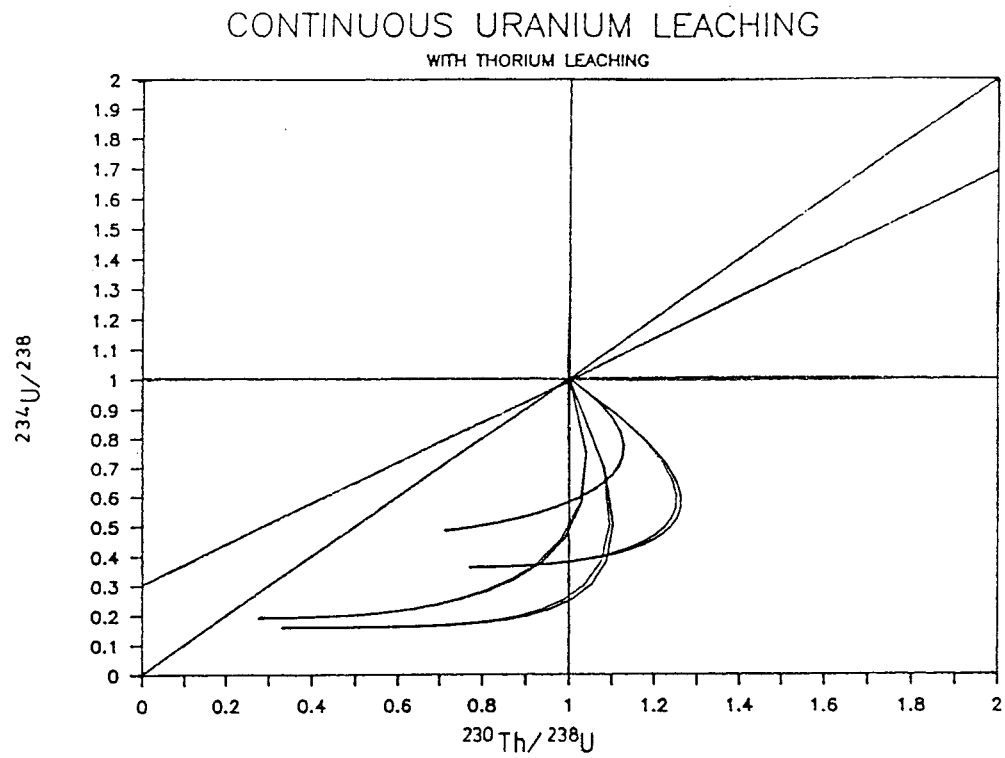


Figure 4. Evolution of the activity ratios during continuous processes with and without a small amount of thorium mobility.

the origin are achieved when the values of λ'_1 , and λ'_2 are of the order of magnitude of the decay constants (Fig. 4), but that the activity ratios increase exponentially unless the condition $\lambda_3 + \lambda'_3 > \lambda'_1$, which in practice means $\lambda_3 > \lambda'_1$, is met. Values of λ'_1 exceeding this limit are capable of generating large values of A_3/A_1 within times of the order of 1 My.

1.2.2. Continuous deposition

Suppose the conditions are such that uranium is being added continuously to the rock from a source which is not being depleted in the process, so that the supply is at a constant rate. Then, if K_1 atoms of ^{238}U are supplied per unit interval of time,

$$\frac{dN_1}{dt} = K_1, \text{ since decay of } ^{238}\text{U} \text{ is neglected}$$

and therefore

$$A_1 = R + \lambda_1 K_1 t$$

if the rock is initially in secular equilibrium and deposition commences at $t = 0$. Activity is being supplied at a rate $\lambda_1 K_1$ per unit time and the ^{238}U activity increases linearly. Suppose, again for the sake of generality, that the probability of recoil loss of ^{234}U is non-zero, then in the previous notation

$$\frac{dN_2}{dt} = f_1 A_1 - \lambda_2 N_2 + K_2$$

and

$$A_2 = f_1 A_1 + (\lambda_2 K_2 - f_1 \lambda_1 K_1)(1 - \exp(-\lambda_2 t))/\lambda_2 + R(1 - f_1)\exp(-\lambda_2 t)$$

For ^{230}Th ,

$$\frac{dN_3}{dt} = f_2 A_2 - \lambda_3 N_3 + K_3$$

Here, f_2 has the same significance as before and would be expected to be very close to unity in conditions under which uranium was being deposited in a low-temperature rock-water interaction. K_3 is the supply term and, if thorium were strictly insoluble and therefore immobile, would arise from the decay of the ^{234}U present in solution. It would therefore be small. Hence

$$A_3 = f_1 f_2 A_1 + [K_3 + f_2(\lambda_2 K_2 - f_1 \lambda_1 K_1) / \lambda_2 - f_1 f_2 K_1 \lambda_1 / \lambda_3] (1 - \exp(-\lambda_3 t)) \\ + [f_2 R (1 - f_1) - f_2(\lambda_2 K_2 - f_1 \lambda_1 K_1) / \lambda_2] (\exp(-\lambda_2 t) - \exp(-\lambda_3 t)) \lambda_3 / (\lambda_3 - \lambda_2) \\ + R (1 - f_1 f_2) \exp(-\lambda_3 t).$$

Once more, these expressions reduce to the simpler forms given by Alexander *et al.* (1989b) in the absence of recoil and with no supply of thorium. At long times,

$$A_2 \rightarrow f_1 A_1 + (\lambda_2 K_2 - f_1 \lambda_1 K_1) / \lambda_2$$

which means that if recoil losses can be neglected and if, for reasons outlined already, $\lambda_2 K_2 \geq \lambda_1 K_1$, then the ^{234}U would tend to be in constant excess. As the activity of the rock increased, the ratio A_2/A_1 would, however, tend towards unity. If $f_1 \neq 1$, it is theoretically possible that $A_2 < A_1$, a result contrary to that expected to arise from uranium deposition. However, it must be admitted that any ^{234}U atoms ejected from the rock surface during the succession of α - and β -decays would become a potential supply to the rock if the chemical conditions were such that deposition was taking place, and the supply term should really become a function of time. This is a further complication in a system which is already underdetermined.

Also,

$$A_3 \rightarrow f_2 A_2 - f_1 f_2 \lambda_1 K_1 / \lambda_3 + K_3$$

and, since $f_2 \approx 1$ and K_3 is small, A_2 will exceed A_3 by a constant amount, but the activity ratio A_3/A_2 will again tend to unity as the rock becomes more active. Disequilibrium can be maintained at an experimentally observable level (say at activity ratios < 0.95 and > 1.05) over several millions of years given suitable values of K_1 and K_2 , that is values such that $\lambda_1 K_1$ and $\lambda_2 K_2$ are of the order of $(10^{-5}R \rightarrow 10^{-6}R)/a$. Under such conditions the activity of the rock will increase by a sizeable factor over a period of a million years. The values of $\lambda_1 K_1$ and $\lambda_2 K_2$ will reflect the ^{238}U and ^{234}U activities in the

water, in particular the ratio $\lambda_1 K_1 / \lambda_2 K_2$ should be identical to the activity ratio in the water since there will be no chemical differentiation of uranium isotopes there. This does not imply, however, that the activity ratio of the rock should be equal to that of the water. Thus, neglecting recoil, we have

$$A_2 = A_1 + (\lambda_2 K_2 - \lambda_1 K_1)(1 - \exp(-\lambda_2 t)) / \lambda_2 \rightarrow A_1 + (\lambda_2 K_2 - \lambda_1 K_1)t = R + \lambda_2 K_2 t$$

at times such that $\lambda_2 t \ll 1$, whereas $A_1 = R + \lambda_1 K_1 t$, so that the activity ratio on the rock surface would be equal to that in the water at short times after the onset of deposition and then only if the value of R were zero. Some plots of the evolution during deposition are shown in Figure 4, where the effect of thorium mobility is also indicated.

1.2.3. Timescales in continuous processes

In contrast to the situation for sudden events, it is difficult to say anything quantitative about the time over which a continuous process has been operating. Considering removal, it has already been pointed out that, under the usual assumptions concerning thorium, $f_2 \approx 1$ and A_3/A_2 will always be greater than unity so that the time previously denoted by T_{23} does not exist. Also, the asymptotic expression for A_3/A_1 can be greater than, equal to or less than unity, depending on the magnitudes of λ'_1 and λ'_2 , and the evolution on the Thiel plot can therefore stop in either the third or the fourth quadrants. If the system crosses the ordinate then T_{13} exists, but there is no analytical expression for it. There is nothing in the position of a point on the allowed parts of the plot, therefore, which indicates that a system undergoing continuous removal has reached a steady state (in which case removal probabilities can be estimated) or, indeed, if it is ever going to do so. However, it is fair to say that if a steady state is going to be attained at all, then this will be the case only after at least 1 Ma from the onset of the removal process. The solutions of the equations for continuous removal predict that A_2/A_1 is a monotonically decreasing function of time if $\lambda'_2 > \lambda'_1$ but that A_3/A_1 has a turning point (if the conditions for an eventual steady state are met) given by

$$t = \ln [(a + b - 1) (\lambda_3 + \lambda'_3 - \lambda'_1) / \{b(\lambda_2 + \lambda'_2 - \lambda'_1)\}] / (\lambda_3 + \lambda'_3 - \lambda_2 - \lambda'_2)$$

where a and b are as defined previously.

The relationship is largely of academic interest, but it is interesting that an analytical expression can be derived and used instructively to see how this time varies over a range of values of λ'_1 and λ'_2 . Thus, assuming no recoil losses and that thorium is immobile, if $\lambda'_1 = 1.1 \times 10^{-6}a$, $\lambda'_2 = 1.5 \times 10^{-6}a$ then $t = 0.2 \times 10^6a$, whereas if $\lambda'_1 = 4 \times 10^{-6}a$, $\lambda'_2 = 10^{-5}a$, which represents a faster removal but which still leads to a steady state, then $t = 0.08 \times 10^6a$.

The situation with respect to deposition is similar, but there are some differences in detail. Again, the time T_{23} does not exist, so that the ^{230}Th activity never overtakes that of ^{234}U , and the evolution path might or might not cross from the second into the first quadrant. Ignoring thorium removal and recoil losses, the condition for such a crossing (T_{13} therefore exists) is that

$$\lambda_2 K_2 / \lambda_1 K_1 > (\lambda_3 + \lambda_2) / \lambda_3 = 1.306$$

Thus, points in the second quadrant can represent either recent or old events, but points in the allowed section of the first quadrant represent the result of processes operating for times $> T_{13}$. Again, there is no analytical solution for T_{13} and its magnitude depends upon the ratio $\lambda_2 K_2 / \lambda_1 K_1$. For instance, a ratio of 2.5 gives $T_{13} = 0.14$ Ma while a ratio of 2 gives 0.2 Ma and one of 10 gives 0.02 Ma. The ratio A_2/A_1 has one turning point and A_3/A_1 has either one or two depending on whether or not the system evolves into the first quadrant, but there are no analytical solutions for the times at which these occur. The system therefore traces out loops in quadrants 1 and 2 with eventual constant differences in activity implying that the tendency is back towards the origin, a situation which is distinct from the case of continuous removal where the system evolves towards some point in quadrant 4 or in the allowed region of quadrant 3.

1.2.4. The behaviour of ^{226}Ra

The half-life of ^{226}Ra (1600a) is very much shorter than that of its long-lived precursors in the decay chain and the natural conclusion to be drawn from this is that the state of disequilibrium of ^{226}Ra will be an indicator of very recent processes, either of removal or of deposition.

If ^{230}Th is taken to be immobile, then in the case of pulsed inputs (the deposition time now must be much less than 1600a) of magnitude P_1 , P_2 and P_4 where the notation is extended in the obvious way,

$$\begin{aligned}
A_4 = & R + P_1 (1 - \exp(-\lambda_4 t)) + P_4 \exp(-\lambda_4 t) \\
& + P_1 \lambda_4 (\exp(-\lambda_4 t) - \exp(-\lambda_3 t)) / (\lambda_4 - \lambda_3) \\
& + (P_2 - P_1) \lambda_3 \lambda_4 [(\exp(-\lambda_2 t) - \exp(-\lambda_4 t)) / \\
& (\lambda_4 - \lambda_2) - (\exp(-\lambda_3 t) - \exp(-\lambda_4 t)) / \\
& (\lambda_4 - \lambda_3)] / (\lambda_3 - \lambda_2)
\end{aligned}$$

and, as soon as $\exp(-\lambda_4 t)$ becomes negligible, $A_4 = A_3$ since $\lambda_4 \gg \lambda_3$ or λ_2 . The fact that $\lambda_4 / (\lambda_4 - \lambda_2)$ and $\lambda_4 / (\lambda_4 - \lambda_3)$ are so near unity means that the transient equilibrium effect of the daughter activity exceeding that of the parent, such as occurs with ^{230}Th growing in towards an excess of ^{234}U , does not occur, at least not to an experimentally measurable extent. The above shows that if uranium is deposited suddenly in the absence of radium, then the radium is never appreciably out of equilibrium with ^{230}Th as it grows in, and that a sudden deposition of radium alone gives disequilibrium which can persist for only a few ^{226}Ra half-lives. Similar considerations apply, of course, to situations where there are sudden losses.

Continuous removal of ^{226}Ra , including recoil loss, is represented by:

$$\frac{dN_4}{dt} = f_3 A_3 - \lambda_4 N_4 - \lambda'_4 N_4$$

with the notation as before. Hence

$$\begin{aligned}
A_4 = & R [\exp(-(\lambda_4 + \lambda'_4)t) \\
& + f_3 \{ a \lambda_4 (\exp(-\lambda'_1 t) - \exp(-(\lambda_4 + \lambda'_4)t)) / \lambda_4 + \lambda'_4 - \lambda'_1 \} \\
& + b \lambda_4 (\exp(-(\lambda_2 + \lambda'_2)t) - \exp(-(\lambda_4 + \lambda'_4)t)) / ((\lambda_4 + \lambda'_4) - (\lambda_2 + \lambda'_2)) \\
& + c \lambda_4 (\exp(-(\lambda_3 + \lambda'_3)t) - \exp(-(\lambda_4 + \lambda'_4)t)) / ((\lambda_4 + \lambda'_4) - (\lambda_3 + \lambda'_3)) \}]
\end{aligned}$$

where a, b and c are as previously defined. Thus, at long times

$$A_4/A_1 \rightarrow f_1 f_2 f_3 \lambda_2 \lambda_3 \lambda_4 / \{ (\lambda_2 + \lambda'_2 - \lambda'_1) (\lambda_3 + \lambda'_3 - \lambda'_1) (\lambda_4 + \lambda'_4 - \lambda'_1) \}$$

$$\text{and } A_4/A_3 \rightarrow f_3 \lambda_4 / (\lambda_4 + \lambda'_4 - \lambda'_1)$$

with the relations previously derived for A_2/A_1 and A_3/A_1 also applying. The interesting ratio is A_4/A_3 , since the disequilibrium of ^{226}Ra relative to the uranium isotopes is

governed by the behaviour of ^{230}Th , and it is evident that disequilibrium can be maintained over long times only if there is appreciable recoil loss or if λ_4 is of the order of magnitude of λ_3 . That is, the probability per unit time of the removal of a ^{226}Ra atom must be very much greater than that of a uranium atom. If these probabilities are nearly equal, however, then at times much greater than the ^{226}Ra half-life (say 10^4a), $A_4 = A_3$.

Similar considerations apply to the addition of ^{226}Ra from a non-depleting source, but the final expression for A_4 , including the possibility of recoil, is somewhat complicated. The situation when $\exp(-\lambda_4 t)$ can be neglected is that a constant difference between the ^{226}Ra and ^{230}Th activities is predicted:

$$A_4 \rightarrow f_3 A_3 + (\lambda_4 K_4 - f_1 f_2 f_3 \lambda_1 K_1) / \lambda_4$$

1.3. Natural radionuclide studies of rock samples at the Osamu Utsumi mine and Morro do Ferro: background and objectives

Detailed descriptions of the geology, hydrology, mineralogy and geochemistry relating to the large uranium and thorium plus rare-earth element deposits at the Osamu Utsumi mine and Morro do Ferro respectively are provided in other reports in this series (Waber *et al.*, Waber, Holmes *et al.* and Nordstrom *et al.*, this report series; Reps. 2, 3, 5 and 6). In addition to the presence of the ore bodies, a geochemical feature of major importance for the present section of the work is the occurrence of redox fronts on a regional scale, generated by the downward penetration of oxidizing groundwater into the reduced rock. At the Osamu Utsumi mine in particular, the redox front is visually obvious as a clearly defined, sharp colour change resulting from the Fe(II)/Fe(III) transition in the oxidation of pyrite.

Within the context of the natural analogue studies at these locations, the natural radioactive decay series work has been focussed upon a number of specific objectives, namely:

- (1) Identification of radionuclide dissolution, transport and deposition processes within the study sites in general, and at the redox fronts in particular.
- (2) Attempts to establish the timescales appropriate to the above processes and to evaluate the rate of movement of the redox fronts.

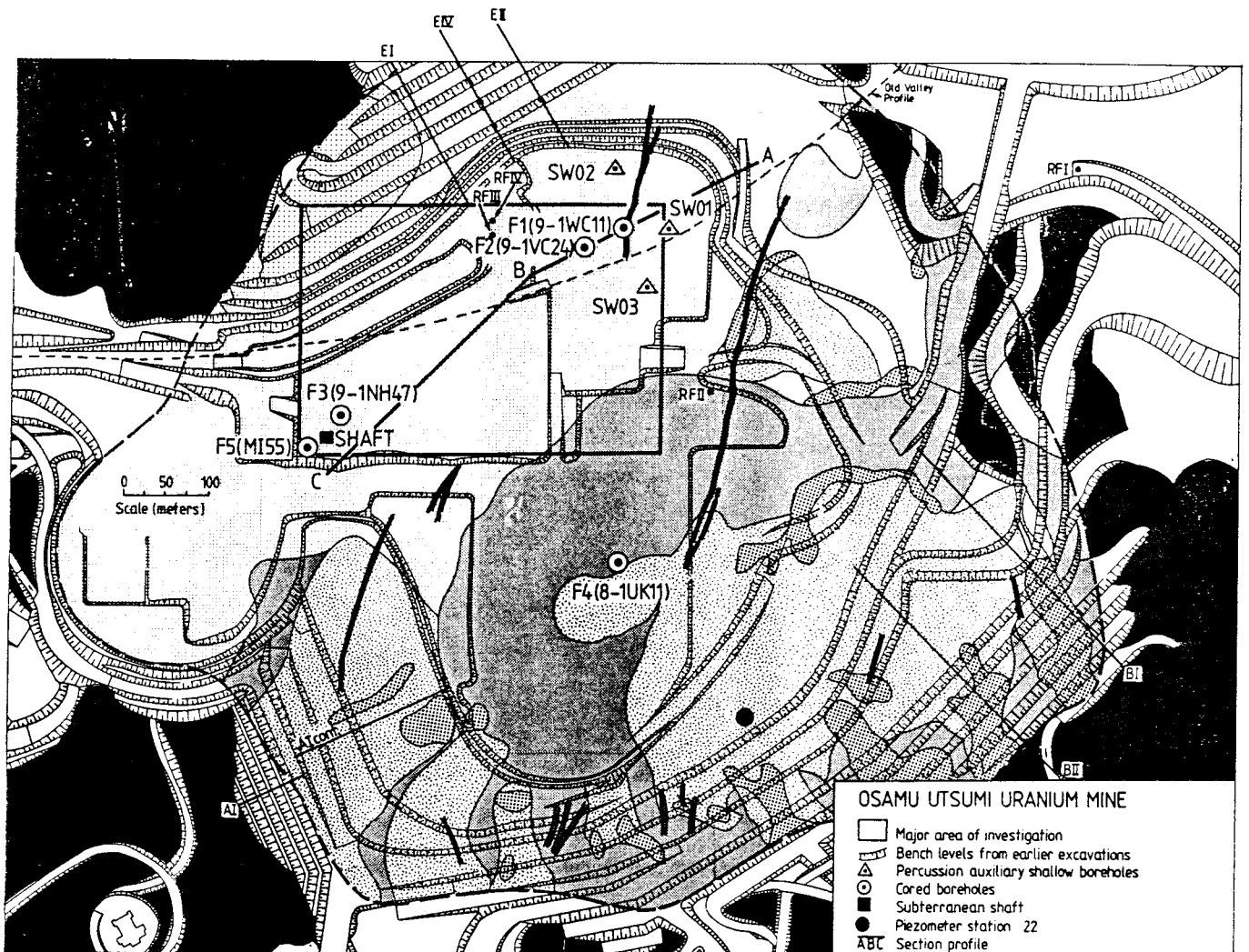
- (3) Provision of information relating to the long-term ($10^5 - 10^6$ a) direction of groundwater flow.
- (4) Investigation of the growth rates of uranium nodules.

The natural decay series measurements were complemented by an extensive series of stable element analyses and an additional section of the work involved analyses for naturally occurring plutonium.

The redox front investigations were of central importance in this part of the project since, in addition to the requirement that any safety assessment should be able to predict the behaviour of radionuclides at naturally occurring redox fronts in the far-field, it has been estimated that, subsequent to the ingress of water, oxidizing conditions could be established within a repository and could eventually extend outwards into the far-field. The postulated mechanism leading to such a situation is that, while initially reducing conditions would apply to the repository itself and to the contiguous host rock, radiolysis of invasive water and subsequent preferential loss of hydrogen relative to oxygen could lead to the development of oxidizing conditions within the repository (Neretnieks, 1982; Chapman *et al.*, 1984; NAGRA, 1985; Guppy and Atkinson, 1989). Subsequent fissure flow has been estimated to be capable of extension of oxidized conditions, with possible associated transport of oxidized radionuclides (e.g. U, Np, Tc) into the host rock at a rate of up to 50 m in 10^6 years (Neretnieks and Åslund, 1983a, b; Chapman *et al.*, 1984).

Given the feasibility of this model, it is clearly important that an adequate understanding of redox front processes should be available for repository safety assessment purposes. The difficulty in studying the evolution of redox conditions in a repository by means of extrapolation from laboratory-based experiments has, however, been described by Guppy and Atkinson (1989), who identified experimental problems such as the selective response of electrodes and kinetic controls over redox equilibria as significant limitations on this approach. These problems are obviously exacerbated in attempts to extrapolate from laboratory conditions and timescales to those applicable to a repository, and the importance of empirical characterization of long-term, natural redox processes is thus apparent.

The main research effort in the natural decay series investigations at the Osamu Utsumi mine was devoted to samples from the F1 drillcore, including detailed study of transects across three sections of the core where it intersected the redox front. An extensive range of stable elements was also analyzed in F1 drillcore samples using inductively coupled plasma mass spectrometry (ICP-MS). Additional redox front



- Limit of mapped area.
- (Oldest)
- Subvolcanic phonolite with very weak hydrothermal alteration, no pyrite impregnation.
 - Mainly subvolcanic & minor volcanic phonolites, fractured if near 4.
 - Abyssal & hypabyssal intrusive nepheline syenites (intrusive in 1), fractured if near 4.
 - Subvolcanic pseudotachyrite phonolites (intrusive in 1 and 2); fractured if near 4.
 - Subvolcanic conduit breccia, locally grading to extremely xenolithic ultra fine-grained, flow textured phonolites.
 - End of major hydrothermal event (formation of "potassic rock" and U - Mo - Zr - REE - pyrite hydrothermal mineralizations).
- (Youngest)
- Biotite - lamprophyre dykes (late-stage intrusive).
- RF I, II, III, IV : Location of redox fronts for detailed investigations.
 E I, II, IV : Vertical profiles in ore-body 'E'
 B I, II : Vertical profiles in ore-body 'B'
 A I : Vertical profiles in ore-body 'A'

Figure 5. Plan of the Osamu Utsumi mine showing the location of the F1 drillcore.

transects on varying scales were analyzed using samples collected from surface exposures in the mine. Uranium nodules from the mine were analyzed for uranium and thorium isotopes; one was analyzed for natural plutonium. In the case of Morro do Ferro, samples were analyzed from two drillcores (MF10 and 12), one of which was from a position in the mineralization zone (MF10) while the other was located downhill from the mineralization (MF12). Subsequent sections of this report describe each of these studies in turn.

Most of the samples were collected, prepared and distributed by Nick Waber of the University of Bern who, together with Hans Schorscher of the University of São Paulo, has also provided mineralogical and geochemical data for many of the samples in other reports in this series (Waber *et al.* and Waber, this report series; Repts. 2 and 3). Established radioanalytical methods were used for analysis of whole-rock samples in three different laboratories and, in order to ensure compatibility in the results obtained, an interlaboratory comparison exercise was performed with generally satisfactory results as described in Appendix 1.

2. Osamu Utsumi uranium mine

2.1. F1 drillcore studies

2.1.1. Natural decay series studies

The F1 drillcore sampling position in the Osamu Utsumi mine is shown in Figures 5 and 6. Figure 6 also shows in schematic form the general features of the position of the main redox fronts and the present groundwater flow pattern within the mine. More detailed descriptions of the hydrogeology, mineralogy and geomorphology of relevance to the F1 drillcore and other redox front studies in the mine are contained in other reports in this series (Waber *et al.* and Holmes *et al.*, this report series; Repts. 2 and 5).

It is apparent from Figure 6 that the redox front, marked by the colour change associated with the Fe(II)/Fe(III) transition, occurs at an irregular depth below the ground surface, with preferential downward extension of oxidized conditions in areas around major fractures. The F1 drillcore intersects one such finger of oxidized rock penetrating into the reduced phonolite, with the oxidized conditions extending in a downward-pointing wedge shape around a major fracture system intersected at a depth of about 50 m. The drillcore consequently intersects the redox front at three depths: at 33.4 m and 66.2 m, with oxidized rock overlying reduced rock, and at 42.0 m where the sequence is reversed and the reduced rock overlies the oxidized rock.

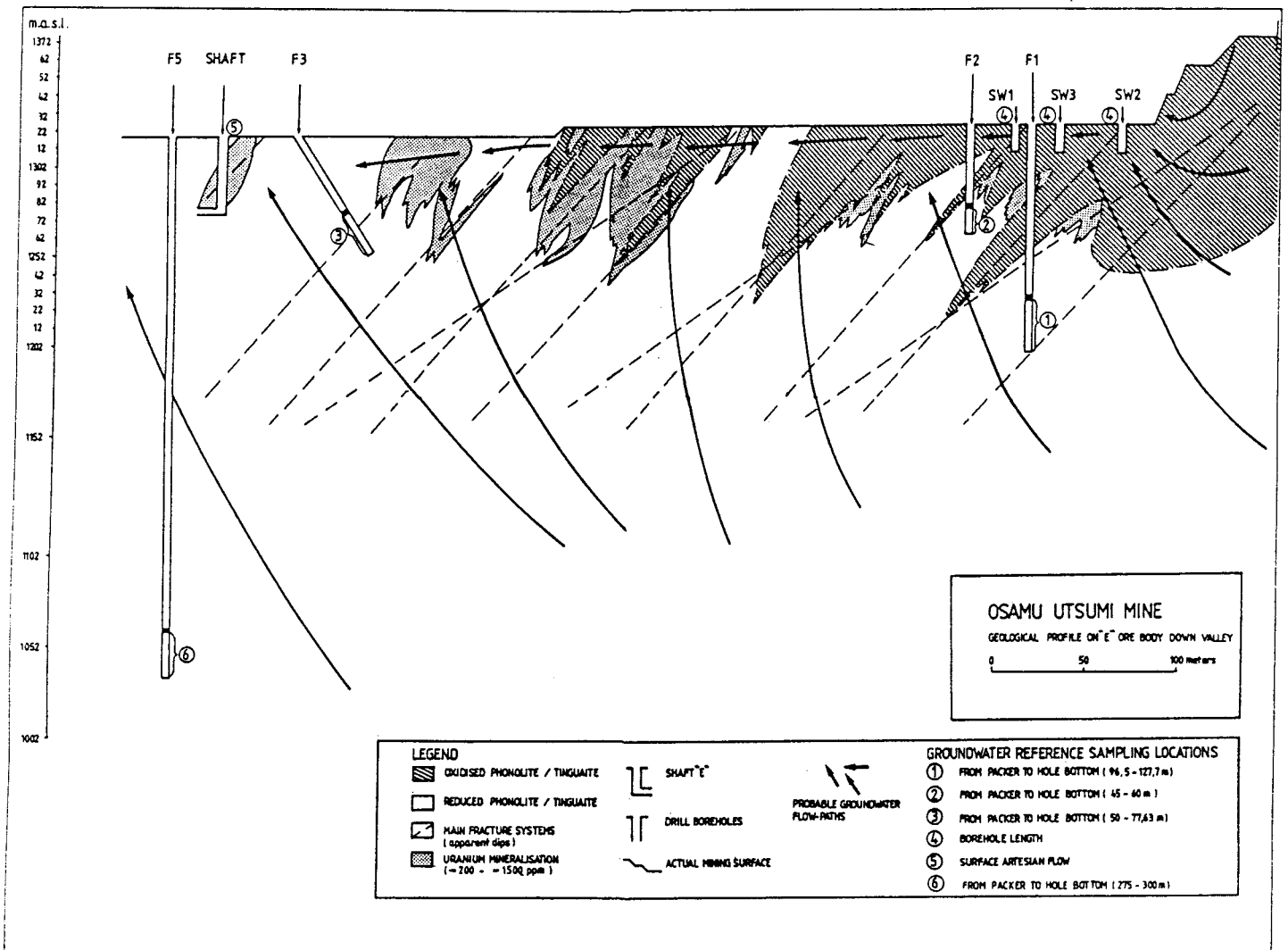


Figure 6. Section through the Osamu Utsumi mine showing the location of the F1 drillcore.

Table I provides a list of samples from the F1 drillcore which were analyzed for natural decay series radionuclides, along with the sample depths and a brief description of the rock type, while Figure 7 shows in detail the sampling positions for some of the samples collected from points close to the redox fronts. The analytical results of the samples for natural decay series radionuclides are given in Table II, while Table III provides a more extensive, composite set of uranium and thorium concentrations (in ppm), comprising results obtained by alpha spectrometry and ICP-MS analysis in this section of the study and by X-ray fluorescence (XRF) in the mineralogy and geochemistry section (Waber *et al.*, this report series; Rep. 2). A set of samples was also examined by semi-quantitative ICP-MS analysis in order to provide complementary information on concentrations of stable elements in F1 drillcore samples and the resultant data are presented in Table V. Finally, a limited number of samples were subjected to quantitative ICP-MS analysis for the rare-earth elements (Table VI).

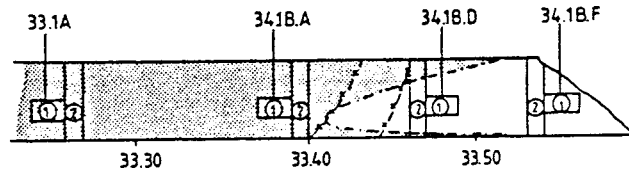
Before detailed discussion of the specific activity results for the natural decay series radionuclides, it is initially useful to consider the overall distribution of uranium in the drillcore and in the mine in general. Figure 8 shows the general distribution of uranium in the rock from the original (pre-mine) surface to the bottom of borehole F1 (Waber *et al.*, this report series; Rep. 2). The uranium profile shows concentrations decreasing from about 30 ppm in the uppermost weathered (laterite) section to values of 10 ppm or less throughout most of the oxidized phonolite overlying the depth range covered by the F1 drillcore. The drillcore itself traverses the redox fronts, as described above, and major enhancements of the concentrations of both uranium and thorium occur in the vicinity of the fronts as shown in Figure 8, and in more detail for the drillcore in Figures 9 and 10. It is clear from Figures 9 and 10 that the enhancement of uranium concentrations near the fronts is much greater than the corresponding enhancement of thorium concentrations, with uranium exhibiting a maximum concentration of 2.8% in the reduced rock just above the 42 m redox front, while the maximum thorium concentration observed was 387 ppm. Thus, while significant variations in the thorium content of the rock do occur in the vicinity of the redox fronts (either as a result of dissolution and redeposition after transport or by preferential concentration of thorium in resistate phases), the extent of such effects appears to be about two orders of magnitude lower than the corresponding increase in uranium concentrations. This is a significant observation in the light of discussions in section 1.2 above on the effects of the relative mobility of uranium and thorium during rock-water interactions on $^{230}\text{Th}/^{234}\text{U}$ disequilibrium, and possible concomitant limitations on interpretation and modelling of such data. Thus, the very much lower degree of enhancement of thorium concentration

TABLE I

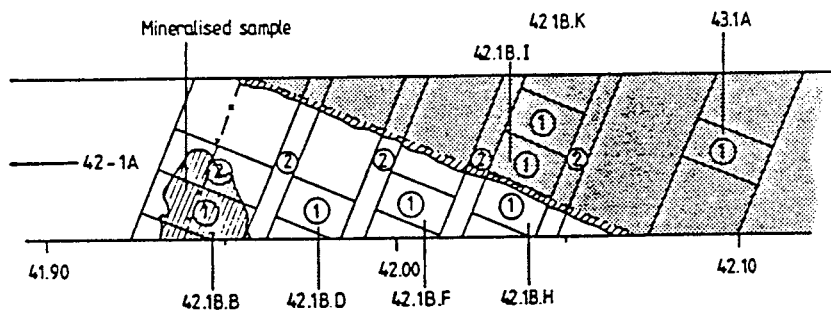
List of samples from the F1 drillcore which were analyzed for natural decay series radionuclides.

Sample code	Depth (m)	Rock description
6-1A	6.00	Porous, strongly fractured, oxidized phonolite.
10-1A	9.84	Porous, fine-grained porphyritic, oxidized phonolite.
16-1A	15.07	Oxidized phonolite, average sample, low U content.
26-1A	25.22	Oxidized phonolite, average sample, low U content.
33-1A	32.89	Redox front, oxidized side, low U content.
34-1B-A	33.40	Redox front, oxidized side, low U content.
34-1B-D	33.51	Redox front, reduced side, low U content.
34-1B-F	33.65	Redox front, reduced side, low U content.
34-1C	34.00	Very porous, fine-grained porphyritic, reduced phonolite.
35-1A	34.31	Porous, fine-grained porphyritic, reduced phonolite, fractured.
41-1A	40.05	Massive, medium-grained porphyritic, reduced phonolite.
42-1A	41.85	Redox front, reduced side, low U content.
42-1B-B	41.95	Redox front, reduced side, U mineralization.
41-1B-D	41.97	Redox front, reduced side, weak U mineralization.
42-1B-F	42.01	Redox front, reduced side, weak U mineralization.
42-1B-H	42.03	Redox front, reduced side, weak U mineralization.
42-1B-I	42.04	Redox front, oxidized side, low U content.
42-1B-K	42.05	Redox front, oxidized side, low U content.
43-1A	42.10	Redox front, oxidized side, low U content.
45-1A	44.87	Massive, medium-grained porphyritic, oxidized phonolite.
47-1A	46.10	Porous, inequigranular porphyritic, oxidized phonolite, strongly fractured.
50-1A	49.83	Porous, fine-grained porphyritic, oxidized phonolite, fractured.
55-1A	54.30	Porous, inequigranular porphyritic, oxidized phonolite, fractured.
60-1A	59.80	Porous, medium-grained, oxidized phonolite.
65-1A	64.50	Porous, medium-grained, oxidized phonolite.
66-1A-A	65.93	Redox front, oxidized side, low U content.
67-1A-B	66.19	Redox front, oxidized side, low U content.
67-1A-D	66.26	Redox front, reduced side, low U content.
68-1A-A	67.03	Redox front, reduced side, low U content.
71-1A	70.10	Porous, argillic, medium-grained, reduced phonolite.
75-1A	74.25	Porous, fine-grained, reduced phonolite.
75-1B	74.96	Massive, fine-grained, reduced phonolite.
80-1A	79.80	Reduced phonolite, average sample.
96-1A	96.00	Reduced phonolite, average sample.
101-1A	100.32	Reduced phonolite, average sample.
104-1A	104.00	Reduced phonolite, average sample.
110-1A	110.00	Reduced phonolite, conductive zone, low U content.
111-1B	111.00	Reduced phonolite, conductive zone, low U content.
113-1B	113.00	Reduced phonolite, average sample.
114-1A-A	113.09	Hydrothermally altered, porous reduced phonolite.
114-1A-B	113.19	Hydrothermally altered, leached, porous reduced phonolite.
114-1A-C	113.20	External part of fracture filling, mainly K-feldspar, pyrite and zircon.
114-1A-D	113.21	Internal part of fracture filling, mainly clay minerals and pyrite.
121-1A	120.19	Reduced phonolite, average sample, low U content.
123-1B	123.00	Reduced phonolite.

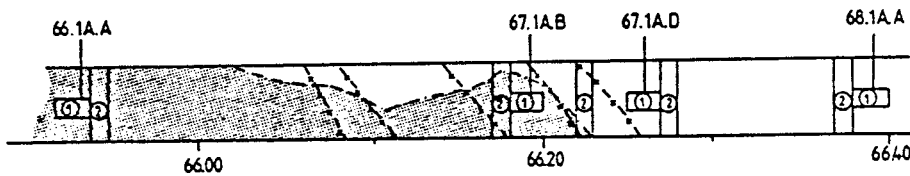
BOREHOLE F1 (9.1WC-11) : OSAMU UTSUMI MINE.



A. Redox front at 33.40m, borehole F1 (9.1WC-11)



B. Redox front at 42.00m, borehole F1 (9.1WC-11)



C. Redox front at 66.20m, borehole F1 (9.1WC-11)








- Symbols in A-C :
-  Reduced phonolite.
 -  Oxidized phonolite.
 -  White clay-layer.
 -  Redox front.
 -  Fissure.
 -  Radionuclide analyses.
 -  Mineralogical and geochemical analyses.

Figure 7. Sections of the F1 drillcore showing details of sampling positions close to the redox fronts.

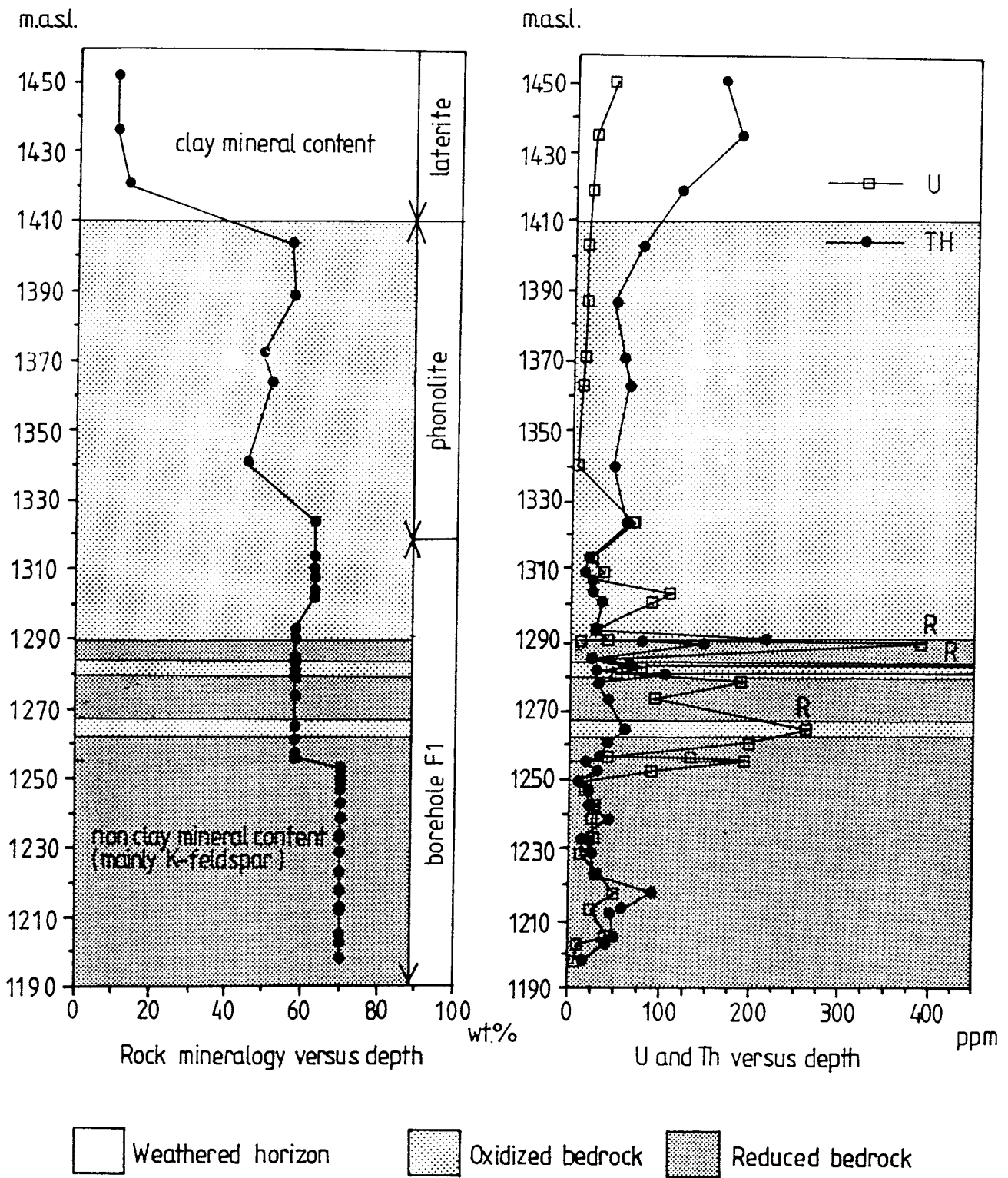


Figure 8. Uranium, thorium and clay mineral distributions as a function of depth (metres above sea level) in the Osamu Utsumi mine (Waber et al., this report series; Rep. 2).

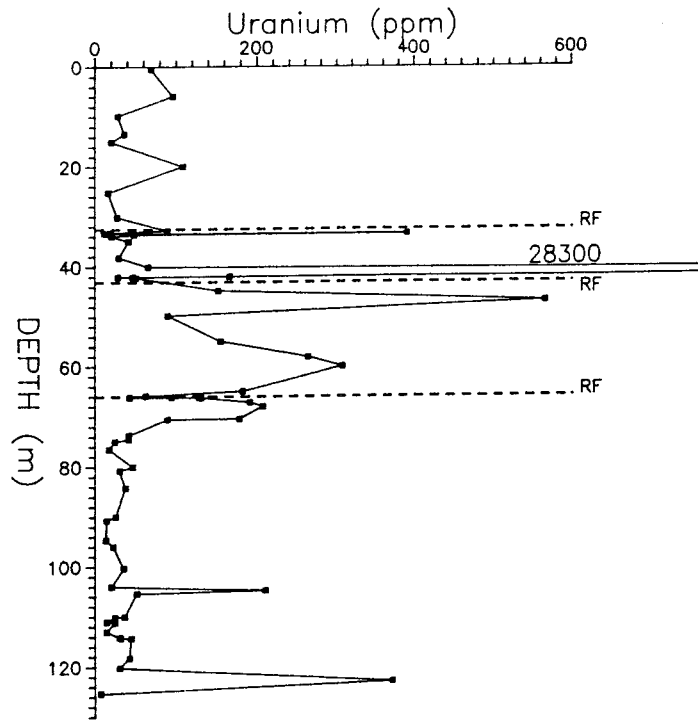


Figure 9. Uranium concentrations as a function of depth (metres below ground level – mbgl) for samples from the F1 drillcore.

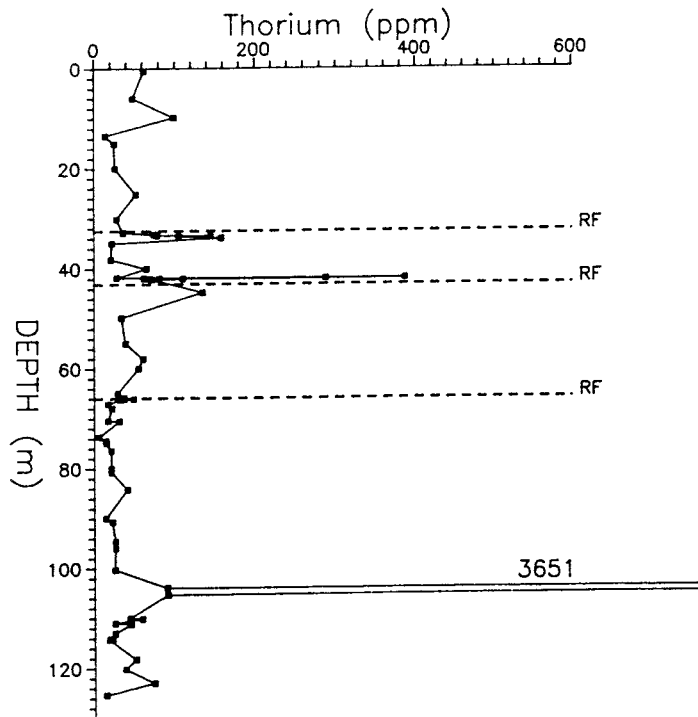


Figure 10. Thorium concentrations as a function of depth for samples from the F1 drillcore.

TABLE II

Natural decay series analyses of rock samples from the F1 drillcore, Osamu Utsumi uranium mine.

Sample	Depth (m)	^{238}U	$^{234}\text{U}/^{238}\text{U}$	$^{230}\text{Th}/^{234}\text{U}$	$^{226}\text{Ra}/^{230}\text{Th}$	$^{231}\text{Pa}/^{235}\text{U}$	^{232}Th
		Concentr. Bq kg ⁻¹	Activity ratio	Activity ratio	Activity ratio	Activity ratio	Concentr. Bq kg ⁻¹
6-1A	6.00	1167 ± 17	1.01 ± 0.02	1.06 ± 0.04	0.076 ± 0.05	NA	193 ± 9
10-1A	9.84	384 ± 8	1.05 ± 0.03	1.09 ± 0.04	0.68 ± 0.05	NA	402 ± 20
16-1A	15.07	248 ± 5	1.03 ± 0.02	0.99 ± 0.04	1.49 ± 0.09	NA	103 ± 5
26-1A	25.22	198 ± 7	1.10 ± 0.03	0.96 ± 0.04	3.90 ± 0.25	NA	213 ± 8
33-1A	32.89	1085 ± 27	1.03 ± 0.02	1.02 ± 0.03	0.61 ± 0.04	NA	150 ± 7
34-1B-A	33.40	227 ± 5	1.00 ± 0.02	0.95 ± 0.04	3.36 ± 0.20	NA	302 ± 8
34-1B-D	33.51	212 ± 7	0.97 ± 0.03	6.00 ± 0.05	3.26 ± 0.24	NA	320 ± 15
34-1B-F	33.65	582 ± 15	0.98 ± 0.02	0.94 ± 0.04	2.16 ± 0.15	NA	427 ± 22
34-1C	34.00	243 ± 8	0.94 ± 0.03	1.55 ± 0.09	2.56 ± 0.13	NA	642 ± 35
35-1A	34.31	503 ± 13	0.85 ± 0.02	0.81 ± 0.06	1.78 ± 0.16	NA	88 ± 11
41-1A	40.05	794 ± 14	1.23 ± 0.04	1.01 ± 0.04	1.05 ± 0.04	NA	256 ± 10
42-1A	41.85	31300 ± 1000	1.15 ± 0.03	0.94 ± 0.03	0.57 ± 0.04	0.97 ± 0.07	250 ± 10
42-1B-B	41.95	345000 ± 9000	1.08 ± 0.02	0.96 ± 0.03	0.62 ± 0.04	1.03 ± 0.06	1570 ± 200
42-1B-D	41.97	110000 ± 2300	1.10 ± 0.02	0.97 ± 0.03	0.48 ± 0.03	0.95 ± 0.06	250 ± 80
42-1B-F	42.01	52500 ± 1300	1.02 ± 0.02	0.88 ± 0.03	0.51 ± 0.03	1.06 ± 0.07	1167 ± 117
42-1B-H	42.03	2020 ± 50	0.51 ± 0.01	1.00 ± 0.03	4.43 ± 0.27	1.05 ± 0.08	327 ± 10
42-1B-I	42.04	336 ± 7	1.02 ± 0.02	1.09 ± 0.04	9.20 ± 0.59	2.84 ± 0.41	280 ± 12
42-1B-K	42.05	557 ± 18	0.93 ± 0.03	1.00 ± 0.05	6.50 ± 0.43	1.13 ± 0.10	447 ± 22
43-1A	42.10	607 ± 15	0.99 ± 0.02	1.00 ± 0.05	6.60 ± 0.38	0.97 ± 0.07	293 ± 10
45-1A	44.87	1849 ± 50	1.02 ± 0.03	1.23 ± 0.03	0.91 ± 0.06	NA	549 ± 30
47-1A	46.10	6891 ± 119	0.96 ± 0.04	NA	NA	NA	NA
50-1A	49.83	1085 ± 16	1.07 ± 0.04	0.94 ± 0.04	1.28 ± 0.10	NA	136 ± 7
55-1A	54.30	1884 ± 33	1.09 ± 0.01	0.97 ± 0.03	0.92 ± 0.06	NA	158 ± 15
60-1A	59.80	3741 ± 100	0.79 ± 0.02	0.81 ± 0.06	0.92 ± 0.06	NA	222 ± 8
65-1A	64.50	2217 ± 32	0.94 ± 0.02	0.89 ± 0.03	1.04 ± 0.06	NA	119 ± 6
66-1A-A	65.93	750 ± 17	0.94 ± 0.02	1.27 ± 0.03	1.03 ± 0.06	NA	150 ± 5
67-1A-B	66.19	1150 ± 27	0.84 ± 0.02	1.69 ± 0.08	1.69 ± 0.12	NA	197 ± 23
67-1A-D	66.26	1560 ± 38	0.86 ± 0.02	1.04 ± 0.04	0.79 ± 0.05	NA	135 ± 12
68-1A-A	67.00	2530 ± 67	0.88 ± 0.02	1.04 ± 0.03	0.76 ± 0.04	NA	88 ± 7
75-1A	74.25	500 ± 10	1.03 ± 0.03	1.07 ± 0.04	1.11 ± 0.07	NA	55 ± 7
80-1A	79.80	560 ± 13	1.01 ± 0.02	1.00 ± 0.03	0.90 ± 0.05	NA	87 ± 3
101-1A	100.32	428 ± 15	1.08 ± 0.03	1.35 ± 0.07	0.80 ± 0.06	NA	102 ± 10
110-1A	110.00	462 ± 12	1.04 ± 0.02	1.01 ± 0.03	1.09 ± 0.07	NA	175 ± 8
111-1B	110.13	170 ± 5	1.09 ± 0.03	0.99 ± 0.03	0.91 ± 0.06	NA	102 ± 5
121-1A	120.19	365 ± 8	1.00 ± 0.02	1.12 ± 0.04	0.85 ± 0.06	NA	153 ± 10

NA = not analyzed.

N.B. Errors are based on one sigma counting statistics plus one percent uncertainty in the spike.

than uranium concentration supports the assumption used in interpretation of the $^{230}\text{Th}/^{234}\text{U}$ activity ratio data that thorium is, to a first approximation, insoluble in comparison with uranium. Further evidence of this is provided by the plot of the uranium/thorium concentration ratio versus depth for the F1 drillcore (Fig. 11) which shows values ranging from less than 1 in sections of the rock remote from the redox fronts up to a maximum value of 145 in the reduced rock at the 42.0 m redox front.

The section of the drillcore below about 75 m lies well away from any redox front and consists entirely of reduced rock. This section of the core thus represents the best available material for characterizing the composition of the phonolite before it has been influenced by the penetration of oxidizing water. The uranium concentrations of most of the samples from this section of the core show irregular variations within the range 7 to 51 ppm, but two of the samples have notably higher concentrations, namely sample 105-1A with 210 ppm and sample 123-1A with 371 ppm. The higher concentrations of uranium at these locations presumably indicates some mineralogical variation which is also reflected in higher concentrations of thorium and other trace elements in these samples (Fig. 10 and Table IV). If the two anomalously high uranium content samples are excluded, the average uranium concentration in the samples below 75 m depth is 27 ppm whereas an average value of 35 ppm is obtained if samples 105-1A and 123-1A are included.

Above 75 m, the uranium content of the rock increases sharply and remains generally high, but with a pronounced series of maxima and minima between 70 m and 30 m. The variations in uranium concentration in this section of the core in fact form a systematic pattern with a maximum in uranium concentration being observed on each side of each redox front and a minimum at each front as shown in Figures 12 to 14. This correlation of the distribution of uranium with the position of the redox front as marked by the Fe(II)/Fe(III) colour change, and in particular the very sharp increase in uranium concentration immediately inside the reduced section of rock, indicates that the redox-controlled reactions affecting uranium occur at effectively the same place as those affecting iron, thus suggesting that the redox potential shows a sharp variation over a very short distance (of the order of 1 cm). In the redox fronts at 33.4 m and 42.0 m, the uranium peak is very narrow (less than 20 cm) on the reduced side of the front and, in both cases, much higher concentrations are observed in the reduced rock than in the oxidized rock where the peaks are smaller in magnitude but extend over several metres. In the case of the 66.2 m redox front, the same broad maximum structure is observed in the uranium distribution on the oxidized side of the front but a broader peak is present on the reduced side, extending over a distance of about 4 m and with a maximum value

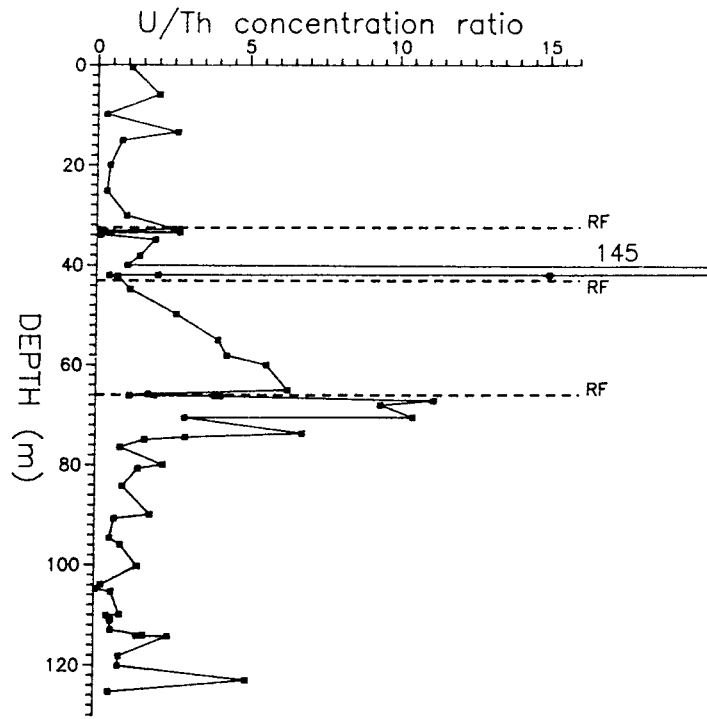


Figure 11. Uranium/thorium concentration ratio as a function of depth for samples from the F1 drillcore.

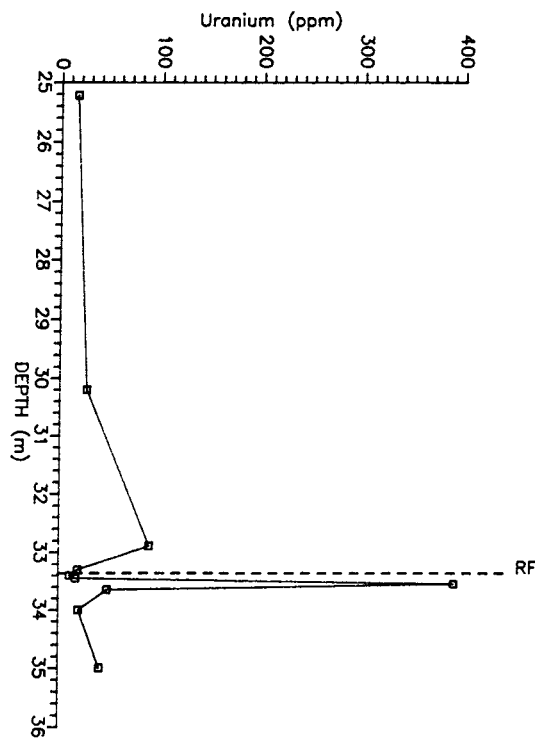


Figure 12. Uranium concentration profile across the redox front at 33.4 m in the F1 drillcore.

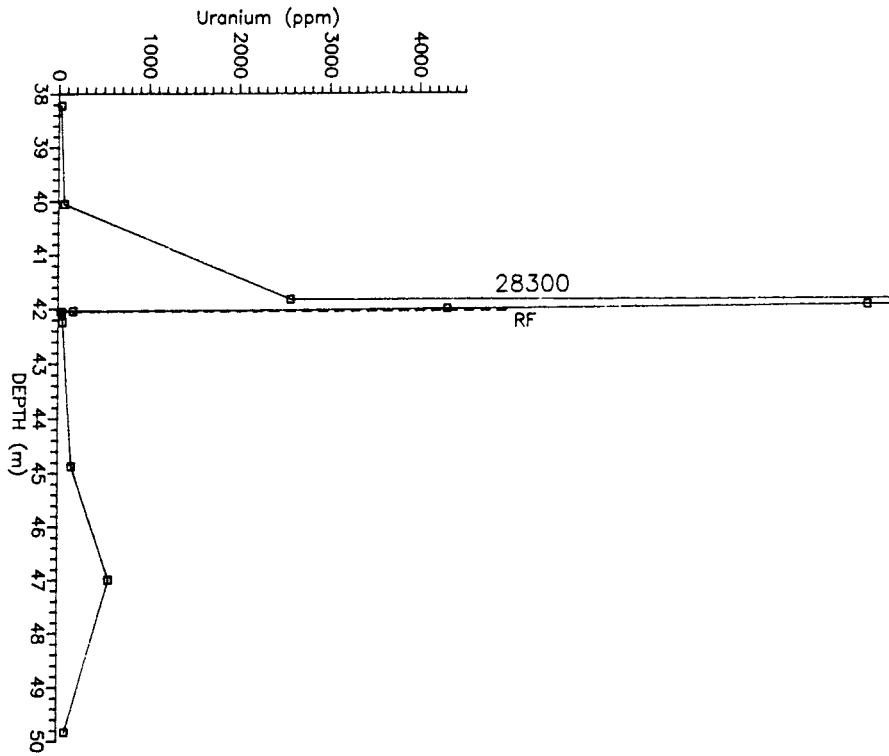


Figure 13. Uranium concentration profile across the redox front at 42.0 m in the F1 drillcore.

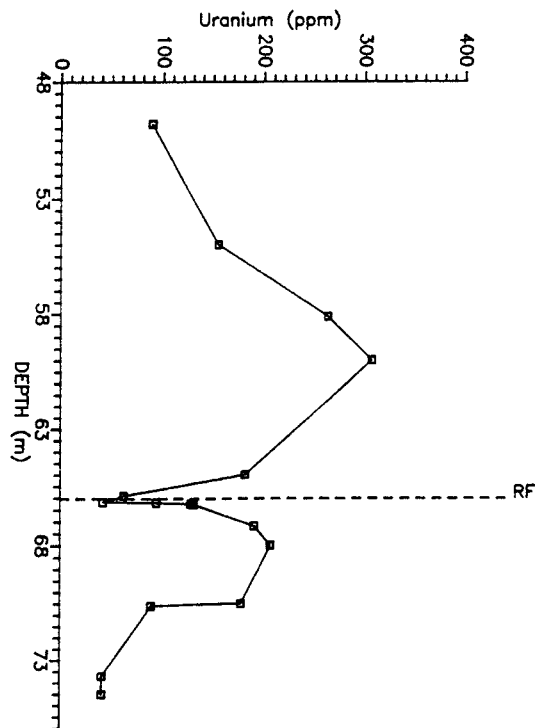


Figure 14. Uranium concentration profile across the redox front at 66.2 m in the F1 drillcore.

of 207 ppm, which is lower in this case than the corresponding maximum of 307 ppm observed on the oxidized side of the front. A final point which should be noted about the distribution of uranium at the redox fronts is that the minimum concentration values of 11, 28 and 42 ppm, observed at 33.45, 42.04 and 66.17 m depth respectively, fall within the range of values observed for the reduced rock below 75 m, indicating that there is no major depletion in the uranium content of the rock relative to the average reduced rock at these positions.

Thus, while dissolution of uranium is evidently occurring just on the redox front, the distribution of uranium indicates that the general area around the fronts is a zone of uranium deposition and that similar processes are operating at all three fronts. The presence of the peaks in uranium concentration on the oxidized side of each front clearly demonstrates that the process involved is not a simple transfer of soluble U(VI) from the oxidized section to the reduced section to be deposited as U(IV).

The distribution of uranium about the three redox fronts places a constraint upon the direction of groundwater flow which has given rise to this system. Thus, any significant upward flow of water across the redox fronts would be difficult to reconcile with the existence of peaks in the uranium concentration on the lower sides of the fronts, particularly since two of these occur in reduced rock while the third is in oxidized rock. Similarly, any large downward advective movement of water would be difficult to reconcile with the existence of peaks in the uranium concentration above the redox fronts. The flux of uranium in any direction at the redox front will clearly be the result of the advective and diffusive processes operating. Dissolution of uranium as oxidizing water contacts the reduced rock is likely to generate a maximum in uranium concentration in the groundwater just on the oxidized side of the front. This process would generate a concentration gradient in the groundwater which would result in diffusive movement of uranium away from the front into both the oxidized and the reduced rock. In the latter case, redeposition of the uranium in the solid phase would be extremely likely when it encounters reducing conditions. On the oxidized side of the front, the dissolved uranium is likely to be inherently stable in solution but other processes, in particular deposition of oxides of iron and manganese, may lead to removal of uranium from solution.

On the basis of these considerations, the mechanism most likely to have generated the observed uranium distribution in the F1 drillcore would involve advective flow of groundwater downwards through the rock in a direction approximately in line with the redox fronts (i.e. parallel with the line of the fracture that intersects the core at 50 m). Preferential flow of oxidizing water down the fracture would lead initially to the

extension of oxidized conditions along the line of the fracture and subsequently outwards into the adjoining rock. The extent of oxidized conditions about any point in the fracture would increase with the time elapsed since oxidizing water first penetrated to that level, resulting in the observed wedge-shaped distribution of the oxidized rock about the fracture. Associated with this would be a net transfer of uranium from the oxidized to the reduced rock.

Operation of a system of this type, with outward propagation of oxidized conditions from the fracture at 50 m, would be consistent with the observed minimum in uranium concentration at sample 50-1A in the porous, fractured area of rock, and with the bimodal distribution of uranium around the 42.0 m and 66.2 m redox fronts (Fig. 9).

A simple one-dimensional system of this type would, however, result in a net depletion of uranium in the oxidized wedge of rock around the fracture and this is inconsistent with the data. Thus, the average uranium concentration of the samples from the oxidized finger is 174 ppm and the lowest value (for sample 50-1A in the fracture zone) is 89 ppm. Thus the uranium concentrations throughout this section of rock are substantially higher than those typically observed for the reduced (unaltered) rock (Table III), which has an average uranium content of 27 ppm. The oxidized finger of rock is therefore apparently enriched in uranium rather than depleted as would be predicted by a simple one-dimensional system. Such an enrichment of uranium at this location could require a lateral input in addition to an outward propagation of oxidizing conditions away from the fissure.

Furthermore, a simple one-dimensional system involving transfer of uranium from oxidized to reduced rock across a propagating redox front is not capable of generating the very high concentrations of uranium observed on the reduced sides of the redox fronts if there is any significant diffusion (or advection) of uranium into the oxidized rock. This can be demonstrated by simple box model calculations in which the redox front is considered to move away from the fissure in both directions in a series of steps and, at each step, some fraction of the uranium (both primary and secondary) in the section containing the redox front is dissolved and is transported by diffusion into both the oxidized and the reduced rock. The maximum uranium concentrations that can be generated in this way are derived if it is assumed that there is no net loss of uranium from the section of rock being considered and that the uranium dissolved at the front is deposited in the rock immediately on each side of the redox front (by reduction to insoluble U(IV) on the reduced side and by, for example, scavenging by iron oxide on the oxidized side). The role of the groundwater in this model is simply to allow transport of oxidant to the redox front and diffusive movement of uranium at the front.

TABLE III

Uranium and thorium concentrations (ppm) for samples from the F1 drillcore. (Composite data set derived from alpha spectrometry and ICP-MS analyses in this section of the study and XRF analyses in Waber *et al.*, this report series; Rep. 2.)

Sample	Depth (m)	Uranium Concentration (ppm)	Thorium Concentration (ppm)	<u>Uranium</u> Thorium Concentration ratio
1-1B	0.60	69	62	1.1
6-1A	6.00	96	48	2.0
10-1A	9.84	28	99	0.28
14-1A	13.46	36	14	2.6
16-1A	15.07	20	25	0.80
20-1B	20.00	108	26	0.42
26-1A	25.22	16	52	0.31
31-1A	30.20	27	28	0.96
33-1A	32.89	89	36	2.5
34-1B-A	33.40	19	74	0.26
34-1B-B	33.45	11	78	0.14
34-1B-D	33.51	17	78	0.21
34-1B-E	33.55	391	145	2.7
34-1B-F	33.65	48	105	0.46
34-1C	34.00	20	158	0.13
35-1A	34.31	41	22	1.9
39-1A	38.22	29	21	1.4
41-1A	40.05	65	65	1.0
42-1A	41.85	2567	28	92
42-1B-B	41.95	28300	387	73
42-1B-D	41.97	9020	62	145
42-1B-F	42.01	4305	288	15
42-1B-H	42.03	166	81	2.0
42-1B-I	42.04	28	69	0.41
42-1B-K	42.05	46	110	0.42
43-1A	42.10	50	72	0.69
45-1A	44.87	152	135	1.1
47-1A	46.10	565	NA	NA
50-1A	49.83	89	34	2.6
55-1A	54.30	155	39	4.0
59-1A	58.12	263	61	4.3
60-1A	59.80	307	55	5.6
63-1A	62.92	198	42	4.7
65-1A	64.50	182	29	6.3
66-1A-A	65.93	62	37	1.7
67-1A-A	66.17	42	37	1.1
67-1A-B	66.19	94	49	1.9
67-1A-D	66.26	128	33	3.9
67-1A-E	66.27	131	32	4.1
68-1A	67.00	191	17	11.2
68-1A-A	67.03	207	22	9.4
71-1A-A	70.10	178	17	10.5
71-1B	70.60	89	31	2.9
74-1A	73.71	41	6	6.8
75-1B	74.96	24	15	1.6
77-1A	76.49	17	21	0.81
80-1A	79.80	46	21	2.2
81-1A	80.73	30	21	1.4
85-1A	84.22	37	41	0.90
90-1B	89.95	25	14	1.8
91-1A	90.74	14	22	0.64
95-1A	94.65	13	26	0.50
96-1A	96.00	22	26	0.85
101-1A	100.32	35	25	1.40
104-1A	104.00	20	90	0.22
105-1A	104.83	210	3651	0.058
106-1A	105.42	51	91	0.56
110-1A	110.00	36	43	0.84
111-1A	110.13	24	59	0.41
111-1B	111.00	14	25	0.56
112-1B	111.17	24	45	0.53
113-1B	113.00	14	25	0.56
114-1A-A	113.09	30	19	1.6
114-1A-B	114.19	31	22	1.4
114-1A-C	114.20	44	18	2.4
119-1A	118.22	42	51	0.82
121-1A	120.19	30	38	0.79
123-1A	123.00	371	74	5.0
126-1A	126.00	7	14	0.5

A variety of distributions of uranium about the redox front can be produced in such models by varying the fraction of uranium that dissolves at the front, the relative amounts of the dissolved uranium that diffuse into the oxidized and reduced rock and the positions of redeposition of the uranium. Two significant points emerge if a series of calculations of this type is performed, namely (a) if any diffusion of uranium into the oxidized rock occurs at all, then the uranium concentration in the reduced rock tends towards a saturation value beyond which it will not increase no matter how far the front moves into the reduced rock, and (b) for all conditions that generate enhanced uranium concentrations in the reduced rock there is necessarily a net depletion of uranium in the oxidized rock. An illustrative example of such a model is presented in Figure 15.

The inability of such one-dimensional models to generate uranium distributions with very high concentrations in the reduced rock close to the front and generally enhanced concentrations in the oxidized rock, as observed in the F1 drillcore, indicates that a lateral input of uranium to the section of rock being considered is required – in the case of the F1 drillcore by downward movement of uranium from the overlying rock in solution in groundwater.

The distribution of uranium in the F1 drillcore thus suggests that the long-term direction of groundwater flow at this location has been downwards, approximately parallel with the fracture system which intersects the drillcore at 50 m depth. This conclusion is inconsistent with the observed flow of water in the mine at this location at present, which is generally upwards, but is consistent with the probable direction of groundwater flow prior to mine excavations when the redox fronts were formed (Holmes *et al.*, this report series; Rep. 5).

Above 33.4 m, uranium concentrations in the F1 drillcore show irregular variations in the range 16 to 108 ppm, with an average value of 50 ppm. Thus the oxidized rocks in this depth interval show higher uranium concentrations than both the average reduced phonolite below 75 m and the oxidized phonolite above the level of the F1 drillcore (Fig. 8). The section of rock from 0 to 33.4 m depth in the drillcore must therefore be regarded as a deposition zone for uranium and, since U(VI) would be expected to show relatively soluble behaviour under the prevailing oxidizing conditions, the removal of uranium from solution will almost certainly involve scavenging by some species such as iron oxide. The observed uranium concentrations in this uppermost section of the drillcore are consistent with the above concept of the water flow having been dominantly downwards, with dissolution of uranium at the redox front and subsequent diffusion into both the oxidized and reduced rock.

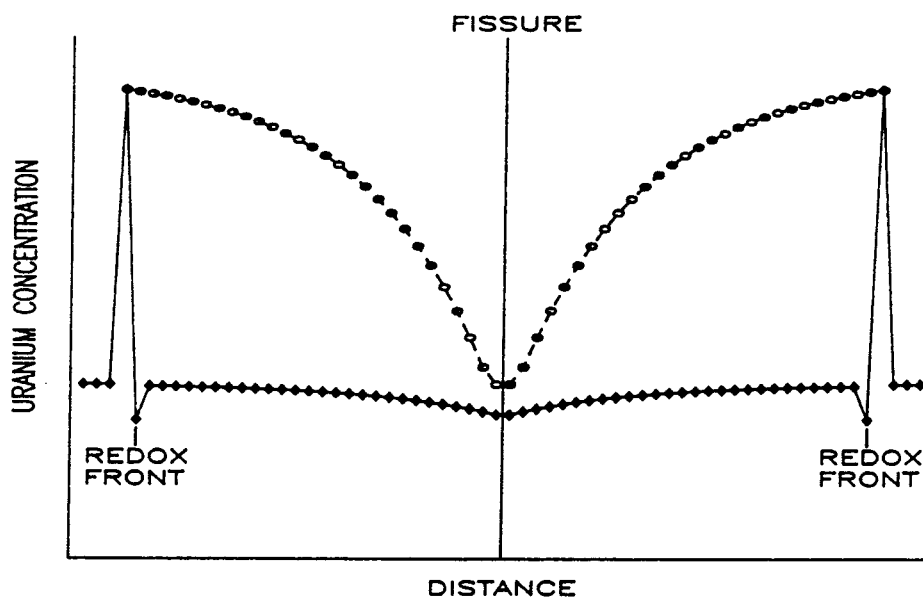


Figure 15. Example of a model uranium concentration profile generated by one-dimensional movement of oxidizing conditions away from a fissure. The figure represents a box model in which dissolution of uranium occurs at the redox front and some of the uranium moves into both the oxidized and the reduced rock. In this particular case, 20% dissolution of uranium contained in primary minerals and 100% dissolution of secondary uranium is assumed to occur. 90% of the dissolved uranium is assumed to enter the reduced rock where it is immediately deposited while 10% enters the oxidized rock and is again immediately deposited. It is assumed that there is no net loss of uranium to groundwater or gain of uranium from groundwater in the section of rock being considered. The solid diamonds represent the model uranium distribution about the fissure after 28 steps of the model, while the open ovals show the stepwise evolution of the uranium maximum in the reduced rock as the redox fronts move away from the fissure.

In the discussion of the natural decay series radionuclide specific activities and activity ratios (Table II) it is again useful to start with a consideration of the general variations in the activity ratios over the entire length of the drillcore and plots of the $^{234}\text{U}/^{238}\text{U}$, $^{230}\text{Th}/^{234}\text{U}$ and $^{226}\text{Ra}/^{230}\text{Th}$ activity ratios are shown in Figures 16 to 18.

Considering initially the $^{234}\text{U}/^{238}\text{U}$ data in Figure 16, it is apparent that all of the values for samples from the reduced rock below 75 m lie on or above unity. This is an interesting observation since the implication of these results is that ^{234}U can be effectively transported by groundwater in this section of the rock and that deposition of ^{234}U is occurring at depths as low as 110 m in the drillcore, about 44 m below the lowest redox front.

Between 75 m and 30 m, the $^{234}\text{U}/^{238}\text{U}$ activity ratio shows large and irregular variations ranging between extreme values of 0.51 and 1.23. These large variations in the $^{234}\text{U}/^{238}\text{U}$ activity ratio over the section of the core containing the redox fronts reveal that the processes of uranium dissolution, transport and redeposition implied by the variations in the concentration profile have been actively operating within the last 10^6 years. A detailed discussion of the $^{234}\text{U}/^{238}\text{U}$ activity ratio variations in this section of the core is given below.

In the section of the core above 30 m, the $^{234}\text{U}/^{238}\text{U}$ activity ratio shows a systematic decrease from a value of 1.10 at sample 26-1A to 1.01 at sample 6-1A. These results suggest that recent (on a 10^6 a timescale) deposition of uranium has occurred in this section of oxidized rock, consistent with the conclusion derived above in consideration of the uranium concentration data.

Considering next the $^{230}\text{Th}/^{234}\text{U}$ data plotted in Figure 17, it can be seen that all of the values for samples in the reduced rock below 75 m lie on or above unity. The values of 1.35 for sample 101-1A and 1.12 for sample 121-1A are particularly significant since they indicate a substantial loss of ^{234}U relative to ^{230}Th from this section of the rock. This observation confirms the conclusion derived from the $^{234}\text{U}/^{238}\text{U}$ data that ^{234}U must be capable of being transported by groundwater within the reduced rock. Alpha recoil effects can be invoked as a mechanism enhancing the rate of transfer of ^{234}U from the solid phase to solution, but it should be noted that such effects will apply equally to ^{230}Th . Thus any ^{230}Th ejected into solution in this way must rapidly return to the solid phase, whereas the ^{234}U must remain in solution in order to generate the observed $^{230}\text{Th}/^{234}\text{U}$ activity ratios. It can therefore be concluded either that ^{234}U enters solution in the 6+ oxidation state as a consequence of oxidation during alpha decay and remains oxidized for a sufficient length of time to be moved out of this section of rock by groundwater transport (although this seems unlikely on the basis of the apparently high efficiency of

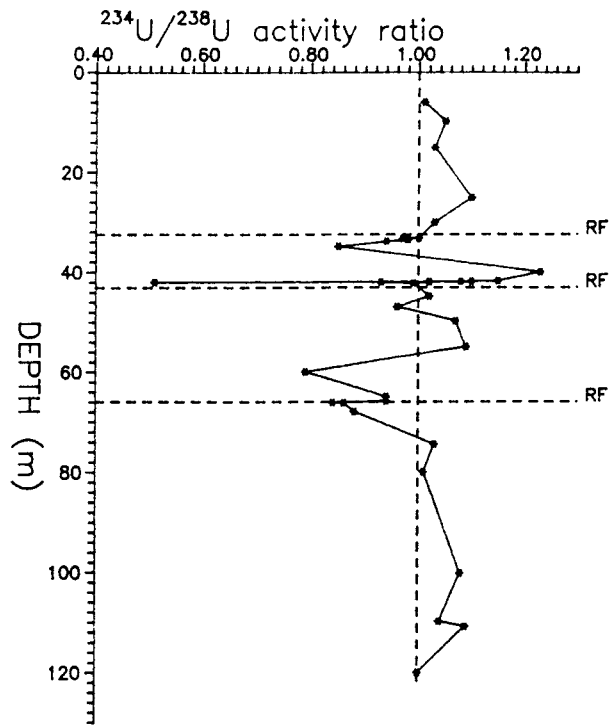


Figure 16. $^{234}\text{U}/^{238}\text{U}$ activity ratios as a function of depth for samples from the F1 drillcore.

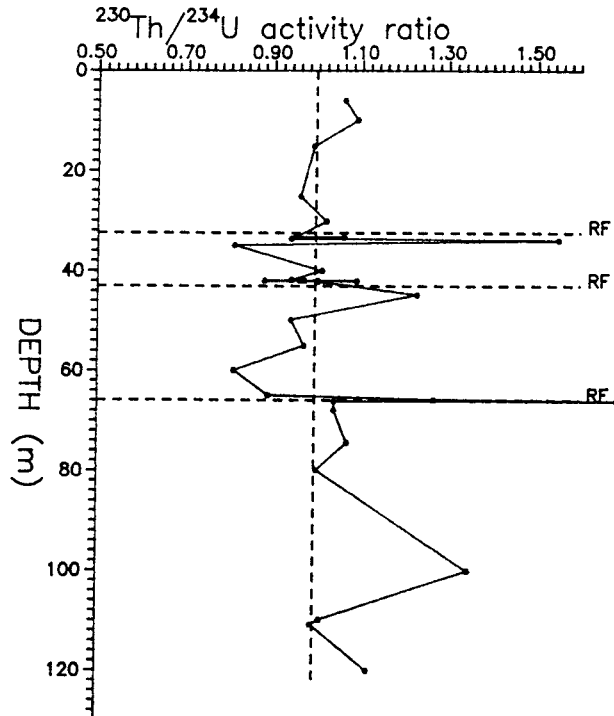


Figure 17. $^{230}\text{Th}/^{234}\text{U}$ activity ratios as a function of depth for samples from the F1 drillcore.

reduction of uranium in the reduced rock at each of the redox fronts), or else that U(IV) is capable of being transported over significant distances by groundwater within the reduced phonolite. It should be noted that the combinations of $^{234}\text{U}/^{238}\text{U}$ and $^{230}\text{Th}/^{234}\text{U}$ activity ratios observed for this section of the core can only be produced by the onset of a sudden process or by operation of a complex process involving deposition followed by removal.

As with the $^{234}\text{U}/^{238}\text{U}$ activity ratio, the $^{230}\text{Th}/^{234}\text{U}$ activity ratio shows major deviations from equilibrium in the section of the core from 70 to 30 m, with values varying irregularly from 0.88 to 1.69. These deviations from equilibrium in the $^{230}\text{Th}/^{234}\text{U}$ activity ratio imply that dissolution, transport and deposition processes affecting uranium have been operating within the last 3×10^5 years.

Above 30 m, the $^{230}\text{Th}/^{234}\text{U}$ activity ratios of samples from the oxidized phonolite lie close to or slightly above unity and there is no obvious trend in the results. It can, however, be noted that, if these samples have at some time experienced uranium deposition, then subsequently sufficient time has elapsed to allow ^{230}Th to grow in to equilibrium.

The $^{226}\text{Ra}/^{230}\text{Th}$ activity ratios (Fig. 18) for samples from the reduced phonolite below 75 m are generally less than unity, indicating a net loss of ^{226}Ra from this section of the rock, although sample 110-1A lying in a conductive zone is an exception to this general behaviour. Once again, large deviations from equilibrium are observed across the section of the core containing the redox fronts, with values of the $^{226}\text{Ra}/^{230}\text{Th}$ activity ratio varying from 0.51 to 9.20. These results clearly indicate that groundwater processes are capable of significant transport of ^{226}Ra within a timescale of the order of 10^3 years.

Above 30 m, the $^{226}\text{Ra}/^{230}\text{Th}$ activity ratio exhibits a marked decrease from a value of 3.90 for sample 26-1A to less than unity for samples 10-1A and 6-1A.

The natural decay series activity ratio data therefore demonstrate that dissolution, transport and deposition processes have affected uranium and radium, both in the vicinity of the redox fronts and in other sections of the drillcore. Further information concerning the rates and mechanisms of the processes involved can be derived by more detailed consideration of the results and the following section provides a discussion of the data for the various sections of the core working downwards from the surface.

The results for samples 6-1A, 10-1A, 16-1A and 26-1A from the oxidized phonolite are plotted on a $^{234}\text{U}/^{238}\text{U}$ versus $^{230}\text{Th}/^{238}\text{U}$ diagram in Figure 19 from which it can be seen that 16-1A and 26-1A lie on the uranium deposition sector of the graph while 6-1A and 10-1A lie in the complex process zone. If the redox front is assumed to have moved downwards through this section of rock in response to groundwater movement and

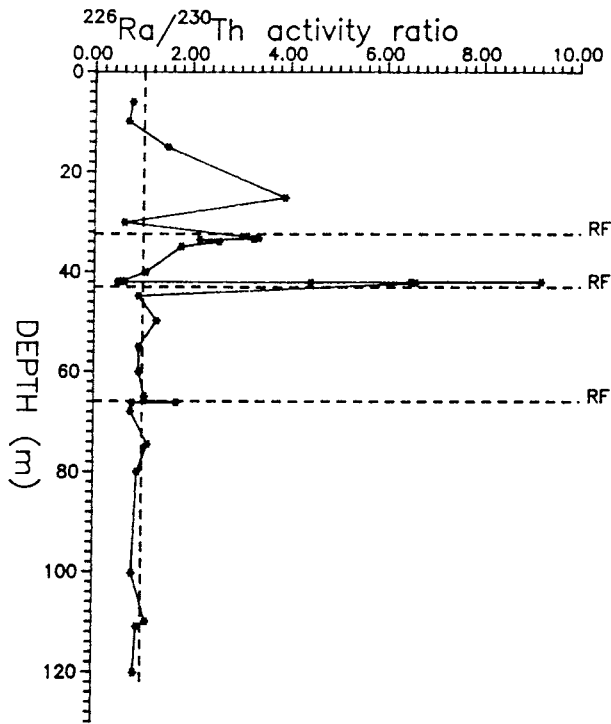


Figure 18. $^{226}\text{Ra}/^{230}\text{Th}$ activity ratios as a function of depth for samples from the F1 drillcore.

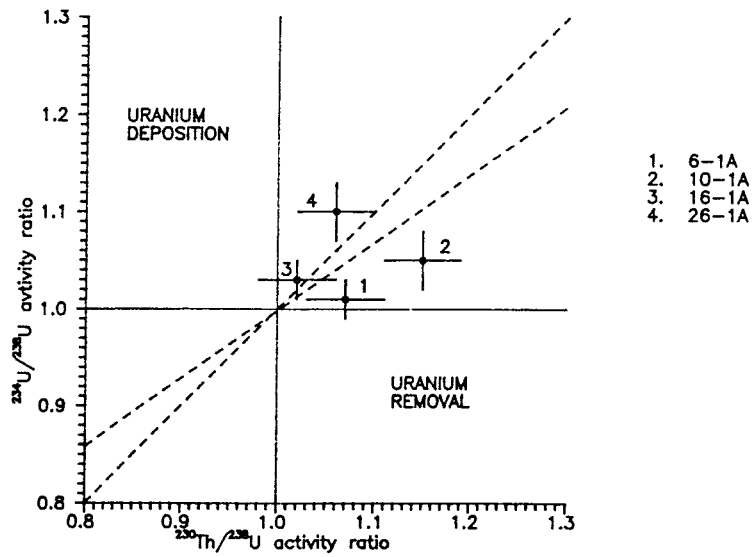


Figure 19. $^{234}\text{U}/^{238}\text{U}$ activity ratio versus $^{230}\text{Th}/^{238}\text{U}$ activity ratio diagram for samples from the oxidized rock in the F1 drillcore above the 33.4 m redox front.

erosion of the land surface (Holmes *et al.*, this report series; Rep. 5) then the influence of the redox front processes would have affected sample 26-1A more recently than sample 16-1A, and the position of these two samples on the activity ratio plot is consistent with this, with 16-1A lying closer to equilibrium than 26-1A. As noted above, the $^{234}\text{U}/^{238}\text{U}$ activity ratio decreases from a value of 1.10 at 25.22 m to reach equilibrium at 6.0 m. If the simplest possible approach is taken then it could be assumed that this decrease in the $^{234}\text{U}/^{238}\text{U}$ activity ratio represents the return to equilibrium of the $^{234}\text{U}/^{238}\text{U}$ system via decay of excess ^{234}U which had been deposited as a consequence of the movement of the redox front through the rock. Thus, if it is assumed that the excess ^{234}U would have decayed to non-detectable levels in the course of four half-lives, the observed decrease in $^{234}\text{U}/^{238}\text{U}$ activity ratio would suggest a rate of downward movement of the redox front of the order of 20 m in 10^6 years. Considerable caution must be employed in assessing the confidence which can be placed in this conclusion since it is evident from the uranium concentration versus depth plot (Fig. 9) and from Figure 19 that, subsequent to the passage of the redox front, further processes have started to act upon samples 6-1A and 10-1A.

The processes operating appear to be complicated since the higher concentrations observed for samples 6-1A and 10-1A than for 16-1A and 26-1A would suggest that the upper samples had experienced uranium deposition (Fig. 9). In contrast, the relative positions of the samples in Figure 19 suggest that samples 6-1A and 10-1A have experienced uranium loss relative to samples 16-1A and 26-1A. This apparently complicated situation is consistent with the observation that samples 6-1A and 10-1A lie in the upper complex process sector in Figure 19. Thus the decrease in the $^{234}\text{U}/^{238}\text{U}$ activity ratio between 25 m and 6 m almost certainly does not represent a simple decay of excess ^{234}U .

The $^{226}\text{Ra}/^{230}\text{Th}$ activity ratio decreases from a value of 3.90 at sample 26-1A to 1.49 at sample 16-1A and, if this was taken to represent a closed system return towards equilibrium following perturbation by passage of the redox front, then an even greater rate of downward movement of the redox front of the order of 1 m in 10^3 years would be derived. The fact that the $^{226}\text{Ra}/^{230}\text{Th}$ activity ratio decreases to values of 0.70 and 0.68 for samples 6-1A and 10-1A argues that it is of dubious validity to assume closed conditions for ^{226}Ra in this rock, and casts severe doubt upon this very high value for the rate of movement of the front.

As outlined above, and as shown in Figure 12, the uranium concentration in the section of the core containing the redox front at 33.4 m exhibits a minimum at the redox front itself, with a sharp maximum just inside the reduced rock at 33.5 m, along with a smaller

peak in the overlying oxidized rock. Not all of the samples from this section were analyzed for natural decay series radionuclides and, notably, sample 34-1B-E with the uranium maximum at 33.55 m was not included in the natural decay series analyses. However, the available $^{234}\text{U}/^{238}\text{U}$, $^{230}\text{Th}/^{234}\text{U}$ and $^{226}\text{Ra}/^{230}\text{Th}$ activity ratio results are plotted in Figures 20 to 22.

The $^{234}\text{U}/^{238}\text{U}$ activity ratios for samples close to the redox front all lie close to unity, indicating that any removal of uranium from this section of the rock must be occurring at a sufficiently rapid rate to prevent the development of $^{234}\text{U}/^{238}\text{U}$ disequilibrium, i.e. bulk dissolution is much faster than the rate of preferential recoil loss of ^{234}U . On the reduced side of the front, the $^{234}\text{U}/^{238}\text{U}$ values show a systematic decrease to a minimum of 0.85 for sample 35-1A at a depth of 34.31 m. This indicates that the rate of preferential recoil loss of ^{234}U systematically increases relative to the rate of bulk dissolution of uranium on moving into the reduced section of the rock, consistent with the expected low solubility of U(IV) in this regime. The $^{234}\text{U}/^{238}\text{U}$ data do, however, require that ^{234}U lost from sections of the rock up to 1 m from the redox front remains in solution in the groundwater for a sufficient length of time to allow for its removal from this section of the rock. The $^{234}\text{U}/^{238}\text{U}$ activity ratio increases again on moving deeper into the reduced rock to a value of 1.23 at sample 41-1A. This may represent redeposition of ^{234}U removed from the section of rock just below the 33.4 m redox front (consistent with downward flow of water) or could be the influence of the uranium mineralization associated with the deeper redox front at 42.0 m.

In the oxidized rock above the 33.4 m redox front, sample 33-1A, which has the highest uranium concentration in this section of the rock, exhibits a $^{234}\text{U}/^{238}\text{U}$ activity ratio close to unity. This indicates that the leaching process which generated the uranium now deposited at this depth either was a rapid process in which there was insufficient time for ^{234}U preferential loss to occur or else took place at least about 7×10^5 years ago in order to allow re-equilibration of ^{234}U with ^{238}U . The latter possibility appears unlikely in view of the radioactive disequilibrium apparent in samples from other positions both above and below this depth, so the observed $^{234}\text{U}/^{238}\text{U}$ ratio for sample 33-1A probably indicates the operation of rapid dissolution and deposition processes associated with the 33.4 m redox front. The higher $^{234}\text{U}/^{238}\text{U}$ activity ratio of 1.10 observed for sample 26-1A is indicative of uranium deposition and suggests that the uranium deposited may have been derived from a more slowly dissolving source than that deposited at sample 33-1A, i.e. this observation again argues for a significant lateral movement of uranium relative to the drillcore.

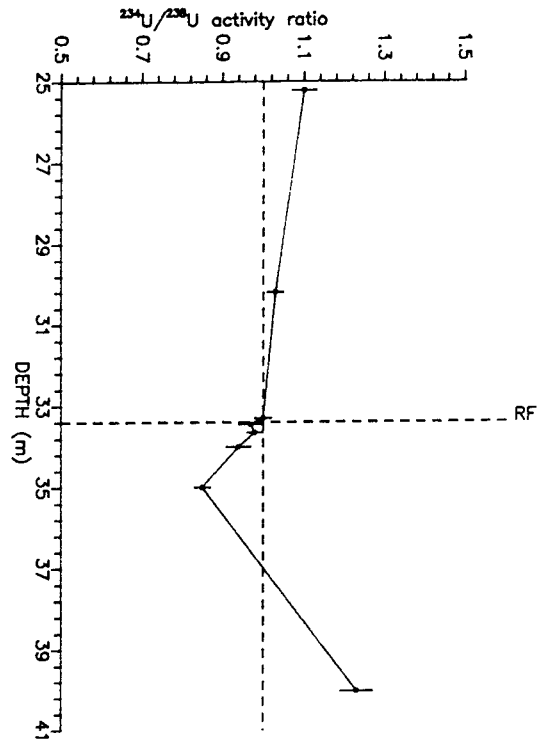


Figure 20. $^{234}\text{U}/^{238}\text{U}$ activity ratio profile across the 33.4 m redox front in the F1 drillcore.

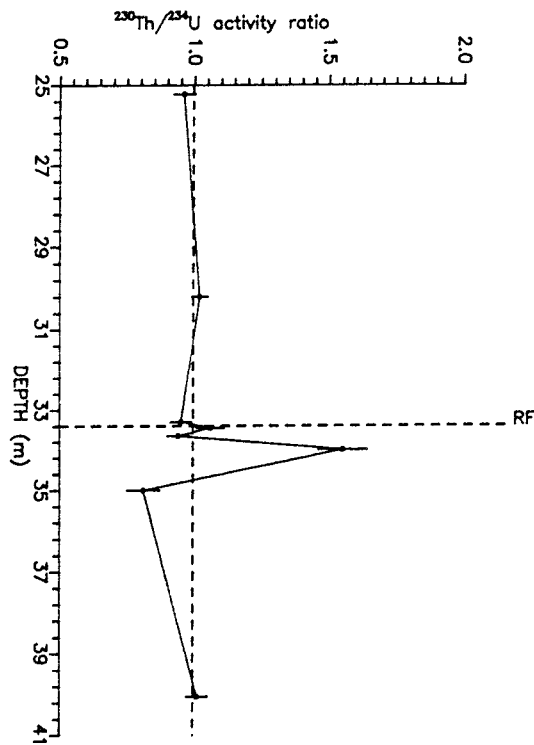


Figure 21. $^{230}\text{Th}/^{234}\text{U}$ activity ratio profile across the 33.4 m redox front in the F1 drillcore.

The $^{230}\text{Th}/^{234}\text{U}$ activity ratios (Fig. 21) for samples from 25.22 m down to 33.65 m on the oxidized side of the 33.4 m redox front all lie within the limits of the analytical uncertainty of equilibrium. Thus if the maximum in uranium concentration at 32.89 m is taken to represent a location of uranium deposition, then the uranium was deposited here at least about 3×10^5 years ago, from which an estimated maximum rate of downward movement of the redox front of the order of 2 m in 10^6 years can be derived.

The $^{230}\text{Th}/^{234}\text{U}$ activity ratio below the redox front increases to 1.55 at sample 34-1C, suggesting that removal of uranium has occurred at this depth, but falls to 0.81 on moving deeper to sample 35-1A, suggesting uranium deposition here. Both of these samples occur at greater depth than the uranium maximum observed at 33.55 m (sample 34-1B-E) on the reduced side of the redox front. Thus, while the uranium concentration profile indicates that uranium dissolved at the redox front is very efficiently deposited as soon as it enters the reduced rock, the $^{230}\text{Th}/^{234}\text{U}$ data suggest that significant dissolution and redeposition processes are acting upon uranium at depths of up to 1 m into the reduced rock. Thus the influence of the redox front could be taken to extend over a distance of 1 m or more and the pronounced disequilibrium between ^{230}Th and ^{234}U would suggest that, if this is the case, then the rate of movement of the front on a scale of 1 m is rapid relative to the 7.5×10^4 a half-life of ^{230}Th .

The $^{226}\text{Ra}/^{230}\text{Th}$ data (Fig. 22) also indicate that the influence of the redox front extends over several metres and that the processes involved are more complex than a simple redox-controlled flux of selected elements across the redox front. Thus the $^{226}\text{Ra}/^{230}\text{Th}$ ratio shows a minimum value of 0.61 at sample 33-1A revealing significant loss of ^{226}Ra at this depth. Deposition of ^{226}Ra is, however, apparent in both the overlying rock at 25.22 m and at the 33.4 m redox front where a value of 3.36 is observed for sample 34-1B-A, after which the ratio gradually decreases with increasing depth in the reduced rock, with sample 41-1A having a value close to equilibrium.

In summary, therefore, the radionuclide activity ratios over this section of the drillcore indicate that dissolution and redeposition effects influence uranium and radium over a relatively wide range of about 10 m across the redox front, that ^{234}U is mobile within the reduced rock and that the processes involved are rapid and complex. The results would be consistent with a downward movement of the front at this location at a rate between 2 and 20 m per 10^6 years.

The $^{234}\text{U}/^{238}\text{U}$ versus $^{230}\text{Th}/^{238}\text{U}$ diagram for the samples in the vicinity of the 33.4 m redox front is shown in Figure 23 and presents a concise summary of the preceding discussion. The samples close to the redox front (33-1A to 34-1BF) all lie close to the (1,1) position, indicating the operation of recent, rapid processes or processes which

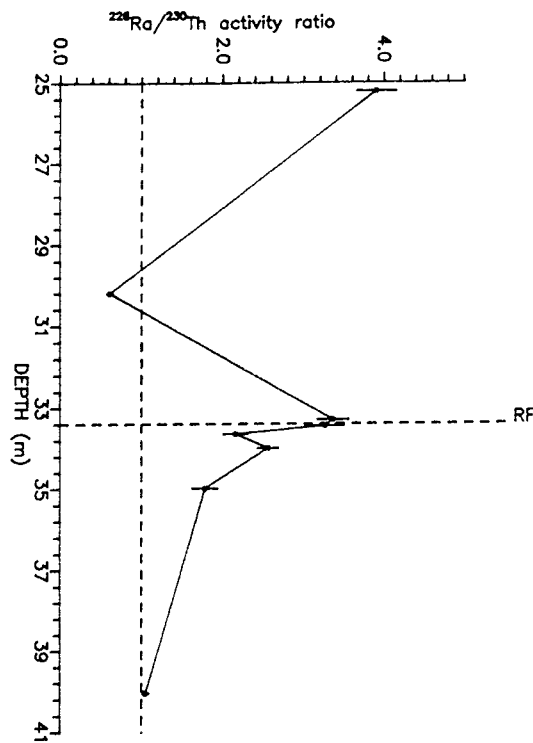


Figure 22. $^{226}\text{Ra}/^{230}\text{Th}$ activity ratio profile across the 33.4 m redox front in the F1 drillcore.

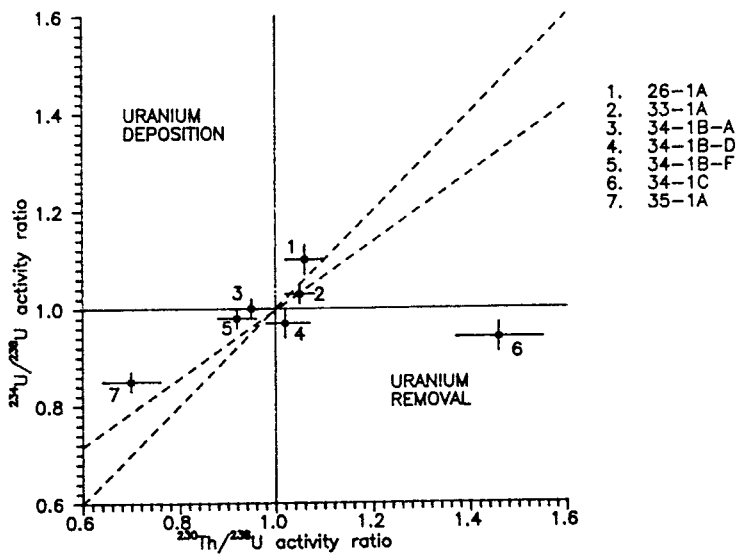


Figure 23. $^{234}\text{U}/^{238}\text{U}$ activity ratio versus $^{230}\text{Th}/^{238}\text{U}$ activity ratio diagram for samples from the vicinity of the 33.4 m redox front in the F1 drillcore.

took place a long time ago relative to the ^{234}U and ^{230}Th half-lives. Sample 26-1A lies further away from the equilibrium position in the uranium deposition sector whereas, on the reduced side of the front, sample 34-1C lies in the uranium removal area and sample 35-1A lies in the complex process sector.

Considering next the transect of samples across the redox front at 42.0 m, it is immediately apparent that the uranium concentration (Fig. 13) shows a very similar distribution about the redox front to that observed at the 33.4 m redox front (Fig. 12), despite the different orientations of the two fronts. The uranium concentrations are, however, very much higher at the 42.0 m redox front, with a maximum of 2.83% at sample 42-1B-B lying just inside the reduced rock (Fig. 7) and a broader peak of lower magnitude in the oxidized rock with a maximum concentration in this case of 565 ppm at sample 47-1A.

The $^{234}\text{U}/^{238}\text{U}$ data for these samples are plotted in Figure 24, from which it can be seen that the samples in the area of the reduced rock containing the uranium mineralization all have $^{234}\text{U}/^{238}\text{U}$ activity ratios greater than unity. There is a systematic increase in the activity ratio moving into the reduced rock from sample 42-1B-F with a value of 1.01 to sample 41-1A with a value of 1.23 and a number of interesting implications follow from those results.

Firstly, it is clear that the uranium at the mineralization has been deposited on a timescale that is recent relative to the 2.45×10^5 a half-life of ^{234}U . Secondly, if the degree of disequilibrium is taken to represent how recently the uranium was deposited, then the results indicate that the uranium closest to the front was deposited before the uranium further from the front. This would be consistent with a movement of the front from the oxidized rock into the reduced rock, but the fact that the sample 42-1B-D has a $^{234}\text{U}/^{238}\text{U}$ activity ratio of 1.10 while sample 42-1B-F, which lies only 4 cm closer to the front, has an activity ratio within error of equilibrium suggests that the front is moving extremely slowly. Finally, the observation of a $^{234}\text{U}/^{238}\text{U}$ activity ratio of 1.23 for sample 41-1A, which lies at a distance of 2 m from the redox front, provides further evidence that significant movement of ^{234}U (and, in this case, almost certainly ^{238}U also) can take place within the reduced rock. Thus, while the uranium concentration profile suggests that uranium is highly efficiently deposited immediately inside the reduced section of rock, the uranium isotope activity results indicate some degree of uranium mobility to distances of up to 2 m into the reduced rock.

On moving a distance of 2 cm towards the redox front from sample 42-1B-F, the $^{234}\text{U}/^{238}\text{U}$ activity ratio decreases from 1.02 to the extremely low value of 0.51 for sample 42-1B-H, which lies just on the reduced side of the front. A value of 0.51 for the $^{234}\text{U}/^{238}\text{U}$

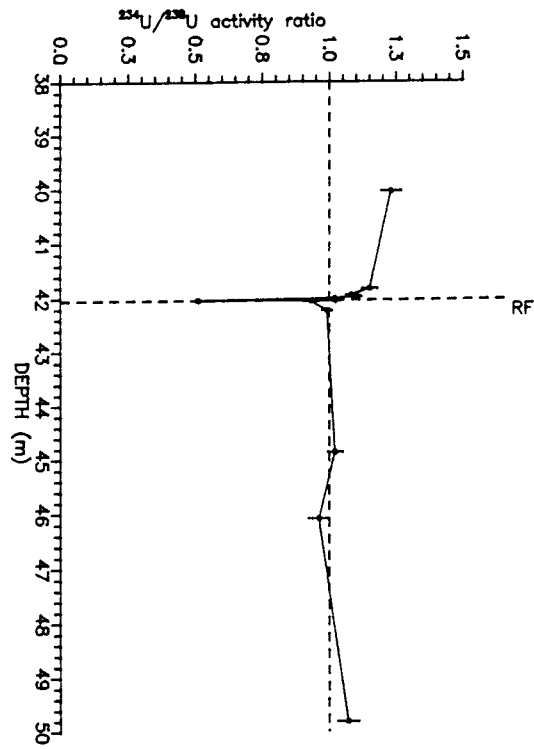


Figure 24. $^{234}\text{U}/^{238}\text{U}$ activity ratio profile across the 42.0 m redox front in the F1 drillcore.

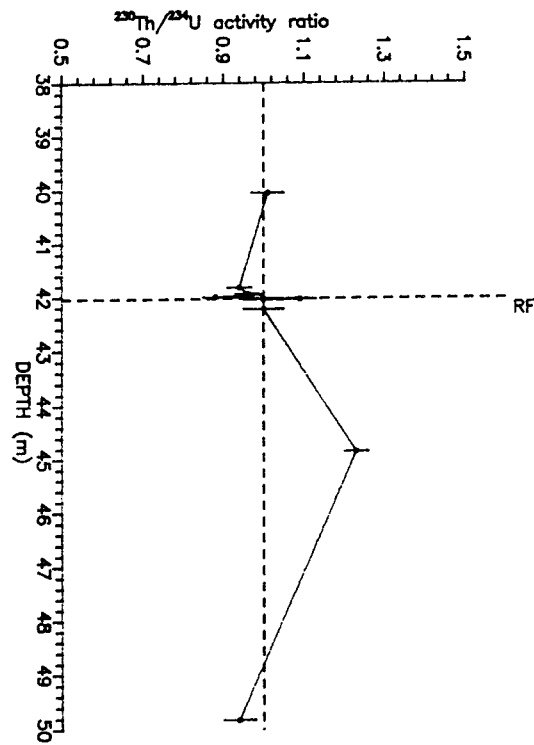


Figure 25. $^{230}\text{Th}/^{234}\text{U}$ activity ratio profile across the 42.0 m redox front in the F1 drillcore.

activity ratio is very unusual and, in order to develop and maintain such a ratio, it may be postulated that effectively half of the ^{234}U atoms being produced by the decay of ^{238}U are being preferentially lost to the aqueous phase. It therefore follows that the uranium must be present at this location either as a thin coating on the surfaces of the mineral grains or else must be located in the outermost layers of minerals since the preferential recoil loss of ^{234}U is only effective to a depth of about 100 μm in a mineral. This ratio value, moreover, indicates that the rate of bulk dissolution of uranium must be low (consistent with the position of the sample on the reduced side of the front) relative to the rate of preferential recoil loss of ^{234}U , but the ^{234}U atoms ejected must clearly remain in solution for a sufficient length of time to ensure their total removal from this section of the rock. Highly specific conditions must therefore affect sample 42-1B-H which do not apply to samples on either side of it at distances of 1-2 cm in either the reduced or the oxidized rock, since these samples have, within error, an equilibrium value for the $^{234}\text{U}/^{238}\text{U}$ activity ratio. It is also highly significant that a time of the order of 7×10^5 years is required to develop this degree of disequilibrium between ^{234}U and ^{238}U . In this context it should be noted that this time constraint is still valid even if the uranium is present as a very thin layer deposited on the surfaces of minerals since, upon deposition, the ^{234}U and ^{238}U are chemically identical and will not be subject to fractionation. Only upon replacement of the original population of ^{234}U atoms by a new population of in situ produced atoms in the deposit would there be potential for development of such a low $^{234}\text{U}/^{238}\text{U}$ activity ratio and this would take at least 7×10^5 years.

The analytical results therefore indicate that the conditions affecting sample 42-1B-H have operated for a time of at least 7×10^5 years during which they have not influenced samples only 1-2 cm away, i.e. the system has been effectively static for this time. Thus if the observed $^{234}\text{U}/^{238}\text{U}$ disequilibrium in this section of the core is accepted as being related to redox front processes then the implication is that, at this location, the redox front has moved a negligible distance on a cm scale over a period of 7×10^5 years.

On the oxidized side of the 42.0 m redox front, the $^{234}\text{U}/^{238}\text{U}$ activity ratios show small variations about the equilibrium value, suggesting that any uranium dissolution or deposition processes in this section of rock occur at a rapid rate relative to recoil loss of ^{234}U . It is also notable that there is no general depletion of ^{234}U relative to ^{238}U on the oxidized side of the front, indicating that the uranium deposited in the overlying mineralization has almost certainly not been simply transported across the redox front. The fact that the excess ^{234}U present in the mineralization on the reduced side of the 42.0 m redox front cannot be balanced by supply from sample 42-1B-H, or from samples on

the oxidized side of the front, demonstrates even more clearly that an input of uranium in a lateral sense to the core must have occurred.

The $^{230}\text{Th}/^{234}\text{U}$ data for samples from the vicinity of the 42.0 m redox front are shown in Figure 25, from which it can be seen that there is a slight deficiency of ^{230}Th relative to ^{234}U over the uranium mineralization area on the reduced side of the front, with values varying from 0.88 to 1.01. The fact that ^{230}Th , although still deficient, is approaching equilibrium with ^{234}U means that at least several ^{230}Th half-lives have elapsed since the start of uranium deposition at this point. Significantly, sample 42-1B-H (which has the $^{234}\text{U}/^{238}\text{U}$ activity ratio of 0.51) has a $^{230}\text{Th}/^{234}\text{U}$ ratio of 1.0, confirming that the processes resulting in selective removal of ^{234}U from this sample have been operating for at least some 3×10^5 years. On the oxidized side of the front, only sample 45-1A shows any significant deviation of the $^{230}\text{Th}/^{234}\text{U}$ activity ratio from equilibrium with a value of 1.23, suggestive of uranium removal at this point on a timescale recent with respect to the ^{230}Th half-life of 7.54×10^4 years. The $^{234}\text{U}/^{238}\text{U}$ activity ratio for sample 45-1A is within error of equilibrium indicating that the process taking place could be long-term removal of uranium, now approaching a steady state. If this is assumed, then a uranium removal probability of $1.7 \times 10^{-6} \text{a}^{-1}$ can be derived on the basis of the arguments advanced in section 1.2. Similarly, if long-term removal of ^{226}Ra is assumed to have occurred then a removal probability of $4.5 \times 10^{-5} \text{a}^{-1}$ can be calculated for ^{226}Ra . The implied removal of uranium on the basis of the $^{230}\text{Th}/^{234}\text{U}$ activity ratios contrasts with the apparent deposition of uranium at this location on the basis of the uranium concentration trend (Fig. 13) suggesting that complex processes may be operating within this section of the oxidized rock.

The $^{226}\text{Ra}/^{230}\text{Th}$ results for the transect across the 42.0 m redox front, which are plotted in Figure 26, show pronounced deviations from equilibrium, with a systematic pattern of ^{226}Ra depletion on the reduced side of the front and ^{226}Ra excess on the oxidized side. Thus the samples 42-1A to 42-1B-F have $^{226}\text{Ra}/^{230}\text{Th}$ activity ratios in the range 0.48 to 0.57, meaning that approximately half the ^{226}Ra atoms being produced by decay of ^{230}Th are being lost to the aqueous phase, again arguing for a very high porosity of the rock or for the natural decay series radionuclides being contained in very thin surface deposits in this area. The $^{226}\text{Ra}/^{230}\text{Th}$ activity ratio increases abruptly from 0.51 at sample 42-1B-F to 4.43 for sample 42-1B-H just on the reduced side of the front, and the excess of ^{226}Ra is maintained in samples 42-1B-I to 43-1A on the oxidized side of the front with values in the range 6.5 – 9.2. The observed $^{226}\text{Ra}/^{230}\text{Th}$ results strongly suggest dissolution of ^{226}Ra from the reduced rock followed by downward transport across the redox front and redeposition on the oxidized side. This apparent flux of radium is in the opposite direction to both the apparent direction of the main uranium flux involved in the

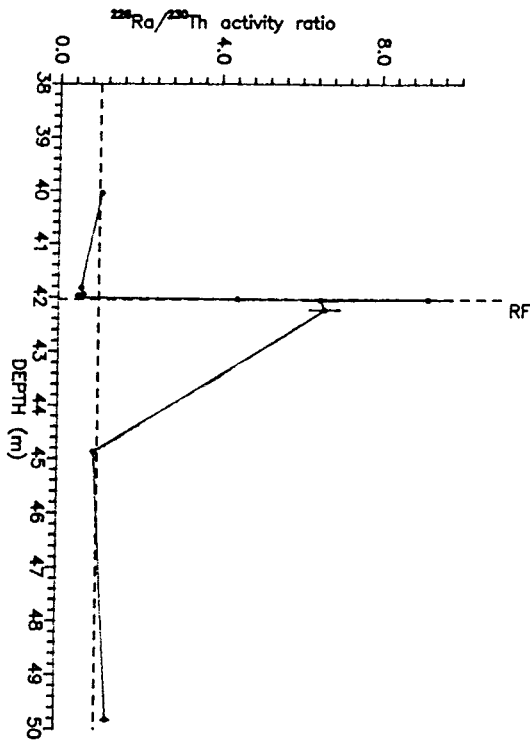


Figure 26. $^{226}\text{Ra}/^{230}\text{Th}$ activity ratio profile across the 42.0 m redox front in the F1 drillcore.

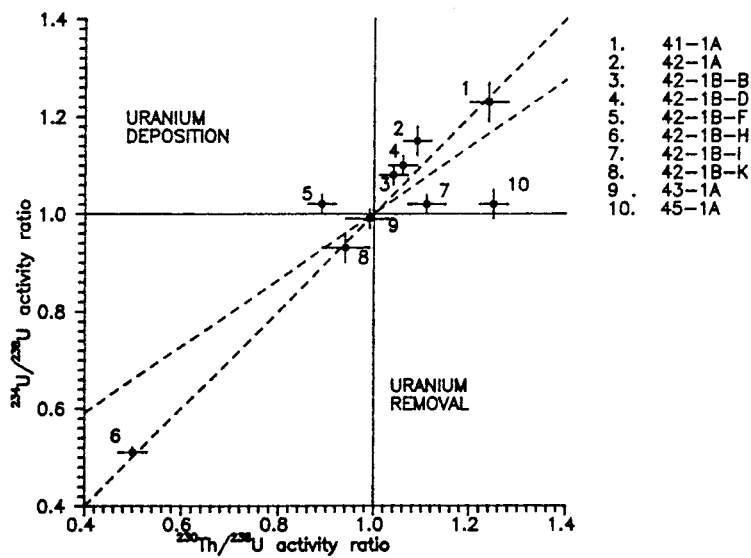


Figure 27. $^{234}\text{U}/^{238}\text{U}$ activity ratio versus $^{230}\text{Th}/^{238}\text{U}$ activity ratio diagram for samples from the vicinity of the 42.0 m redox front in the F1 drillcore.

mineralization and the proposed present-day direction of groundwater flow. The ^{226}Ra data therefore provide further support for the argument that, in the longer term, there has been no major advective movement of groundwater across the redox front, and that the flux of uranium and radium across the front can be more readily explained by diffusive transport driven by concentration gradients which develop in the groundwater at or near the redox front.

In the reduced rock, ^{226}Ra clearly demonstrates a mobility (with alpha recoil enhanced ejection into the aqueous phase) compatible with transport over about 20 cm in a time that is short relative to its 1.6×10^3 year half-life. In contrast, ^{226}Ra is highly efficiently retarded within the first few cm of the oxidized rock. Since radium itself is clearly not directly subject to redox reactions, existing only in the 2+ oxidation state, the observed differences in behaviour of radium across the front must be controlled by other processes. The sulphide-sulphate system is one possible controlling mechanism, with radium being readily soluble in the sulphide-dominated system in the reduced rock but being subject to removal from the aqueous phase by coprecipitation in species such as BaSO_4 on the sulphate-dominated oxidized side of the front. An alternative mechanism for radium removal in the oxidized sector could be scavenging by iron or manganese oxides.

The $^{234}\text{U}/^{238}\text{U}$ versus $^{230}\text{Th}/^{238}\text{U}$ diagram for the samples from the vicinity of the 42.0 m redox front is shown in Figure 27. It is immediately apparent from Figure 27 that five of the six samples from the reduced rock lie in the uranium deposition sector, with the only exception being sample 42-1B-H which lies just on the reduced side of the front (Fig. 7). Samples 41-1A, 42-1A, 42-1B-B and 42-1B-D lie in a part of the graph which suggests that these samples have been subject to deposition of uranium over a timescale of the order of 7×10^5 a and that the deposition process has started to influence sample 41-1A more recently than sample 42-1A, which in turn started to experience deposition more recently than samples 42-1B-B and 42-1B-D. The distribution of these samples in this diagram is thus consistent with their positions in the reduced rock, with their high uranium concentrations and with the concept of the very slow movement (on a cm scale) of the front into the reduced rock.

Sample 42-1B-F, from a position in the reduced rock closer to the front than the above samples, also lies in the uranium deposition section of the graph but in a different position from the other reduced samples, in this case indicative of more recent, near-equilibrium deposition of uranium. The last sample in the reduced rock, 42-1B-H, is located immediately at the front and plots in an entirely different position in the graph from all the other reduced samples, being located in the uranium removal sector far removed

from the (1,1) equilibrium position and at a point corresponding to a combination of activity ratios which would take in the order of 7×10^5 years to evolve.

These extreme differences in position of the reduced samples in Figure 27, in conjunction with the implied timescales for the processes affecting them and the small distances (on a cm scale) between them, provide strong support for the concept of a very slow rate of movement of the front at this position.

The four oxidized samples all lie in (or within error of) the uranium removal sector. Sample 42-1B-I lies just inside the upper complex process sector, but within the limits of the analytical uncertainty could be taken to represent recent, near-equilibrium removal of uranium from this position. Sample 42-1B-K is located at a point in the diagram consistent with long-term (on a 7×10^5 a timescale) removal of uranium, while sample 43-1A lies close to the (1,1) position in the uranium removal sector, suggesting deposition of uranium at some time in the past sufficient to have allowed the system to revert almost to equilibrium. Finally, sample 45-1A, like sample 42-1B-I, is located in the upper complex process area close to the $^{234}\text{U}/^{238}\text{U} = 1$ line, possibly indicating near-equilibrium removal of uranium.

Presentation of the data for the 42.0 m redox front in this way thus clearly demonstrates the compatibility of the analytical data with the expected geochemical behaviour of uranium and thorium and with the previous discussion based upon concentration and activity ratio trends by (a) confirming the general removal of uranium from the oxidized rock and deposition of uranium in the reduced rock, (b) showing positions for the samples in the graph which are consistent with their locations in the rock relative to the redox front, (c) indicating a slow rate of movement of the front into the reduced rock and (d) revealing a striking similarity between the sample data points and the lines describing the theoretical evolution of $^{234}\text{U}/^{238}\text{U}$ and $^{230}\text{Th}/^{238}\text{U}$ activity ratios described above.

The $^{231}\text{Pa}/^{235}\text{U}$ data for the 42 m redox front (Table II) are also consistent with the transfer of uranium from the oxidized to the reduced rock (on the assumption that U(VI) will exhibit a substantially greater solubility than Pa(V)). Thus the $^{231}\text{Pa}/^{235}\text{U}$ activity ratios for all the reduced samples are within error of equilibrium, confirming that the deposited uranium at this location is old relative to the 3.28×10^4 year half-life of ^{231}Pa . On the oxidized side of the front the $^{231}\text{Pa}/^{235}\text{U}$ ratio increases sharply to 2.84 at sample 42-1B-I but falls again to 1.13 by sample 42-1B-K and has returned to equilibrium by sample 43-1A. These results therefore confirm the loss of uranium relative to protactinium from the oxidized rock and the return of the $^{231}\text{Pa}/^{235}\text{U}$ ratio to equilibrium over a distance of

less than 5 cm again suggests a slow rate of movement of the front (of the order of centimetres in 10^5 a at most).

The uranium concentration profile across the 66.2 m redox front has, like the two higher redox fronts, a minimum at the front itself and distinct maxima in both the oxidized and reduced rock on each side of the front (Fig. 14). The peaks in the uranium distribution are, however, much broader for the 66.2 m redox front than for the other two (Figs. 12 and 13), particularly on the reduced side of the front. The $^{234}\text{U}/^{238}\text{U}$ activity ratios for samples in the vicinity of the 66.2 m redox front are plotted in Figure 28, which reveals a broad minimum, with all of the samples from 60-1A to 68-1A-A having ratios of less than unity. Samples 50-1A and 55-1A lying in the oxidized rock well away from the front have $^{234}\text{U}/^{238}\text{U}$ ratios greater than unity while sample 75-1A, 8 metres below the redox front in the reduced rock, has a $^{234}\text{U}/^{238}\text{U}$ ratio within error of equilibrium. Thus, in addition to the distribution of uranium about the 66.2 m redox front being much broader than for the other two fronts, the isotopic disequilibrium exhibited by uranium extends over a greater distance at the 66.2 m redox front. This persistence of radioactive disequilibrium between ^{234}U and ^{238}U over a distance of at least 8 m around the redox front could be used as an argument for an estimate of the downward rate of movement of the redox front of the order of 10 m in 10^6 a. This would, however, require the assumption of closed conditions for the uranium in this section of rock after the initial $^{234}\text{U}/^{238}\text{U}$ disequilibrium had been established and the detailed structure of the $^{234}\text{U}/^{238}\text{U}$ activity ratio plot, in conjunction with the uranium concentration profile, indicates that this assumption is not likely to be valid. Comparison of these two plots reveals a qualitatively inverse relationship between the uranium concentration and the $^{234}\text{U}/^{238}\text{U}$ activity ratio, with the lower $^{234}\text{U}/^{238}\text{U}$ values being obtained for samples which have the maximum uranium concentrations in both the oxidized and the reduced phonolite. It is therefore apparent that preferential recoil loss is relatively much more efficient than bulk dissolution for samples with higher uranium concentrations and the implication of this is that the uranium at the areas of peak concentration is present in a form which is relatively stable under the ambient conditions, but which is either highly porous or else exists as a very thin coating on the surface of other minerals, and is highly prone to preferential recoil loss of ^{234}U . It is notable that, where the uranium concentration decreases on approaching the redox front from the oxidized side, the $^{234}\text{U}/^{238}\text{U}$ activity ratio tends towards unity, consistent with the concept of more rapid, (probably redox-induced) bulk dissolution of uranium in this section of rock.

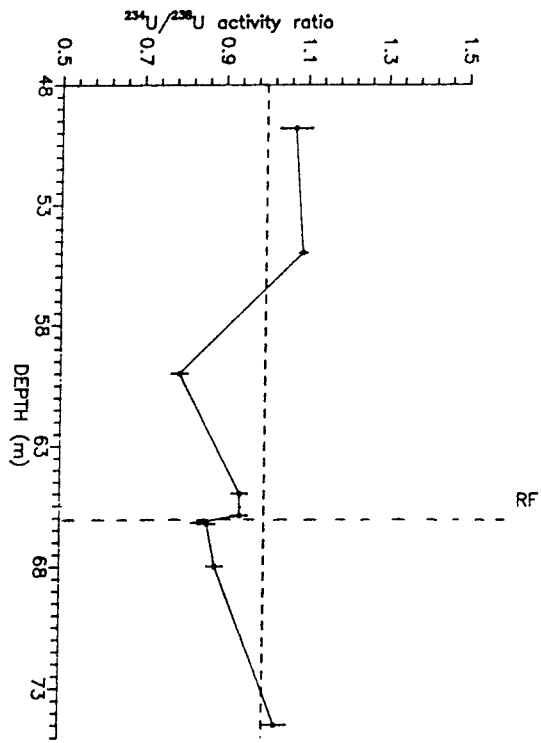


Figure 28. $^{234}\text{U}/^{238}\text{U}$ activity ratio profile across the 66.2 m redox front in the F1 drillcore.

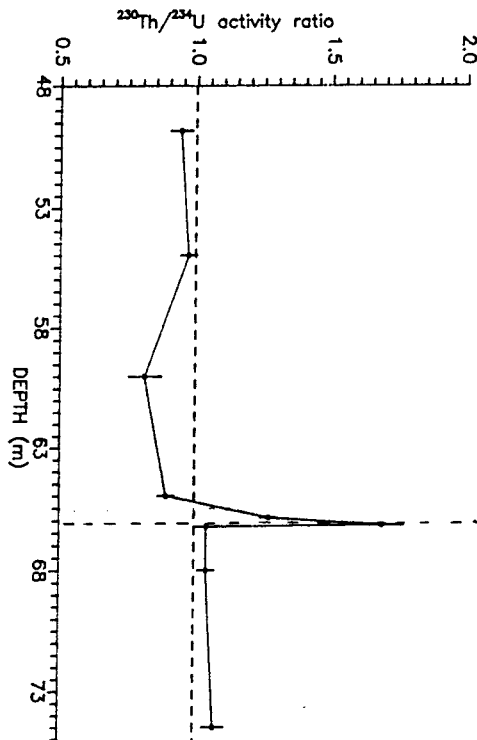


Figure 29. $^{230}\text{Th}/^{234}\text{U}$ activity ratio profile across the 66.2 m redox front in the F1 drillcore.

The $^{230}\text{Th}/^{234}\text{U}$ activity ratios also exhibit disequilibrium over a wide section of rock around the 66.2 m redox front as shown in Figure 29. Sample 67-1A-B, which lies just on the oxidized side of the redox front, has the highest $^{230}\text{Th}/^{234}\text{U}$ activity ratio (with a value of 1.69) of the samples in this section of the core. The $^{230}\text{Th}/^{234}\text{U}$ activity ratio decreases with increasing distance from the front on the oxidized side, falling to a value of 0.89 at sample 65-1A. The ^{230}Th deficiency relative to ^{234}U is maintained at sample 60-1A but, on moving further up the core, the $^{230}\text{Th}/^{234}\text{U}$ activity ratio is within error of equilibrium at sample 55-1A. This pattern in the $^{230}\text{Th}/^{234}\text{U}$ activity ratios in the oxidized rock is entirely consistent with the conclusion inferred above from the uranium concentration profile, i.e. uranium dissolution near the front (corroborated by $^{230}\text{Th}/^{234}\text{U}$ values of greater than unity) but uranium deposition in the oxidized rock away from the front (corroborated by $^{230}\text{Th}/^{234}\text{U}$ values of less than unity). If the return of the $^{230}\text{Th}/^{234}\text{U}$ activity ratio to equilibrium over a distance of between 5 and 10 m is assumed to be purely the result of decay of ^{234}U and associated ingrowth of ^{230}Th after the initial $^{230}\text{Th}/^{234}\text{U}$ disequilibrium has been established, then a rate of downward movement of the redox front at this location of the order of 20 m in 10^6 a is implied. The active deposition of uranium and preferential loss of ^{234}U in this area (apparent from the uranium concentration and $^{234}\text{U}/^{238}\text{U}$ activity ratio data), however, clearly invalidate a closed system assumption for this system and severely limit the level of confidence that can be placed upon this estimate of the rate of movement of the redox front.

The $^{230}\text{Th}/^{234}\text{U}$ activity ratio also falls abruptly on moving from sample 67-1A-B on the oxidized side of the front with a value of 1.69 to samples 67-1A-D and 68-1A-A which lie just on the reduced side of the front and have $^{230}\text{Th}/^{234}\text{U}$ activity ratios within error of equilibrium. Two significant observations follow from this pattern in the $^{230}\text{Th}/^{234}\text{U}$ activity ratios over the redox front. Firstly, it is apparent that the sharp maximum in the $^{230}\text{Th}/^{234}\text{U}$ ratio at the position of the front, in conjunction with the corresponding sharp minimum in uranium concentration at the same point, indicates that with respect to uranium dissolution, the position of the colour change marking the Fe(II)/Fe(III) transition also corresponds to the U(IV)/U(VI) transition, i.e. the redox gradient between the oxidized and reduced rock must be very steep and probably extends over a few cm at most. Secondly, it is evident (on the basis of the observed $^{230}\text{Th}/^{234}\text{U}$ equilibrium) that the uranium contained in samples 67-1A-D and 68-1A-A, which lie on the uppermost edge of the peak in uranium concentrations in the reduced rock, was deposited at least $3\text{--}4 \times 10^5$ years ago and that this location, just on the reduced side of the front, is not at present a location of significant uranium deposition. ICP-MS and XRF results (Table IV) reveal that the section of rock containing high uranium concentrations extends into the reduced

rock from the front to at least the position of sample 71-1A-A, i.e. 3.9 m. Unfortunately none of the other samples from this section has been analyzed for the natural decay series radionuclides so it is not possible to draw any definite conclusions concerning the present location (if any) of uranium deposition. If, however, it is assumed that uranium deposition currently takes place at the lower edge of the section of rock exhibiting enhanced concentrations (as would be necessary for movement of this structure into the reduced rock) then a rate of downward movement of the front of the order of 12 m in 10^6 years is suggested.

At greater depth in the reduced rock, below the peak in uranium concentrations, samples 75-1A and 80-1A show $^{230}\text{Th}/^{234}\text{U}$ activity values equal to or slightly greater than unity.

The $^{226}\text{Ra}/^{230}\text{Th}$ data for the transect across the 66.2 m redox front, which are plotted in Figure 30, show a similar trend to that observed at the 42.0 m redox front, with a pronounced ^{226}Ra deficiency relative to ^{230}Th on the reduced side of the front and a step change at the front to an excess of ^{226}Ra in the oxidized rock. These results thus suggest once again that ^{226}Ra is relatively mobile in the reduced rock close to the front, with recoil loss from the solid phase enhancing the dissolution rate, but is rapidly removed from solution upon entry into the oxidized rock with sulphate precipitation or uptake in iron oxides being likely mechanisms for transfer to the solid phase. The results thus strongly suggest a flux of ^{226}Ra across the redox front in the same sense, with respect to redox conditions (i.e. reduced to oxidized), as observed at the 42.0 m redox front, but in almost exactly the opposite direction as a consequence of the opposing orientations of the two redox fronts. Once more, this provides a strong argument against any significant advective flow of groundwater across the redox fronts.

If the decrease in the $^{226}\text{Ra}/^{230}\text{Th}$ activity ratio from 1.69 at sample 67-1A-B to equilibrium at sample 66-1A-A, some 26 cm away, is assumed to result purely from excess ^{226}Ra decay after passage of the front through the rock, a rate of movement of the front of about 26 m in 10^6 years is derived.

Samples 55-1A and 60-1A, which lie in the oxidized rock at a distance of 6 to 12 m from the front, have $^{226}\text{Ra}/^{230}\text{Th}$ activity ratios significantly below unity, indicative of ^{226}Ra loss (probably alpha recoil-enhanced) from this section of the rock. Thus the process which is responsible for retardation of ^{226}Ra close to the front in the oxidized rock is not so effective at these greater distances from the front. This provides support for the concept that the mechanism of removal of radium from solution close to the front involves coprecipitation or scavenging by some species forming at this location following

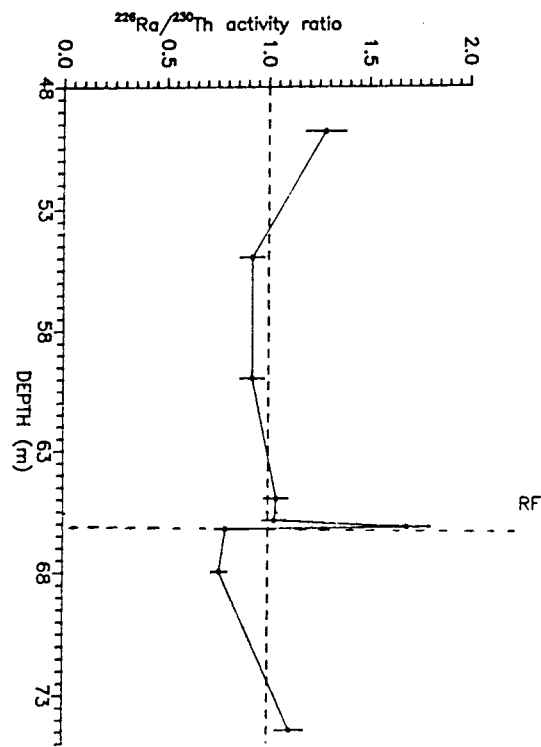


Figure 30. $^{226}\text{Ra}/^{230}\text{Th}$ activity ratio profile across the 66.2 m redox front in the F1 drillcore.

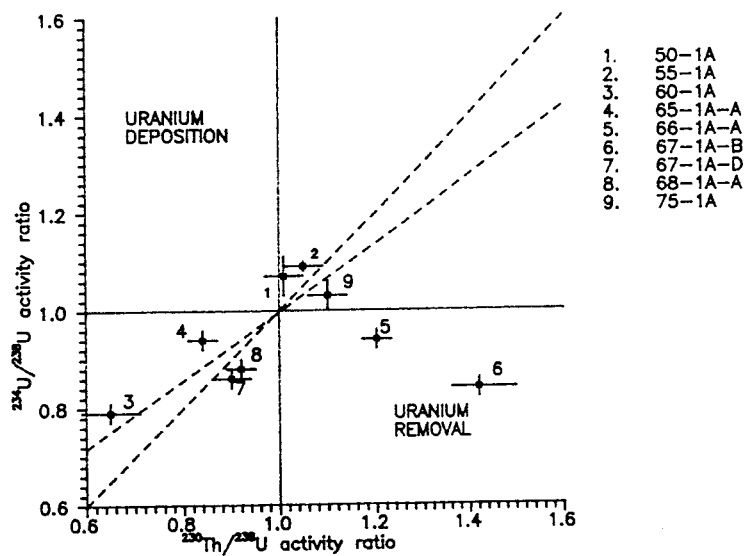


Figure 31. $^{234}\text{U}/^{238}\text{U}$ activity ratio versus $^{230}\text{Th}/^{238}\text{U}$ activity ratio diagram for samples from the vicinity of the 66.2 m redox front in the F1 drillcore.

dissolution of the constituent elements at the redox front (i.e. a situation of high aqueous phase concentrations).

The $^{234}\text{U}/^{238}\text{U}$ versus $^{230}\text{Th}/^{238}\text{U}$ diagram for the samples from the vicinity of the 66.2 m redox front is shown in Figure 31 and inspection of this plot leads to conclusions consistent with the preceding discussion. Thus, samples 50-1A and 55-1A from the oxidized rock at distances of 16.37 and 11.9 m respectively from the redox front lie in the uranium deposition sector in positions consistent with a process which has been operating on a timescale of about 7×10^5 years and which started to influence sample 50-1A before sample 55-1A. This supports the concept of oxidizing conditions spreading outwards from the fracture system at about 50 m depth in the drillcore and suggests a rate of movement of the front in the order of about 20 m in 10^6 years.

As discussed in section 1.2, uranium deposition rates can be calculated if a long-term deposition system is assumed to be operating and samples 50-1A and 55-1A give values of 8.6×10^{-4} Bq $\text{kg}^{-1}\text{a}^{-1}$ and 5.7×10^{-4} Bq $\text{kg}^{-1}\text{a}^{-1}$ respectively for the estimated rate of deposition of ^{238}U on the basis of such considerations. If these deposition rates are assumed to have applied for 10^6 a then the initial whole rock uranium concentrations for these samples can be calculated as 441 Bq kg^{-1} and 1315 Bq kg^{-1} respectively. The fact that these values are significantly higher than the unaltered reduced rock uranium concentrations suggests that the estimated uranium deposition rates may be too low. Closer to the front, samples 60-1A and 66-1A-A lie in the complex process zone while samples 66-1A-A and 67-1A-B from the oxidized rock close to the front are located in the uranium removal sector in positions which could be indicative of recent uranium dissolution. On crossing the front, the two samples from the reduced rock close to the front, 67-1A-D and 68-1A-A, also lie in the uranium removal sector but in a markedly different position from the samples from the oxidized side of the front. The reduced samples in fact lie in a position suggesting the operation of a process of uranium loss over a timescale of the order of 7×10^5 years. Uranium removal probabilities can be calculated for these samples as described in section 1.2. Sample 67-1A-D gives removal probabilities of $0.36 \times 10^{-6}\text{a}^{-1}$ and $0.82 \times 10^{-6}\text{a}^{-1}$ for ^{238}U and ^{234}U respectively, while sample 68-1A-A generates corresponding removal probabilities of $0.36 \times 10^{-6}\text{a}^{-1}$ and $0.75 \times 10^{-6}\text{a}^{-1}$. Thus, in both cases, a higher probability of removal is observed for ^{234}U than for ^{238}U in the reduced rock, consistent with the concept of recoil enhanced loss of ^{234}U . It is also notable that the removal probability for ^{238}U in the reduced rock ($0.36 \times 10^{-6}\text{a}^{-1}$) is an order of magnitude lower than that derived above for sample 45-1A in the oxidized rock ($1.7 \times 10^{-6}\text{a}^{-1}$) but that the removal probability of ^{234}U in the reduced rock is similar to the ^{238}U removal probability in the oxidized rock. Finally, sample 75-1A from the reduced

rock below the uranium concentration peak lies in the complex process sector of the graph but relatively close to the (1,1) position, suggesting that no major dissolution or deposition processes are affecting this sample.

The final set of samples from the F1 drillcore which was analyzed for natural decay series radionuclides was from the reduced rock below 75 m (Table II). Despite the fact that all of these samples lie well below the redox front, pronounced radioactive disequilibrium is still observed in a number of cases, indicating that significant redistribution processes are influencing uranium and radium at these depths.

Samples 101-1A and 111-1B have respective $^{234}\text{U}/^{238}\text{U}$ activity ratios of 1.08 and 1.09, suggesting recent (on a 2.5×10^5 a timescale) deposition of uranium at these locations. The fact that sample 111-1B lies in the conductive zone may be significant in this context. All of the other samples in this group have equilibrium values for their $^{234}\text{U}/^{238}\text{U}$ activity ratios. Sample 101-1A also exhibits pronounced $^{230}\text{Th}/^{234}\text{U}$ disequilibrium with an activity ratio of 1.35, indicating recent (relative to the ^{230}Th half-life) removal of uranium from this sample. This is in contrast to the conclusion inferred from the $^{234}\text{U}/^{238}\text{U}$ ratio for this sample, indicating that the processes operating are complex. Nevertheless the results do clearly indicate that, even at a depth of 100 m in the drillcore, active dissolution and redeposition processes are affecting uranium. Sample 121-1A also shows evidence of uranium loss with a $^{230}\text{Th}/^{234}\text{U}$ activity ratio of 1.12.

With the exception of sample 110-1A, all of the samples from this section of reduced phonolite have $^{226}\text{Ra}/^{230}\text{Th}$ activity ratios of less than unity (within the range 0.80 to 0.91). The implied loss of ^{226}Ra from the reduced rock is in good agreement with the above observation of radium loss from the reduced rock to the oxidized rock close to the redox fronts and suggests that ^{226}Ra (with a mean lifetime of 2300a) may be subject to substantial movement within the rock since there is a general depletion of ^{226}Ra on a scale of tens of metres in the reduced rock. As noted above, sample 110-1A with a value of 1.09 is the only one of this group of samples to have a $^{226}\text{Ra}/^{230}\text{Th}$ activity ratio greater than unity. Once again, this sample comes from the conductive zone and the observed activity ratios for this sample and sample 111-1B may be influenced by an enhanced flow of groundwater at this depth.

The $^{234}\text{U}/^{238}\text{U}$ versus $^{230}\text{Th}/^{238}\text{U}$ activity ratio diagram for the samples from the reduced phonolite is shown in Figure 32, from which it can be seen that four of the samples lie in, or on the boundary of, the upper complex process sector while the fifth lies in the uranium deposition sector. Samples 80-1A and 110-1A in fact lie relatively close to the (1,1) position, indicating that any dissolution or deposition processes influencing uranium at these positions are relatively minor or very old. Sample 101-1A, however, is

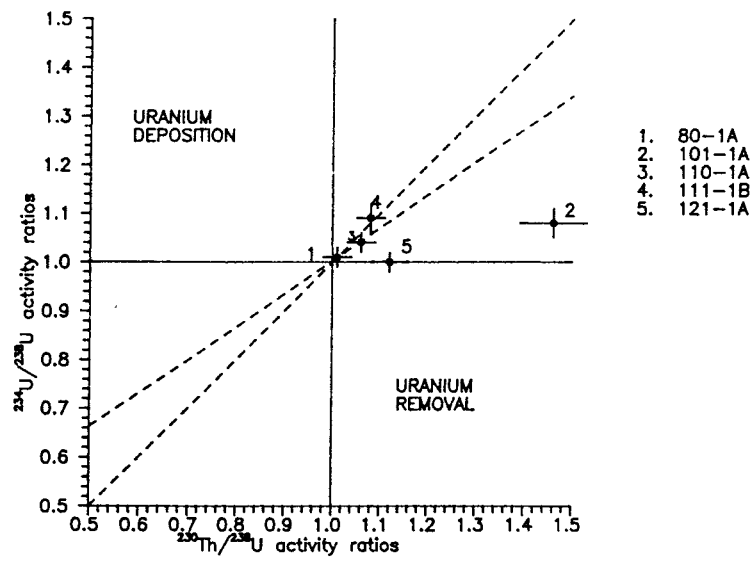


Figure 32. $^{234}\text{U}/^{238}\text{U}$ activity ratio versus $^{230}\text{Th}/^{238}\text{U}$ activity ratio diagram for samples from the reduced rock below the 66.2 m redox front.

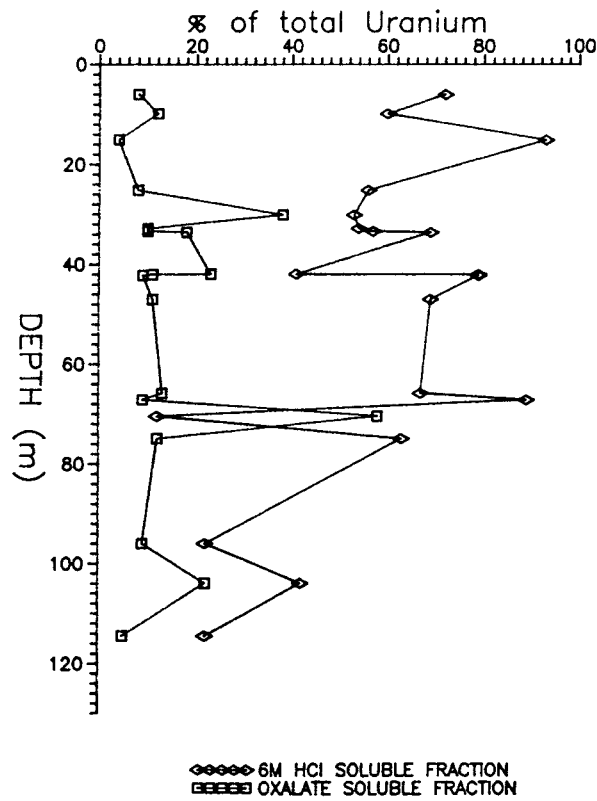


Figure 33. Profile showing the % of total uranium dissolved by leaching with oxalate solution and 6M HCl for samples from the F1 drillcore.

clearly subject to more significant and complex redistribution of uranium on the basis of its position in the plot. Sample 111-1B lies in the uranium deposition sector in a position indicating a process which has been influencing the sample for about 7×10^5 years. Finally, sample 121-1A lies on the $^{234}\text{U}/^{238}\text{U} = 1$ line in a position suggesting relatively rapid, equilibrium dissolution of uranium.

Despite recent controversy concerning the validity of sequential leaching as a means of investigating the speciation of elements in the solid phase, this technique remains one of the limited number of ways of obtaining information about the relative ease of distribution of elements from different samples. Thus, while it is probably erroneous to rigorously assign a "speciation" to an element on the basis of sequential leaching, this approach can provide useful information and, in the present work, a leaching scheme based loosely upon that employed by Cook *et al.* (1984) was used to extract uranium from samples from the F1 drillcore. The leaching scheme employed three solutions for sequential dissolution of the samples, namely (a) Tamms Acid Oxalate, which was attributed with selective dissolution of authigenic iron and manganese in the work by Cook *et al.* (1984), (b) Cold 6M HCl, and finally (c) total dissolution of the residue in aqua regia/HF. The results of the sequential leaching study are given in Table IV and in graphical form in Figures 33 to 37.

TABLE IV

Sample	Oxalate soluble		6M HCl soluble		Residue	
	% U	$^{234}\text{U}/^{238}\text{U}$	% U	$^{234}\text{U}/^{238}\text{U}$	% U	$^{234}\text{U}/^{238}\text{U}$
6-1A	8	0.87 ± 0.02	72	1.12 ± 0.01	20	1.07 ± 0.04
10-1A	12	0.93 ± 0.04	60	1.15 ± 0.03	28	1.07 ± 0.03
16-1A	4	1.28 ± 0.07	93	0.83 ± 0.01	3	1.00 ± 0.04
26-1A	8	1.29 ± 0.08	56	1.12 ± 0.02	36	1.04 ± 0.04
31-1A	38	1.01 ± 0.02	53	1.07 ± 0.03	9	0.95 ± 0.03
33-1A	10	1.07 ± 0.06	54	1.22 ± 0.03	36	0.88 ± 0.03
34-1B-D	10	1.27 ± 0.18	57	0.91 ± 0.03	33	1.2 ± 0.2
34-1B-F	18	1.30 ± 0.05	69	0.92 ± 0.02	13	1.11 ± 0.04
42-1B-D	23	1.17 ± 0.04	41	1.08 ± 0.02	36	1.11 ± 0.01
42-1B-H	11	0.57 ± 0.01	79	0.41 ± 0.09	10	1.26 ± 0.06
43-1A	9	1.15 ± 0.03	79	0.93 ± 0.03	12	0.97 ± 0.02
47-1A	11	1.01 ± 0.02	69	0.90 ± 0.01	20	1.05 ± 0.02
66-1A-A	13	0.84 ± 0.03	67	0.91 ± 0.02	20	1.24 ± 0.05
68-1A-A	9	0.77 ± 0.01	89	0.94 ± 0.04	2	1.59 ± 0.03
71-1A	58	0.81 ± 0.02	12	1.05 ± 0.03	30	1.12 ± 0.03
75-1B	12	1.41 ± 0.06	63	0.93 ± 0.03	25	0.91 ± 0.04
96-1A	9	1.42 ± 0.04	22	0.97 ± 0.02	69	1.26 ± 0.02
104-1A	22	1.34 ± 0.07	42	0.85 ± 0.02	36	0.83 ± 0.01
114-1A-D	5	1.15 ± 0.05	22	1.37 ± 0.07	73	0.96 ± 0.02

The fraction of uranium released by the oxalate leach (Fig. 33) varied from 4% to 58%, with notably higher values occurring for samples 34-1B-F, 42-1B-D and 71-1A, all of which lie in the reduced rock near the redox fronts. Sample 31-1A, which lies in the oxidized rock above the uppermost redox front, and sample 104-1A also had a relatively high release of uranium into the oxalate solution. As noted above, it is probably unwise to interpret these data in the sense of defining a strict speciation for uranium, but it is reasonable to say that, at these locations, all but one of which would represent sites of recent uranium deposition on the basis of the preceding discussion, the fraction of the total uranium which is very easily dissolved is high. Moreover, the results are consistent with, but cannot be taken to prove, association of the uranium with secondary iron or manganese minerals at these locations.

The 6M HCl leach (Fig. 33) also showed a maximum at sample 104-1A in the reduced rock along with generally high values for all of the samples above 75 m. Exceptions to this occurred at points where a high dissolution efficiency of uranium in the oxalate solution had been obtained. These lower results cannot therefore be taken to represent a lower solubility of uranium in 6M HCl for samples from these locations, since a high fraction of the uranium had already been removed from the sample before this leach was performed.

In order to provide an overall picture of the distribution of readily soluble uranium, Figure 34 shows the percentage of uranium dissolved in total by the oxalate plus 6M HCl leaches, while Figure 35 shows the percentage of the total uranium in the residual fraction. A very clear pattern emerges in these two graphs, with all of the samples above 75 m showing a high percentage of readily dissolved uranium (values ranging from 64 to 98%) and correspondingly low percentages of uranium in the residual phase (in the range 2 to 36%). Below 75 m, sample 104-1A shows a distinct maximum in the percentage of readily dissolved uranium with a value of 64%. The other two samples from the reduced rock both show high percentages (around 70%) for the uranium in the residual phase with corresponding readily dissolved values of around 30%. The data thus clearly demonstrate a much greater ease of dissolution of uranium in the sections of the core which have been influenced by the redox front than those which have not.

The $^{234}\text{U}/^{238}\text{U}$ activity ratio data for the combined oxalate plus 6M HCl leaches and for the residual fraction are plotted in Figures 36 and 37. The readily dissolved uranium in the combined oxalate plus 6M HCl leaches shows variations, as would be expected, similar to the total sample $^{234}\text{U}/^{238}\text{U}$ variations (Fig. 36) above 75 m. Interestingly, many of the residual phase samples above 75 m (Fig. 37) have $^{234}\text{U}/^{238}\text{U}$ activity ratios greater than unity, suggesting that some of the uranium which has been redistributed within the

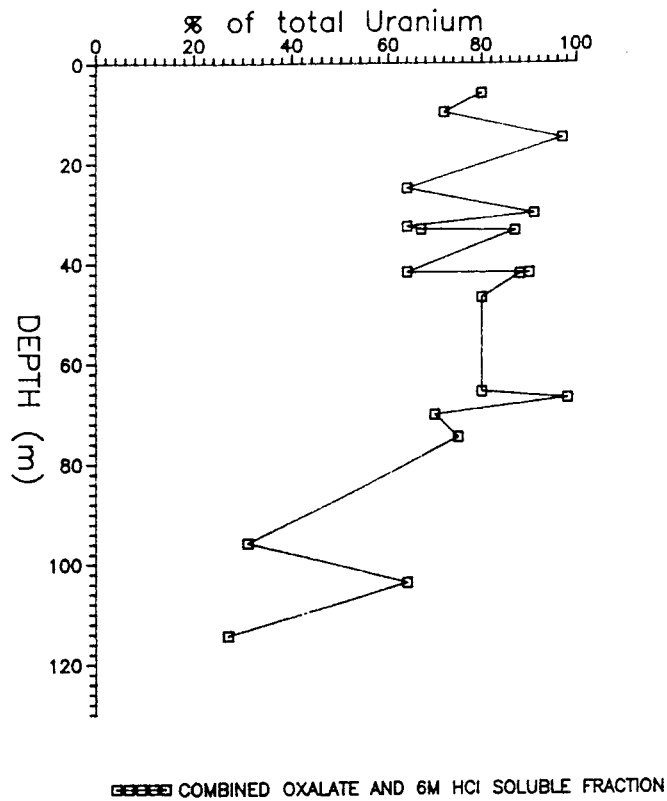


Figure 34. Profile showing the % of total uranium dissolved by combined oxalate plus 6M HCl leaching of samples from the F1 drillcore.

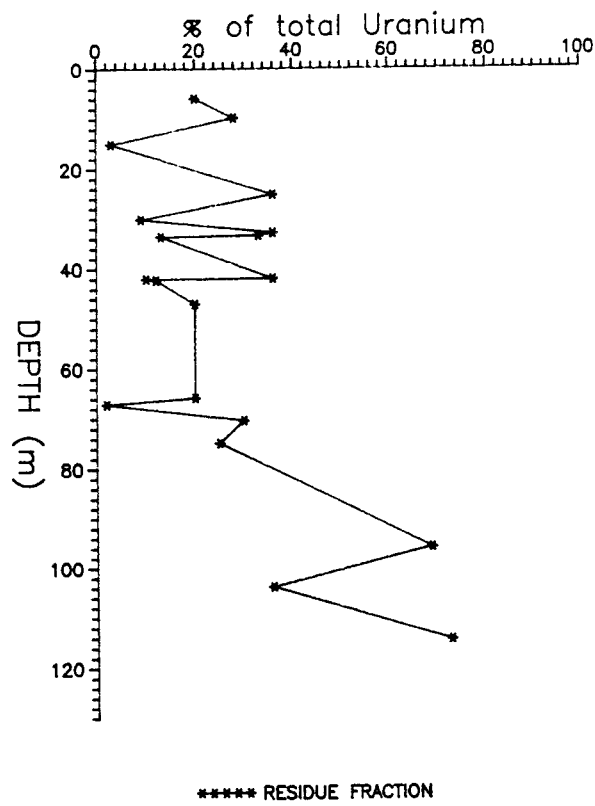


Figure 35. Profile showing the % of total uranium in the residual fraction following oxalate and 6M HCl leaching of samples from the F1 drillcore.

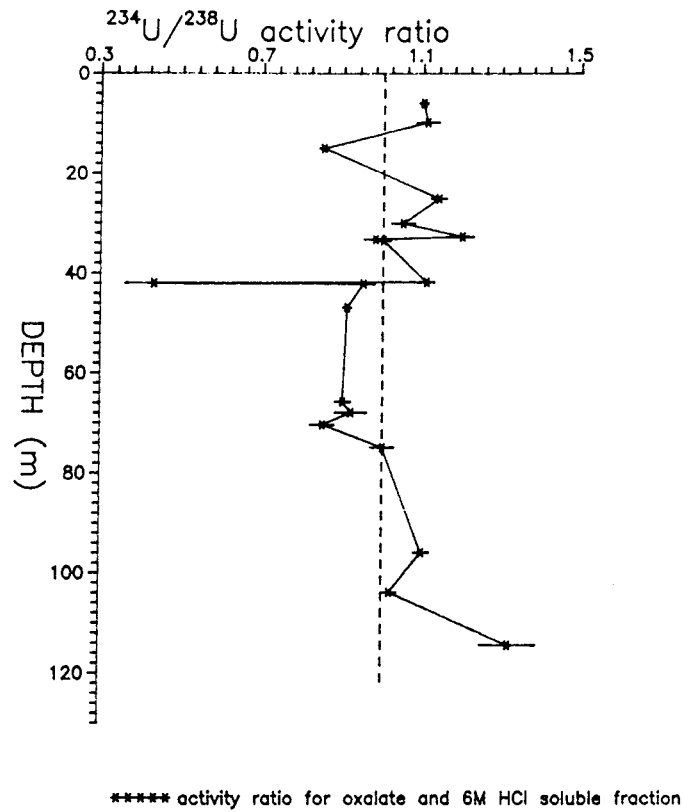


Figure 36. Profile showing $^{234}\text{U}/^{238}\text{U}$ activity ratios for combined oxalate plus 6M HCl leaching of samples from the F1 drillcore.

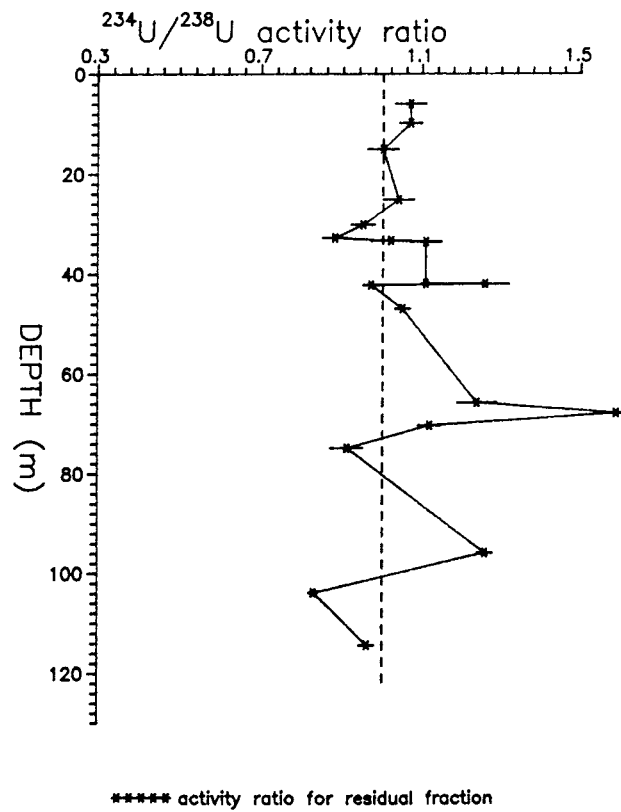


Figure 37. Profile showing $^{234}\text{U}/^{238}\text{U}$ activity ratios for the residual fraction following oxalate and 6M HCl leaching of samples from the F1 drillcore.

rock has been incorporated in a relatively resistate mineral phase. An alternative, although possibly less likely, explanation that could be advanced to explain this observation would be to invoke alpha recoil of uranium nuclei from thin surface coatings resulting in the embedding of ^{234}U atoms in resistate minerals.

A notable feature of the $^{234}\text{U}/^{238}\text{U}$ results for the samples from deeper than 75 m is that the readily dissolved values are all greater than or equal to equilibrium, while three out of the four residual phase results are less than unity. Moreover, as shown in Table IV, the high $^{234}\text{U}/^{238}\text{U}$ values for the readily dissolved component are derived predominantly from the oxalate leach. This strongly suggests a two component system for the reduced phonolite comprising residual phase minerals which have been subject to preferential loss of ^{234}U to groundwater along with a secondary mineral deposit of recent origin with a $^{234}\text{U}/^{238}\text{U}$ signature greater than unity. This system would be consistent with the positioning of the reduced phonolite samples in the upper complex process sector in Figure 32.

2.1.2. Stable element studies

In addition to the natural radionuclide studies described above, selected samples from the F1 drillcore were also analyzed for a range of stable elements by ICP-MS and the results of these analyses are contained in Tables III, V and VI. The following discussion of this aspect of the work is restricted to a comparison of the behaviour of uranium with that of other elements in the F1 drillcore and attempts to provide further details of processes occurring at the redox fronts. A more extensive geochemical and mineralogical study, including work on the F1 drillcore, was carried out as a complementary section of the Poços de Caldas Project and is described in detail in another report in this series (Waber *et al.*, this report series; Rep.2).

Comparison of the behaviour of uranium with that of thorium is of particular importance, firstly because the virtually complete insolubility of thorium relative to uranium is a fundamental assumption in interpretation of the natural decay series data and, secondly, because thorium exists only as Th(IV) and is not intrinsically sensitive to redox processes, it shows contrasting behaviour to the redox-sensitive properties of uranium and can provide information of relevance to the behaviour of U(IV) in this system. As previously discussed, the variations in the concentration of thorium in the F1 drillcore are sufficiently small relative to those of uranium (Figs. 9 to 11) that, to a first approximation, the assumption, in the context of natural decay series radionuclide

TABLE V
Concentrations (ppm) of elements in samples from the F1 drillcore obtained by semi-quantitative ICP-MS analysis.

Sample	Depth	B	Al	Ga	Ge	As	Se	Sn	Sb	Te	Tl	Pb	Bi
6-1A	6	2.8	62900	85	3.7	19	1.9	13	0.9	0.1	0.55	83	0.02
10-1A	9.84	4.4	55700	56	2.6	4.6	1.6	4	0.6	0.2	1.8	49	0.01
16-1A	15.07	2.2	46000	35	1.1	3.8	0.1	2.7	0.4		2.2	9.6	0.02
26-1A	25.22	7.4	68200	64	0.5	6.6	0	7.8	0.8	0.2	3.7	14	0.09
31-1A	30.2	17	42400	107	1.2	20	46	4	1	0.03	2.3	27	0.02
33-1A	32.89	25	57700	219	1.2	3.9	0	5.1	1	0	2.8	29	0.38
34-1B-D	35.51	4.2	59700	59	1.1	0.4	0.2	4.2	0.6	0.02	4.5	11	0.01
34-1B-F	33.65	0.7	39600	78	1.4	0.2	0.4	2.2	0.8	0.02	5.8	120	0.01
34-1C	34	2.2	54300	37	1.5	0.7	2	9.8	0.4	0.13	5.2	26	0.01
35-1A	34.31	2.3	60800	58	3.1	3.4	1.4	5.4	1.9	0.17	3.9	93	0.02
41-1A	40.05	1.8	4210	64	1.4	3	8.3	2.5	0.4	0.03	1.1	49	0.02
42-1A	41.85	0.8	60900	45	1.2	0.2	0.2	3.9	0.5	0	0.311	25	0
42-1B-B	41.95	85	93200	66	35	11	117	20	13	20	6.6	130	3.5
42-1B-D	41.97	60	117000	69	32	9.4	84	19	6.6	9.4	13	20	2.6
42-1B-H	42.03	58	157000	65	35	22	76	15	7.5	11	9.9	12	1.7
42-1B-I	42.04	74	144000	53	31	7.9	128	12	7.1	14	11	23	4.5
42-1B-K	42.05	54	120000	51	28	26	71	15	5.5	9.4	9.2	15	3.2
43-1A	42.1	47	12700	154	2.7	5.3	1.5	5.3	1.3	0.2	3.6	12	0.01
45-1A	44.87	4	60700	61	2.3	11	1.7	10	0.8	0.1	2.7	41	0.01
47-1A	46.1	0	43500	52	2.4	25	76	6.6	1.6	0.52	7.5	178	0.02
66-1A-A	65.93	4.2	13900	208	2.5	3	2.5	5.2	0.5	0	1.3	22	0.08
67-1A-D	66.26	6.1	13100	66	2.4	0.3	0.2	7	1	0	1.6	39	0.09
68-1A-A	67.03	7.7	14400	78	2.2	0.5	0.4	7.4	1.4	0	1.9	29	0.04
71-1A	70.1	1	52200	54	2	0.6	1.5	3.2	0.4	0	1.1	20	0.02
75-1A	74.25	2.4	50900	53	2.6	1.7	3.6	3.8	0.3	0.2	0.6	19	0
75-1B	74.96	1.6	55100	53	2.6	1.7	3.6	4	0.3	0	0.7	21	0.03
80-1A	79.8	1	63000	59	0.8	0.2	0	4	0.3	0	1.3	34	0.02
96-1A	96	2.9	60700	75	3.2	1.4	2.7	6.2	0.4	0.07	1	30	0
101-1A	100.32	3.9	69200	66	0.9	5.8	0	4.2	6	0	1	8.4	0.02
104-1A	104	0	47100	83	1.5	8.3	15	11	0.8	0.12	1.2	49	0.08
110-1A	110	19	42800	81	2	0.5	0	5.5	0.6	0.03	0.8	44	0.06
111-1B	111	2.4	48100	66	2.9	3	5	4.4	0.3	0	0.58	81	0.05
113-1B	113	1.6	57600	50	2	1.3	1.6	2.2	0.2	0.02	0.9	16	0
114-1A-A	114.1	174	42600	58	1.8	5.8	2.2	6	0.4	0.06	1	30	0.04
114-1A-B	114.2	0	41900	66	1.9	5.8	2	2.3	0.4	0.05	0.6	94	0.05
114-1A-C	114.3	9	39300	44	2.1	6.6	2	2.1	0.6	0	0.65	55	0.04
114-1A-D	114.4	5.2	49700	82	2.7	18	37	6.9	0.5	0.23	1.3	24	0.04
121-1A	120.19	31	62300	75	0.5	1	0.3	1.9	0.4	0	0.8	35	0.03
123-1B	123	12	44300	65	4	141	6.8	9.4	2.2	0.34	2	51	0.18

TABLE V (contd.).

Sample	Depth	Li	Be	Mg	Ca	Rb	Sr	Cs	Ba
6-1A	6	213	10	731	353	236	34	0.2	313
10-1A	9.84	66	3	273	233	303	199	0.3	735
16-1A	15.07	41	5	107	891	258	102	0.4	350
26-1A	25.22	55	4	116	2000	294	212	0.7	1080
31-1A	30.2	61	6	412	786	316	183	0.8	2600
33-1A	32.89	97	5	664	718	226	152	0.3	6320
34-1B-D	35.51	38	4	635	881	279	147	0.4	985
34-1B-F	33.65	20	3	1990	2880	325	173	0.4	1210
34-1C	34	19	3	70	242	302	227	0.4	1020
35-1A	34.31	106	6	364	256	300	210	0.4	771
41-1A	40.05	58	7	497	800	307	173	0.6	2600
42-1A	41.85	53	6	147	105	247	162	0.3	425
42-1B-B	41.95	135	65	819	2280	314	210	5.5	1560
42-1B-D	41.97	179	68	1400	3380	399	325	3.3	577
42-1B-H	42.03	140	65	359	3340	327	257	3.5	490
42-1B-I	42.04	137	41	2260	5240	354	347	4.9	575
42-1B-K	42.05	120	66	304	4870	378	348	4	550
43-1A	42.1	69	10	852	1400	280	213	0.2	1700
45-1A	44.87	101	6	236	274	290	219	0.3	717
47-1A	46.1	31	3	215	531	299	219	0.6	741
66-1A-A	65.93	123	3	1840	351	178	178	0.4	2500
67-1A-D	66.26	109	4	1470	1720	399	179	0.2	320
68-1A-A	67.03	112	3	1830	2340	349	254	0.6	431
71-A	70.1	95	2	250	195	242	130	0.6	521
75-1A	74.25	62	3	1960	4210	264	324	1.7	830
75-1B	74.96	101	3	367	2220	274	311	0.9	557
80-1A	79.8	87	4	680	734	245	120	0.4	699
96-1A	96	118	9	314	586	316	327	0.8	1330
101-1A	100.32	73	4	609	2560	198	104	0.3	996
104-1A	104	61	8	193	531	284	106	0.5	1250
110-1A	110	141	9	3960	5650	277	361	0.5	632
111-1B	111	92	5	1170	1850	323	297	0.6	1050
113-1B	113	88	4	137	2770	305	282	0.5	1060
114-1A-A	114.1	94	4	2610	5810	248	165	0.7	535
114-1A-B	114.2	75	3	2720	7330	276	237	0.5	1560
114-1A-C	114.3	61	2	2320	6020	242	215	0.5	661
114-1A-D	114.4	263	6	428	820	242	226	1	665
121-1A	120.19	43	3	375	1300	308	180	0.6	1610
123-1B	123	79	10	292	8260	251	398	0.8	2600

TABLE V (contd.).

Sample	Depth	Ce	Pr	Nd	Sm	Eu	Gd	Tb	Dy	Ho	Er	Tm	Yb	Lu
6-1A	6	15	21	56	6.6	2.6	7.6	1.7	11	2.5	8.4	1.3	7.5	1.1
10-1A	9.84	13	9.1	26	3.1	0.9	2.7	0.5	3.1	0.97	3.4	0.47	3.3	0.4
16-1A	15.07	181	22	67	7.1	2.1	6.5	1	5.3	0.95	3.4	0.34	2.5	0.26
26-1A	25.22	81	11	31	4.1	1.7	5.1	1	7.9	1.7	4.4	0.65	3.7	0.63
31-1A	30.2	99	13	35	5.1	1.7	4.9	0.85	6	1.4	4.5	0.69	5.2	0.64
33-1A	32.89	136	10	29	5.4	2.4	3.9	0.58	4.6	1.1	3.6	0.59	3.8	0.54
34-1B-D	35.51	165	18	55	8.5	3.3	13	2.4	16	2.7	7.2	1	5.4	0.73
34-1B-F	33.65	263	29	85	15	6.2	21	4.2	22	4	9.9	1.1	6.4	0.96
34-1C	34	201	23	64	10	4.5	14	3.1	17	2.9	7.1	0.84	4.5	0.58
35-1A	34.31	349	40	108	12	4.3	15	2.5	15	3.4	9.6	1.47	8.6	1.1
41-1A	40.05	427	46	116	12	3.7	14	1.7	8	1.4	4.3	0.36	2.7	0.33
42-1A	41.85	90	16	51	13	5.1	14	3.1	22	4	12	1.6	9.4	1.2
42-1B-B	41.95	141	95	312	107	46	118	32	183	34	85	13	94	7.8
42-1B-D	41.97	161	44	138	54	18	68	19	84	16	42	7.7	40	8.7
42-1B-H	42.03	99	18	61	13	8.3	17	3.3	14	3.9	12	2.8	12	3.3
42-1B-I	42.04	235	27	93	12	5.3	23	3.9	18	3.9	6.2	4.1	15	4.9
42-1B-K	42.05	196	23	71	19	13	25	4.1	15	5.2	9.2	3.6	22	3.9
43-1A	42.1	262	30	83	9.8	3	9.2	1.5	8.4	1.6	3.7	0.43	2.7	0.28
45-1A	44.87	1112	31	82	11	3.8	17	2.1	12	2.4	6.9	0.94	6.3	0.83
47-1A	46.1	6279	45	111	17	5.1	73	4	15	2.5	7.2	1	6.2	0.77
66-1A-A	65.93	172	24	68	8.5	2.7	7.7	1.2	7.9	1.8	5.7	0.8	5.2	0.78
67-1A-D	66.26	290	28	77	8.5	2.5	7.9	1.2	6.9	1.4	4	0.58	2.9	0.38
68-1A-A	67.03	248	21	54	6.1	1.7	5.4	0.8	5.2	1.2	3.8	0.51	3.7	0.53
71-1A	70.1	249	28	73	8.6	2	7	0.94	3.6	0.79	2.4	0.28	1.7	0.29
75-1A	74.25	3219	417	1208	115	33	130	18	93	19	55	6.6	35	4.8
75-1B	74.96	303	28	76	7.6	2.1	8.3	0.99	4.6	0.91	3.1	0.43	2.7	0.35
80-1A	79.8	189	18	47	4.6	1.5	5	0.56	3.4	0.64	2.1	0.27	1.7	0.23
96-1A	96	337	30	82	8.6	2.4	9	1.4	9.5	1.7	5.3	0.56	3.8	0.63
101-1A	100.32	188	13	36	4	1.4	5.7	1.1	6.2	1.3	3.1	0.4	2.1	0.3
104-1A	104	333	27	69	7.2	2.6	11	2	1	2.2	5.3	0.63	3.3	0.39
110-1A	110	445	35	93	13	4.1	14	2.6	15	2.8	6.7	0.8	4.3	0.61
111-1B	111	496	41	107	12	3.7	15	2	9.2	1.3	3.5	3.4	1.7	0.2
113-1B	113	470	42	113	13	3.7	13	2.1	12	2.2	5.4	0.52	3.1	0.44
114-1A-A	114.1	540	24	68	7.2	2	10	1.1	7.1	1.5	3.7	0.46	2.6	0.39
114-1A-B	114.2	173	15	40	5.8	1.9	6.6	1.2	9.6	2.1	6.5	0.92	5.5	0.66
114-1A-C	114.3	181	13	38	5.2	1.4	6.5	1.1	9	2.2	6	0.83	5.1	0.64
114-1A-D	114.4	428	38	102	13	4.2	17	2.9	21	5	15.5	1.9	12	1.7
121-1A	120.19	536	46	117	13	3.2	11	1.5	10	2.7	7.4	0.83	5	0.48
123-1B	123	484	43	125	17	5.7	24	4.5	36	8.3	22	2.9	16	2.4

TABLE V (contd.).

Sample	Depth	Sc	Ti	V	Cr	Mn	Fe	Co	Ni	Cu	Zn
6-1A	6	3.3	3560	653	3.2	72	43100	1	0.8	12	66
10-1A	9.84	1.5	2090	233	1.3	27	14700	0.3	1.5	14	30
16-1A	15.07	1.2	232	75	0.9	26	2530	0.1	0.2	3.4	5.4
26-1A	25.22	2.5	2450	200	2.1	65	5820	0.2	0.8	1.3	16
31-1A	30.2	2.9	2500	252	3.7	20	7080	0.2	7	31	36
33-1A	32.89	2.6	2360	240	0.4	30	19800	0.8	0.1	1	6.8
34-1B-D	35.51	1.8	1190	112	0.3	27	4150	0.1	0.1	1.2	6.6
34-1B-F	33.65	7.8	900	43	2.1	18	4900	1	1.3	2.7	7.3
34-1C	34	1.4	1290	69	0.7	18	2370	1	2.5	5.1	19.9
35-1A	34.31	3.7	3070	242	2.9	73	16900	1.7	2.4	5.9	31
41-1A	40.05	1.7	1020	196	4.1	66	4360	1.2	6.5	16	75
42-1A	41.85	1	1937	160	0.4	34	9570	0.7	1.7	0.8	6.5
42-1B-B	41.95	162	2900	318	32	93	19600	9.4	54	508	59
42-1B-D	41.97	122	3270	299	22	83	14700	14.5	64	399	28
42-1B-H	42.03	57	4750	313	22	91	14600	9.9	43	168	41
42-1B-I	42.04	75	1210	151	40	45	15600	8.7	47	191	38
42-1B-K	42.05	62	1470	195	28	115	16700	8.3	60	158	38
43-1A	42.1	3.8	1780	300	1.3	34	21100	0.1	0.2	4.8	15
45-1A	44.87	1.8	3160	261	0.5	72	17800	0.3	1.5	7.5	49
47-1A	46.1	2	7450	217	4.3	69	12500	0.7	4.3	11	71
66-1A-A	65.93	5.2	3060	313	1.8	44	23300	0.1	0.7	3.4	11
67-1A-D	66.26	4.2	3380	244	1.2	63	23100	1.5	0.8	7	67
68-1A-A	67.03	5.4	2850	274	1.2	69	23100	1	0.8	4.4	13
71-1A	70.1	1.1	1210	113	0.3	27	3120	0.9	4.8	3.4	18
75-1A	74.25	1.5	2080	174	1.6	282	20800	1.6	5.3	5.7	1250
75-1B	74.96	1.1	2340	175	0.5	73	1390	0.3	1.1	3.2	1020
80-1A	79.8	1.3	2080	115	0.4	44	1620	0.3	0.7	1	26
96-1A	96	2.5	2940	600	2.2	82	14800	1	5.2	85	144
101-1A	100.32	3.4	2210	222	0.8	44	19000	0.3	0.9	0.6	124
104-1A	104	0.81	2810	539	3.5	43	11000	1.2	5.1	16	231
110-1A	110	14.4	3880	316	2.7	134	18900	0.9	1	3.8	185
111-1B	111	8.2	3150	259	1.3	43	14300	0.7	6.5	16	75
113-1B	113	1.2	2030	177	2.5	35	4390	0.3	0.7	0.4	222
114-1A-A	114.1	20	1740	433	1.3	50	5320	0.5	2.3	7.8	42
114-1A-B	114.2	18.9	531	192	1.5	31	8310	0.6	2.7	6.4	270
114-1A-C	114.3	18.7	474	203	1.8	31	9720	0.8	2.8	7.3	520
114-1A-D	114.4	4.7	716	654	2	88	12100	1.1	9.8	11.4	404
121-1A	120.19	1.7	966	56	3.1	191	5330	0.02	0.3	0.5	27
123-1B	123	32.5	1980	673	1.5	223	19900	0.85	2.2	6.9	99

TABLE V (contd.).

Sample	Depth	La	Hf	Ta	W	Re	Os	Ir	Pt	Au	Hg
6-1A	6	138	12	3.1	11	0	0	0.02	0.2	0.11	0.2
10-1A	9.84	67	5.1	4.8	6.6	0.01	0.04	0.02	0.07	0.09	0.2
16-1A	15.07	117	2.8	2.2	2.1	0	0.02	0	0	0.01	0.1
26-1A	25.22	54	6	7	13.5	0.3	0.04	0.01	0	0.05	0.1
31-1A	30.2	97	9.5	2.5	11.9	0	0.03	0.03	0.03	0.22	0.4
33-1A	32.89	59	14.9	7.9	10.6	0	0	0.02	0.01	0.05	0.23
34-1B-D	35.51	98	3.9	2.9	7.2	0	0	0	0	0	0.04
34-1B-F	33.65	142	3.5	1.9	4.9	0.04	0	0	0.03	0.02	0.2
34-1C	34	138	3.9	2.9	7.2	0	0	0.01	0.01	0.09	0.04
35-1A	34.31	276	14.7	8.7	6.8	0.02	0.03	0.05	0.17	0.41	0.26
41-1A	40.05	327	2.6	5.1	4.1	0.03	0	0	0	0.24	0.22
42-1A	41.85	92.7	8.2	7.2	15.6	1	0.02	0	0.02	0.07	0.13
42-1B-B	41.95	222	14.1	7.3	34.4	6.1	9.4	2.8	6.2	2.8	19.8
42-1B-D	41.97	190	14.4	5.1	18.2	5.4	4.9	4.6	8.4	2.8	6.6
42-1B-H	42.03	171	15.6	8.7	28	3.9	9.9	3	6.6	2.5	10.3
42-1B-I	42.04	192	13.4	5.2	20	5.1	5.1	4.9	8.2	3.9	14
42-1B-K	42.05	173	19.6	6.1	20	4.1	4.6	6.6	9.1	3.1	3.2
43-1A	42.1	186	4.2	7.8	12	0	0	0.01	0.01	0.03	0.07
45-1A	44.87	191	9.2	11.2	8	0	0	0.02	0.02	0.38	0.12
47-1A	46.1	327	5.9	12.7	23.7	0	0.05	0	0	0.71	0.34
66-1A-A	65.93	166	13.9	8	6.2	0	0	0.013	0.05	0.04	0.01
67-1A-D	66.26	163	8.3	8.3	8.9	0.07	0	0	0.02	0.03	0
68-1A-A	67.03	160	13.9	8	6.3	0	0	0.01	0.05	0.03	0.01
71-1A	70.1	186	3.9	9.2	5.3	0.01	0.01	0.02	0.11	0.25	0.08
75-1A	74.25	3225	6.3	7.9	8.5	0	0.1	0.02	0.02	0.17	0.08
75-1B	74.96	218	6.4	5.6	6.8	0	0.05	0.03	0.1	0.23	0.15
80-1A	79.8	105	6.5	7.9	7.6	0	0	0.02	0.04	0.08	0.08
96-1A	96	222	8.5	8.2	15.4	0	0.02	0.02	0.06	0.3	0.13
101-1A	100.32	83	12.9	8.2	11.1	0.03	0.01	0	0.12	0.02	0.21
104-1A	104	201	3.4	3.8	9.7	0	0	0	0	0.71	0.34
110-1A	110	226	13.5	7.5	11	0	0.01	0.05	0.18	0.08	0.07
111-1B	111	283	2.9	7.5	12.2	0	0	0	0	0.28	0.35
113-1B	113	304	4.3	4.9	10.7	0	0.01	0.01	0.06	0.24	0.12
114-1A-A	114.1	94	12.2	4.9	7.8	0	0	0.02	0.12	0.23	0.23
114-1A-B	114.2	79	18.8	1.4	3.3	0	0.03	0.05	0.08	0.09	0.11
114-1A-C	114.3	265	24.2	1.3	3.3	0	0.023	0.05	0.15	0.1	0.11
114-1A-D	114.4	283	37.8	0.68	2.6	0	0.081	0.07	0.29	0.17	0.29
121-1A	120.19	281	10.3	5.7	9.6	0	0	0.04	0.02	0.01	0.07
123-1B	123	332	194	6.2	13.1	0	0.23	0.52	1.5	0.61	0.23

TABLE V (contd.).

Sample	Depth	Y	Zr	Nb	Mo	Ru	Rh	Pd	Ag	Cd
6-1A	6	68	547	101	182	0.04	0.005	2.8	1.4	0.8
10-1A	9.84	23	220	94	49	0.04	0.014	1.2	1.3	0.7
16-1A	15.07	20	118	17	58	0	0	0.4	0.2	0.6
26-1A	25.22	37	265	119	91	0	0	0.5	0.9	1
31-1A	30.2	42	583	89	166	0.03	0.01	3	1.3	2.8
33-1A	32.89	27	782	160	404	0	0	2.1	1.1	0.8
34-1B-D	35.51	56	226	59	83	0	0	0.7	0.4	0.5
34-1B-F	33.65	96	211	44	84	0	0	1.4	0.6	7.8
34-1C	34	63	180	58	60	0	0	0.9	0.7	1.7
35-1A	34.31	84	867	217	166	0	0	3.9	3	0.8
41-1A	40.05	41	126	133	117	0.02	0	0.6	1.8	4.6
42-1A	41.85	67	328	141	266	0	0	0.9	0.9	0.6
42-1B-B	41.95	761	262	148	330	17.2	4.6	23	9.4	41
42-1B-D	41.97	367	292	145	191	25	7.7	21	6	48
42-1B-H	42.03	80	520	217	290	12	7.9	16	6.7	36
42-1B-I	42.04	60	375	87	402	19	4.9	12	5.9	37
42-1B-K	42.05	88	632	90	411	15	7.1	26	10.2	53
43-1A	42.1	45	234	134	824	0	0	0.7	0.7	0.5
45-1A	44.87	53	390	257	190	0	0	1.8	3.2	2.1
47-1A	46.1	57	324	211	409	0.01	0.01	3.1	3.1	7.1
66-1A-A	65.93	59	754	300	39	0	0	1.7	1.5	3.9
67-1A-D	66.26	34	484	326	82	0	0	5	1.6	117
68-1A-A	67.03	46	782	280	141	0	0	2.1	1.4	9.4
71-1A	70.1	22	198	274	45	0.03	0.02	0.9	3.3	0.3
75-1A	74.25	561	331	257	27	0.03	0.01	1.5	3.3	0.03
75-1B	74.96	30	252	154	35	0.02	0.01	1.2	2	0.3
80-1A	79.8	16	285	284	25	0	0	0.8	1.4	0.5
96-1A	96	47	362	186	14	0	0	1.6	2.9	8.8
101-1A	100.32	27	513	195	9	0	0	1.7	1.5	1.2
104-1A	104	67	165	129	44	0.01	0.01	0.86	2.1	1.8
110-1A	110	75	684	279	18	0	0.01	2.7	2.4	2.2
111-1B	111	45	159	231	23	0.01	0.02	0.84	2.9	3.5
113-1B	113	58	223	72	12	0	0	0.9	0.8	0.3
114-1A-A	114.1	38	758	102	39	0.05	0.01	3.9	1.4	2.7
114-1A-B	114.2	67	1140	35	21	0.02	0.01	5.3	0.6	3.1
114-1A-C	114.3	56	1560	33	15	0.02	0.01	7.1	0.7	3
114-1A-D	114.4	180	2670	37	21	0.06	0.01	12.4	0.9	11
121-1A	120.19	74	548	78	12	0.05	0	1.3	0.6	0.2
123-1B	123	274	1730	201	266	0	0.02	92	6.1	20

studies, of negligible solubility of thorium relative to that of uranium is valid. Nevertheless, significant variations in thorium concentrations are observed in the F1 drillcore and, as shown in Figures 38 to 40, are most pronounced in the vicinity of the redox fronts. At the 33.4 m redox front, thorium concentrations rise sharply from values of 28 to 78 ppm in the oxidized rock to reach values of up to 158 ppm in the reduced rock (Fig. 38), with the zone of enhanced thorium concentrations extending for a distance of at least 0.5 m into the reduced rock. The thorium maximum occurs below the area of maximum dissolution at the front (as indicated by minima in the uranium and iron concentrations), suggesting that this is a genuine case of transport of thorium to this location at low concentration in groundwater, followed by uptake in some mineral forming on the reduced side of the front, rather than an increase of thorium concentration as a consequence of its insolubility and preferential enrichment in resistate phases when more labile elements are dissolved at the redox front. A similar situation pertains at the 42.0 m redox front where thorium concentrations exhibit a very sharp peak in the reduced rock at the same position as uranium deposition occurs (Fig. 39). While the thorium concentration at the 42.0 m redox front rises to a higher level than at the 33.4 m redox front, with a maximum of 387 ppm for sample 42-1B-B, these higher concentrations of thorium are only maintained over a distance of about 6 cm, i.e. an order-of-magnitude lower than the extent of enrichment of thorium in the reduced rock at 33.4 m. Thus the total quantity of thorium contained in the reduced rock at 33.4 m is probably greater than the corresponding quantity on the reduced side of the 42.0 m front. At the 66.2 m redox front (Fig. 40), there is evidence of only slight thorium enrichment, with sample 67-1A-B having the maximum concentration of only 49 ppm, which is in fact lower than concentrations of thorium observed in the overlying oxidized rock.

The quantity of thorium deposited at the three redox fronts thus decreases with increasing depth and this provides an interesting comparison with the pattern of uranium concentration down the drillcore. At the 33.4 m redox front (Fig. 12), there is only a weak and narrow enrichment of uranium in the reduced rock with a maximum concentration at sample 34-1B-E of 391 ppm. At 42.0 m, the uranium concentration increases to a value of 2.8% at sample 42-1B-B but decreases rapidly on moving further into the reduced rock (Fig. 13), with an order-of-magnitude reduction in concentration over a distance of 10 cm. Unfortunately the exact extent of the uranium enrichment into the reduced rock cannot be ascertained as a result of limitations in the sampling frequency, but the available evidence suggests a narrow band of highly enriched rock close to the front.

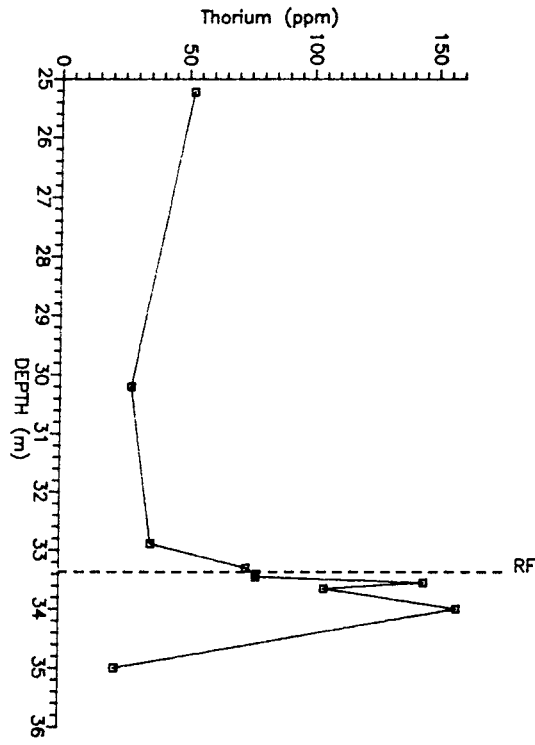


Figure 38. Thorium concentration profile across the 33.4 m redox front in the F1 drillcore.

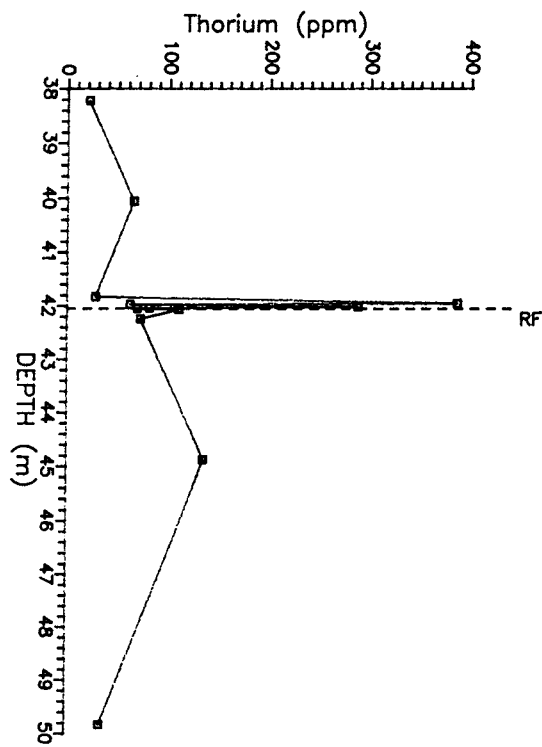


Figure 39. Thorium concentration profile across the 42.0 m redox front in the F1 drillcore.

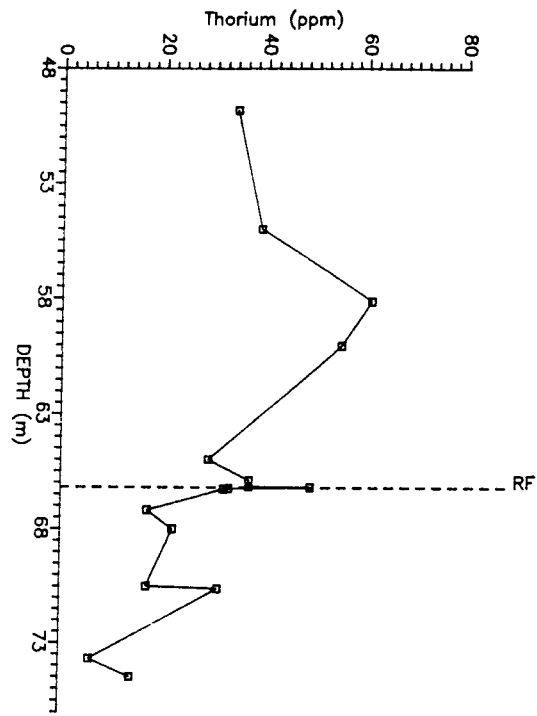


Figure 40. Thorium concentration profile across the 66.2 m redox front in the F1 drillcore.

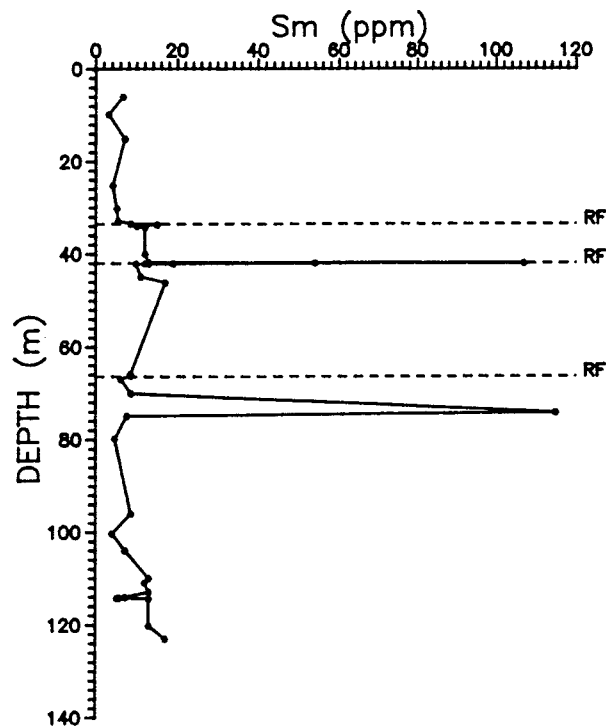


Figure 41. Samarium concentration profile in the F1 drillcore.

In contrast, the uranium enrichment in the reduced rock close to the 66.2 m redox front is less intense, with a maximum concentration of 207 ppm, but extends over a distance of some 4 m into the reduced rock. Thus, while markedly higher concentrations of uranium are observed in the reduced rock at the 42.0 m front than at the 66.2 m front, the total quantity of uranium in the reduced rock in both cases is probably similar. Moreover, the oxidized rock adjoining the 66.2 m redox front has a more pronounced enrichment of uranium extending over a greater distance than does the corresponding oxidized rock adjoining the 42.0 m redox front. Thus the total enrichment of uranium around the 66.2 m redox front is almost certainly greater than that at 42.0 m.

The uranium enrichment pattern is thus the opposite of that for thorium in the F1 drillcore, with the downward movement of the redox front system clearly separating the two elements, with preferential downward displacement of the redox-sensitive and more mobile uranium relative to the much less soluble thorium. It should be noted that this pattern of relative enrichment of the two elements is entirely consistent with the previously postulated long-term direction of water flow being downwards along the front, with the degree of separation of the two elements increasing with increasing length of water flow path. The narrower band of enrichment at the 42.0 m redox front than at the other two is also consistent with the conclusion, derived above from the natural decay series radionuclide data, that the 42.0 m redox front has been effectively static on a 10^6 year timescale while the other two fronts are moving downwards at a rate of metres to tens of metres in 10^6 years. Finally, it can be observed that the apparent mobility of thorium for distances of up to 0.5 m in the reduced rock supports the argument derived in the natural decay series discussion that uranium is mobile over significant distances in the reduced phonolite (presumably as U(IV)).

The rare-earth elements, like thorium, generally exhibit a low solubility in groundwater, being highly prone to removal from solution by hydrolysis and by particulate scavenging, and (generally) being preferentially concentrated in resistates during weathering. The data in Table VI reveal that the rare-earth element distributions in the F1 drillcore are dominated by a mineralization at sample 75-1A but otherwise show enrichment patterns similar to thorium at the redox fronts, with a broad, low maximum in the reduced rock at 33.4 m, a narrower but more intense enrichment at 42.0 m, and almost no enrichment at 66.2 m. This pattern is illustrated for Sm and Lu in Figures 41 and 42 and the details of the distribution of Lu in the transect across the 33.4 m and 42.0 m redox fronts in Figures 43 and 44 clearly parallel those of thorium shown in Figures 38 and 39. Eu, which can participate in redox-controlled geochemical processes by reduction to the 2+ oxidation state from the 3+ state normally exhibited by the

TABLE VI
Quantitative ICP-MS results (ppm) for analyses of F1 drillcore sample for rare-earth elements.

Sample	La	Ce	Pr	Nd	Sm	Eu	Gd	Tb	Dy	Ho	Er	Tm	Yb	Lu	Hf
16-1A	160 ± 2	203 ± 2	21.8 ± 0.2	56.5 ± 0.4	5.88 ± 0.17	1.68 ± 0.03	5.55 ± 0.16	0.78 ± 0.02	5.13 ± 0.23	0.99 ± 0.02	2.77 ± 0.17	0.39 ± 0.03	2.14 ± 0.08	0.28 ± 0.02	
26-1A	98 ± 1	98 ± 1	11.8 ± 0.1	30.8 ± 0.5	3.94 ± 0.34	1.56 ± 0.01	5.35 ± 0.05	1.12 ± 0.02	8.03 ± 0.11	1.4 ± 0.02	3.47 ± 0.04	0.56 ± 0.03	3.48 ± 0.06	0.45 ± 0.01	
33-1A	122 ± 1	208 ± 3	–	39.2 ± 0.8	4.25 ± 0.12	3.24 ± 0.10	5.59 ± 0.17	0.85 ± 0.03	–	1.44 ± 0.05	–	0.73 ± 0.03	4.66 ± 0.20	0.72 ± 0.07	–
34-1B-D	120 ± 2	172 ± 1	–	53.7 ± 0.8	6.82 ± 0.22	3.36 ± 0.12	11.2 ± 0.2	2.10 ± 0.02	–	2.52 ± 0.04	–	0.81 ± 0.06	4.43 ± 0.22	0.60 ± 0.16	–
34-1B-F	95.2 ± 1	160 ± 1	165 ± 0.1	46.3 ± 0.7	7.27 ± 0.14	3.24 ± 0.05	10.8 ± 0.3	2.14 ± 0.04	13.3 ± 0.24	2.20 ± 0.11	4.74 ± 0.11	0.67 ± 0.01	3.87 ± 0.10	0.47 ± 0.02	
42-1A	107 ± 1	89 ± 1	–	48.1 ± 1.2	9.70 ± 0.30	4.47 ± 0.11	12.0 ± 0.3	2.60 ± 0.05	–	3.34 ± 0.03	–	1.25 ± 0.08	7.60 ± 0.27	0.94 ± 0.03	
42-1B-H	167 ± 1	102 ± 1	16.6 ± 0.1	42.8 ± 0.5	5.19 ± 0.14	1.73 ± 0.06	6.1 ± 0.2	1.21 ± 0.02	9.1 ± 0.24	1.89 ± 0.03	5.33 ± 0.06	0.86 ± 0.05	5.32 ± 0.13	0.70 ± 0.01	
42-1B-I	197 ± 1	204 ± 2	21.7 ± 0.1	55.8 ± 0.7	6.16 ± 0.10	1.84 ± 0.03	6.4 ± 0.1	1.13 ± 0.04	7.8 ± 0.12	1.60 ± 0.04	4.18 ± 0.07	0.65 ± 0.01	3.84 ± 0.12	0.50 ± 0.04	
42-1B-K	208 ± 1	216 ± 1	23.9 ± 0.1	61.4 ± 0.7	6.96 ± 0.12	2.18 ± 0.05	7.7 ± 0.1	1.46 ± 0.02	11.0 ± 0.19	2.31 ± 0.04	6.39 ± 0.06	1.00 ± 0.03	6.14 ± 0.20	0.81 ± 0.03	
42-1B-K	196 ± 5	204 ± 4	21.6 ± 0.4	54.1 ± 1.8	6.12 ± 0.18	1.99 ± 0.07	7.2 ± 0.3	1.20 ± 0.07	9.3 ± 0.28	1.82 ± 0.06	5.47 ± 0.40	0.86 ± 0.06	5.06 ± 0.17	0.64 ± 0.03	
43-1A	129 ± 3	209 ± 4	15.2 ± 0.2	38.5 ± 1.3	4.21 ± 0.19	1.27 ± 0.11	3.85 ± 0.15	0.56 ± 0.02	3.92 ± 0.14	0.83 ± 0.06	2.55 ± 0.24	0.40 ± 0.1	2.70 ± 0.01	0.37 ± 0.01	
66-1A-A	170 ± 1	161 ± 1	20.7 ± 0.1	55.2 ± 0.4	6.40 ± 0.19	2.15 ± 0.04	6.60 ± 0.19	1.08 ± 0.04	7.56 ± 0.14	1.61 ± 0.02	4.62 ± 0.16	0.76 ± 0.01	4.95 ± 0.32	0.69 ± 0.05	
67-1A-D	161 ± 6	286 ± 12	21.0 ± 0.4	53.4 ± 0.8	6.05 ± 0.11	1.92 ± 0.02	6.74 ± 0.35	0.93 ± 0.02	5.88 ± 0.26	1.18 ± 0.06	2.98 ± 0.12	0.46 ± 0.01	2.62 ± 0.16	0.35 ± 0.02	
67-1A-D	157 ± 1	269 ± 1	20.5 ± 0.2	53.0 ± 0.3	5.98 ± 0.06	1.82 ± 0.06	6.57 ± 0.17	0.90 ± 0.01	5.65 ± 0.10	1.09 ± 0.02	2.88 ± 0.09	0.41 ± 0.01	2.43 ± 0.10	0.33 ± 0.04	
68-1A-A	146 ± 1	237 ± 1	17.2 ± 0.2	43.8 ± 0.5	4.77 ± 0.12	1.43 ± 0.05	4.36 ± 0.11	0.63 ± 0.02	4.45 ± 0.30	0.94 ± 0.02	2.90 ± 0.11	0.46 ± 0.03	3.06 ± 0.12	0.42 ± 0.01	
80-1A	77.9 ± 1	127 ± 1	9.91 ± 0.07	25.8 ± 0.4	2.67 ± 0.09	0.88 ± 0.04	2.71 ± 0.25	0.32 ± 0.02	1.57 ± 0.07	0.35 ± 0.02	0.98 ± 0.07	0.16 ± 0.01	1.00 ± 0.11	0.13 ± 0.01	
101-1A	195 ± 1	285 ± 1	23.1 ± 0.12	5.92 ± 0.3	5.96 ± 0.04	2.11 ± 0.02	7.02 ± 0.15	1.19 ± 0.02	8.33 ± 0.06	1.40 ± 0.01	3.12 ± 0.12	0.39 ± 0.01	2.49 ± 0.08	0.33 ± 0.01	
110-1A	158 ± 3	313 ± 5	21.0 ± 0.4	54.4 ± 1.3	6.77 ± 0.27	2.27 ± 0.08	8.54 ± 0.26	1.44 ± 0.07	9.46 ± 0.13	1.67 ± 0.06	3.52 ± 0.16	0.50 ± 0.03	2.74 ± 0.24	0.36 ± 0.02	
121-1A	208 ± 4	310 ± 6	24.2 ± 0.5	60.8 ± 1.4	5.28 ± 0.12	1.77 ± 0.07	5.45 ± 0.11	0.69 ± 0.04	5.23 ± 0.43	1.22 ± 0.11	3.28 ± 0.09	0.41 ± 0.02	2.14 ± 0.07	0.26 ± 0.02	

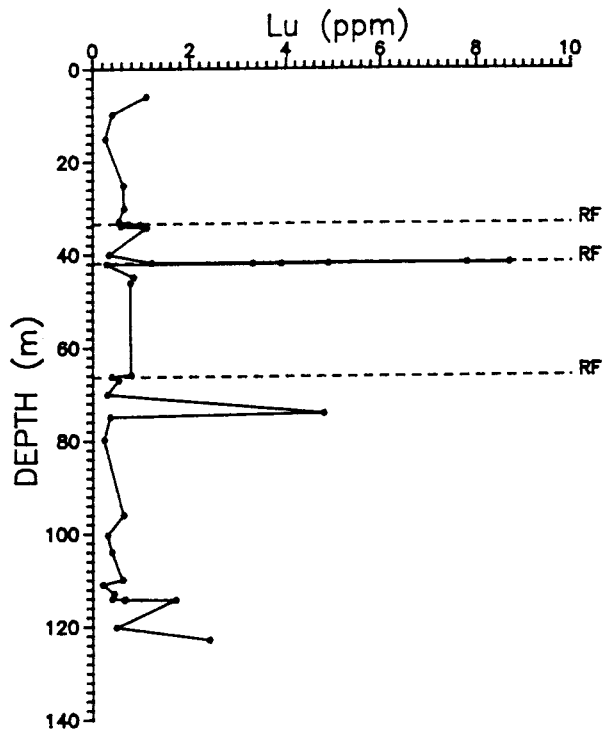


Figure 42. Lutetium concentration profile in the F1 drillcore.

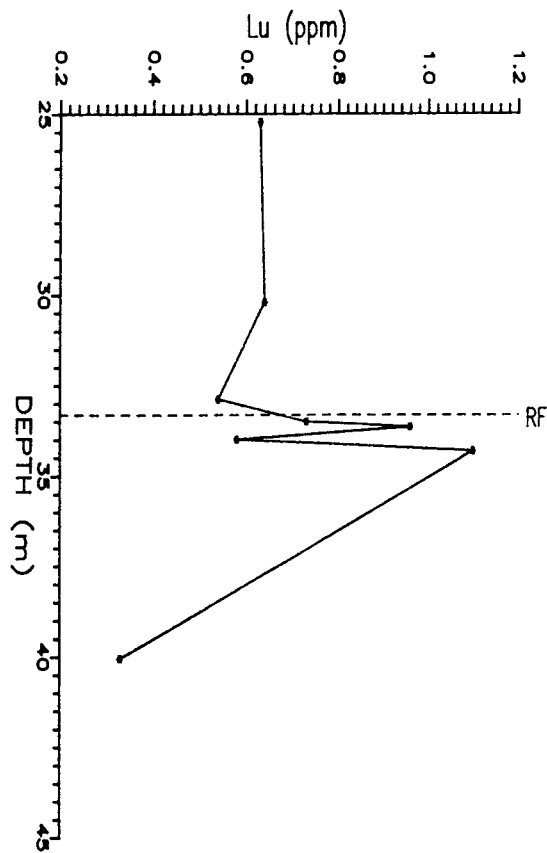


Figure 43. Lutetium concentration profile across the 33.4 m redox front in the F1 drillcore.

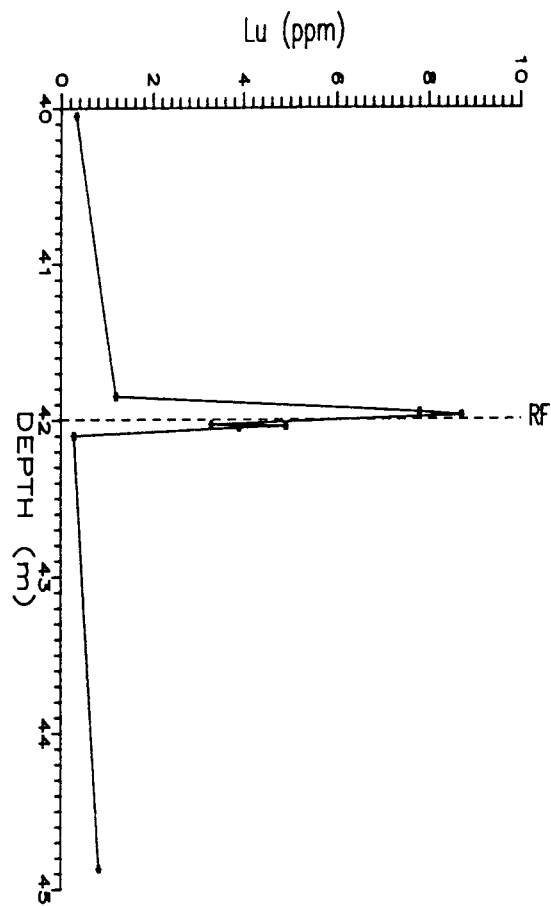


Figure 44. Lutetium concentration profile across the 42.0 m redox front in the F1 drillcore.

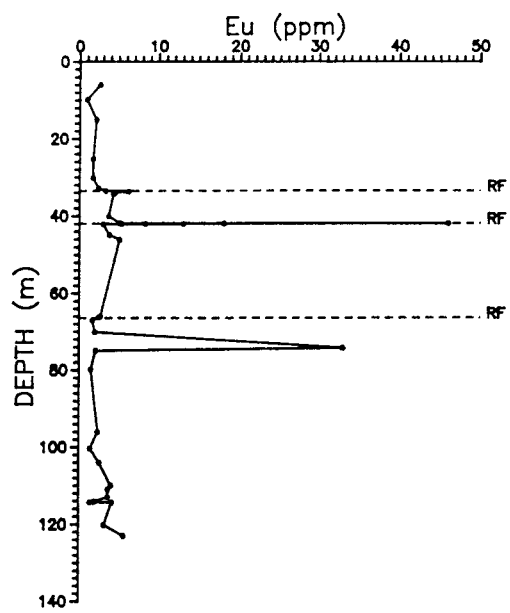


Figure 45. Europium concentration profile in the F1 drillcore.

rare-earth elements, shows no significant evidence of the operation of such effects in the concentration profiles for the F1 drillcore as illustrated in Figures 45 to 47. Sc and Y, which also exist in the 3+ oxidation state, show similar concentration trends to the rare-earth elements, although Sc does not exhibit a high concentration at sample 75-1A whereas Y does.

In sharp contrast to the other rare-earth elements, Ce (which is recognized as participating in redox reactions by oxidation from the normal 3+ to the 4+ oxidation state) has a concentration profile in the F1 drillcore which is dominated by a large peak in the oxidized rock between the 42.0 m and 66.2 m redox fronts, with a maximum concentration of 6279 ppm at sample 47-1A (Fig. 48). An enrichment in Ce concentration is observed on the reduced side of the 33.4 m redox front (Fig. 49), but not at the 42.0 m or 66.2 m fronts (Figs. 48 and 50).

The general conclusion can therefore be drawn from the above observation that non-redox-sensitive, refractory 3+ and 4+ oxidation state species behave in a systematic manner at the redox fronts, with preferential concentration in the reduced rock close to the fronts. Eu, which is involved in geochemical processes by reduction, does not exhibit any major deviation from the behaviour of the other rare-earth elements, but Ce (which is susceptible to oxidation to the 4+ oxidation state) does show a radically different distribution, with pronounced concentration in the oxidized phonolite between the 42.0 m and 66.2 m redox fronts.

Chondrite normalized concentration plots for the rare-earth elements can provide further details about the processes occurring and Figures 51 and 52 provide plots for samples 16-1A and 121-1A, the highest and lowest samples analyzed from the drillcore. It is immediately obvious from these graphs that there is a slight depletion of the light rare-earth elements in sample 16-1A relative to sample 121-1A, but otherwise the concentrations and trends in the two plots are very similar. This observation could lead to the conclusion that passage of the redox front through the phonolite results in very little change in the rare-earth element concentrations and, notably, there is no evident effect on the two redox-sensitive rare-earth elements Ce and Eu. This is, however, too simple a picture as is revealed by the chondrite normalized concentration plots for other samples from the drillcore. Sample 26-1A (Fig. 53), for example, shows a pronounced depletion of the light rare-earths and an enrichment of the heavy rare-earths relative to sample 121-1A, indicative of decreasing reactivity along the series during weathering. A similar situation applies to sample 34-1B-F from the reduced side of the 33.4 m redox front (Fig. 54), with the enrichment of heavy and middle rare-earth elements being even more pronounced in this case.

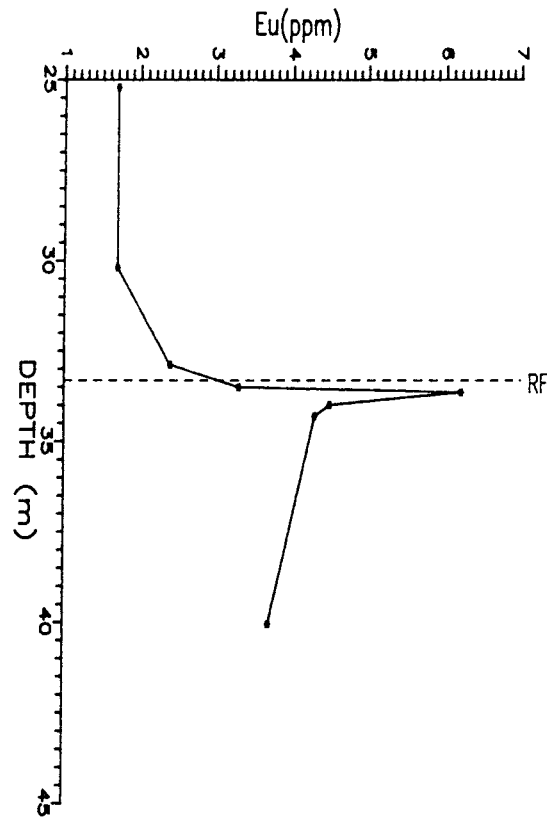


Figure 46. Europium concentration profile across the 33.4 m redox front in the F1 drillcore.

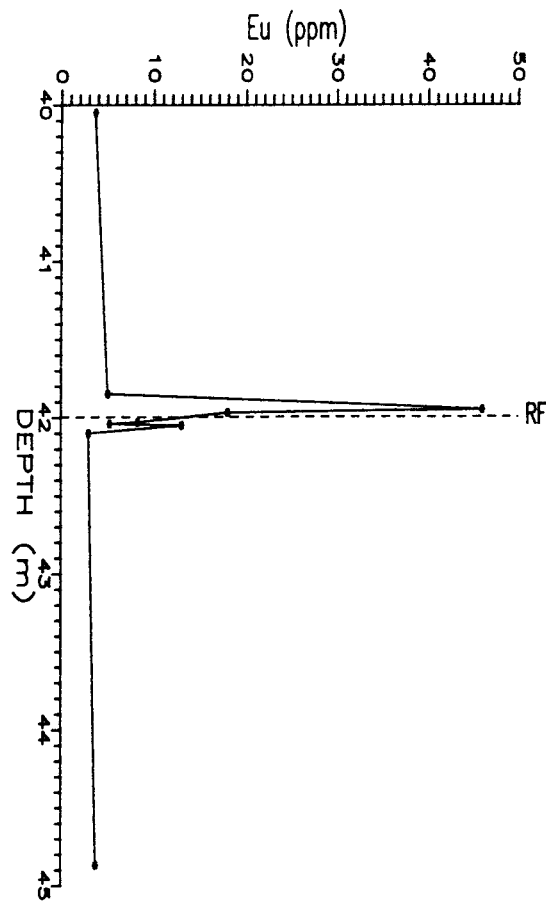


Figure 47. Europium concentration profile across the 42.0 m redox front in the F1 drillcore.

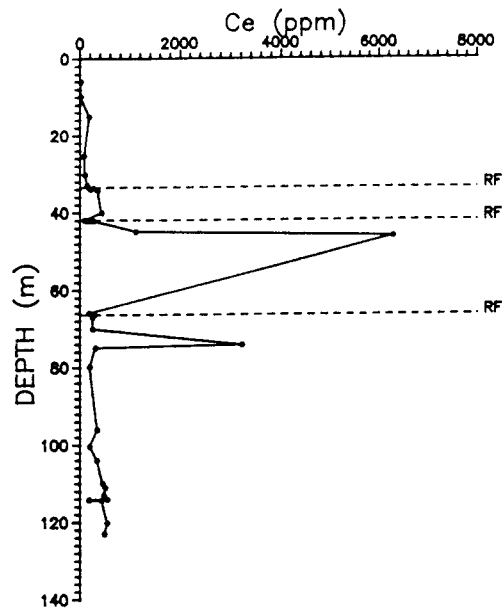


Figure 48. Cerium concentration profile in the F1 drillcore.

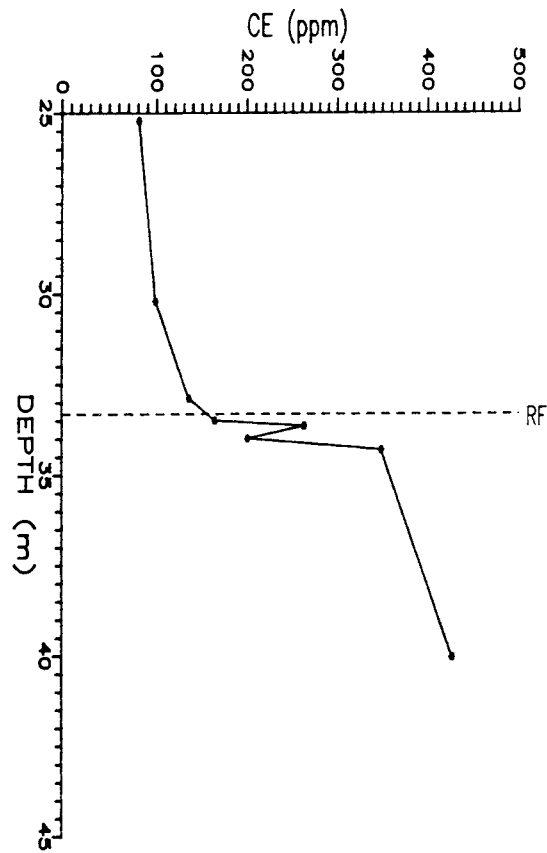


Figure 49. Cerium concentration profile across the 33.4 m redox front in the F1 drillcore.

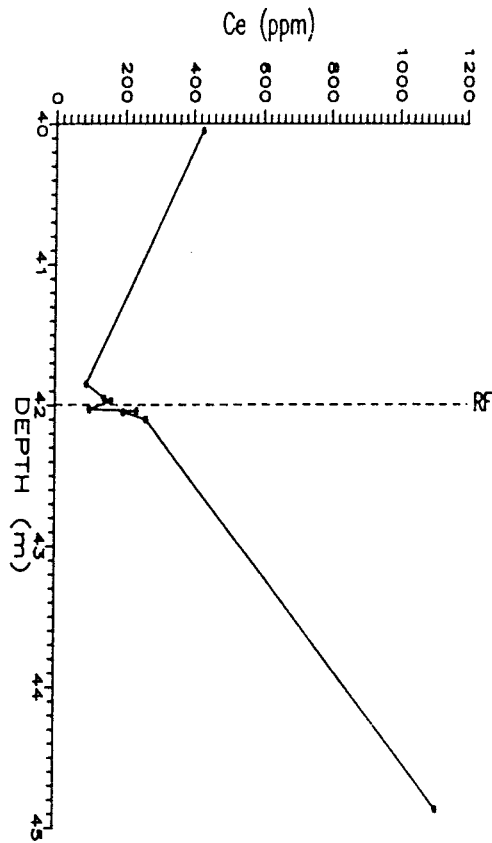


Figure 50. Cerium concentration profile across the 42.0 m redox front in the F1 drillcore.

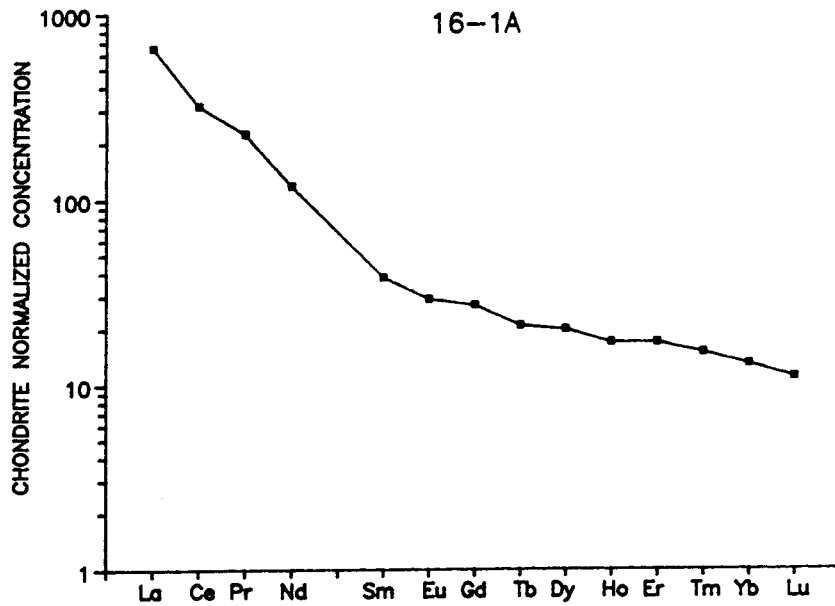


Figure 51. Chondrite normalized concentration ratio plot for rare-earth elements in sample 16-1A from the F1 drillcore.

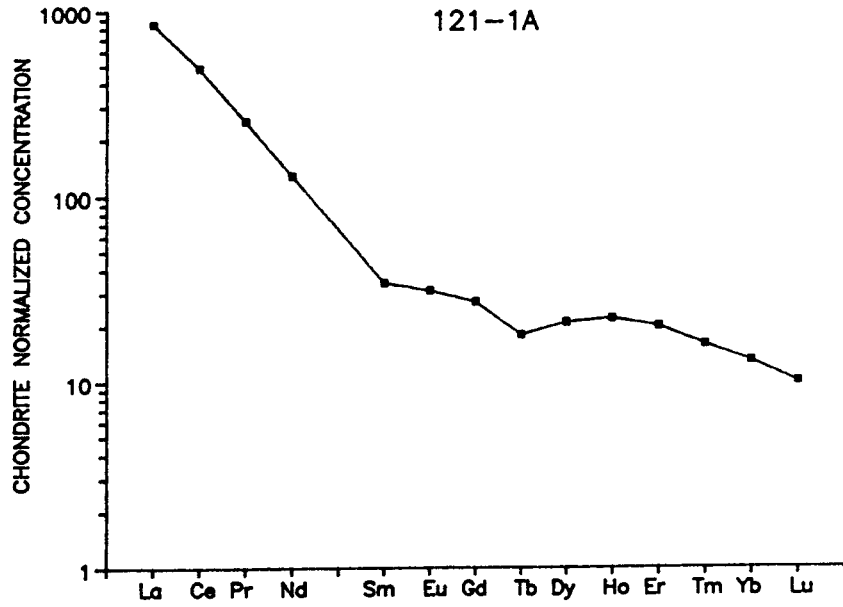


Figure 52. Chondrite normalized concentration ratio plot for rare-earth elements in sample 121-1A from the F1 drillcore.

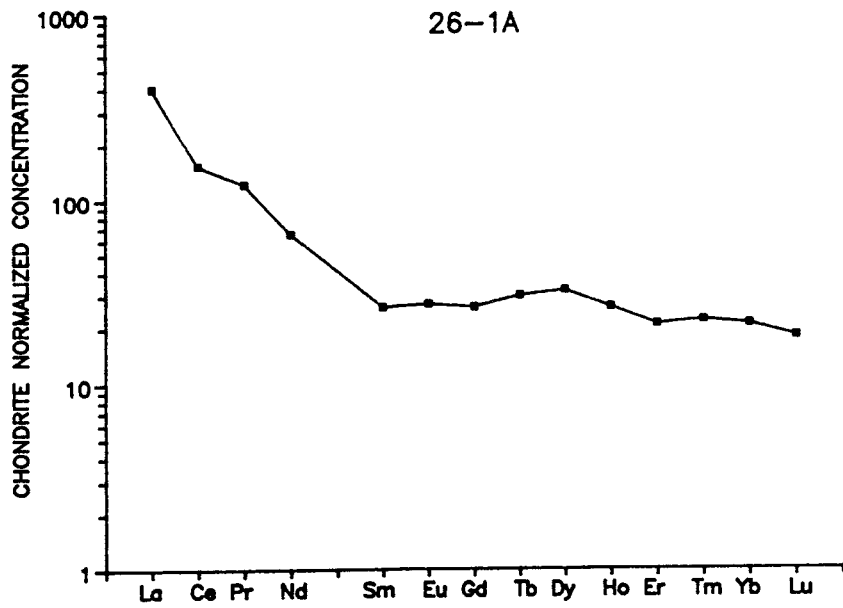


Figure 53. Chondrite normalized concentration ratio plot for rare-earth elements in sample 26-1A from the F1 drillcore.

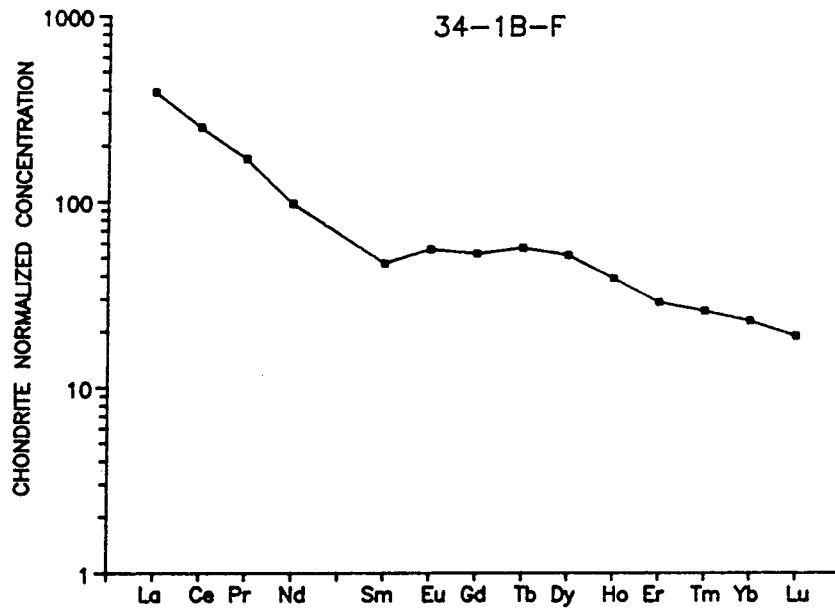


Figure 54. Chondrite normalized concentration ratio plot for rare-earth elements in sample 34-1B-F from the F1 drillcore.

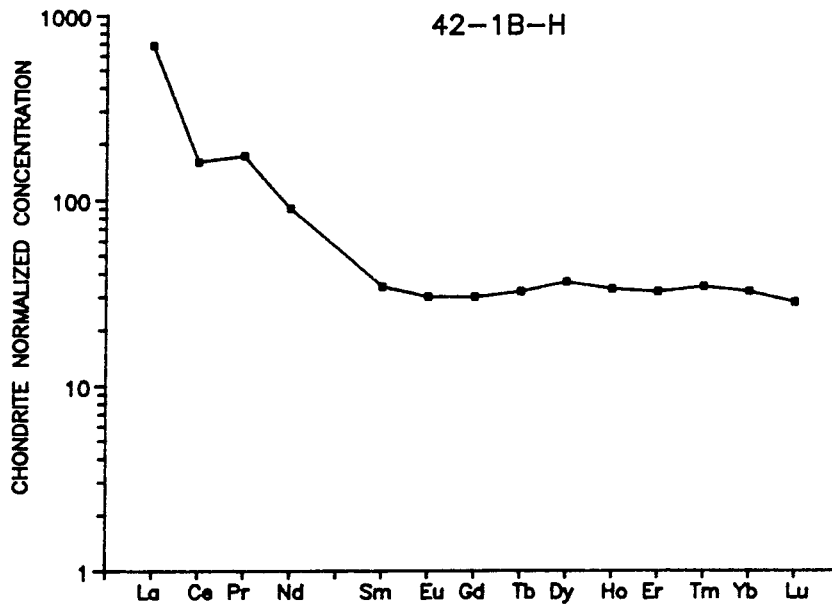


Figure 55. Chondrite normalized concentration ratio plot for rare-earth elements in sample 42-1B-H from the F1 drillcore.

There is some evidence of preferential loss of Ce from the reduced rock close to the redox front, as shown for sample 42-1B-H in Figure 55, where a distinct negative Ce anomaly is observed, consistent with the minimum in Ce concentration at this position (Fig. 55). In contrast, a pronounced Ce maximum occurs at sample 47-1A (Fig. 56), presumably due to oxidation of Ce to the 4+ oxidation state at this location close to the fissure at 50 m, where the downward flow of oxidizing water might be expected to be a maximum. Sample 47-1A also shows an unusual and strong anomalous enrichment in Gd and Tb.

The pronounced fractionation observed in sample 47-1A is in contrast to the rare-earth element pattern for sample 75-1A from the reduced phonolite, which shows very high rare-earth element concentrations. In the case of sample 75-1A (Fig. 57), there is evidence that the degree of enrichment of the light rare-earth elements is somewhat lower than that of the heavy rare-earth elements relative to other reduced phonolites, e.g. sample 121-1A, and there is a slight negative Ce anomaly, but in general there is no evidence of major fractionation within the series.

Thus, while there is no major difference apparent between the concentrations of the rare-earth elements in samples 16-1A and 121-1A (with the exception of a slight depletion of the light rare-earths in 16-1A), it is clear that the situation is more complex in other parts of the drillcore, and in some cases pronounced fractionation can occur. In an attempt to assess the overall effect of the processes occurring at different depths in the drillcore, the average rare-earth element concentrations were calculated for the rock in the following depth intervals: 0 to 33.4 m (oxidized rock above the uppermost redox front); 33.4 to 42.0 m (reduced rock below the 33.4 and 42.0 m fronts); 42.0 m to 66 m (oxidized rock between the 42.0 and 66.2 m redox fronts); 66 m to 75 m (reduced rock below the 66.2 m redox front, in the area of high uranium content); greater than 75 m (average reduced rock). The ratio of the average rare-earth element concentrations in the first 4 sections to the average concentrations in the reduced rock below 75 m were then calculated, with the results being given in Table VII and plotted in Figures 58 to 61. In this form of presentation, pronounced variations in the rare-earth element distributions are apparent. It is clear from Figure 58 that the average oxidized rock above 33.4 m is generally depleted in the rare-earth elements relative to the average reduced rock and that the degree of depletion decreases along the series. Moreover, a distinct Eu anomaly is evident along with, arguably, a positive La or negative Gd anomaly. The trend of this plot is reasonable in terms of reflecting decreased reactivity along the series during weathering and the positive Eu anomaly might also be expected on the basis of the preferential loss of Eu(II) from the reduced rock. Figure 59 indicates that the

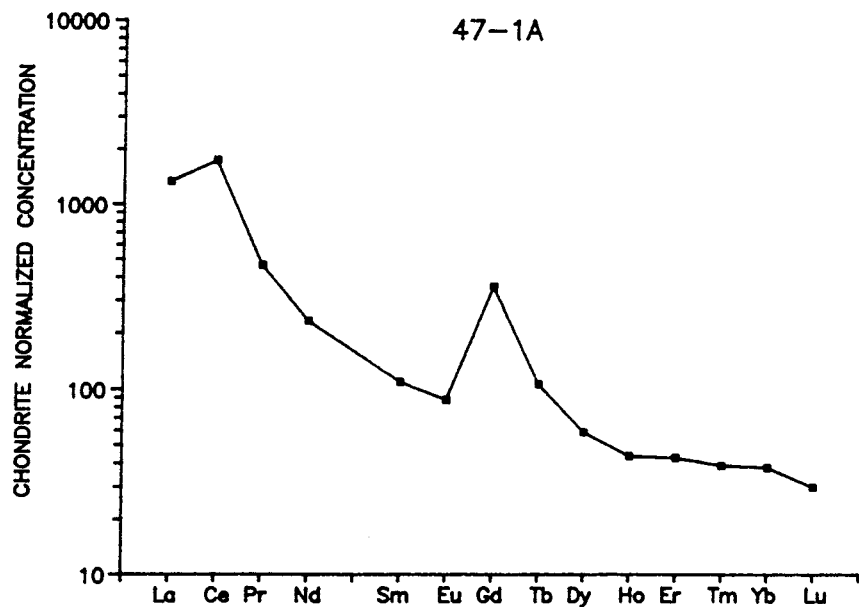


Figure 56. Chondrite normalized concentration ratio plot for rare-earth elements in sample 47-1A from the F1 drillcore.

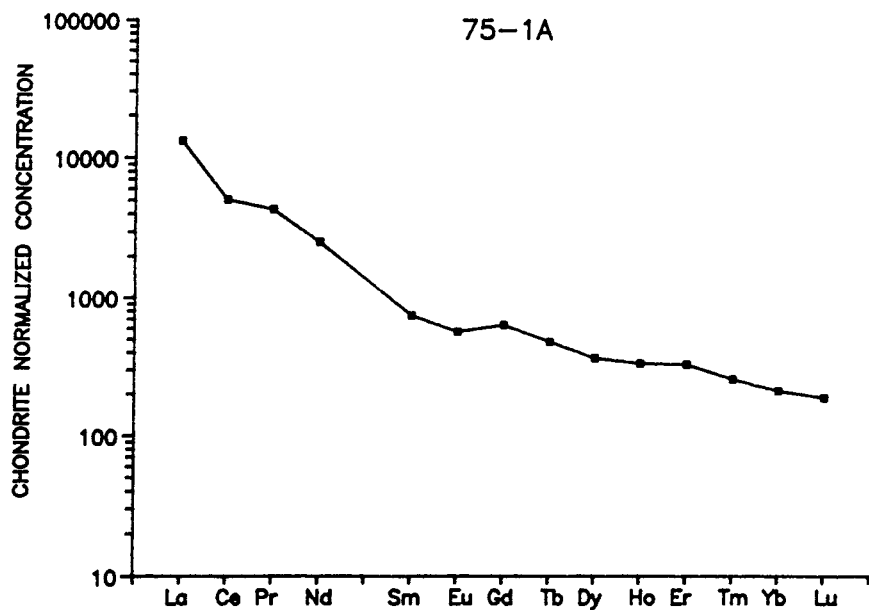


Figure 57. Chondrite normalized concentration ratio plot for rare-earth elements in sample 75-1A from the F1 drillcore.

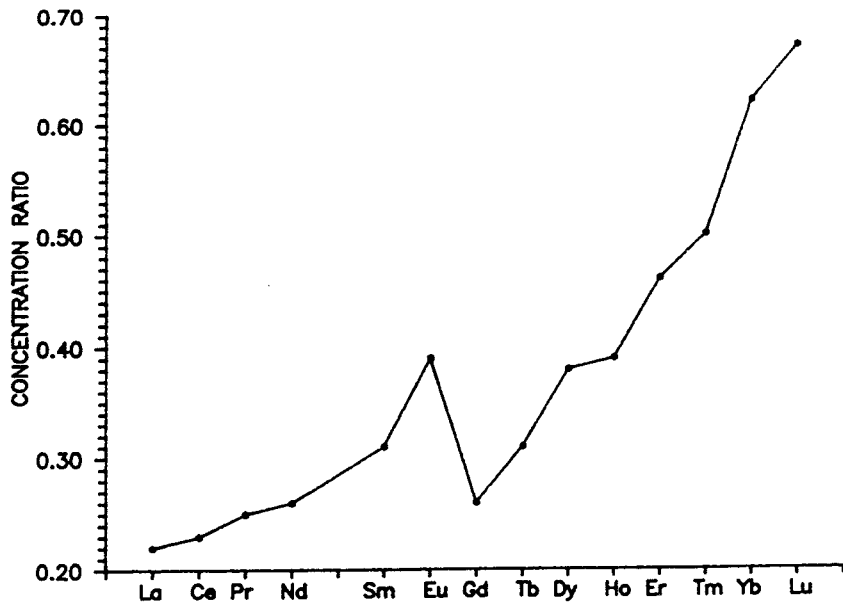


Figure 58. Plot showing the ratio of average rare-earth element concentrations in the 0 to 33 m section of the F1 drillcore to average concentrations in the section below 75 m.

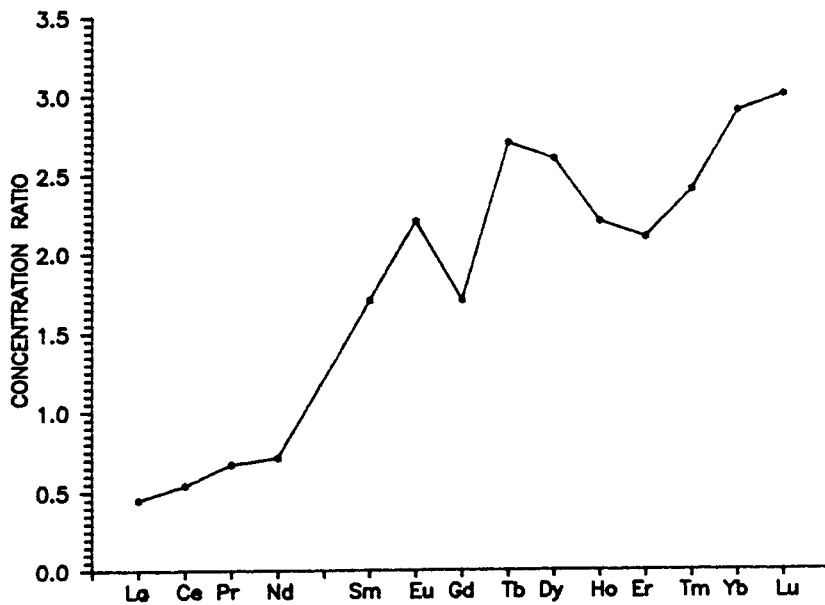


Figure 59. Plot showing the ratio of average rare-earth element concentrations in the 33.4 to 42.0 m section of the F1 drillcore to average concentrations in the section below 75 m.

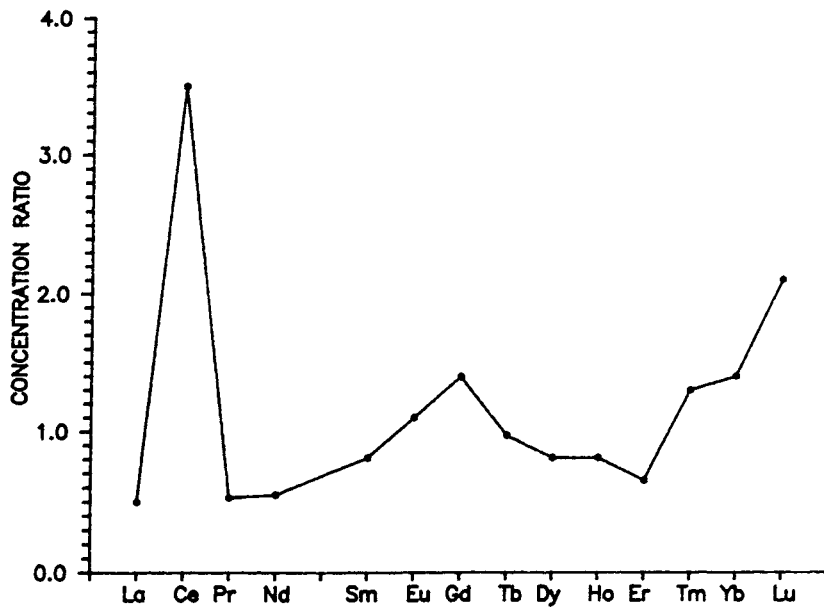


Figure 60. Plot showing the ratio of average rare-earth element concentrations in the 42.0 to 66.2 m section of the F1 drillcore to average concentrations in the section below 75 m.

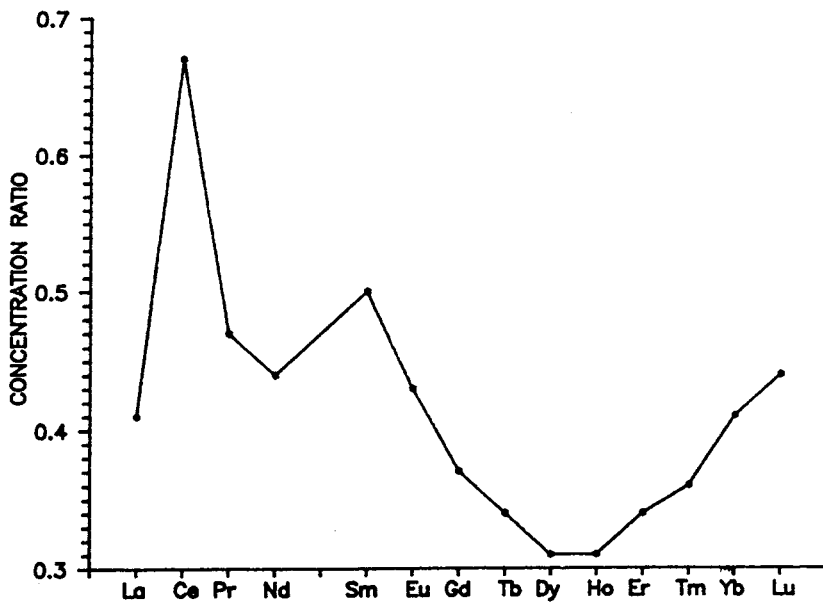


Figure 61. Plot showing the ratio of average rare-earth element concentrations in the 66.2 to 75 m section of the F1 drillcore to average concentrations in the section below 75 m.

reduced rock lying between the 33.4 m and 42.0 m redox fronts is depleted in the high light rare-earth elements (La-Na) but enriched in the others relative to the average reduced rock. There is, moreover, a complex structure in the graph within the enrichment sector with maxima at Eu and Tb and minima at Gd and Er. The oxidized rock between the 42.0 m and 66.2 m redox fronts (Fig. 60) shows a different pattern of relative rare-earth element abundance to that observed for the oxidized rock above 33.4 m (Fig. 58). For the rock between 42.0 and 66.2 m, there is a pronounced enrichment in Ce and lesser enrichments of Eu, Gd, Tm, Yb and Lu relative to the average reduced phonolite, while the other rare-earth elements show varying degrees of depletion. The major enhancement of the Ce concentration in this case is consistent with the preferential fixation of Ce(IV) in the prevailing oxidizing conditions. Finally, Figure 61 reveals a general depletion of the rare-earth elements in the reduced rock from 66 m to 75 m relative to the underlying rock, with the degree of depletion being most pronounced for Dy and Ho and with distinct maxima for Ce and Sm.

In summary, therefore, the rare-earth element data reveal a general loss of these elements from the oxidized rock as the redox front moves down through the phonolite, with the degree of loss being greater for the light rare-earth elements. Fractionation of Eu and Ce from the other rare-earth elements is observed, but in some other cases there is also fractionation of elements in the series which are not normally regarded as being redox-sensitive, e.g. Gd.

The approach of comparing the average concentration of elements in the reduced rock below 75 m to the average concentrations in the overlying sections of rock, employed above for the rare-earth elements, can be usefully extended to other elements and the concentration ratios derived in this way from the data in Table V are presented in Tables VIII to XII. A summary table showing various combinations of enrichment or depletion of different elements in the various depth increments of the drillcore is presented in Table XIII. A number of systematic trends and groupings of elements in accordance with their position in the periodic table are apparent in this summary. Thus, as might be expected, the most soluble elements such as Mg, Ca and Sr are grouped together by being depleted in all of the overlying rock relative to the reduced phonolite, indicating a general removal of the species from the system by groundwater. Interestingly, the redox-sensitive elements As and Mn also appear in this group, as do La, Hf and the light rare-earth elements Pr and Nd. Ce and Li are grouped together as being enriched in the oxidized rock between 42.0 m and 66.2 m while Y, Sm, Tb, Dy, Ho and Er are enriched only in the reduced rock between the 33.4 and 42.0 m redox fronts. A large group of elements including the remaining rare-earths, the noble metals, Sc, Cu,

TABLE VII

Ratios of average rare-earth element and thorium and uranium concentrations in upper sections of the F1 drillcore to average concentrations in the section below 75 m.

Section	Ce	Pr	Nd	Sm	Eu	Gd	Tb	Dy	Ho	Er	Tm	Yb	Lu	U	Th
Oxidized rock above 33.4 m	0.23	0.25	0.26	0.31	0.39	0.26	0.31	0.38	0.39	0.46	0.50	0.62	0.67	1.4	1.4
Reduced rock 33.4 – 42.0 m	0.54	0.67	0.71	1.7	2.2	1.7	2.7	2.6	2.2	2.1	2.4	2.9	3.0	96	3.5
Oxidized rock 42.0 – 66 m	3.5	0.53	0.55	0.81	1.1	1.4	0.97	0.81	0.81	0.65	1.3	1.4	2.1	4.4	1.8
Reduced rock 66 – 75 m	0.67	0.47	0.44	0.50	0.43	0.37	0.34	0.31	0.31	0.34	0.36	0.41	0.44	3.8	0.78

TABLE VIII

Ratios of average S-block element concentrations in upper sections of the F1 drillcore to average concentrations in the section below 75 m.

Section	Li	Be	Mg	Ca	Rb	Sr	Ca	Ba
Oxidized rock above 33.4 m	0.93	1.2	0.31	0.25	1.01	0.53	0.71	1.78
Reduced rock between 33.4 and 42 m	0.86	5.0	0.56	0.46	1.15	0.75	2.29	1.00
Oxidized rock between 42 and 66 m	1.01	4.4	0.79	0.63	1.10	0.92	2.43	1.06
Reduced rock between 66 and 75 m	1.09	0.6	0.98	0.42	1.22	0.68	0.71	0.40

TABLE IX

Ratios of average d-block (Sc-Zn) element concentrations in upper sections of the F1 drillcore to average concentrations in the section below 75 m.

Section	Sc	Ti	V	Cr	Mn	Fe	Co	Ni	Cu	Zn
Oxidized rock above 33.4 m	0.26	1.11	0.87	1.06	0.43	1.39	0.61	0.55	0.91	0.09
Reduced rock between 33.4 and 42 m	4.6	1.49	0.61	5.3	0.60	0.91	6.27	6.30	10.7	0.10
Oxidized rock between 42 and 66 m	2.9	1.51	0.75	7.1	0.68	1.60	4.33	6.13	5.44	0.12
Reduced rock between 66 and 75 m	0.41	1.24	0.67	0.5	0.57	1.47	1.61	0.68	0.43	1.53

TABLE X

Ratios of average d-block (Y-Cd) element concentrations in upper sections of the F1 drillcore to average concentrations in the section below 75 m.

Section	Y	Zr	Nb	Mo	Ru	Rh	Pd	Ag	Cd
Oxidized rock above 33.4 m	0.33	0.55	0.85	4.05	1.0	0.5	0.54	0.50	0.28
Reduced rock between 33.4 and 42 m	1.66	0.44	1.18	4.50	301	224	2.5	1.7	4.0
Oxidized rock between 42 and 66 m	0.56	0.60	1.18	9.72	284	200	2.5	2.1	4.4
Reduced rock between 66 and 75 m	0.31	0.64	1.93	2.28	0.5	1.0	0.90	1.1	10.8

TABLE XI

Ratios of average d-block (La-Hg) element concentrations in upper sections of the F1 drillcore to average concentrations in the section below 75 m.

Section	La	Hf	Ta	W	Re	Os	Ir	Pt	Au	Hg
Oxidized rock above 33.4 m	0.22	0.35	0.85	1.06	5.0	0.5	0.03	0.28	0.41	1.2
Reduced rock between 33.4 and 42 m	0.45	0.37	1.02	1.6	183	29	19	13	4.5	25
Oxidized rock between 42 and 66 m	0.50	0.46	1.6	1.7	153	48	32	16	6.2	17
Reduced rock between 66 and 75 m	0.41	0.36	1.6	0.77	3	-	0.17	0.33	0.45	0.18

TABLE XII

Ratios of average p-block element concentrations in upper sections of the F1 drillcore to average concentrations in the section below 75 m.

Section	B	Al	Ga	Ge	As	Se	Sn	Sb	Te	Tl	Pb	Bi
Oxidized rock above 33.4 m	0.55	1.1	1.4	0.81	0.72	1.3	1.2	0.89	1.3	2.2	0.90	2.3
Reduced rock between 33.4 and 42 m	1.35	1.4	1.5	5.9	0.42	5.9	1.9	3.9	64	5.6	1.4	22
Oxidized rock between 42.0 and 66 m	1.7	1.3	1.5	5.5	0.96	8.5	1.8	3.1	57	5.9	1.3	33
Reduced rock between 66 and 75 m	0.28	0.51	1.0	1.0	0.04	0.13	1.2	1.0	0	6.5	0.74	1.3

TABLE XIII

Summary of enrichment (E) and depletion (D) patterns for average elemental concentrations in upper sections of the F1 drillcore relative to average concentrations in the section below 75 m.

Section																
0 – 33.4 m	E	E	E	E	D	E	E	E	D	D	D	E	D	D	D	D
33.4 – 42 m	E	D	E	E	E	D	E	D	D	E	E	D	E	D	D	D
42 – 66.2 m	E	E	D	E	E	D	D	E	E	D	E	D	D	E	D	D
66.2 – 75 m	E	E	E	D	E	E	D	D	E	E	D	D	D	D	E	D

	Ga			Al	Ge						B				As	
	Sn			Se	Sb					Pb						
	Tl			Te												
	Bi															

	Rb			Be						Cs		Li		Mg		
				Ba										Ca		
														Sr		

	Ti	Fe			Co		Cr			Sc			Zn	V		
										Ni				Mn		
										Cu						
	Mo			Ru	Nb					Pd	Y			Zr		
					Rh											
					Ag											
					Cd											

	Re			W	Ta					Os				La		
				Hg						Ir				Hf		
										Pt						
										Au						

										Eu	Sn	Ce		Pr		
										Gd	Tb			Nd		
										Tm	Dy					
										Yb	Ho					
										Lu	Er					

	U			Th												

Pb and B are enriched in the middle two divisions considered, but depleted in the other two. The remaining elements are all enriched in at least 3 of the overlying sections of rock and include U, many of the redox-sensitive d-block elements (e.g. W, Ru, Co, Mo), most of the p-block elements analyzed, Rb, Ba and Th. Notably, Fe is the only element to be depleted in the reduced rock between 33.4 and 42.0 m (consistent with relatively soluble behaviour of Fe(II)) but enriched in the other three sections. The elements which are grouped along with U as being enriched in all four sections relative to the reduced phonolite are Re, Mo, Ti, Rb, Bi, Tl, Sn and Ga.

This approach thus provides a useful general guide to the behaviour of different elements within the F1 drillcore and it is worthwhile considering the distribution of

selected elements from different groups in Table XIII, both in the drillcore in general and in detail across the redox fronts. The distribution of Mo in the drillcore is shown in Figure 62, from which it is clear that the enrichment of Mo is most pronounced in the oxidized rock close to the redox fronts. This is illustrated in more detail in Figures 63 and 64 which show the concentration profiles for Mo across the 33.4 m and 42.0 m redox fronts. Two features are significant in these graphs, namely (a) the bimodal distribution of Mo around the position of the front, providing support for the hypothesis developed above for uranium of negligible advective flow of groundwater across the front and the distribution of elements dissolved at the front being dominated by diffusion away from the front into both the oxidized and reduced rock, and (b) the asymmetry of the distribution about the fronts with, in both cases, much higher concentrations in the oxidized rock indicative of deposition of some oxidized form of Mo or else highly effective uptake by iron oxides forming at these locations.

Rb is the only S-block element to exhibit general enrichment in the rocks above the reduced phonolite and its distribution across the uppermost two redox fronts is shown in Figures 65 and 66. Once more, a bimodal distribution of concentration about the two fronts is observed with a much narrower distribution about the 42.0 m front than the 33.4 m front, consistent with the previously developed concepts of water movement and relative rates of movement of these two fronts. This argument is in fact supported by the distribution of almost all of the elements which are enriched in at least 3 of the upper sections of rock as illustrated by selected examples in Figures 67 to 74 and by the noble metals as shown for Pd in Figures 75 and 76. Notable features in these graphs are the deposition of Fe on both sides of the redox fronts, giving the potential for scavenging of other elements at these positions, and the deposition of Ba in the oxidized rock close to the fronts, which could lend support to the concept of removal of ^{226}Ra from solution at these locations by coprecipitation with BaSO_4 .

The distribution of elements about the redox fronts can therefore be bimodal or asymmetric and the species exhibiting bimodal distribution include redox-sensitive elements such as U and Mo as well as elements which are not intrinsically involved in redox-controlled processes, such as Cs. In the case of the non-redox-sensitive elements, removal from solution in the vicinity of the redox fronts requires either that the solution phase concentrations of appropriate ions are high enough to lead to precipitation or that the mechanism involved is scavenging or coprecipitation with some major mineral species.

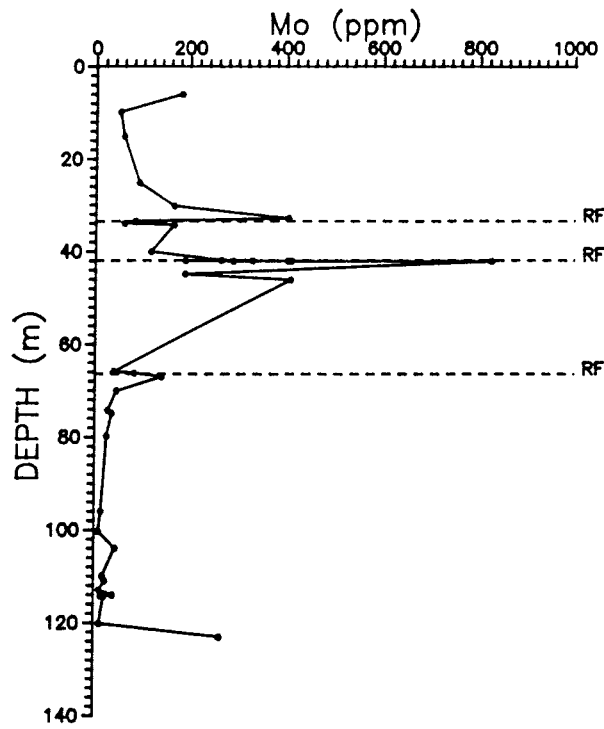


Figure 62. Molybdenum concentration profile in the F1 drillcore.

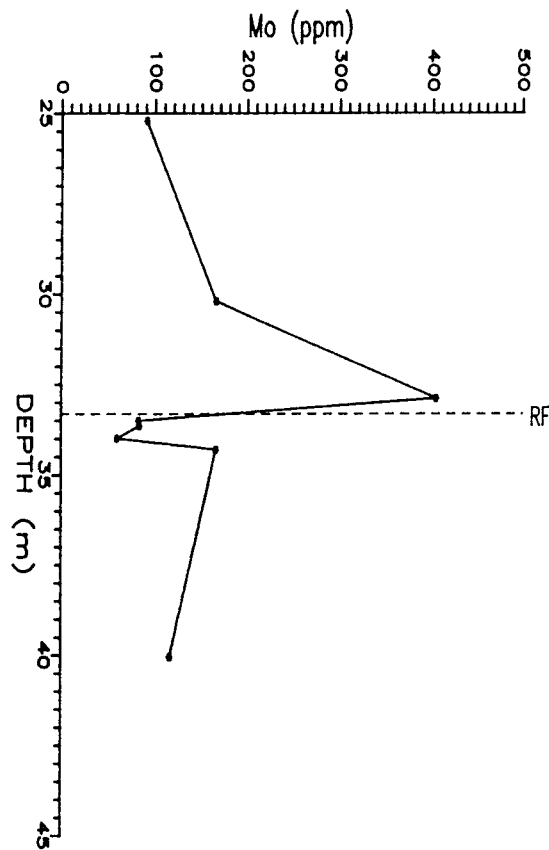


Figure 63. Molybdenum concentration profile across the 33.4 m redox front in the F1 drillcore.

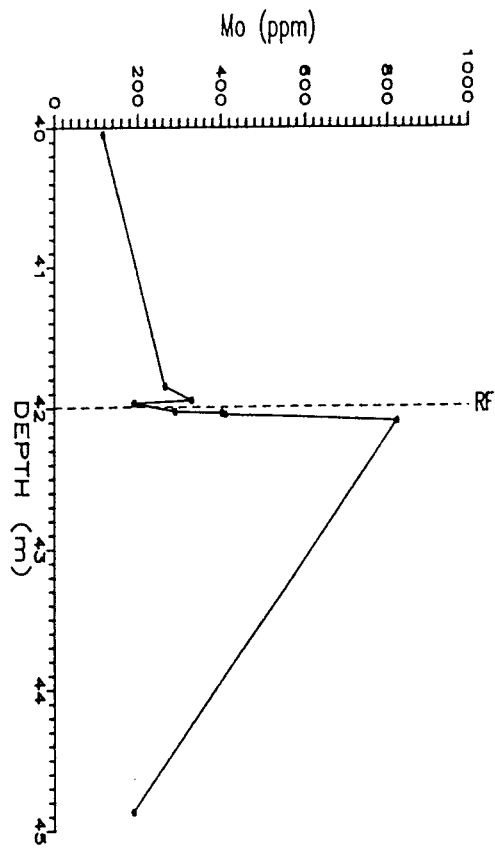


Figure 64. Molybdenum concentration profile across the 42.0 m redox front in the F1 drillcore.

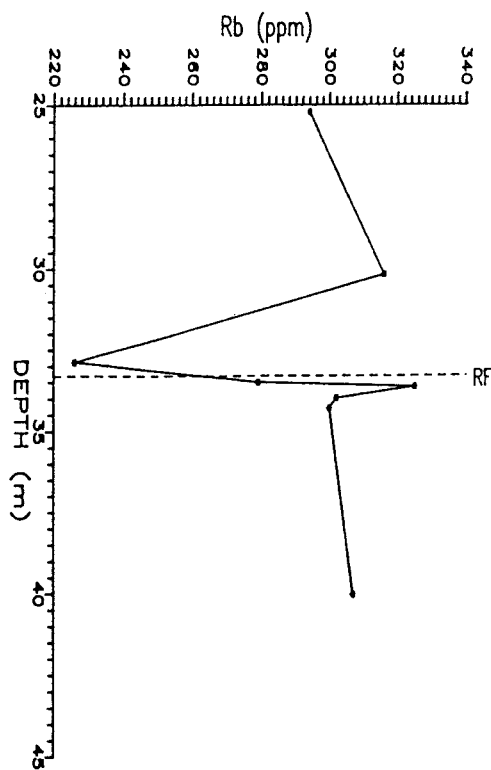


Figure 65. Rubidium concentration profile across the 33.4 m redox front in the F1 drillcore.

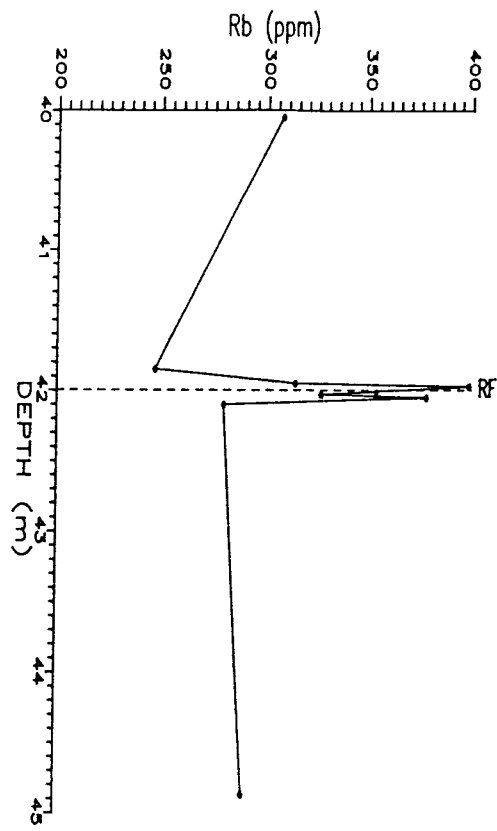


Figure 66. Rubidium concentration profile across the 42.0 m redox front in the F1 drillcore.

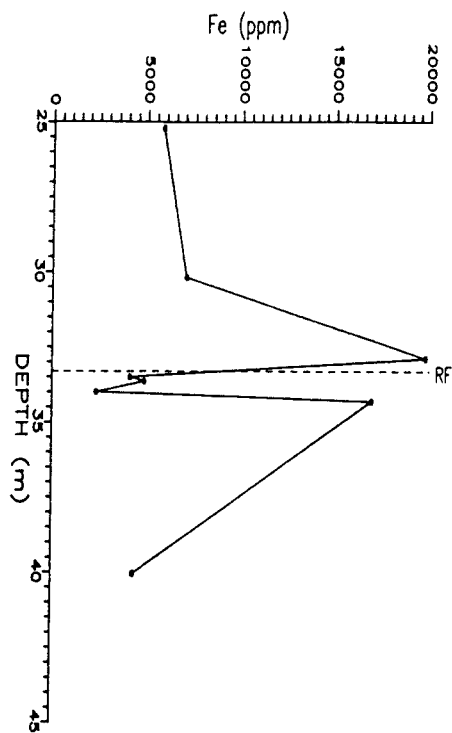


Figure 67. Iron concentration profile across the 33.4 m redox front in the F1 drillcore.

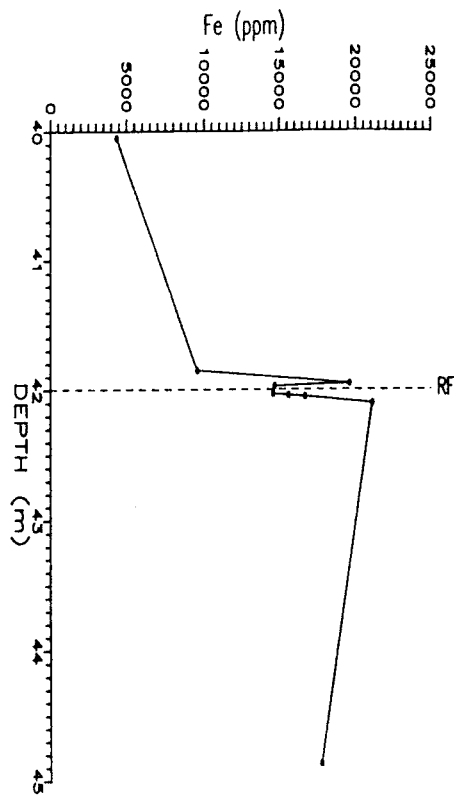


Figure 68. Iron concentration profile across the 42.0 m redox front in the F1 drillcore.

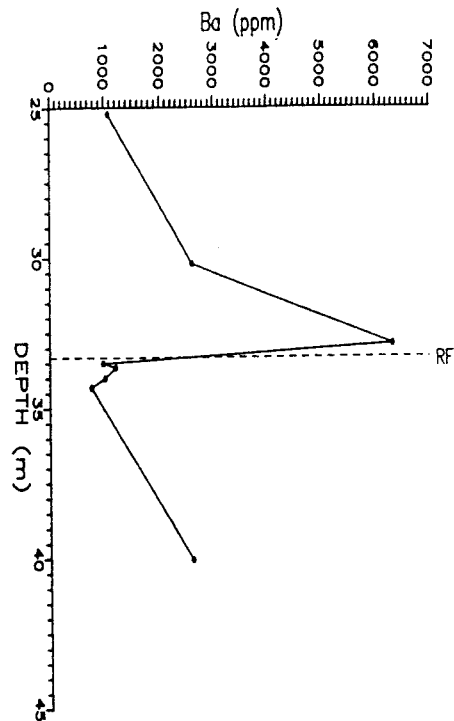


Figure 69. Barium concentration profile across the 33.4 redox front in the F1 drillcore.

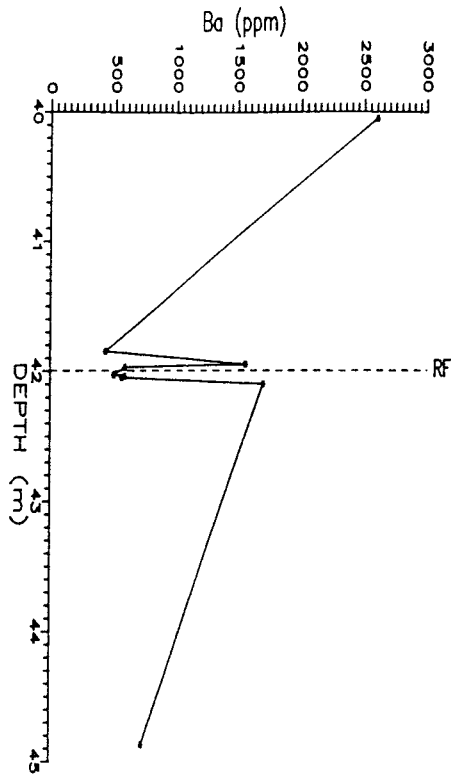


Figure 70. Barium concentration profile across the 42.0 m redox front in the F1 drillcore.

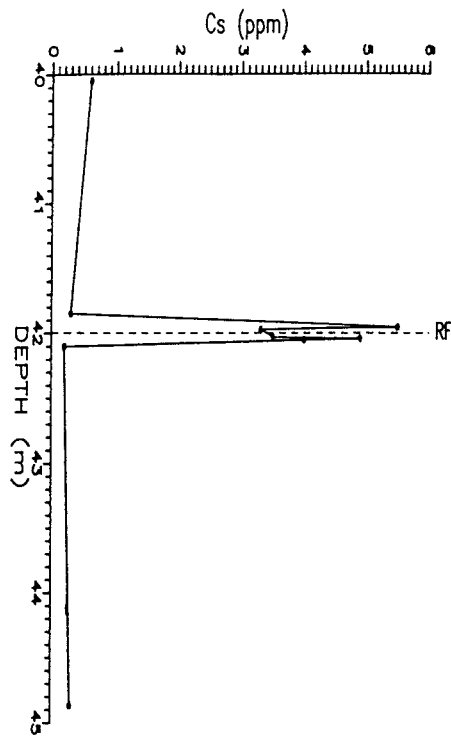


Figure 71. Cesium concentration profile across the 42.0 m redox front in the F1 drillcore.

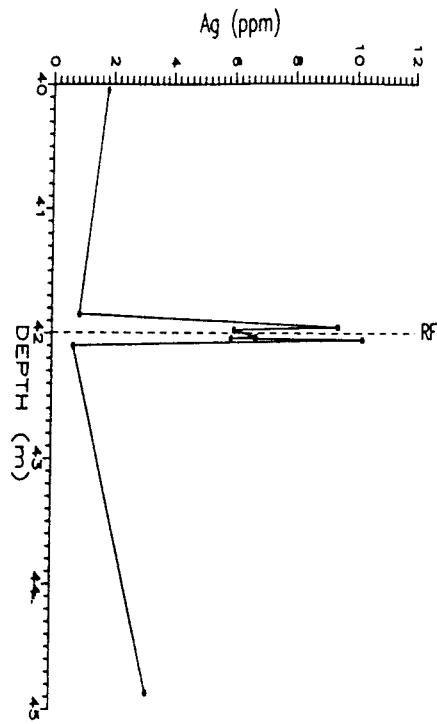


Figure 72. Silver concentration profile across the 42.0 m redox front in the F1 drillcore.

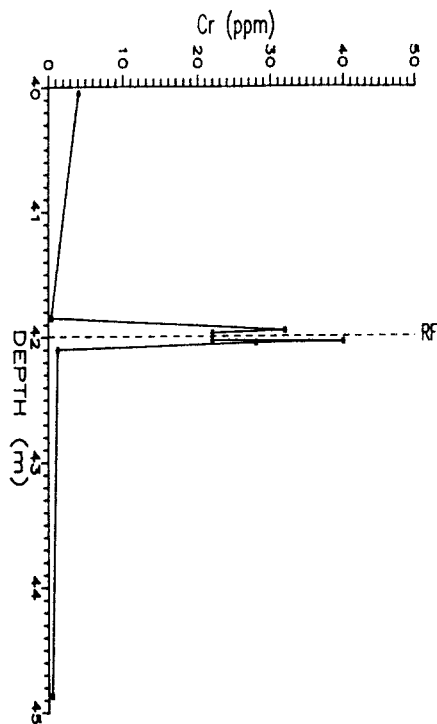


Figure 73. Chromium concentration profile across the 42.0 m redox front in the F1 drillcore.

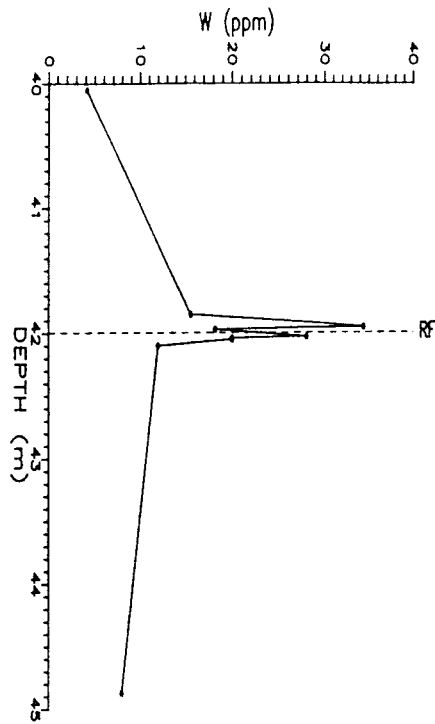


Figure 74. Tungsten concentration profile across the 42.0 m redox front in the F1 drillcore.

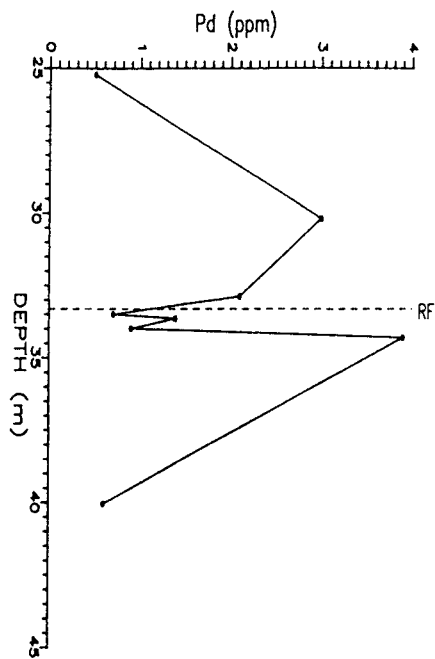


Figure 75. Palladium concentration profile across the 33.4 m redox front in the F1 drillcore.

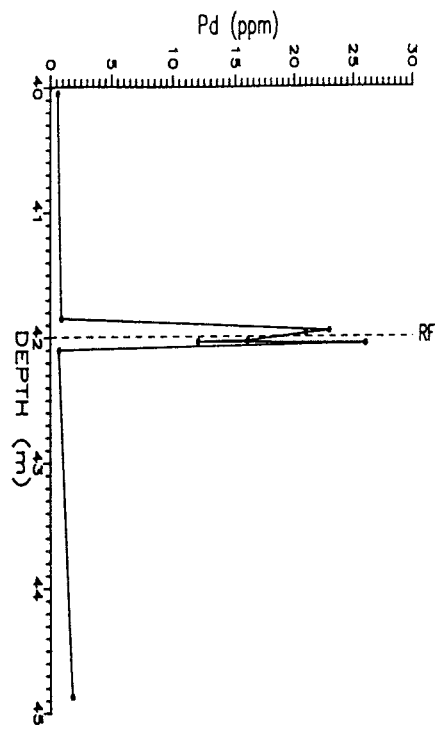


Figure 76. Palladium concentration profile across the 42.0 m redox front in the F1 drillcore.

2.2. Other redox front studies

2.2.1. Redox front 71ZE23

Six samples were extracted from a hand section (code 71ZE23) obtained from the wall of the mine at a point approximately 120 m south-west of the position of drillcore F1, and at a level about 16 m higher than the top of the F1 drillcore. The orientation of the redox front at this position was almost vertical and the phonolite in this section was relatively homogeneous with few fractures. The six samples were extracted from positions on either side of the redox front at distances of 0.5 cm, 2.5 cm and 4.5 cm as indicated in Figure 77. The analytical results for these samples are shown in Table XIV and are summarized graphically in Figures 78 to 81.

The average uranium concentrations in the reduced and oxidized rock respectively of 234 Bq kg⁻¹ (19 ppm) and 84 Bq kg⁻¹ (6.8 ppm) are lower than the values typically encountered throughout the F1 drillcore, consistent with the general features of uranium distribution in the mine presented in Figure 8.

The uranium specific activity profile (Fig. 78) and the ²³⁸U/²³²Th activity ratio values (Table XIV) clearly reveal an excess of uranium in the reduced rock relative to the oxidized rock in this sample. However, the generally low values for the uranium concentration suggest that this difference may be due to removal of uranium from the oxidized rock rather than deposition of uranium in the reduced rock. This suggestion is supported by the average ²³⁸U/²³²Th activity ratios of 2.8 and 1.1 for the reduced and oxidized rock respectively, which correspond to concentration (ppm) ratios of 0.31 and 0.24 respectively and are consequently low relative to samples from the F1 drillcore, even from depths greater than 75 m. The ²³⁴U/²³⁸U activity ratio data (Fig. 79) for these samples further suggest general loss of uranium from this section of rock, with all of the results lying below unity except sample D from just on the oxidized side of the front which has a value of 1.03 ± 0.02.

In contrast, however, the ²³⁰Th/²³⁴U activity ratios (Fig. 80) strongly suggest transfer of uranium across the redox front, with values in the reduced rock all being less than one while those for the oxidized rock are all in excess of one.

The uranium and thorium results suggest that this section of rock is subject to general removal of uranium, with significant preferential loss of ²³⁴U, but may also be experiencing transfer of uranium from the oxidized to the reduced rock. The ²³⁴U/²³⁸U versus ²³⁰Th/²³⁸U diagram for these samples (Fig. 82) presents a similar picture, with samples E and F from the oxidized rock lying in the uranium removal sector, sample D from the oxidized rock close to the front lying in the upper complex process area, samples

TABLE XIV

Natural decay series radionuclide specific activities (Bq kg^{-1}) and activity ratios for samples from section 71ZE23.

Sample	^{238}U	^{234}U	^{230}Th	^{226}Ra	^{232}Th	$^{238}\text{U}/^{232}\text{Th}$	$^{234}\text{U}/^{238}\text{U}$	$^{230}\text{Th}/^{234}\text{U}$	$^{226}\text{Ra}/^{230}\text{Th}$
A	243 ± 7	212 ± 5	183 ± 7	221 ± 11	88 ± 5	2.8 ± 0.2	0.87 ± 0.02	0.87 ± 0.03	1.21 ± 0.08
B	200 ± 5	173 ± 3	162 ± 8	206 ± 10	78 ± 5	2.6 ± 0.2	0.87 ± 0.02	0.93 ± 0.04	1.27 ± 0.09
C	258 ± 5	212 ± 5	190 ± 5	266 ± 13	82 ± 3	3.1 ± 0.1	0.82 ± 0.02	0.90 ± 0.03	1.40 ± 0.08
D	127 ± 3	137 ± 3	170 ± 8	193 ± 10	142 ± 7	0.89 ± 0.05	1.03 ± 0.02	1.24 ± 0.05	1.14 ± 0.08
E	123 ± 3	103 ± 3	119 ± 3	170 ± 9	88 ± 3	1.03 ± 0.06	0.84 ± 0.03	1.15 ± 0.03	1.43 ± 0.08

TABLE XV

Natural decay series radionuclide specific activities (Bq kg^{-1}) and activity ratios for samples from redox front II.

Sample	^{238}U	^{234}U	^{230}Th	^{226}Ra	^{232}Th	$^{238}\text{U}/^{232}\text{Th}$	$^{234}\text{U}/^{238}\text{U}$	$^{230}\text{Th}/^{234}\text{U}$	$^{226}\text{Ra}/^{230}\text{Th}$
A (200 cm)	998 ± 22	940 ± 21	1101 ± 39	1183 ± 59	120 ± 16	8.3 ± 1.1	0.94 ± 0.01	1.17 ± 0.03	1.07 ± 0.06
B (150 cm)	1736 ± 43	1738 ± 43	1684 ± 61	1777 ± 89	315 ± 18	5.5 ± 0.3	1.00 ± 0.02	0.97 ± 0.03	1.06 ± 0.06
C (100 cm)	1282 ± 31	1291 ± 31	1442 ± 40	1540 ± 77	213 ± 8	6.0 ± 0.3	1.01 ± 0.02	1.12 ± 0.02	1.07 ± 0.06
D (50 cm)	126 ± 29	1222 ± 26	1176 ± 58	1353 ± 68	202 ± 18	6.2 ± 0.6	0.89 ± 0.01	1.12 ± 0.05	1.15 ± 0.08
E (20 cm)	1554 ± 41	1483 ± 34	1734 ± 38	1647 ± 82	256 ± 9	4.6 ± 0.2	0.95 ± 0.01	1.18 ± 0.02	0.95 ± 0.05
F (ox)	1554 ± 23	1392 ± 36	1511 ± 44	1700 ± 85	335 ± 15	5.8 ± 0.3	0.90 ± 0.02	1.37 ± 0.03	1.13 ± 0.07
F (red)	927 ± 21	890 ± 20	1020 ± 33	1216 ± 61	268 ± 13	3.5 ± 0.2	0.96 ± 0.01	1.15 ± 0.03	1.19 ± 0.07
G (20 cm)	1176 ± 31	1085 ± 29	980 ± 31	1110 ± 56	217 ± 11	5.4 ± 0.3	0.92 ± 0.02	0.90 ± 0.03	1.13 ± 0.07
H (50 cm)	943 ± 23	851 ± 21	863 ± 16	1163 ± 58	182 ± 5	5.2 ± 0.2	0.90 ± 0.02	1.06 ± 0.02	1.35 ± 0.07
I (100 cm)	1364 ± 25	1110 ± 21	1141 ± 38	1507 ± 75	224 ± 12	6.1 ± 0.3	0.81 ± 0.01	1.03 ± 0.03	1.32 ± 0.08
K (150 cm)	994 ± 21	979 ± 20	849 ± 39	1230 ± 62	151 ± 13	6.6 ± 0.5	0.99 ± 0.01	0.87 ± 0.03	1.45 ± 0.09
L (200 cm)	1324 ± 31	1216 ± 29	1061 ± 31	1413 ± 71	156 ± 8	8.5 ± 0.5	0.92 ± 0.01	0.87 ± 0.02	1.33 ± 0.08

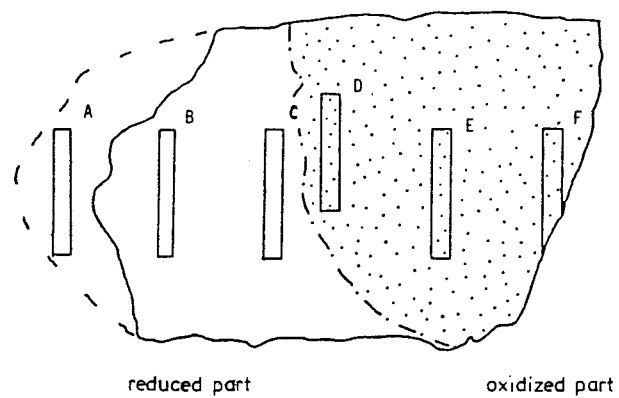


Figure 77. Sampling positions for hand section 71ZE23 obtained from the wall of the mine.

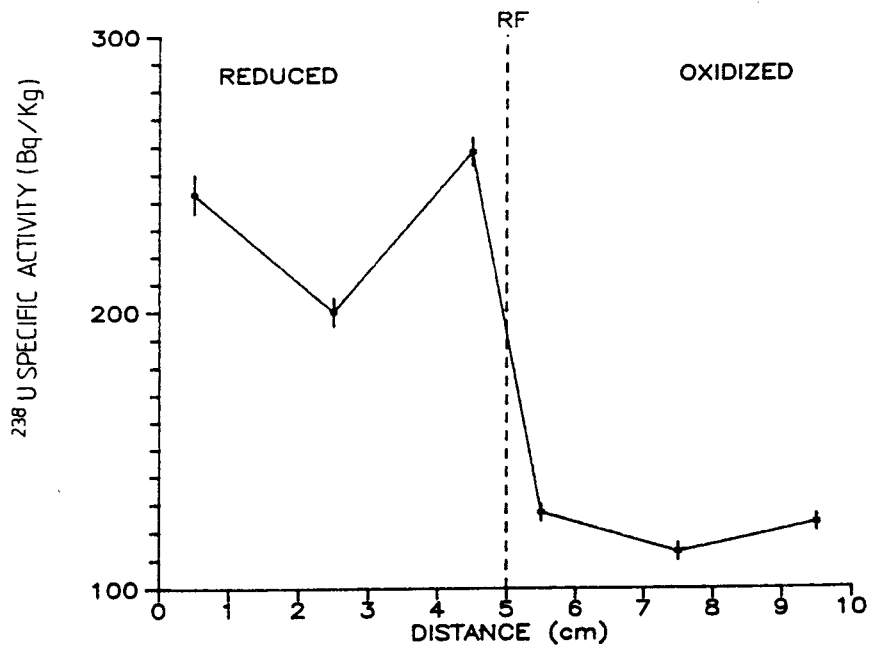


Figure 78. ^{238}U specific activity profile for samples from hand section 71ZE23.

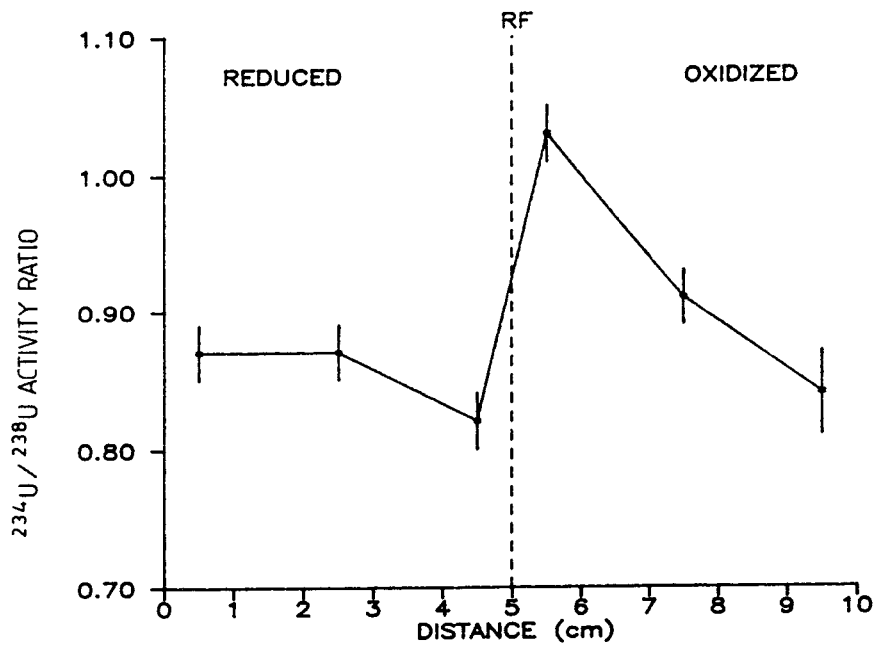


Figure 79. $^{234}\text{U}/^{238}\text{U}$ activity ratio profile for samples from hand section 71ZE23.

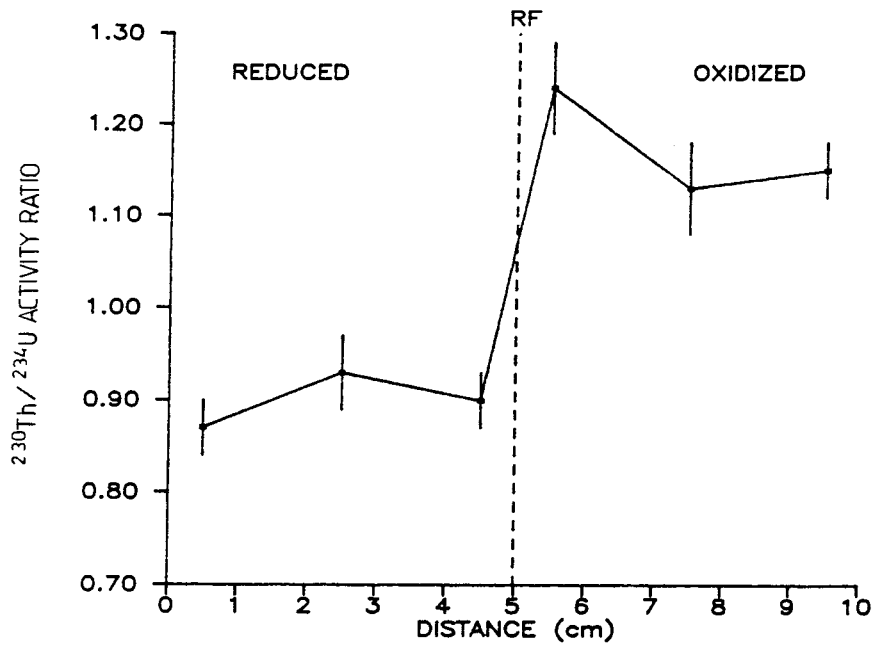


Figure 80. $^{230}\text{Th}/^{234}\text{U}$ activity ratio profile for samples from hand section 71ZE23.

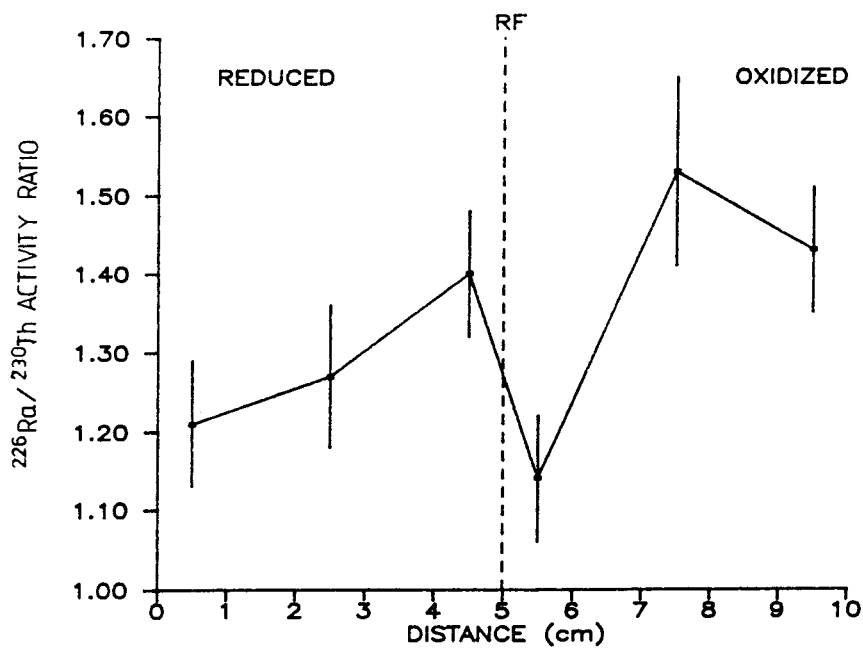


Figure 81. $^{226}\text{Ra}/^{230}\text{Th}$ activity ratio profile for samples from hand section 71ZE23.

B and C from 2.5 and 0.5 cm respectively away from the front lying on the boundary between the uranium removal and lower complex process areas, i.e. a position which cannot be reached by a continuous uranium removal process, and sample A from 4.5 cm into the reduced rock lying in the lower complex process area.

The positions of the reduced samples A, B and C in this diagram could be taken to indicate the return towards equilibrium of these samples following a perturbation involving uranium loss at some time in the past which is long relative to the 7.54×10^4 a half-life of ^{230}Th . In contrast, the positions of the oxidized samples D, E and F in the diagram could be taken to represent more recent removal of uranium, consistent with the movement of the redox front into the reduced rock.

Finally, as shown in Figure 81, the $^{226}\text{Ra}/^{230}\text{Th}$ activity ratios for all of the samples from section 71ZE23 lie significantly above unity. There is therefore an apparent systematic change in the behaviour of ^{226}Ra at the redox fronts as a function of depth in the mine. Thus, as at the 66.2 m and 42.0 m redox fronts in the F1 drillcore, there is a distinct transfer of ^{226}Ra from the reduced to the oxidized rock. At 33.4 m in the F1 drillcore, ^{226}Ra deposition was apparent in all but one of the samples, and in the 71ZE23 samples ^{226}Ra deposition is evident in all cases. This suggests a more rapid rate of removal of ^{226}Ra from solution on moving upwards in the phonolite, possibly in response to a change in the groundwater characteristics as a function of depth resulting in, for example, enhanced scavenging of ^{226}Ra by sulphate or oxide secondary minerals in the upper rock when more oxidizing conditions are encountered.

2.2.2. Redox front II

A suite of samples was analyzed in a 4 m transect across the redox front in a breccia body in the mine and the analytical results are shown in Table XV.

^{238}U shows a highly irregular variation in concentration across the front as shown in Figure 83, with values ranging from 927 Bq kg^{-1} (75 ppm) on the reduced side of the front to a maximum of 1736 Bq kg^{-1} (141 ppm) at sample B, 150 cm into the oxidized rock. The average uranium concentration is in fact slightly higher in the oxidized than in the reduced rock, with respective values of 1398 Bq kg^{-1} (113 ppm) and 1121 Bq kg^{-1} (91 ppm). However, the average $^{238}\text{U}/^{232}\text{Th}$ activity ratios for the oxidized and reduced sections are respectively 6.1 and 5.9 (corresponding to concentration ratios of 2.0 and 1.9) and are effectively indistinguishable. This suggests that the observed variations in uranium concentration across the transect are probably the result of variations in the

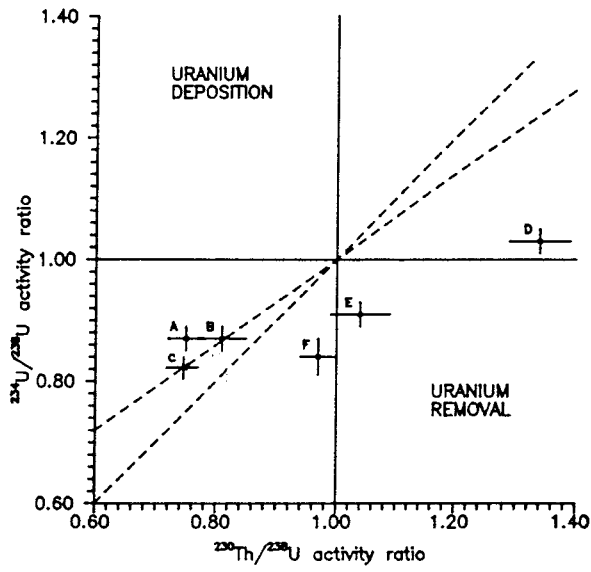


Figure 82. $^{234}\text{U}/^{238}\text{U}$ activity ratio versus $^{230}\text{Th}/^{238}\text{U}$ activity ratio diagram for samples from hand section 71ZE23.

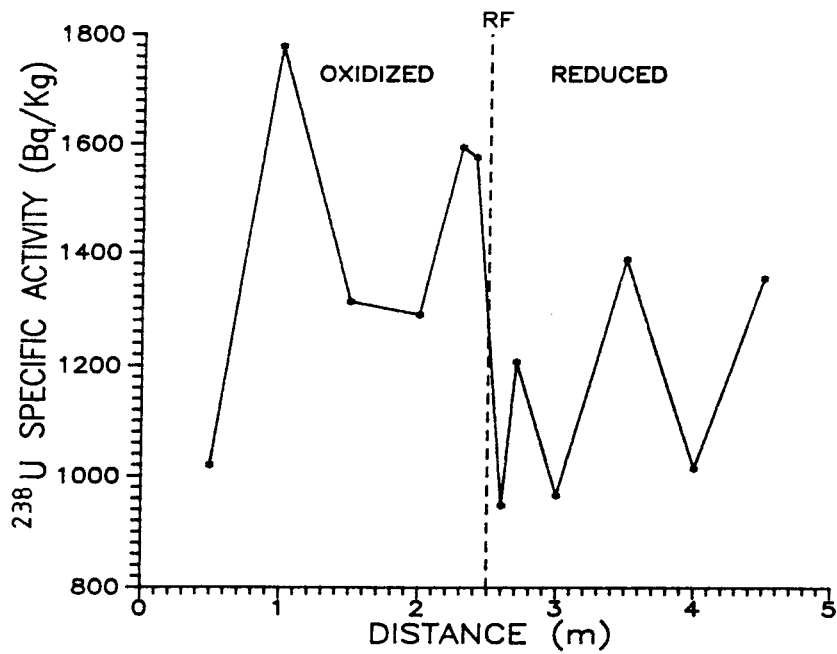


Figure 83. ^{238}U specific activity profile across redox front II.

mineralogy of the rock rather than the effects of redox reactions associated with the front.

The $^{234}\text{U}/^{238}\text{U}$ activity ratios for these samples (Fig. 84) are all less than or equal to unity suggesting general removal of uranium from this rock, with significant preferential loss of ^{234}U . On the oxidized side of the front, $^{234}\text{U}/^{238}\text{U}$ activity ratios lie in the range 0.89 to 0.95 in the half metre of rock closest to the front. On moving further from the front, the oxidized samples at 1.0 and 1.5 m have equilibrium $^{234}\text{U}/^{238}\text{U}$ activity ratios but a further decrease to 0.94 is observed at sample A, 2.0 m from the front. On the reduced side of the front, the $^{234}\text{U}/^{238}\text{U}$ activity ratio decreases from 0.96 at the front to a minimum value of 0.81 at sample I 1 m from the front, rises to equilibrium at 1.5 m from the front but falls again to 0.92 by 2.0 m. The value of 0.81 for sample I implies a rapid rate of preferential recoil loss of ^{234}U relative to bulk dissolution, suggesting that uranium in the solid phase is probably relatively stable at this position, consistent with the prevailing reducing conditions, but once more revealing that ^{234}U must be able to undergo transport in solution over distances of at least metres in the reduced rock.

The $^{230}\text{Th}/^{234}\text{U}$ data for redox front II, plotted in Figure 85, show values generally in excess of unity, indicating the recent (on a 7.54×10^4 a timescale) loss of uranium from these samples, with the ^{230}Th excess being most pronounced for the sample closest to the front, consistent with the movement of the front from the oxidized to the reduced rock. Estimation of a rate of movement of the front is once again complicated by the fact that closed system conditions obviously do not apply to uranium in this rock. The assumption that the return to equilibrium for the $^{230}\text{Th}/^{234}\text{U}$ activity ratio over a distance of 1.5 m is purely due to decay of excess ^{234}U would suggest a rate of movement of the front of the order of about 5 m in 10^6 years. On the reduced side of the front, the $^{230}\text{Th}/^{234}\text{U}$ activity ratio decreases irregularly from a value of 1.15 at the front to 0.87 at 1.5 to 2.0 m from the front. The results therefore suggest removal of uranium from the front and deposition of uranium in the reduced rock with the deposition being most pronounced at a distance of over 1.5 m into the reduced rock, once more indicating that uranium must be mobile in groundwater in the reduced rock over at least this distance.

All of the $^{226}\text{Ra}/^{230}\text{Th}$ activity ratios (Fig. 86), except for sample E which is located 20 cm into the oxidized rock and has a value of 0.95 ± 0.05 , are greater than unity and there is a systematic increase in the ratio on moving from the oxidized to the reduced rock. This section of rock is thus a zone of general ^{226}Ra deposition, with the rate of deposition being more intense or the deposit being more recent in the reduced rock.

The overall picture which emerges for the redox front II samples is therefore complex, with the $^{234}\text{U}/^{238}\text{U}$ ratios indicating uranium loss in general, the $^{230}\text{Th}/^{234}\text{U}$ ratios implying

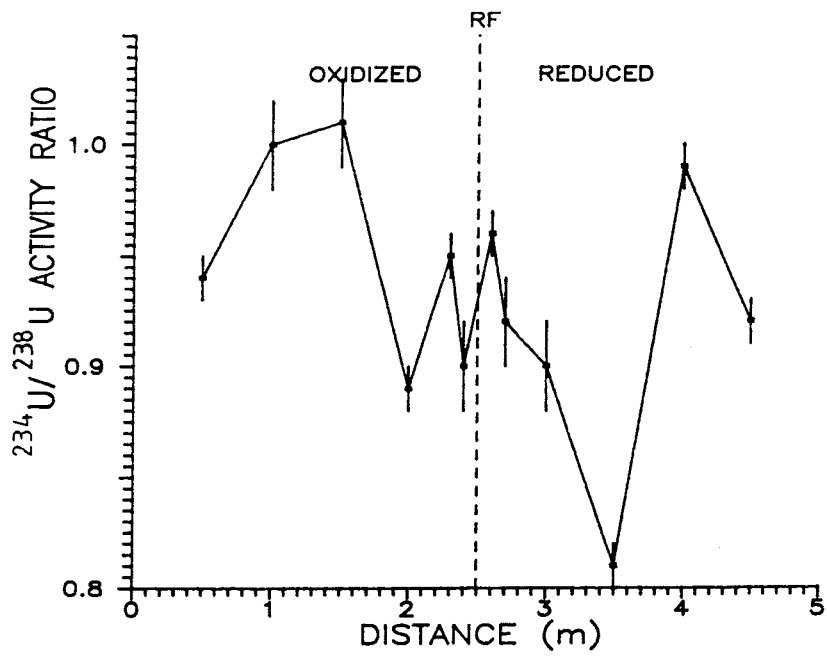


Figure 84. $^{234}\text{U}/^{238}\text{U}$ activity ratio profile for redox front II.

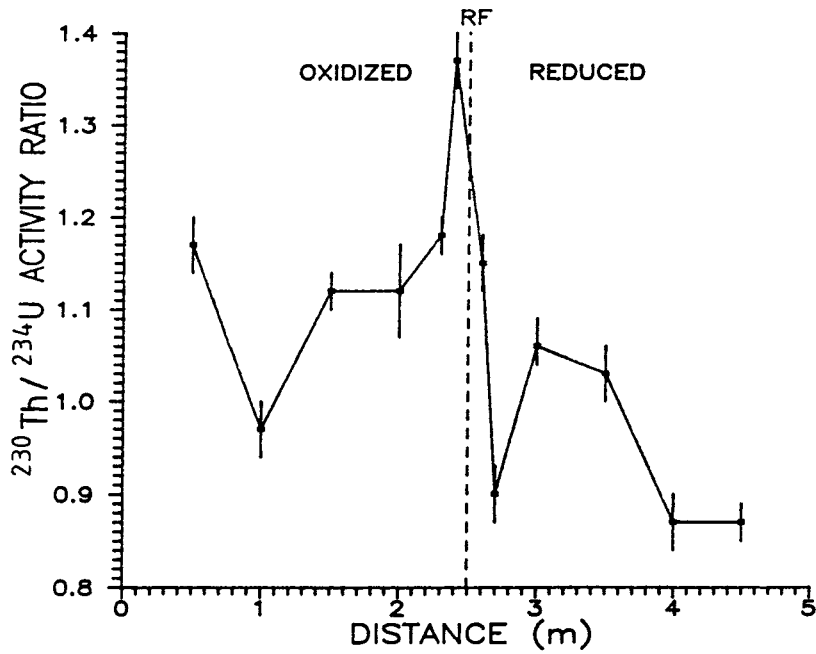


Figure 85. $^{230}\text{Th}/^{234}\text{U}$ activity ratio profile for redox front II.

dissolution of uranium at the front and transfer of uranium from the oxidized to the reduced rock, and the uranium concentrations and uranium/thorium concentration ratios suggesting that mineralogical variations may also be significant.

The $^{234}\text{U}/^{238}\text{U}$ versus $^{230}\text{Th}/^{238}\text{U}$ diagram for these samples (Fig. 87) presents a correspondingly complex distribution of the data points. Samples A, D, E and F (ox) from the oxidized rock are located in the uranium removal area but there is no systematic trend in their positions, which would suggest that samples A (2 m) and E (20 cm) have experienced more recent loss of uranium than sample D (50 cm) and sample F (ox) from just on the oxidized side of the front. Sample B (1.5 m on the oxidized side of the front) lies close to the (1,1) position suggesting very little perturbation of this sample, while sample C (1 m on the oxidized side of the front) lies in the upper complex process area.

On the reduced side of the front, sample F (red) lies in the uranium removal area in a position consistent with recent dissolution of uranium. Samples H (reduced rock 50 cm from the front) and I (reduced rock 100 cm from the front) are also in the uranium removal sector, but in positions indicative of a removal process operating over a timescale of the order of 7×10^5 years. The remaining samples from the reduced rock (G, K and L) all lie in the lower complex process sector.

In general, therefore, the natural decay series data suggest removal of uranium from most of the samples from redox front II, particularly from the oxidized rock, but that recent processes resulting in the redistribution of uranium have been complex and that mineralogical variations may also be significant.

2.2.3. Redox front NM

A hand section of rock was collected from the wall of the mine and a set of 10 samples was extracted from the positions shown in Figure 88. The results for analysis of the samples for natural decay series radionuclides are given in Table XVI and are plotted in $^{234}\text{U}/^{238}\text{U}$ versus $^{230}\text{Th}/^{238}\text{U}$ diagrams in Figure 89.

The complete section represents a zone of uranium enrichment relative to the average reduced phonolite in the deeper sections of the F1 drillcore, and the oxidized samples have a higher uranium content on average than the reduced samples. Thus the oxidized samples have an average ^{238}U specific activity of 7700 Bq kg^{-1} (623 ppm) and an average $^{238}\text{U}/^{232}\text{Th}$ activity ratio of 28 (concentration ratio of 9.1) while the reduced samples have an average ^{238}U specific activity of 4760 Bq kg^{-1} (385 ppm) and an average $^{238}\text{U}/^{232}\text{Th}$ activity ratio of 23 (concentration ratio of 7.5). There is considerable variation of

TABLE XVI
 Natural decay series radionuclide specific activities (Bq kg^{-1}) and activity ratios for samples from section NM.

Sample	^{238}U	^{234}U	^{230}Th	^{232}Th	^{238}Th	$^{238}\text{U}/^{238}\text{Th}$	$^{234}\text{U}/^{238}\text{U}$	$^{230}\text{Th}/^{234}\text{U}$
O-0	9400 ± 400	9100 ± 400	14900 ± 300	230 ± 10	330 ± 10	40.9 ± 2.5	0.96 ± 0.06	1.64 ± 0.08
O-1	6100 ± 300	5500 ± 200	26800 ± 700	330 ± 30	260 ± 20	18.5 ± 1.9	0.91 ± 0.06	4.8 ± 0.2
O-2	5800 ± 200	5900 ± 200	54000 ± 1000	350 ± 30	320 ± 30	16.6 ± 1.5	1.03 ± 0.06	9.1 ± 0.4
O-3	8800 ± 500	7700 ± 500	5900 ± 200	290 ± 20	360 ± 20	30.3 ± 2.7	0.83 ± 0.07	0.77 ± 0.05
O-4	8400 ± 300	7200 ± 300	9800 ± 200	240 ± 10	390 ± 20	35.0 ± 1.3	0.86 ± 0.05	1.36 ± 0.06
R-0	4400 ± 200	3600 ± 100	2290 ± 60	174 ± 9	230 ± 10	25.3 ± 1.7	0.82 ± 0.04	0.64 ± 0.03
R-1	3700 ± 200	2900 ± 100	3130 ± 90	170 ± 10	220 ± 10	21.8 ± 1.7	0.79 ± 0.05	1.08 ± 0.06
R-2	4900 ± 200	3800 ± 200	5100 ± 100	200 ± 20	260 ± 20	24.5 ± 2.6	0.78 ± 0.06	1.34 ± 0.08
R-3	7200 ± 400	5500 ± 300	4700 ± 100	260 ± 20	290 ± 20	27.7 ± 2.6	0.77 ± 0.05	0.85 ± 0.05
R-4	3600 ± 200	2800 ± 200	2580 ± 80	200 ± 10	300 ± 20	18.0 ± 0.9	0.80 ± 0.06	0.91 ± 0.06

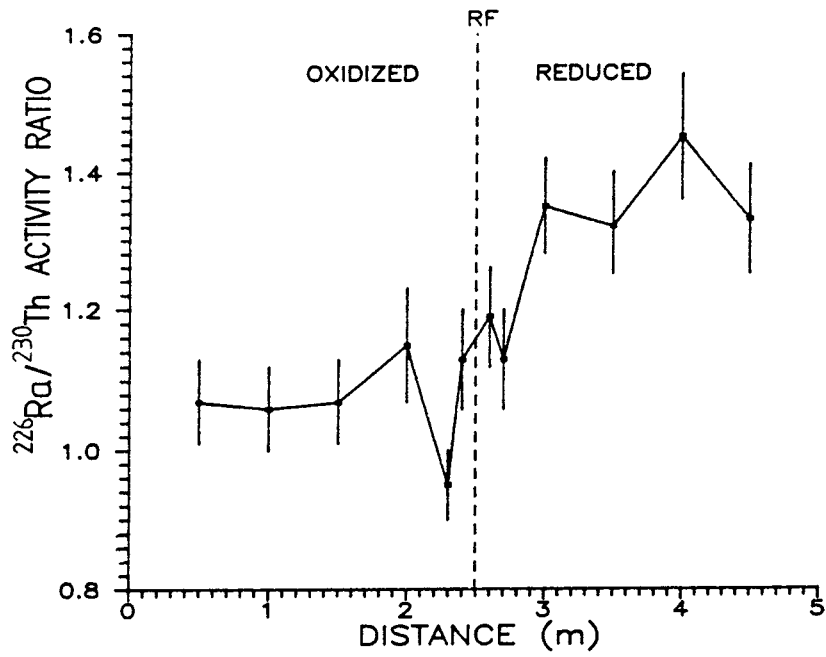


Figure 86. $^{226}\text{Ra}/^{230}\text{Th}$ activity ratio profile for redox front II.

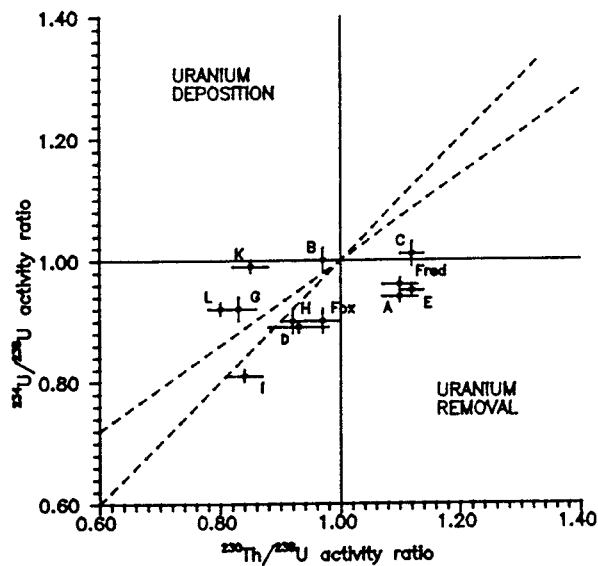


Figure 87. $^{234}\text{U}/^{238}\text{U}$ activity ratio versus $^{230}\text{Th}/^{238}\text{U}$ activity ratio diagram for samples from redox front II.

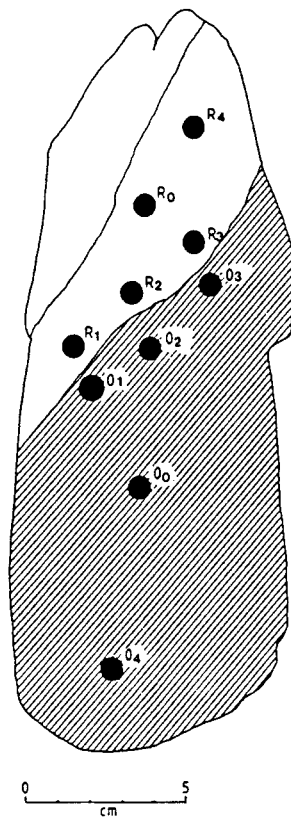


Figure 88. Sampling locations for hand section NM from the wall of the mine.

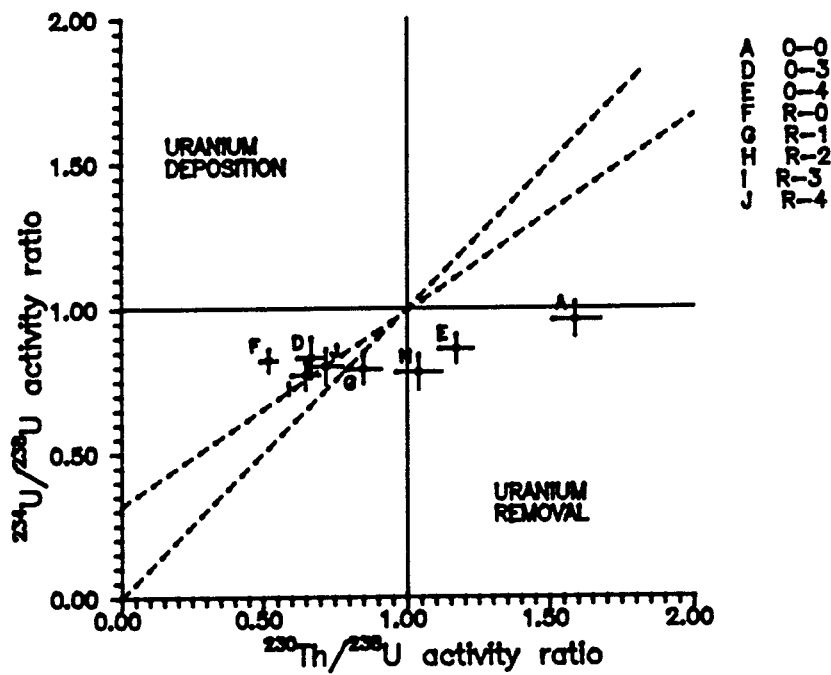
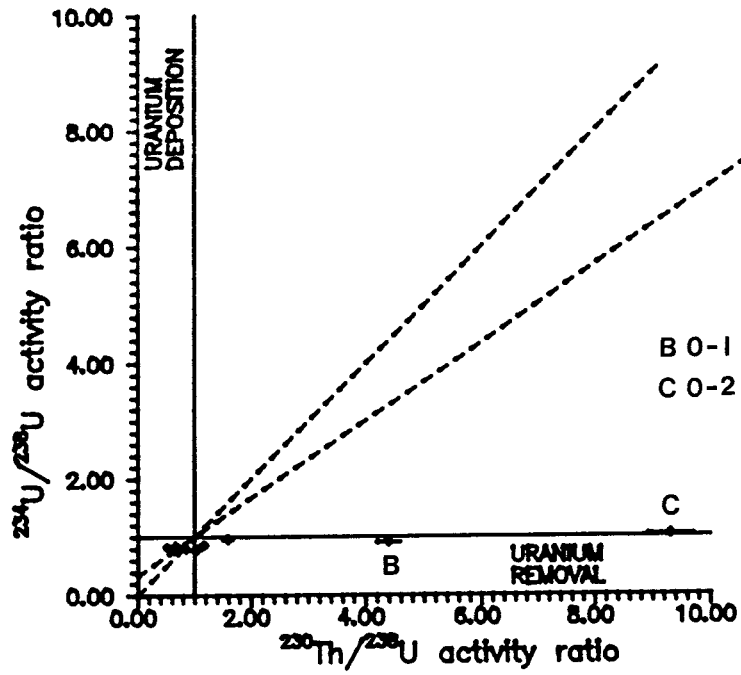


Figure 89. $^{234}\text{U}/^{238}\text{U}$ activity ratio versus $^{230}\text{Th}/^{238}\text{U}$ activity ratio diagrams for samples from hand section NM from the wall of the mine.

uranium concentration both along the length of the redox front and with distance from the front but there is no obvious systematic trend in the results.

Samples O-0 and O-2 from the oxidized rock have $^{234}\text{U}/^{238}\text{U}$ activity ratios within error of equilibrium while all of the other samples have ratios of less than unity, with the ^{234}U deficiency being most pronounced for samples R1, R2 and R3 in the reduced rock close to the redox front. The uranium isotope activity ratios thus suggest active loss of uranium on a timescale that is recent relative to the ^{234}U half-life ($2.45 \times 10^5 \text{a}$), with preferential recoil loss of ^{234}U relative to ^{238}U being most effective in the reduced rock close to the redox front. Sample O-3 has a $^{230}\text{Th}/^{234}\text{U}$ activity ratio of 0.77 indicating recent deposition of uranium at this location but all the other samples from the oxidized section of rock have $^{230}\text{Th}/^{234}\text{U}$ activity ratios greater than unity, with samples O-1 and O-2 having very high values of 4.8 and 9.1 respectively. These results clearly demonstrate that recent, and highly intense, dissolution of uranium has occurred from these samples and the high value of 54000 Bq kg^{-1} for the ^{230}Th content of sample O-2 further suggests that the uranium, which had been contained at this location, had been deposited there at some time in the past significant with respect to the 7.5×10^4 year half-life of ^{230}Th . These results also imply that the ^{238}U content of the rock at sample position O-2 had previously been at least 54000 Bq kg^{-1} , a value which is an order of magnitude higher than the specific activities observed immediately on the reduced side of the front.

The results indicate that the redox front has recently (on a $7.5 \times 10^4 \text{a}$ timescale) passed over a relatively localized area of uranium mineralization and that the uranium has been highly effectively removed. It is also notable that the uranium dissolved in this way has not, as far as can be observed within the sampling frequency, given rise to any corresponding mineralization in the immediately adjoining reduced rock. Thus the uranium removed from the oxidized section of rock must have been deposited in a diffuse manner in the contiguous reduced rock or have been transported to a more remote location before deposition.

The $^{230}\text{Th}/^{234}\text{U}$ activity ratios for the reduced samples vary from values of 1.34 and 1.08 for samples R2 and R1 respectively, indicative of uranium dissolution from these locations close to the front, to values as low as 0.64, indicating uranium deposition in the other three reduced samples.

The data for this section are plotted in $^{234}\text{U}/^{238}\text{U}$ versus $^{230}\text{Th}/^{238}\text{U}$ diagrams in Figure 89, from which it is apparent that all of the samples from the oxidized section of rock except O-3 lie in the uranium removal sector, with O-0, O-1 and O-2 being in positions consistent with recent, intense uranium dissolution. Sample O-3 lies away from the other oxidized samples in the lower complex process sector. Of the reduced samples, R-2 lies

in the uranium removal area, R-3 and R-4 lie on the boundary between the uranium removal area and the lower complex process area, and sample R-0 lies in the lower complex area.

The results for the samples from this section thus provide strong evidence for dissolution of previously deposited uranium as the redox front advances into the reduced rock. The results clearly reveal the complexity of the processes involved when considered on a scale of cm and provide further support for the idea that, subsequent to dissolution at the redox front, uranium is not necessarily deposited in the immediately adjoining reduced rock, but can be transported to more distant sites before deposition.

2.2.4. Redox front IV

A set of 12 samples from a 4 m transect across a redox front in the wall of the mine, redox front IV, was analyzed by selective leaching techniques in an attempt to characterize the uranium migration characteristics at the front as described below.

The labile uranium and thorium were leached in two stages and analyzed isotopically by alpha spectrometry. There was negligible dissolution of rock during the first leach (0.1 N HNO₃ at room temperature for 48 hours) and about 3% dissolution during the second stage (hot 8 N HNO₃ for 48 hours). Ion-exchange procedures were used to remove iron and other leached ions and to separate uranium and thorium before electroplating onto stainless steel planchets. ²³⁶U and ²²⁹Th were used as alpha-emitting yield tracers. The analytical results are presented in Table XVII and are summarized graphically in Figures 90 to 92.

TABLE XVII

Results for sequential leaching analysis of samples from redox front IV.

Sample	0.1 N HNO ₃ soluble			Hot 8 N HNO ₃ soluble		
	Relative U content	²³⁴ U/ ²³⁸ U	²³⁰ Th/ ²³⁴ U	Relative U content	²³⁴ U/ ²³⁸ U	²³⁰ Th/ ²³⁴ U
A	0.65	1.58	0.32	2.56	1.32	1.08
B	0.54	1.23	0.45	3.42	0.95	1.04
C	0.39	1.42	0.48	3.09	0.89	1.87
D	0.57	1.25	0.35	3.15	1.09	1.33
E	0.64	1.21	0.46	3.23	1.15	0.51
F (ox)	1.49	1.28	0.26	7.51	0.99	1.47
F (red)	3.66	1.19	0.81	9.15	0.75	0.49
G	5.99	0.92	3.11	17.61	0.93	0.44
H	6.3	1.12	0.68	9.73	0.91	3.77
I	3.73	1.22	1.96	9.81	1.01	1.13
K	11.18	1.11	0.21	12.85	0.84	0.02
L	5.88	0.98	1.06	11.88	0.91	0.01

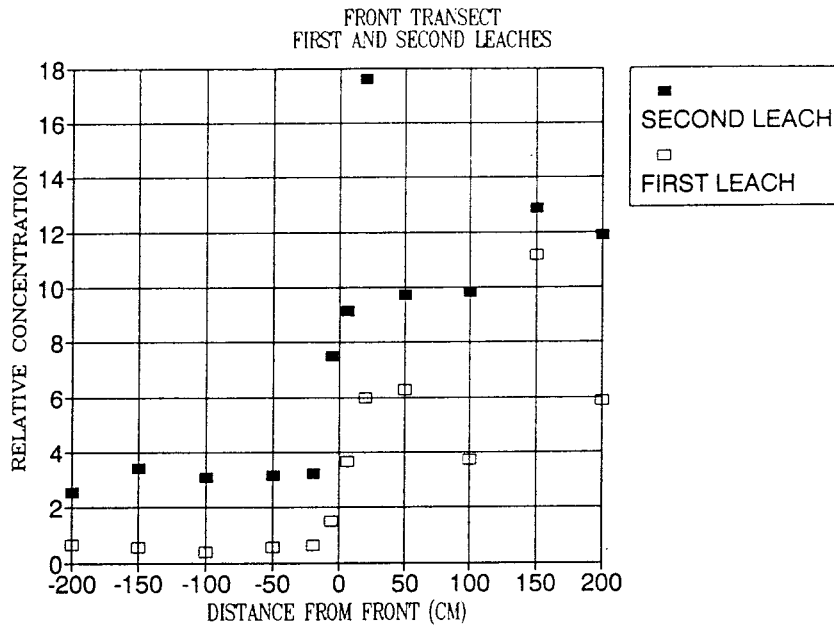


Figure 90. Relative uranium concentrations for first and second leachings of samples from redox front IV.

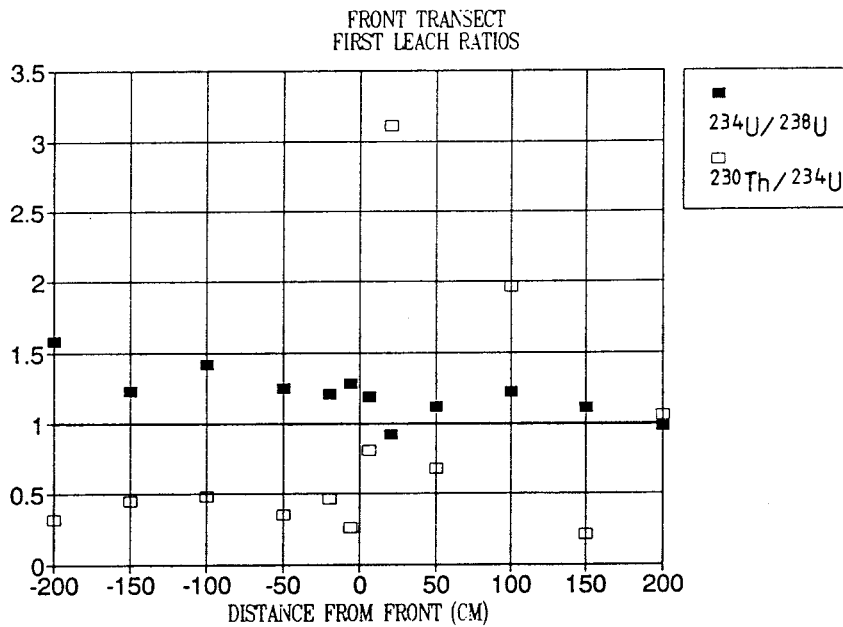


Figure 91. $^{234}\text{U}/^{238}\text{U}$ and $^{230}\text{Th}/^{234}\text{U}$ activity ratio for first leachings of samples from redox front IV.

With respect to the initial, less intensive 0.1 N HNO₃ leach, which should have removed only uranium secondarily precipitated onto grain surfaces along with any daughter thorium which was produced by decay after precipitation:

1. The relative concentration of uranium is quite low on the oxidized side but rises steeply over a distance of two metres on the reduced side of the front (Fig. 90).
2. Thorium is deficient relative to equilibrium on the oxidized side, and irregular on the reduced side with both excess and deficient values relative to 1.0 (Fig. 91).
3. The ²³⁴U/²³⁸U activity ratio is generally in excess of equilibrium (1.0), but is higher on the oxidized side (Fig. 91).

With respect to the second, more intensive leach, less mobile and perhaps earlier deposited uranium and its associated daughters should have been removed:

1. More uranium was leached from the samples on both sides of the front, but again considerably more came from the reduced side; while the ratio of enrichment of reduced relative to oxidized sides averaged about 10 in the first leach, it averaged about 3 in the second leach (Fig. 90).
2. Thorium is present in excess of equilibrium on the oxidized side and is generally deficient on the reduced side (Fig. 92).
3. The ratio of ²³⁴U to ²³⁸U is at about equilibrium on the oxidized side, but averages somewhat below equilibrium on the reduced side (Fig. 92).

Relative to the bulk samples, a median value of about 5 ppm of uranium was extracted from the oxidized samples in the two steps, while the reduced samples yielded about 20 ppm. Relative to just the leachate mass, the corresponding concentrations would be 125 ppm and 450 ppm respectively. Although there is less labile uranium altogether on the oxidized side, a larger proportion of it was vulnerable to the light leach.

The results of the leaching experiment are presented in the form of ²³⁴U/²³⁸U versus ²³⁰Th/²³⁸U diagrams in Figures 93 and 94. It is apparent from Figure 93 that, for the less intense leach, all of the samples from the oxidized side of the front lie in the uranium deposition sector, as do samples F (red), H and K from the reduced rock. Of the remaining samples from the reduced rock, sample L lies close to the (1,1) equilibrium point, sample I lies in the upper complex process zone and sample G lies in the uranium removal area.

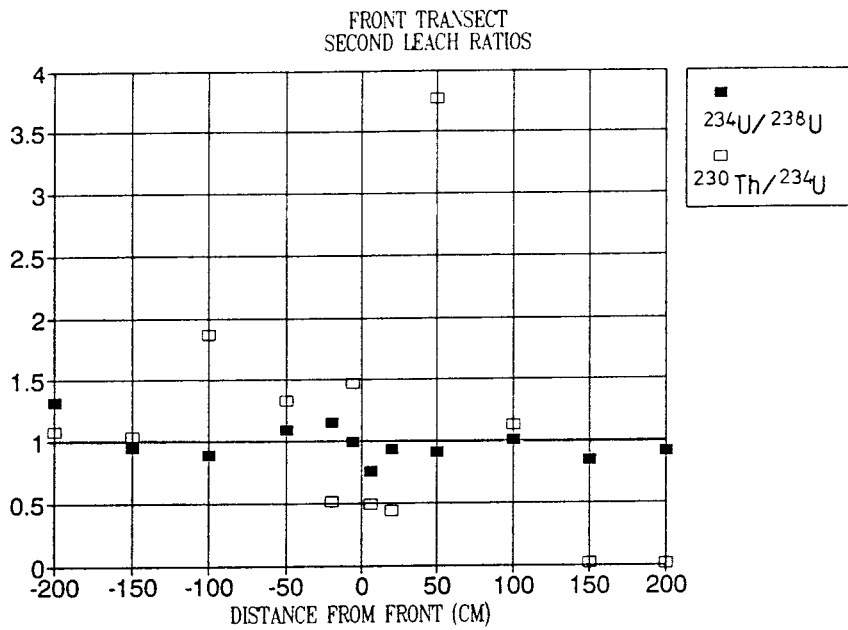


Figure 92. $^{234}\text{U}/^{238}\text{U}$ and $^{230}\text{Th}/^{234}\text{U}$ activity ratio for second leachings of samples from redox front IV.

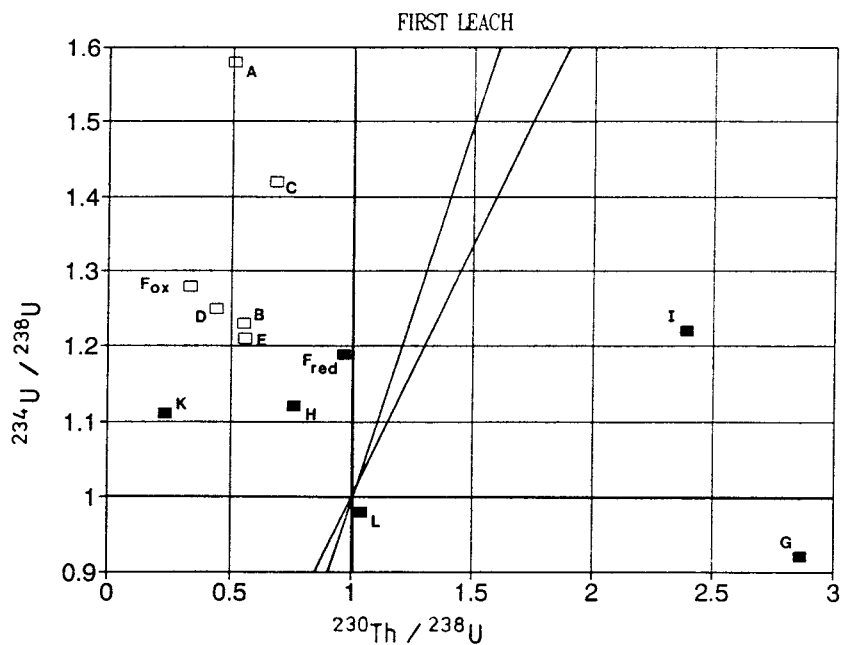


Figure 93. $^{234}\text{U}/^{238}\text{U}$ activity ratio versus $^{230}\text{Th}/^{238}\text{U}$ activity ratio diagram for first leachings of samples from redox front IV.

A significantly more complex picture is presented for the second, more intense leach in Figure 94, in which two of the samples from the oxidized rock (A and E) lie in the uranium deposition sector, three (B, C and F (ox)) lie in the uranium removal area and one (D) lies in the upper complex process area. Of the reduced samples, four (F (red), G, K and L) are in the lower complex process area, one (I) is in the upper complex process area and one (H) is in the uranium removal sector.

Finally, the uranium data for the reduced samples are presented in the form of a plot of the $^{234}\text{U}/^{238}\text{U}$ activity ratio against the reciprocal of the uranium concentration in Figure 95. This type of plot is used to characterize groundwaters and, in this presentation, high concentration waters (low $1/\text{conc.}$ values) are rich in the freshly leached component, while low concentration waters (to the right) tend to reflect the excess ^{234}U content in the aquifer; many aquifer suites show a kind of mixing line between the two end-members. In the plot of the data from the reduced side of the front (Fig. 95), where non-fractionating precipitation is taking place, the higher concentration samples probably form from higher concentration waters, and vice versa. One inference from this diagram is that the mobilized uranium was leached from high concentration surfaces with activity ratios as low as 0.77.

We believe that at this site the ground surface is being lowered at the rate of several centimetres per thousand years, that the redox fronts are advancing in the same general direction and at the same rate, and that the groundwater movement here is generally upwards at present. The questions we are attempting to answer are:

- (a) Has the water movement always had the same vector?
- (b) Has the uranium been moving with or against the water flow direction?

The larger excess of ^{234}U over ^{238}U in the labile component on the oxidized side of the front relative to the reduced side is strong evidence that the water has been flowing towards the oxidized zone for at least 10^5 years. The trend is more pronounced for the more easily leached uranium than for the more tightly bound uranium. One interpretation of the fact that the activity ratio values of the more tightly bound uranium are lower than 1.0 on the reduced side of the front is that this uranium has been in place and serving as a source for recoiling ^{234}U atoms for a very long time.

The movement of uranium itself is best shown by the relative amounts of ^{230}Th and ^{234}U . On the reduced side of the front this ratio exhibits wide variations, from very high to very low; there appears to be considerable local movement within the reduced zone itself. Within the oxidized zone, all of the lightly leached uranium exceeds its daughter

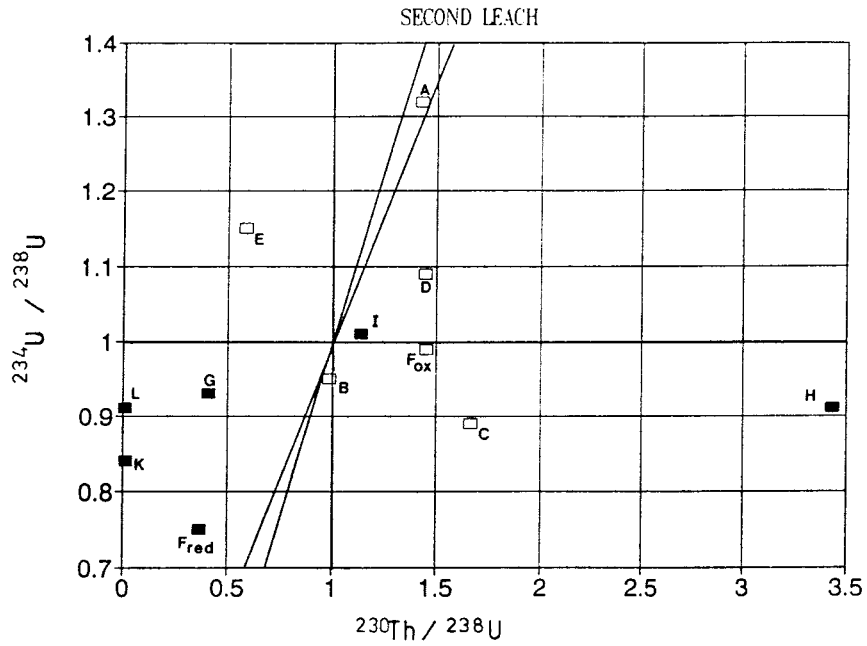


Figure 94. $^{234}\text{U}/^{238}\text{U}$ activity ratio versus $^{230}\text{Th}/^{238}\text{U}$ activity ratio diagram for second leachings of samples from redox front IV.

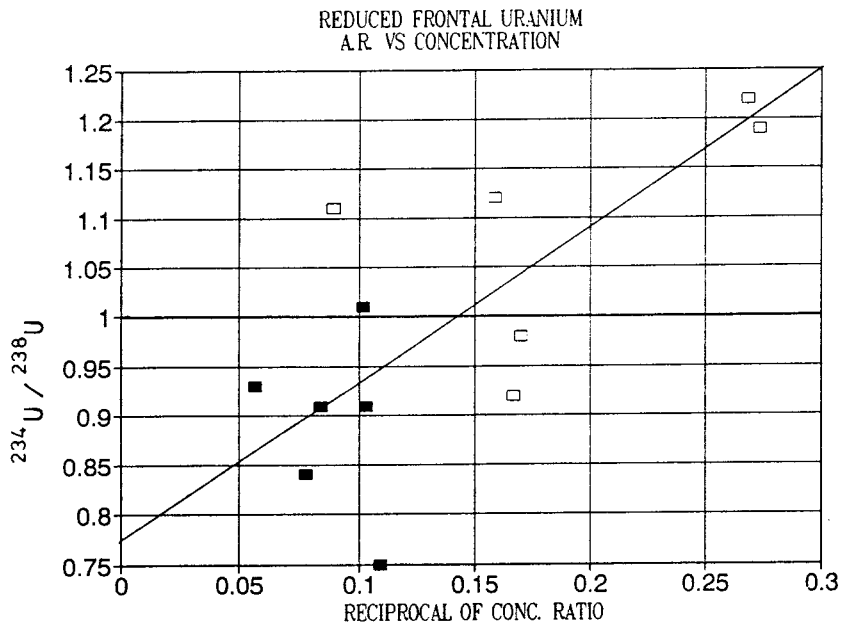


Figure 95. $^{234}\text{U}/^{238}\text{U}$ versus $1/\text{concentration}$ plot for first and second leachings of reduced samples from redox front IV.

thorium, suggesting that the uranium is moving away from the reduced and towards the oxidized side of the front. On the other hand, most of the less available uranium (second leach) of the oxidized zone is accompanied by less than the equilibrium amount of ^{230}Th , suggesting that this uranium is being leached from the oxidized zone. A possible interpretation of this finding is that the older, more tightly bound uranium moved in one direction (towards the reduced zone) while the younger, more labile uranium is moving in the opposite direction, away from the reduced zone.

Some caution in interpreting the Th/U ratio data is advisable inasmuch as the occurrence and leachability of the two elements are not necessarily the same, and fractionations rather than disequilibria are possibly being measured. The uranium isotopes, on the other hand, are not fractionated during natural accumulation, nor in the laboratory leaching process; this explains why the uranium isotope data are so consistent and unambiguous across the front.

In summary, the uranium isotope ratio $^{234}\text{U}/^{238}\text{U}$ provides clear evidence that the direction of water movement has been, on average over a long timescale, from the reducing to the oxidizing side of the front and, by inference, upwards in the area of the Osamu Utsumi deposit. The thorium/uranium ratio variations in the bulk of the leachable uranium suggest that the movement of this uranium has been from the oxidized to the reduced side of the front, in a direction opposite to that of the water flow. However, by the same measure, the movement of the most labile, perhaps most recent uranium has been from the reduced to the oxidized side of the front, in the direction of the water flow. This could be an artifact of the “light” leach process, or it could be a true interpretation of the frontal system as it operates today. If so, it could not have been the long-term (10^5a) prevailing direction of movement, because (a) the “heavy” leach data suggest otherwise, and (b) the ore body would have long since dissipated due to the weathering associated with the regional erosion process.

2.3. Studies of uranium nodules from the Osamu Utsumi mine

2.3.1. Growth rates of two pitchblende nodules

The pitchblende nodules, collected from near the redox front, were analyzed for uranium and thorium isotopes in order to determine their rates of growth. If the nodules grow from a central core outwards, and the uranium precipitates without its daughter thorium, then the age of each layer can be determined by the growth equation. Even if some thorium is present at the time of precipitation, relative ages of the layers can be

deduced, provided that the relative amount of initial thorium has remained approximately constant.

Each nodule consisted of a soft, light-coloured, clay-rich core surrounded by a hard black pitchblende mantle. (In fact, the samples supplied for analysis consisted of two half-nodules.) On their surfaces the nodules carried discontinuous remnants of a lighter-coloured matrix. The smaller nodule was roughly spherical, about two centimetres in diameter, with a mantle of 8 mm and a core of 4 mm. The larger nodule was oblate and less regular in shape, averaging about 4 cm in diameter and with a mantle of 11 mm. Its core was less spherical than the other.

The nodules were sectioned and sampled sequentially, starting with scrapings of the outer rind followed by small samples of the pitchblende, progressing inwards at about 1 to 2 mm intervals and ending with one or two samples of the core material (Fig. 96). The sample weights were 1 to 5 mg for the pitchblende and 10 to 50 mg for the outer matrix and inner core. An equilibrated spike of ^{232}U and ^{228}Th was added at the time of dissolution. The small samples were almost completely dissolved in concentrated nitric acid and the minor amount of residue was discarded.

Analytical yields were high, so that a few hours of counting yielded activity ratio uncertainties of only 2–3 per cent. The analytical results are presented in Table XVIII.

The basic disequilibrium age dating equation is quite simple if the $^{234}\text{U}/^{238}\text{U}$ ratio is close to equilibrium:

$$\frac{R-1}{R_0-1} = e^{-\lambda t}$$

where λ is the decay constant for ^{230}Th , R is the $^{230}\text{Th}/^{234}\text{U}$ alpha activity ratio and t is the time since crystallization. R_0 can be any value; if the initial ratio is >1.0 the excess ^{230}Th ($R - 1$) will decay away with the half-life of ^{230}Th ; if the initial ratio is <1.0 the deficiency of ^{230}Th ($1-R$) will disappear with the half-life of ^{230}Th .

Column 5 of Table XVIII (model age) is the solution for t in kiloyears if R_0 is $= 0$, and the equation becomes:

$$1 - R = e^{-\lambda t}$$

Column 6 of Table XVIII (apparent age) is the solution for t if R_0 is taken to be the lowest observed value of R , i.e. that at the growth surface. This is algebraically the same as subtracting the model age at the growth surface from that of each of the interior laminae.

TABLE XVIII

Analytical results and calculated ages for two uranium nodules from the mine.

NODULE 1: DIAMETER ~2 cm

Distance from rim (mm)	U concentration %	$^{234}\text{U}/^{238}\text{U}$	$^{230}\text{Th}/^{234}\text{U}$	Model age (ka)	Apparent age (ka)
0.0	6.2	0.99	0.30	38	0
0.5	45.2	1.00	0.53	81	43
1.5	41.4	1.00	0.65	113	75
2.5	31.9	0.99	0.64	111	73
3.5	34.7	1.00	0.81	182	144
5.0	20.2	0.98	0.92	276	238
6.5	37.7	1.00	0.89	235	197
7.5	31.0	1.01	0.68	123	85
8.0	15.5	0.93	0.69	127	89

NODULE 2: DIAMETER ~4 cm

Distance from rim (mm)	U concentration %	$^{234}\text{U}/^{238}\text{U}$	$^{230}\text{Th}/^{234}\text{U}$	Model age (ka)	Apparent age (ka)
0.0	54.3	0.99	0.63	106	0
0.5	35.8	0.99	0.66	116	10
1.5	25.1	0.96	0.85	206	100
2.5	32.4	1.02	0.90	253	147
3.5	35.9	0.99	0.77	159	53
6.5	27.1	1.06	0.52	79	0
8.5	30.0	1.05	0.77	160	81
10.0	49.3	1.04	0.91	261	182
11.0	23.7	1.02	0.97	398	319
13.0	7.4	0.91	0.79	169	90

An average growth rate of the nodules is indicated by the slope of a best-fit line on the graph of $\log(1-R)$ plotted against distance from the growth surface (Figs. 96 and 97).

The smaller nodule has a growth rate that is nearly linear at 2.8 mm per 10^5 years, with an R value at the time of deposition of about 0.30. (An alternative model involving recent leaching of the outer surface would allow an initial ratio of 0, but the indicated growth rate would be the same.) The core and innermost surface of the mantle yield younger ages than the interior layers of pitchblende, suggesting that the core region of the nodule is more "open" to uranium migration than are the "crystalline" pitchblende laminae.

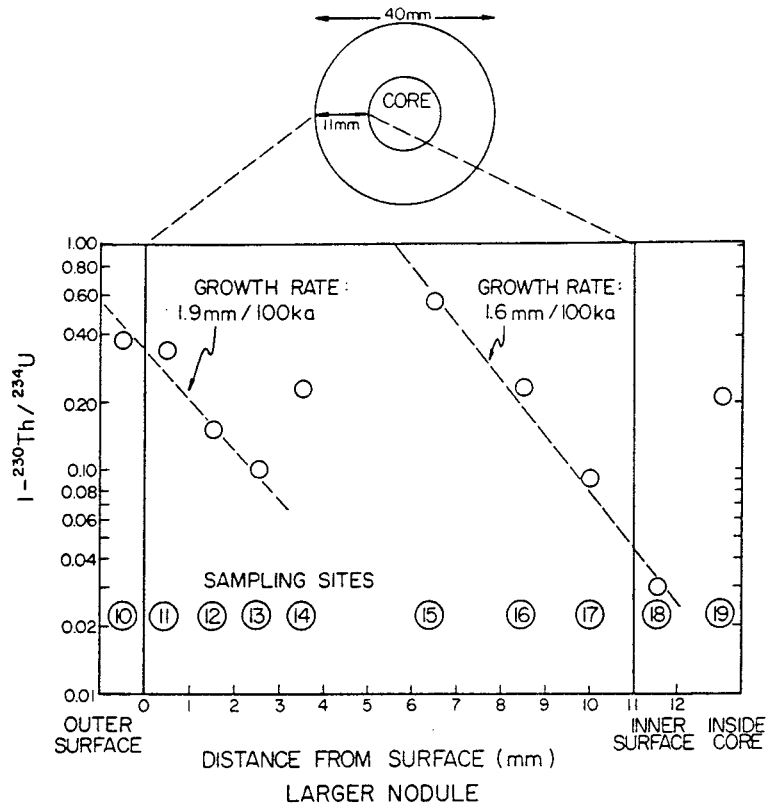


Figure 96. Plot of $\log(1 - {}^{230}\text{Th}/{}^{234}\text{U})$ versus distance for smaller uranium nodule.

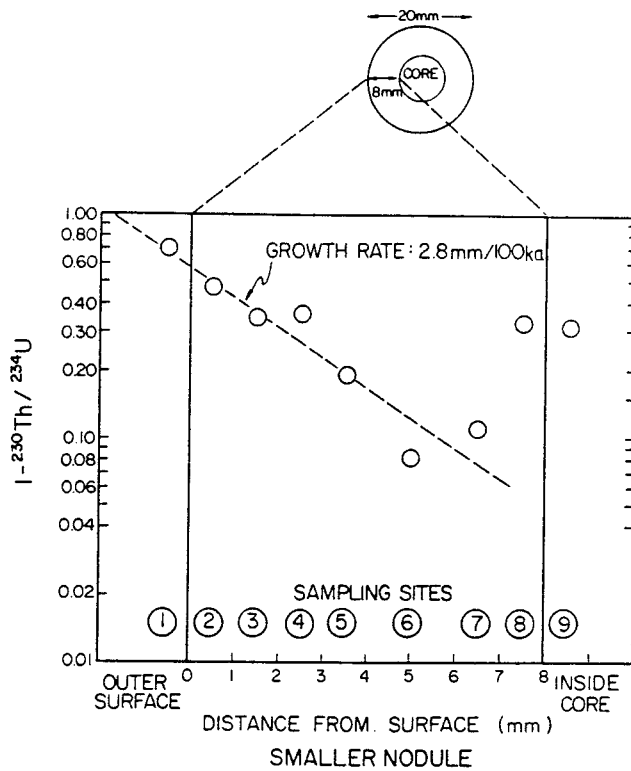


Figure 97. Plot of $\log(1 - {}^{230}\text{Th}/{}^{234}\text{U})$ versus distance for larger uranium nodule.

The larger nodule yielded a more complex pattern of model ages. One possible interpretation, indicated in Figure 97, is that there have been two growth surfaces, one being inside the mantle. If so, this is really a compound nodule. The observed irregularity of the nodule and of the core region support this interpretation. However, there was no obvious discontinuity observed in the region where the mantle was sampled.

Both nodules averaged about 30% uranium, with a slight tendency for the concentration values to diminish inwards from the outer rim to inner core. The lowest values were, as expected, in the core material and in the outermost surface material of the small core. However, the outermost surface material of the large nodule had the highest concentration of any sample. The second highest value was found in sample #17, at the inner edge of the mantle of the larger nodule. Perhaps the higher values near the younger growth surfaces result from the approach of the redox front with time.

Given the known variation of $^{234}\text{U}/^{238}\text{U}$ activity ratio in the mine waters, and in the leachable fraction of mine rock samples, it is surprising to find the prevalence of equilibrium values of $^{234}\text{U}/^{238}\text{U}$ in the nodules. The two samples that are most clearly out of equilibrium are the core samples from each nodule, both of which have a deficiency of the daughter ^{234}U of about 8%. On the other hand, the samples from the inner half of the large nodule appear to have a 5% excess of ^{234}U .

All of the samples from the outer surface and mantle of the small nodule and all of those from the outer surface and outer mantle of the large nodule are at equilibrium with respect to $^{234}\text{U}/^{238}\text{U}$, within analytical uncertainty (1-2%). The disparity of the two parts of the large nodule in this respect is probably another indication of its compound nature.

2.3.2. Uranium decay series characteristics of an old pitchblende nodule

Other nodules which are older (on the basis of near-equilibrium condition in the uranium decay chain) than the two described above also occur in the mine, with an example of one of these being shown in Figure 98 and the results for analysis of 5 samples from the positions indicated being given in Table XIX. These data clearly reveal $^{230}\text{Th}/^{234}\text{U}$ equilibrium for all of the samples except B3, indicating that this is a much older nodule than the two described above and which is growing at a very slow rate (or has stopped growing).

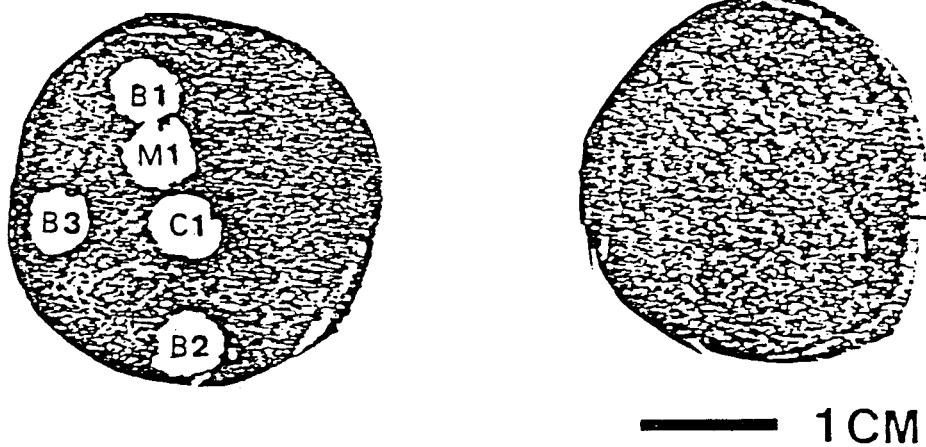


Figure 98. Xerox image of an old uranium nodule showing the sampling positions.

TABLE XIX

Results for uranium/thorium analysis of an old uranium nodule.

Sample	Uranium concentration (%)	$^{234}\text{U}/^{238}\text{U}$	$^{230}\text{Th}/^{234}\text{U}$
C1	45 ± 2	1.04 ± 0.06	1.11 ± 0.06
M1	44 ± 2	1.02 ± 0.06	1.11 ± 0.06
B1	46 ± 2	1.07 ± 0.06	0.95 ± 0.04
B2	38 ± 2	1.01 ± 0.06	1.03 ± 0.05
B3	51 ± 2	1.06 ± 0.05	0.85 ± 0.04

2.3.3. Uranium/thorium disequilibria in uranium-bearing micronodules near a redox front

In these rock samples collected at the redox front, a sharply defined yellow/blue colour discontinuity marked the front and several small nodules were visible on both sides of the colour line. The nodules were too small to permit the annular ring sampling described above for larger nodules. Each nodule thus constitutes a single sample, ranging in size from one to four milligrams. The apparent distances of the nodules from the front, measured on the rock surfaces, were one to four centimetres; direct distances were not determined, but would be somewhat less. In rock sample M2A, four nodules were sampled from the yellow (oxidized) side, two from the blue (reduced) side, and one from directly on the frontal discontinuity. In rock sample U-5, two nodules were sampled from the blue zone and one nodule was taken from the reduced/oxidized boundary. Whereas the reduced nodules were black and dense, the oxidized nodules were more rust-coloured and friable.

All of the samples yielded high alpha-ray count rates so that the uncertainties in concentration and isotope ratio values are quite small, usually less than a few per cent. The analytical results are presented in Table XX.

Because of their small size and friability, it was impossible in most cases to obtain pure pitchblende samples. Therefore the concentrations reported should be regarded as lower limits for the nodular uranium content, with dilution by country rock material being involved. Nevertheless, all of the reduced and borderline nodules contained more uranium than any of the oxidized nodules. The highest concentration sample, at 22% uranium, is probably representative of pure nodular material. The oxidized samples vary

TABLE XX

Analytical results and calculated ages for micronodules collected from positions close to the redox front.

Sample	Rock	Ox/red	Uranium concentration (ppm)	$^{224}\text{U}/^{222}\text{U}$	$^{220}\text{Th}/^{224}\text{U}$	$^{220}\text{Th}/^{222}\text{U}$	Accum. "age" (ka)	Leach "age" (ka)
761	M2A	OX	3680	1.22	14.6	17.81		120
762	M2A	OX	4975	2.25	16.5	37.13		21
763	M2A	OX	2475	1.53	9.8	14.99		140
764	M2A	OX	1017	2.66	5.1	13.57		180
765	M2A	R/O	58740	0.79	1.7	1.34		
766	M2A	RED	7260	1.58	0.33	0.52	40	
767	M2A	RED	222721	1.08	0.62	0.67	95	
768	U-5	RED	73811	1.48	0.64	0.95	100	
769	U-5	RED	22688	1.09	2.7	2.94		
770	U-5	R/O	6644	1.26	0.99	1.25	>300	

from 1000 to 5000 ppm uranium concentration, with the higher figure probably representative of oxidized nodules.

Only one reduced sample has a $^{234}\text{U}/^{238}\text{U}$ activity ratio less than the equilibrium value of 1.00. The remaining values range from 1.08 to 2.66. Although there is some overlap, the lowest values are found in the reduced nodules and the highest in the oxidized nodules. The two highest concentration samples have the lowest ratio values, so that the weighted average of all nodular uranium would yield an activity ratio only slightly greater than equilibrium.

A distinguishing feature of all of the oxidized nodules is their very high ratio of ^{230}Th to ^{234}U . These excess ratios vary from 5 to 17 with respect to the daughter ^{230}Th relative to the parent ^{234}U , and from 14 to 37 relative to the grandparent ^{238}U . In contrast, three reduced nodules have $^{230}\text{Th}/^{234}\text{U}$ ratios in the range 0.33 to 0.64. The two nodules from right on the front have values of 0.99 and 1.7 for the same ratio. Only one sample appears to be somewhat anomalous; although definitely reducing and with a fairly high concentration, sample 769 from rock U-5 has an excess of ^{230}Th over ^{234}U amounting to a ratio of 2.7.

The isotopic data for these small nodules located near the front present an unambiguous picture of uranium migration from the oxidizing to the reducing side of the front. The agent of this movement is the same percolating water that causes the oxidation of the iron minerals. While the uranium moves, its daughter thorium remains immobile, thus producing two regimes of disequilibrium. The loss of uranium from the

oxidized nodules creates an excess of ^{230}Th relative to ^{234}U , at least until the excess ^{230}Th can decay away at a rate determined by its half-life of 7.5×10^4 a. The reprecipitation of the uranium on the reduced side of the front results in minerals which are deficient in the daughter, until the daughter ^{230}Th can grow to its equilibrium value at a rate governed by the same half-life value.

Although it is not possible to determine the rate of growth of these nodules, it is not difficult to generalize to average or limiting values. The model ages of the reduced nodules are estimated, assuming an episode of accumulation of thorium-free uranium, followed by a period of daughter growth. The value of close to 10^5 a determined for two nodules, including the one with the highest uranium concentration, can probably be interpreted as the average age of continuously accumulating nodular uranium in the reduced zone near the front. In turn, the front has moved, either continuously or episodically, some two or three centimetres in this time period.

Less justifiable, but still indicative, are the estimates of the time since oxidation of the leached nodules. In this case we assume that a nodule of pitchblende concentration was in radioactive equilibrium and then suffered an episode of uranium leaching, followed by a period of decay of the remnant ^{230}Th . Specifically, if a nodule like M2A 763 lost most of its uranium and became like M2A 762, it would have an initial $^{230}\text{Th}/^{234}\text{U}$ ratio of about 45. It would take about 10^5 a for this ratio to decay to the value of 15 we find today. Although the several assumptions involved in this estimate are speculative at best, the general time-frame is probably about right, whether the leaching was episodic or continuous.

The agreement of estimates for the two time rates, accumulation and leaching of the nodules, supports the chronology presented here. Furthermore, the degrees of disequilibrium on both sides of the front are such that even the most extreme assumptions yield time-frames less than about 3×10^5 a.

The pattern of disequilibria among the three isotopes in these nodules relative to the front (Fig. 99) has interesting implications for interpretation of the history of the front, groundwater flow and the ore body as a whole. The "normal" pattern for migrating fronts is that low $^{234}\text{U}/^{238}\text{U}$ ratios are associated with high $^{230}\text{Th}/^{238}\text{U}$ ratios, and high $^{234}\text{U}/^{238}\text{U}$ ratios are associated with low $^{230}\text{Th}/^{238}\text{U}$ ratios. This is because, in addition to the leached component of uranium (both ^{238}U and ^{234}U), there exists an additional component of ^{234}U that is mobilized by recoil-related processes. Therefore, the upflow (leaching and recoiling) side of a front should have a deficiency of ^{234}U relative to both ^{238}U and ^{230}Th , while the downflow (precipitation) side of the front should have corresponding excesses of ^{234}U . The fact that the uranium isotope activity ratios tend to be counter to this model

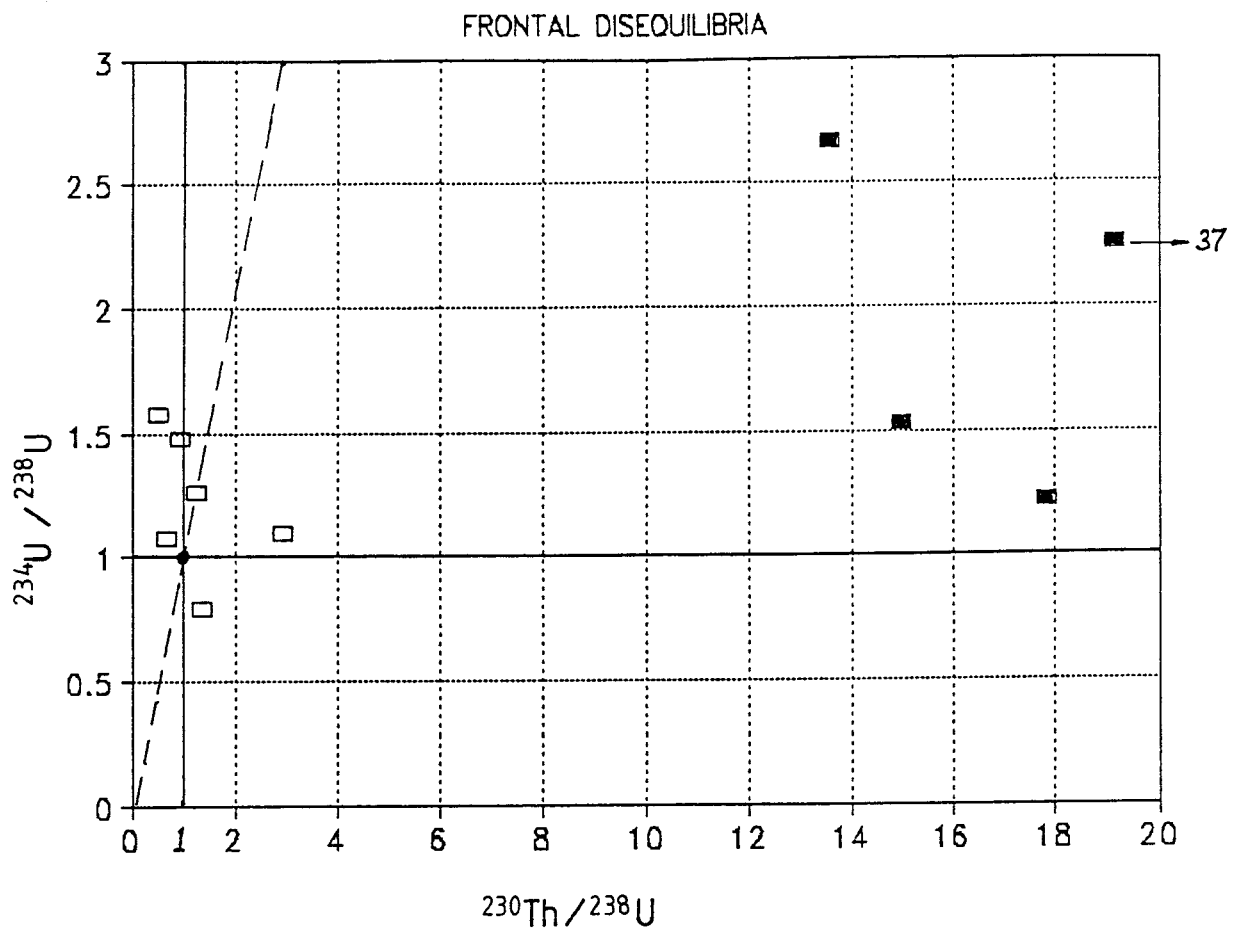


Figure 99. Plot of micronodule uranium and thorium isotopic data. Dot at 1,1 represents system equilibrium. Dashed line shows $^{230}\text{Th}/^{234}\text{U}$ equilibrium; samples to the right have excess ^{230}Th , those to the left have ^{230}Th deficiency. The oxidized nodules (solid) plot in a sector indicating leaching, as expected; however, their high $^{234}\text{U}/^{238}\text{U}$ values indicate a typical or changing water percolation directions.

suggests the history of the front is somewhat more complicated. In all likelihood, the water percolation direction has changed with time, or has a component more closely parallel to the front.

The overall uranium activity ratio greater than unity is also atypical of migratory fronts, which commonly have ^{234}U deficiencies of 5 or 10 per cent. This also suggests a somewhat unusual groundwater percolation pattern, and is perhaps an indication of a dispersal history for the ore body.

2.4. Natural plutonium geochemistry in a redox front

Plutonium, like uranium, is a multivalent element that is more soluble in higher valence states than in lower ones. To characterize the geochemistry of plutonium in an open geological system, the concentration of natural plutonium was measured in a centimetre-sized pitchblende nodule similar to those described above.

Plutonium was measured by isotope dilution mass spectrometry at the Los Alamos Isotope and Nuclear Chemistry Division isotope measurement laboratory. The limit of detection for plutonium measurement by the mass spectrometry procedure is about 10^5 atoms. However, this requires extensive chemical processing to isolate and purify plutonium in preparation for the isotopic analysis. Plutonium detectability is limited by the quantities of plutonium randomly introduced into the sample during this processing. The average measured quantity of ^{239}Pu in twelve blanks, materials containing undetectable quantities of indigenous plutonium, was $7.6 \pm 6.9 \times 10^7$ atoms. The detection limit, defined as three standard deviations greater than the average blank, is 2.8×10^8 atoms. The measured quantity of the natural isotope ^{239}Pu in the pitchblende nodule was twice the limit of detection. Neither of the anthropogenic isotopes ^{238}Pu and ^{240}Pu were detected, showing the lack of observable anthropogenic plutonium contamination in the sample. The Pu concentration in the nodule, corrected for the analytical blank, is $2.3 \pm 0.7 \times 10^8$ atoms per gram. The uranium concentration is $43(\pm 2)\%$ and the atom ratio of Pu/U is $2.1 \pm 0.7 \times 10^{-13}$.

Natural plutonium exists in rocks exclusively as the product of neutron capture by uranium. Models of plutonium production using a Monte Carlo neutron transport code (Briesmeister, 1986) show that the Pu/U ratio in a sample is a function of the composition of the rock within a radius of about 50 cm of the sample, the spatial distribution of elements within that volume, and the length of time that the system has been open to loss and/or gain of uranium or plutonium. In a system that has been closed for about 10^5

years, equivalent to several half-lives of plutonium, a state of secular equilibrium is established between the parent uranium and the radioactive daughter plutonium.

In such a closed system the Pu/U ratio is independent of time. Such model calculations indicate that Pu/U in the pitchblende nodule is consistent with a state of secular equilibrium in a matrix of reduced leucocratic phonolite, containing 3000 ppm U. Although the composition of the rock from which the nodule was taken was not known, the composition used in the model calculations is descriptive of the most uranium-enriched rock that has been observed at the deposit. Most simply, the Pu/U ratio in the nodule suggests that the two elements have resided unfractionated in the most highly uraniferous rock in the deposit for the last 10^5 a.

Uranium and its radioactive daughter ^{230}Th are in disequilibrium in the nodule. The activity ratio $^{230}\text{Th}/^{234}\text{U}$ is 0.62, indicating that thorium has been preferentially lost from, or uranium preferentially added to, the nodule at some time in the last 10^5 a. If there has been no alteration in that time, the plutonium was produced in-situ. If alteration has occurred more recently, the processes did not significantly fractionate plutonium from uranium.

At the uranium concentrations observed in the mine, plutonium production calculations show that, to a first approximation, Pu/U scales with the uranium concentration. Hence, Pu/U in volcanic host rock, which contains in the order of 20 ppm uranium, should be about two orders of magnitude lower than that in the pitchblende nodule. If plutonium in the nodule were formed in the host rock, the processes of nodule formation must have occurred more recently than 10^5 years ago and significantly enriched plutonium relative to uranium. This is a more improbable interpretation of the data than the one involving no fractionation.

It is hypothesized that uranium and plutonium are geochemically similar in the hydrogeochemical system that produced the uranium ore in the Osamu Utsumi mine. Plutonium must have migrated at a rate similar to uranium, and concentrations of uranium in the order of thousands of ppm have existed for at least 10^5 a. The hypothesis can be tested by measuring Pu/U in samples from well characterized regions of the redox front that are in extreme disequilibrium with respect to uranium and its radioactive daughter thorium.

3. Morro do Ferro

The Morro do Ferro area is described in detail by Waber (this report series; Rep. 3). The area marks the highest point (1541 masl) of the Poços de Caldas plateau. The region is dominated by deeply weathered volcanic to subvolcanic rocks of phonolite origin; there are some indications that Morro do Ferro represents a carbonatite complex. The ore body (i.e. where Th \geq 1%) is chiefly confined to the upper 25 m on the south face of the hill. Estimates of the thorium inventory of the ore body of 12,000 metric tonnes (T) and 30,000 T were made independently by Wedow (1967) and Frayha (1962) respectively, based on analyses of cores and shallow trench cuttings. The larger inventory has been utilized in recently published works dealing with thorium mobilization rates because it was based on samples taken to greater depths (up to 100 mbgl) which included a larger halo of lower grade ore (Lei, 1984; Eisenbud *et al.*, 1984; Lei *et al.*, 1986; Campos *et al.*, 1986). Estimates of the inventories of U, ^{228}Ra and the light rare-earth elements (Table XXI), are based on the 30,000 T thorium inventory and the ratios of the geometric mean concentrations of these elements to thorium, which were obtained from earlier X-ray fluorescence analyses of some 95 core sections obtained in 1981 from 5 shallow boreholes (25 to 60 mbgl) drilled dry in and around the vicinity of the ore body. For comparison, Table XXI shows the median concentration of these elements in farm soils (15–20 cm depths) sampled within 10 km of the Morro do Ferro. Based on these analyses,

TABLE XXI

Estimated inventories of some elements and isotopes within the MF ore body and in surface soils of the Poços de Caldas plateau.

Element	Geom. mean. ore. conc. ^I ($\mu\text{g} \cdot \text{g}^{-1}$)	Ore body inventory (T)	Median soil ^{II} conc ($\mu\text{g} \cdot \text{g}^{-1}$)
Th	2 668	30 000 ^{III}	93
U	34	400 ^{IV}	15
La	2 945	33 000 ^{IV}	213
Ce	4 329	49 000 ^{IV}	799
Nd	1 480	17 000 ^{IV}	68
^{228}Ra	10.8 ($\text{Bq} \cdot \text{g}^{-1}$) ^V	$1.2 \cdot 10^{14}$ (Bq) ^V	0.3 ($\text{Bq} \cdot \text{g}^{-1}$)

I Based on XRF analyses of 95 core samples from boreholes MF5, 6, 7, 8 and 9, which were drilled in 1981.

II From Linsalata *et al.* (1989).

III From Frayha (1962).

IV Estimated from the product: ratio of the geometric mean concentrations (e.g. La/Th) \cdot Th inventory.

V Assumes secular equilibrium with ^{232}Th .

MORRO DO FERRO

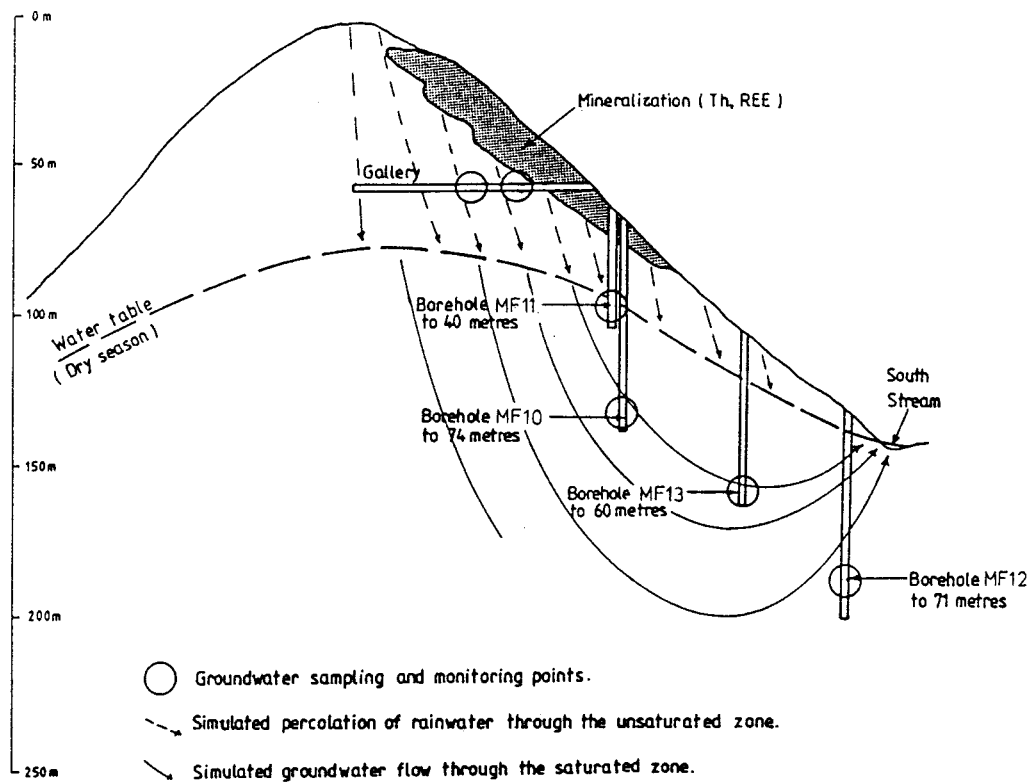


Figure 100. Section through the Morro do Ferro showing the positions of the MF10 and MF12 boreholes.

uranium is presently elevated by only a factor of two within the ore body when compared to local soil concentrations.

Earlier investigations using contemporary samples of suspended particulate matter ($\geq 0.45 \mu\text{m}$) and “dissolved” filtrates ($< 0.45 \mu\text{m}$) collected from the major groundwater seepage points and streams receiving drainage from the hill (the South Stream; Fig. 100) have stressed that erosional (surface) transport of Th and light rare-earth elements (LREEs) from the ore body is occurring at a rate some three orders of magnitude faster than that occurring via dissolution/groundwater seepage and transport (Eisenbud *et al.*, 1984; Lei *et al.*, 1986). Both the relative insolubility of Th and the LREE-bearing solid phases (Krauskopf, 1986) and the location of the mineralization (lying essentially within the unsaturated zone) are clearly reflected in earlier results.

Present-day erosion rates for the south face of the Morro do Ferro are in the order of 0.1 mm a^{-1} based on data observed from both the filling of three 100 m-long prospecting trenches cut along the south face of the hill (15 T a^{-1}) and from the flow-weighted mass transport of suspended particulate matter (110 T a^{-1}) past a flume constructed in the major drainage stream of the Morro do Ferro basin (Lei, 1984). This value appears reasonable based on land surface lowering within the entire caldera, which has recently been estimated by Holmes *et al.* (this report series; Rep. 5) to range between 0.015 and 0.05 mm a^{-1} .

3.1. Objectives

The objectives in this phase of the study were to obtain new data on LREE concentrations and on Th and U series radionuclides and their state of equilibrium within two cores which were drilled and packed off at different depths along the groundwater flow path. Thorough elemental and mineralogical analyses have been performed on the core samples selected for study (Waber *et al.*, this report series; Rep. 3). A schematic illustration of Morro do Ferro showing the approximate locations of the thorium mineralization, the groundwater monitoring points and boreholes MF10 and MF12 is given in Figure 100. The locations of MF10 and MF12 were chosen primarily to encounter groundwater both within and downflow of the mineralization. MF10, which cuts through the mineralization, did not, throughout its 74 m length, penetrate the thick zone of weathering and hydrothermal alteration; hence the material analyzed consists largely of clay minerals. A sequential radiochemical procedure was used for the separation of Th (^{234}Th tracer), U (^{232}U tracer) and LREEs (^{144}Ce tracer) (Linsalata *et al.*,

1987). Radiochemical separation and alpha spectrometry methods were used for the analysis of natural decay series radionuclides and inductively coupled plasma source optical emission spectroscopy (ICP-OES) for light rare-earth elements.

3.2. Results of core sample analyses

3.2.1. Borehole MF10

Thorium, U and LREE concentration data in the MF10 core samples, and corresponding isotopic ratios, are given in Table XXII. Thorium concentrations decrease by a factor of 250 from the surface metre (~230 Bq/g equivalent to 57,072 ppm) to that at 72.7 metres depth (0.90 Bq/g, equivalent to 223 ppm). Thorium decreases very sharply between 0.5 mbgl and 2.4–5.7 mbgl, and then again between 5.7 and 12.0 mbgl (Fig. 101) followed by an increase at 17 mbgl and a fairly smooth decline to depth. The thorium depth profile is fairly well represented ($r^2 = 0.88$) by an exponential function of the form:

$$[\text{Th}] \text{ in ppm} = 17,154e^{-0.0657(d)}$$

where (d) is sample depth in metres below ground level (mbgl). Thus thorium is decreasing over the length of this core with a half-distance of 10.5 metres. Based on samples taken over the length of MF10, neither U nor LREE depth distributions could reasonably be fitted to single exponential functions.

A very heterogeneous clay mineralogy has been described by Waber (this report series; Rep. 3), especially in the upper horizon of this core. Based on semi-quantitative clay mineral abundances described by Waber, Th concentrations in samples 10-4 (3.5 mbgl) to depth (10-73, 72.7 mbgl) are correlated ($r = 0.88$; $n = 8$) with the ratios of illite-sericite/kaolinite. Samples described as having a red or bright red component (Fe-Mn oxyhydroxide coatings) and high illite/kaolinite ratios (e.g. 2-4) appear to be enriched in Th, as opposed to those described as homogeneous white laterite samples (such as 10-12-1B) which exhibit low ratios (e.g. 0.3).

The uranium depth profile (Fig. 101) also reveals a depression in the homogeneous white, kaolinite-rich sample at 12 mbgl (10-12-1B), although U is neither correlated with Th nor with any of the LREEs measured over the length of this core. Uranium ranges from 19.8 (10-12-1B and 10-73-1A) to 76.3 ppm (10-25-1A) and averages 34.5 ± 15.8 ppm (± 1 SD (standard deviation)), in good agreement with earlier XRF results summarized in Table XXI (U geometric mean of 34 ppm). While the distribution of U concentration

Th and U Concentration with Depth in MF10

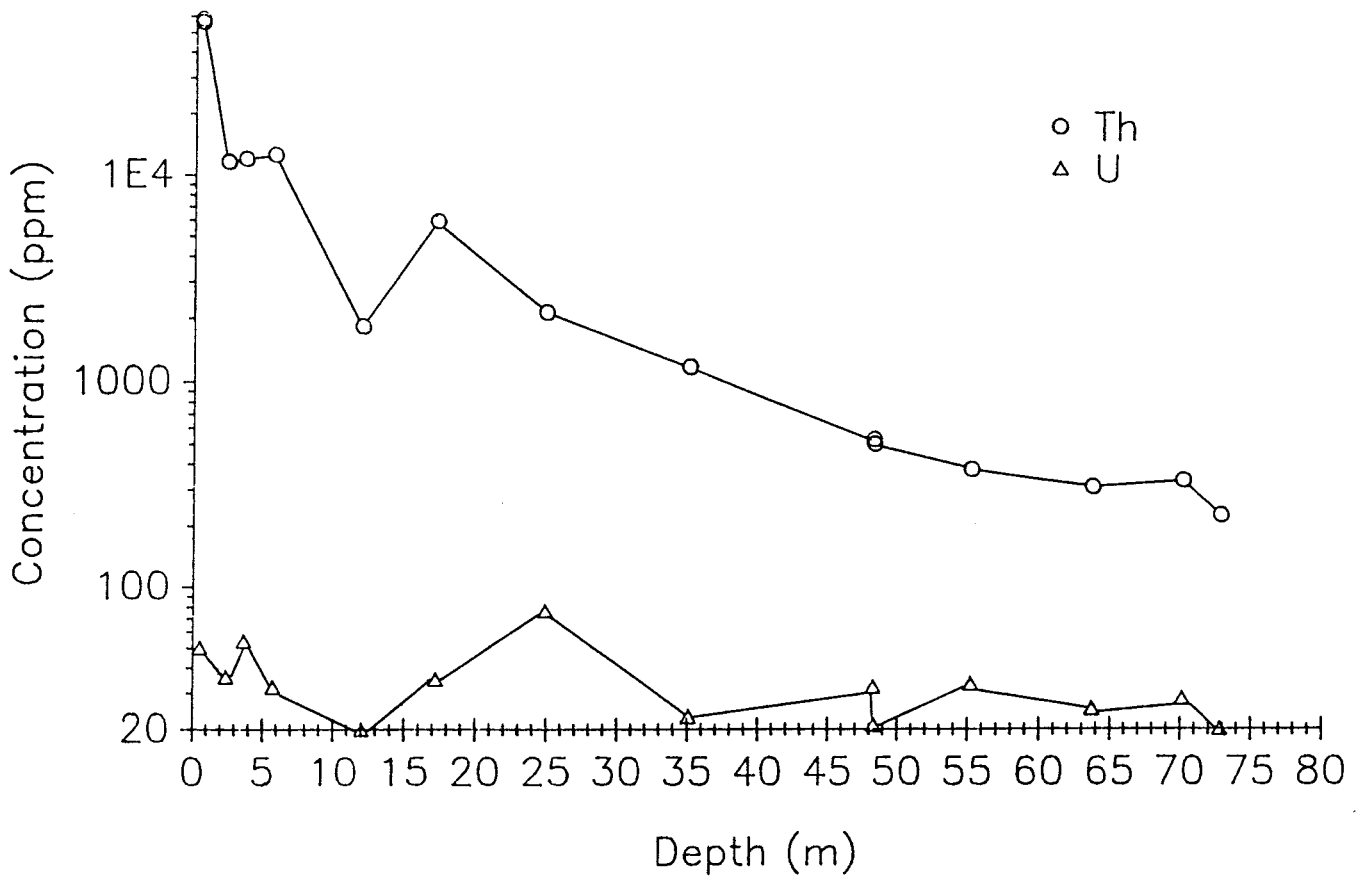


Figure 101. Thorium and uranium concentration profiles for drillcore MF10.

data in previously analyzed core samples from the ore body vicinity can be approximated by the normal distribution, Th and LREEs are lognormally distributed. Median concentrations (based on data given in Table XXII) for Th, La, Ce, Pr, Nd and Sm for the 14 core samples taken over the 74 m length of MF10 are (in ppm) 1496, 3493, 3033, 404, 1678 and 159, respectively. The median concentrations given are factors of two to three less than corresponding arithmetic mean concentrations, with the exception of U, for which the two statistics are the same. These differences among estimators of central tendency are expected for lognormally distributed and normally distributed variables. The median estimates given for Ce and Th in MF10 are lower (by 30 to 44% respectively) than the respective summary (older) data given in Table XXI because the MF10 core includes a higher proportion of samples taken within the lower concentration halo relative to the five earlier core samples referred to. Th and Ce have notably been shown to (1) be more closely correlated with one another than with other lanthanides or U, and (2) be retained in relatively higher concentrations within several metres of the surface than other lanthanides or U (Lei *et al.*, 1986). La and Nd median concentrations in MF10 are shown to be within 19% and 13% (both higher) of the earlier data given in Table XXI respectively.

The LREE data (Table XXII and Fig. 102) indicate highly variable concentrations from the surface to depth, with a steep decrease in the upper five metres as was noted for Th. The surface metre contains the highest LREE content (about 13% by weight for the summation of elemental La, Ce, Nd, Pr and Sm) and Th content (5.7%) reported to date from core sample data. Excluding Ce, the remaining LREEs are highly correlated with one another ($r = 0.99$ for virtually all combinations of any two members). As was found in ore body core samples drilled in 1981 (Lei *et al.*, 1986), Ce appears to be more closely correlated with Th ($r = 0.96$) than with other LREEs ($r = 0.89$), although considering the small sample size this difference in correlation coefficients is not significant. As was noted for Th, Ce concentrations are also correlated with the illite/kaolinite ratios reported for the bulk, unfractionated samples ($r = 0.9$, $n = 8$), although none of the remaining LREEs measured are.

The North American shale-normalized (Haskin and Frey, 1966) LREE concentrations for individual samples from MF10 are given in Figure 103 for samples taken from the unsaturated and saturated zones respectively. The extreme LREE enrichment within the surface metre (10-1-1B) is evident (depth in mbgl is indicated by the number following the core identification code). Below the surface metre, and culminating at the bottom of the unsaturated zone at 36 mbgl, positive Ce anomalies are observed with the exception of sample 10-12-1B. Mineralogically, this sample (as well as

TABLE XXII

REE, Th and U concentrations in core sections from borehole MF10¹. Concentration ($\mu\text{g/g dry} \pm 1 \text{ SD}$).

Sample no		Ce	La	Nd	Pr	Sm	Th	U
10-1-1B-a	Red-brown clay, magnetite	59524 \pm 1291	41170 \pm 885	23624 \pm 526	5772 \pm 270	3110 \pm 70	NC	50 \pm 4
-b	"	52289 \pm 1593	42139 \pm 1282	23229 \pm 694	6810 \pm 282	3031 \pm 98	58196 \pm 1172	NA
-c	"	54682 \pm 1624	44005 \pm 1291	24772 \pm 744	6800 \pm 269	3019 \pm 92	56058 \pm 827	NA
10-3-1A	Bright red + white clay	7545 \pm 153	3151 \pm 62	637 \pm 42	159 \pm 7	100 \pm 22	11633 \pm 744	36 \pm 2
-b	"	6545 \pm 196	3246 \pm 98	827 \pm 322	238 \pm 11	100 \pm 6	11540 \pm 174	NA
10-4-1A-a	Red laterite	18050 \pm 537	4162 \pm 140	1206 \pm 84	251 \pm 8	97 \pm 6	NC	54 \pm 1
-b	"	16864 \pm 505	3696 \pm 108	1963 \pm 106	355 \pm 13	231 \pm 12	11985 \pm 536	NA
10-6-1A	White-red laterite, HFO	1599 \pm 151	1125 \pm 34	150 \pm 14	77 \pm 3	12 \pm 1	12505 \pm 842	32 \pm 1
10-12-1B	Homog. white laterite	2891 \pm 85	5243 \pm 153	1771 \pm 64	789 \pm 24	135 \pm 11	1826 \pm 102	20 \pm 1
10-18-1A	White-red laterite	8226 \pm 516	1448 \pm 211	444 \pm 49	143 \pm 5	32 \pm 2	5905 \pm 370	35 \pm 1
10-25-1A	Brown laterite	14246 \pm 412	2151 \pm 63	594 \pm 92	213 \pm 7	45 \pm 3	2117 \pm 158	76 \pm 3
10-36-1A	Red-white laterite	2679 \pm 99	8744 \pm 265	5520 \pm 170	1623 \pm 59	624 \pm 22	1166 \pm 59	23 \pm 1
10-49-1A-A	White clay, "unaltered?"	1117 \pm 34	7025 \pm 211	3989 \pm 131	1173 \pm 38	473 \pm 15	521 \pm 28	32 \pm 1
10-49-1A-B	Alt. zone around fracture	941 \pm 29	9287 \pm 313	5192 \pm 154	1519 \pm 60	591 \pm 19	496 \pm 29	21 \pm 1
10-56-1A	Brown + white clay	3515 \pm 90	3430 \pm 86	1915 \pm 47	466 \pm 24	255 \pm 7	372 \pm 25	33 \pm 2
10-64-1A	White clay, magnetite nodule	1440 \pm 47	954 \pm 35	588 \pm 19	146 \pm 4	73 \pm 2	305 \pm 19	25 \pm 1
10-70-1A	White clay	3174 \pm 93	2108 \pm 62	1331 \pm 41	341 \pm 11	154 \pm 5	328 \pm 20	28 \pm 1
10-73-1A	White-yellow clay	848 \pm 30	3556 \pm 140	2215 \pm 65	677 \pm 22	231 \pm 11	222 \pm 14	20 \pm 1

¹See Table XXIII for sample depths and mineralogical description.

REEs determined by Inductively Coupled Plasma Source Optical Emission Spectroscopy (ICP-OES), Th and U by alpha spectrometry.

NA refers to not analyzed.

NC refers to not calculated due to inability to accurately assess radiochemical ²²⁹Th yield. Subsequent aliquots utilized ²³⁴Th tracer.

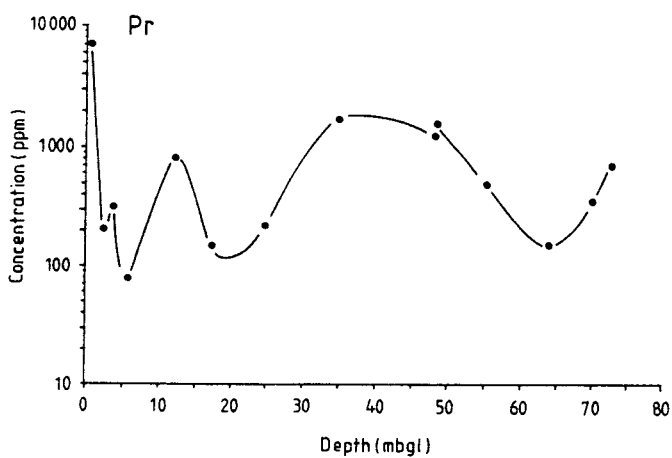
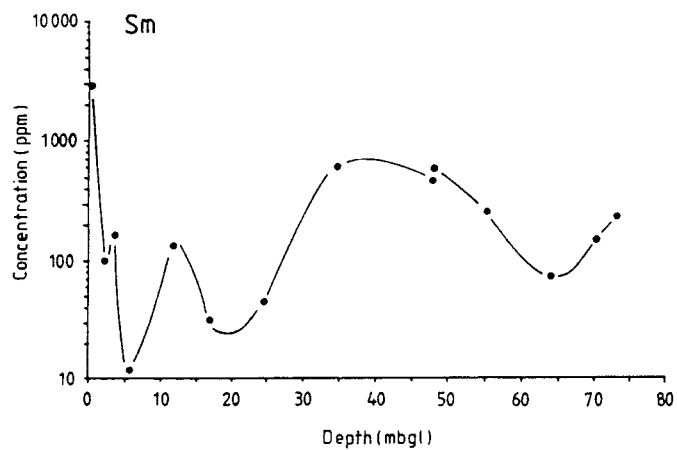
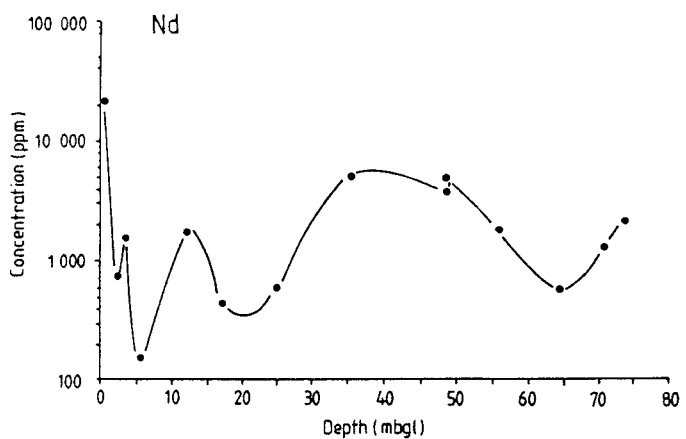
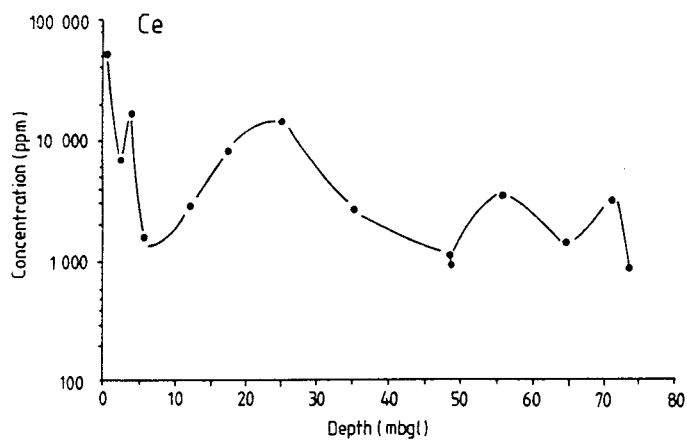
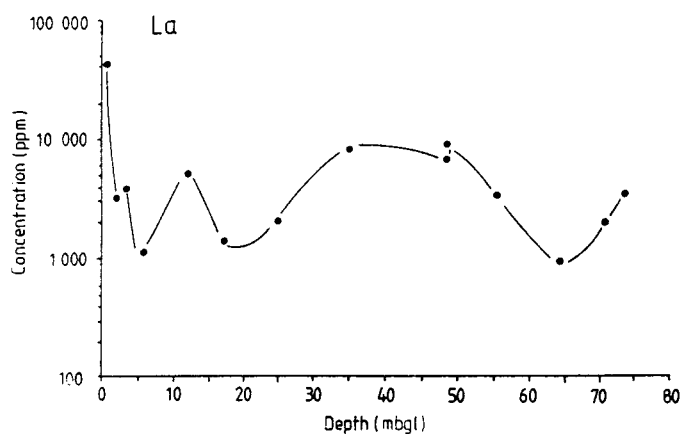


Figure 102. Light rare earth element profiles for drillcore MF10.

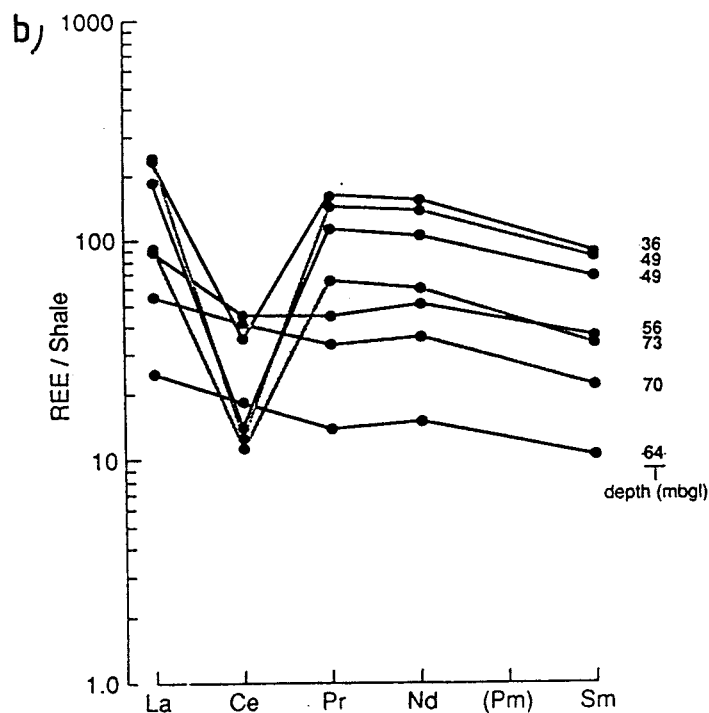
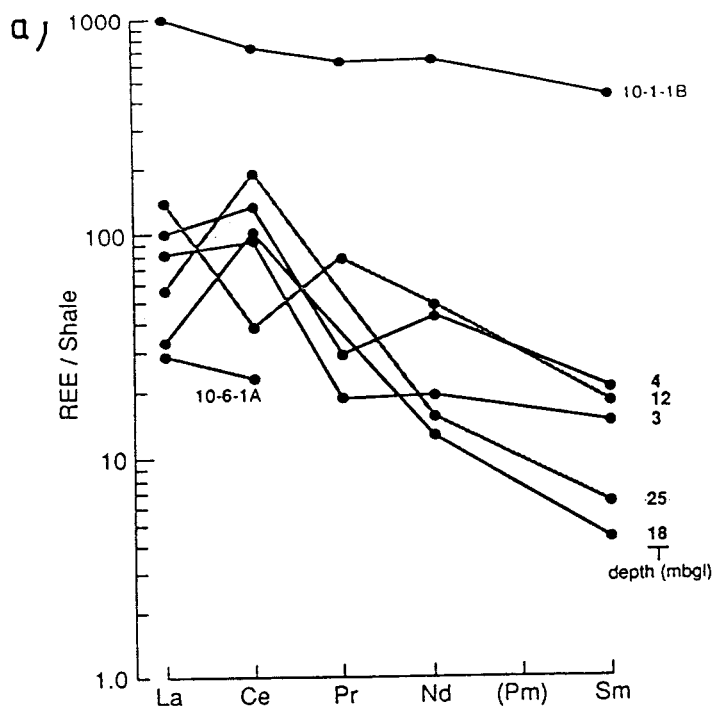


Figure 103.

(a) Shale-normalized concentration ratio diagram for light rare-earth elements for samples from drillcore MF10 in the unsaturated zone.

(b) Shale-normalized concentration ratio diagram for light rare-earth elements for samples from drillcore MF10 in the saturated zone.

its pronounced negative Ce anomaly) is similar to those taken from the weathered, saturated zone beginning at 36 mbgl (see Waber, this report series; Rep. 3). At the top of the saturated zone, some 36 mbgl, strong Ce depletion is observed in samples 10-36-1A, 10-49-1A-A and nearby 10-49-1B, followed by modest to no depletion in samples 10-56-1A, 10-64-1A and 10-70-1A, and again strong depletion in 10-73-1A sampled near the bottom of this core.

Isotopic activity concentrations (Table XXIII) and isotopic ratio data (Table XXIV) indicate that for the thorium series, at least through to ^{228}Th , secular radioactive equilibrium is maintained as the $^{228}\text{Th}/^{232}\text{Th}$ ratios are not, with the exception of one sample (10-3-1A), significantly different from unity considering the uncertainties associated with the ratios. This indicates that ^{228}Ra ($t_{1/2} = 5.75\text{a}$), the parent of ^{228}Th and the likely candidate within the ^{232}Th decay chain to have the potential for in-situ migration because of its relatively high solubility, is either retained where it is radiogenically produced or is migrating from the mineralized zone very slowly relative to its half-life. These results are consistent with the very slow current mobilization rate that has been reported for ^{228}Ra based on annual stream transport of ^{228}Ra away from the ore body in solution ($\leq 0.45 \mu\text{m}$) and the estimate for the ^{228}Ra burden within the ore body, i.e. the flux/inventory ratio (Campos *et al.*, 1986).

The U series activity ratio data are shown in Figure 104 using an interpretive plot of $^{230}\text{Th}/^{238}\text{U}$ against $^{234}\text{U}/^{238}\text{U}$ (after Thiel *et al.*, 1983), the explanation for which has previously been given. With the exception of four points (two which cannot be explained in terms of a single process, e.g. 10-25 and 10-56 and two of the deepest samples which lie in the zone of U-accumulation, e.g. 10-64 and 10-73), the isotopic ratio data indicate uranium loss which can be interpreted as occurring from a single process. Two additional samples, 10-49-1A-A and 10-49-1A-B, which represent clay material sampled in close proximity to a fracture, fall within a region forbidden as originating from a continuous single process, although their uncertainty estimates could easily place them within the zone of U loss from a single process.

As might be expected from infiltrating, oxidizing rainwater which will oxidize U to the more soluble, hexavalent state, samples taken from near the surface, e.g. 10-3 and 10-4, have $^{234}\text{U}/^{238}\text{U}$ activity ratios of unity and $^{230}\text{Th}/^{234}\text{U}$ activity ratios of 1.8 and 1.21 respectively. This indicates that, for these samples, loss of both U isotopes by bulk leaching processes is masking, i.e. occurring at a greater rate than, any preferential removal of ^{234}U (e.g. from alpha recoil and/or accelerated solubilization along alpha tracks). We cannot, however, omit the fact that preferential removal of ^{234}U is also occurring both close to the surface, e.g. 10-1 ($^{234}\text{U}/^{238}\text{U} = 0.93$) and 10-6 ($^{234}\text{U}/^{238}\text{U} =$

TABLE XXIII
Radionuclide concentrations in core samples from borehole MF10.

Sample no	Depth (mbgl)	Concentration (Bq/g dry \pm 1 SD)					
		^{232}Th	^{230}Th	^{228}Th	^{234}U	^{238}U	^{231}Pa
10-1-1B-a	0.42 – 0.50	NC	NC	NC	0.57 ± 0.03	0.61 ± 0.03	NA
-b	0.42 – 0.50	234 ± 5	2.0 ± 0.3	236 ± 5	NA	NA	0.027 ± 0.002
-c	0.42 – 0.50	226 ± 3	1.3 ± 0.2	219 ± 3	NA	NA	NA
10-3-1A	2.35 – 2.40	47 ± 3	0.85 ± 0.18	50 ± 3	0.43 ± 0.03	0.44 ± 0.03	NA
-b	2.35 – 2.40	47 ± 1	0.72 ± 0.07	51 ± 1	NA	NA	0.019 ± 0.001
10-4-1A-a	3.51 – 3.65	NC	NC	NC	0.66 ± 0.01	0.66 ± 0.01	NA
10-4-1A-b	3.51 – 3.65	48 ± 2	0.80 ± 0.10	47.0 ± 2.1	NA	NA	NA
10-6-1A	5.58 – 5.72	50 ± 3	0.42 ± 0.06	49 ± 3	0.35 ± 0.01	0.39 ± 0.01	NA
10-12-1B	11.90 – 12.00	7.36 ± 0.41	0.30 ± 0.03	7.37 ± 0.41	0.23 ± 0.01	0.24 ± 0.01	NA
10-18-1A	17.07 – 17.20	23.8 ± 1.5	0.54 ± 0.05	23.8 ± 1.5	0.42 ± 0.01	0.43 ± 0.01	NA
10-25-1A	24.77 – 24.86	8.53 ± 0.64	0.87 ± 0.06	8.23 ± 0.44	0.93 ± 0.04	0.94 ± 0.04	NA
10-36-1A	34.95 – 35.06	4.70 ± 0.24	0.29 ± 0.03	4.61 ± 0.23	0.27 ± 0.01	0.28 ± 0.01	NA
10-49-1A-A	48.20 – 48.27	2.10 ± 0.11	0.36 ± 0.02	2.14 ± 0.11	0.37 ± 0.01	0.39 ± 0.01	NA
10-49-1A-B	48.27 – 48.30	2.00 ± 0.12	0.24 ± 0.02	2.07 ± 0.12	0.24 ± 0.01	0.26 ± 0.01	NA
10-56-1A	55.20 – 55.25	1.5 ± 0.1	0.33 ± 0.02	1.5 ± 0.1	0.38 ± 0.02	0.41 ± 0.02	NA
10-64-1A	63.65 – 63.75	1.23 ± 0.08	0.27 ± 0.02	1.18 ± 0.07	0.31 ± 0.01	0.31 ± 0.01	NA
10-70-1A	70.30 – 70.13	1.32 ± 0.08	0.35 ± 0.02	1.40 ± 0.08	0.35 ± 0.01	0.35 ± 0.01	NA
10-73-1A	72.61 – 72.81	0.90 ± 0.05	0.25 ± 0.02	0.88 ± 0.05	0.26 ± 0.01	0.24 ± 0.01	NA

NC refers to not calculated due to inability to accurately assess radiochemical ^{229}Th yield. Subsequent aliquots utilized ^{234}Th tracer.
N.B. Errors are based on one sigma counting statistics plus one percent uncertainty in the spike.

Uranium Decay Series Analysis for the MF 10 Borehole

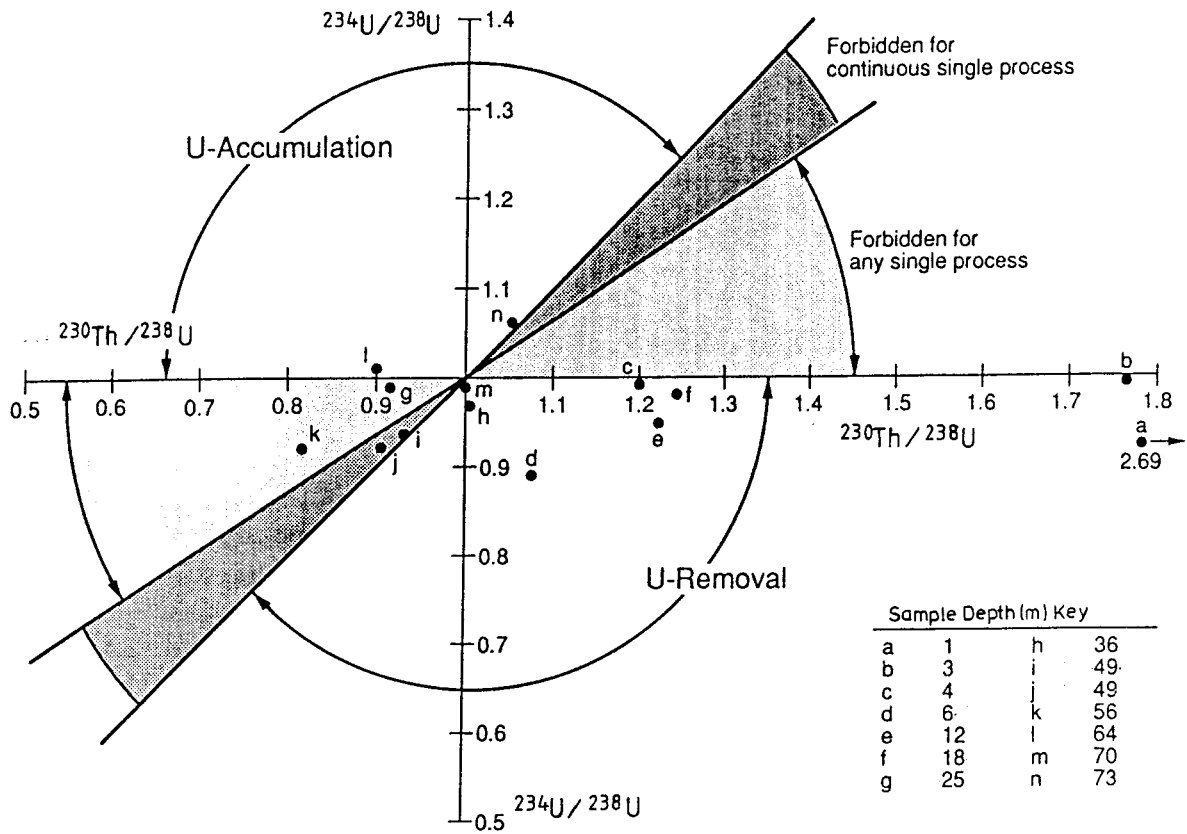


Figure 104. $^{234}\text{U}/^{238}\text{U}$ activity ratio versus $^{230}\text{Th}/^{238}\text{U}$ activity ratio diagram for samples from drillcore MF10.

0.89), and throughout this core up to about 64 mbgl (Fig. 105), as evidenced by $^{234}\text{U}/^{238}\text{U}$ ratios <1.0 . The limited $^{231}\text{Pa}/^{235}\text{U}$ data given in Table XXIV (ratios not significantly different from 1.0 in the two uppermost samples for which data are available) suggest that the rate of bulk U leaching may be slow relative to the 3.28×10^4 year half-life of ^{231}Pa , since it is normally assumed that protactinium is immobile under oxidizing conditions relative to uranium and that a more rapid ^{235}U loss from leaching should be manifest as $^{231}\text{Pa}/^{235}\text{U} > 1.0$. Groundwater data from MF10 are indicative of present-day, preferential loss of ^{234}U , since $^{234}\text{U}/^{238}\text{U}$ ratios from five samples range between 1.11 and 1.39 and average 1.29 ± 0.11 (± 1 SD).

TABLE XXIV
Isotopic ratios in core samples from borehole MF10.

Sample no	Ratio ± 1 SD			
	$^{234}\text{U}/^{238}\text{U}$	$^{230}\text{Th}/^{234}\text{U}$	$^{228}\text{Th}/^{232}\text{Th}$	$^{231}\text{Pa}/^{235}\text{U}$
10-1-1B-a	0.93 ± 0.04	NC	1.04 ± 0.02	0.96 ± 0.09
-b	NA	3.54 ± 0.53	1.01 ± 0.02	NA
-c	NA	2.25 ± 0.36	0.97 ± 0.02	NA
10-3-1A	0.99 ± 0.05	1.98 ± 0.44	1.06 ± 0.03	0.94 ± 0.08
-b	NA	1.58 ± 0.19	1.10 ± 0.02	NA
10-4-1A	0.99 ± 0.03	1.21 ± 0.15	0.97 ± 0.03	NA
10-6-1A	0.89 ± 0.03	1.21 ± 0.18	0.98 ± 0.03	NA
10-12-1B	0.95 ± 0.03	1.28 ± 0.13	1.00 ± 0.02	NA
10-18-1A	0.98 ± 0.04	1.27 ± 0.13	1.00 ± 0.02	NA
10-25-1A	0.99 ± 0.05	0.93 ± 0.07	0.96 ± 0.03	NA
10-36-1A	0.97 ± 0.04	1.04 ± 0.12	0.98 ± 0.03	NA
10-49-1A-A	0.94 ± 0.03	0.99 ± 0.06	1.02 ± 0.02	NA
10-49-1A-B	0.92 ± 0.04	0.99 ± 0.08	1.03 ± 0.02	NA
10-56-1A	0.93 ± 0.04	0.87 ± 0.07	1.00 ± 0.03	NA
10-64-1A	1.01 ± 0.03	0.89 ± 0.07	0.96 ± 0.03	NA
10-70-1A	0.99 ± 0.03	1.01 ± 0.06	1.06 ± 0.03	NA
10-73-1A	1.06 ± 0.04	0.98 ± 0.07	0.98 ± 0.03	NA

* ^{235}U estimated as $0.046(^{238}\text{U}$ activity).

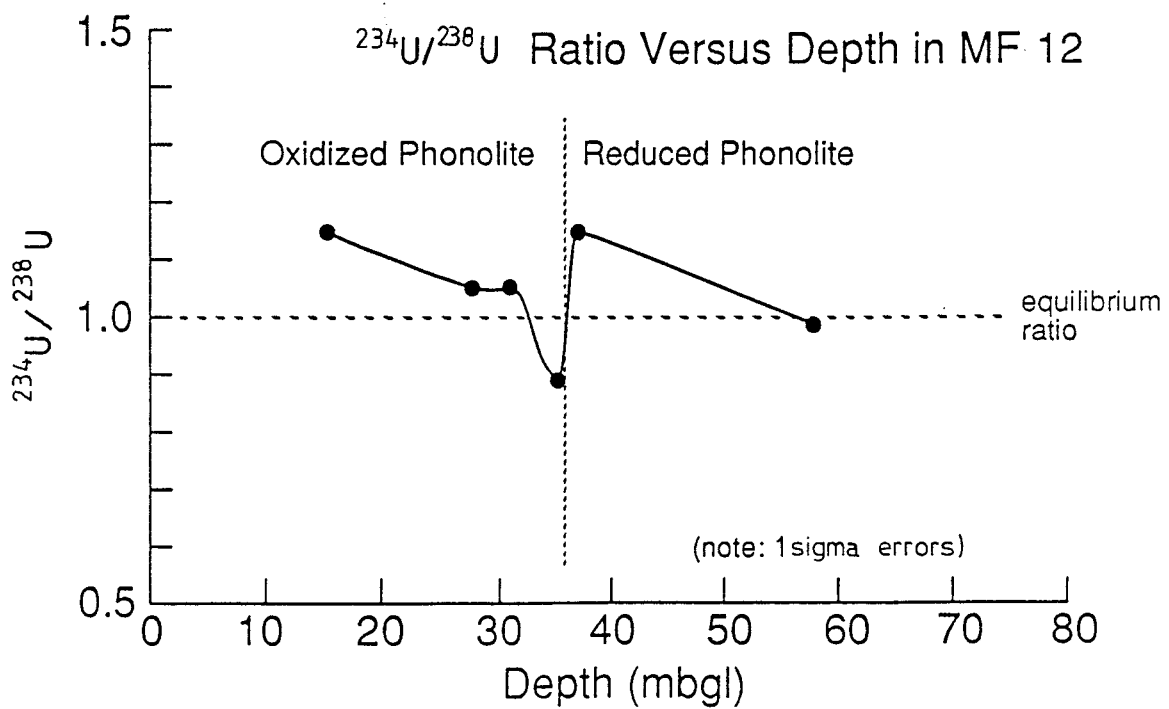
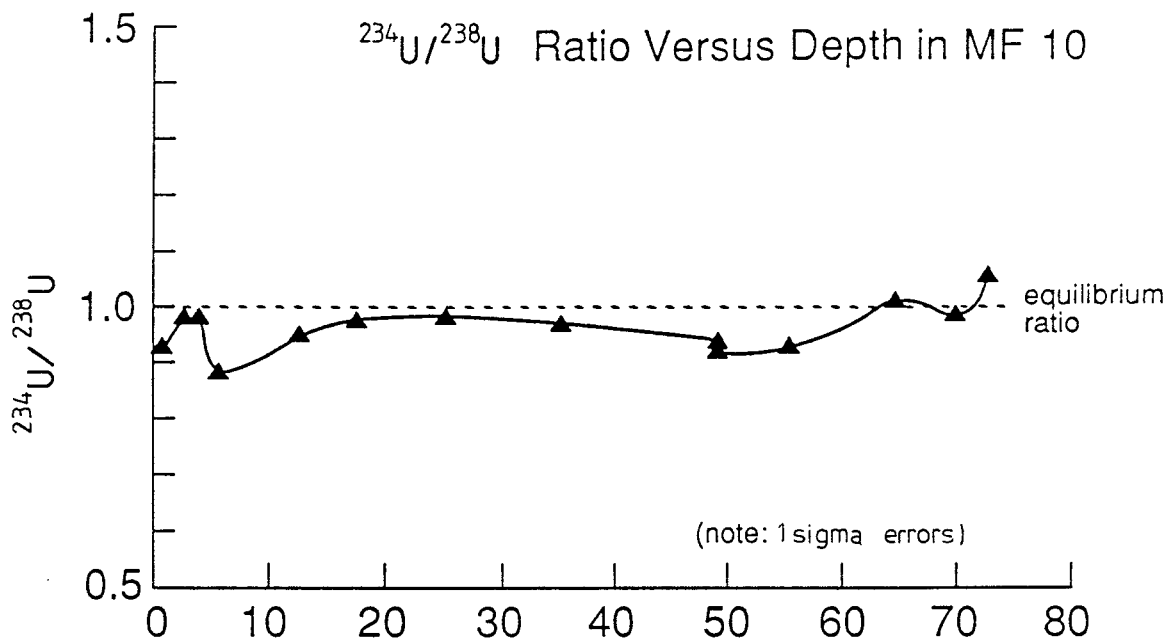


Figure 105. $^{234}\text{U}/^{238}\text{U}$ versus depth profiles for drillcores MF10 and MF12.

3.2.2. Borehole MF12

The MF12 borehole, which was drilled close to the South Stream near the base of the Morro do Ferro (Fig. 100) to a depth of 71 mbgl, is characterized over its first 27.5 metres by an intensely altered and weathered lateritic cover (mainly aluminium hydrates and clay minerals) followed by competent bedrock beginning at this depth and extending to the core bottom. A very dispersed redox front was observed at 35.7 mbgl, and rock samples obtained below this depth are characterized as reduced and those above this front as oxidized. The competent bedrock has been described as a hydrothermally altered and weathered phonolite, similar to the phonolites found at the Osamu Utsumi uranium mine (Waber *et al.*, this report series; Rep. 2). Based on the gamma log and alpha spectrometric results reported here, no obvious Th or U mineralization occurs in either the laterite cover or the competent bedrock below, although the LREEs are considerably enriched.

TABLE XXV

REE, Th and U concentrations in core sections from borehole MF12.

Sample no	Concentration ($\mu\text{g/g dry} \pm 1 \text{ SD}$)*						
	Ce	La	Nd	Pr	Sm	Th	U
12-16-1a	1878 \pm 20	7353 \pm 20	4551 \pm 49	1414 \pm 32	595 \pm 7	129.1 \pm 6.7	63.2 \pm 3.4
12-28-1a	1040 \pm 11	654 \pm 7	258 \pm 3	76 \pm 3	33 \pm 1	60.6 \pm 3.4	23.4 \pm 1.1
12-31-1b	1453 \pm 15	2630 \pm 27	736 \pm 27	261 \pm 4	82 \pm 1	77.7 \pm 4.3	29.5 \pm 1.3
12-35-1a	1318 \pm 13	2090 \pm 21	495 \pm 56	168 \pm 4	55 \pm 2	105 \pm 7	43.1 \pm 2.2
12-37-1b	1639 \pm 18	1362 \pm 15	328 \pm 86	118 \pm 11	47 \pm 1	41.9 \pm 2.2	25.3 \pm 1.1
12-58-1a	1275 \pm 65	987 \pm 29	257 \pm 88	93 \pm 3	35 \pm 1	69.7 \pm 3.8	87.1 \pm 4.4

*REE analysis by ICP-OES, Th and U by alpha spectrometry.

Mass concentrations for the LREEs, Th and U (Table XXV) indicate approximately an order-of-magnitude decrease in LREEs other than Ce between the middle of the laterite cover (12-16-1a) and the sharp transition zone between the cover and competent bedrock at 27.5 mbgl. Ce, Th and U also decline but only by factors of 2 (Ce, Th) to 3 (U). Below the laterite cover, after an initial increase from the minimum concentrations observed at the boundary, the LREEs (again excluding Ce) show a decreasing trend with increasing depth, while Ce, Th and U show no distinct trends. Median concentrations (n=6) for Ce, La, Nd, Pr, Sm, Th and U (in ppm) are 1386, 1726, 411, 143, 51, 74 and 36, respectively. Unlike results obtained from within the mineralized zone, Ce and Th concentrations are not correlated whereas U and Th are ($r = 0.94$, $n = 5$), albeit only

TABLE XXVI
Radionuclide concentrations in core samples from borehole MF12

Sample no	Description	Depth (mbgl)	Concentration (Bq/g dry \pm 1 SD)				
			^{232}Th	^{230}Th	^{228}Th	^{234}U	^{238}U
12-16-1a	Red-brown lateritic cover	16	0.520 ± 0.027	0.750 ± 0.036	0.550 ± 0.028	0.907 ± 0.40	0.777 ± 0.042
12-28-1a	Border between lateritic cover and oxid. phonolite	27.5	0.244 ± 0.014	0.344 ± 0.018	0.247 ± 0.014	0.305 ± 0.014	0.288 ± 0.014
12-31-1b	Oxidized phonolite (mainly nepheline)	31	0.313 ± 0.017	0.425 ± 0.023	0.289 ± 0.017	0.386 ± 0.017	0.363 ± 0.016
12-35-1a	Oxidized phonolite (mainly nepheline)	35	0.425 ± 0.026	0.530 ± 0.032	0.462 ± 0.028	0.469 ± 0.024	0.530 ± 0.027
12-37-1b	Reduced phonolite (argillic alteration)	37	0.169 ± 0.009	0.315 ± 0.016	0.164 ± 0.009	0.367 ± 0.016	0.311 ± 0.014
12-58-1a	Reduced phonolite (argillic alteration)	58	0.28 ± 0.015	1.008 ± 0.048	0.272 ± 0.015	1.045 ± 0.052	1.071 ± 0.054

after the exclusion of the deepest sample obtained (12-58-1a), in which the concentration of U (87 ppm) exceeds that of Th (70 ppm).

The shale-normalized LREE profiles (Fig. 106) indicate a strong negative Ce anomaly within the laterite cover (12-16-1A, 1404 metres above sea-level), which roughly coincides, in terms of sampling height, with the negative anomaly in sample 10-73-1A from the MF10 core (about 1406 masl). This implies a continuity within the weathered zone over a horizontal distance of about 100–200 m, which is consistent with both the current groundwater flow pattern (Fig. 100) and the notion that this flow pattern has been in existence for a long time period. Proceeding deeper into the core, the negative Ce anomaly is absent at 28 mbgl, reappears at 31 and 35 mbgl, and is absent at 37 and 58 mbgl. Thus the recurring, relative Ce enrichment/depletion pattern that was observed in MF10 is somewhat subdued in MF12, as reflected by the absence of any strong, positive Ce anomalies within six samples analyzed.

Natural series radionuclide data (Table XXVI) and corresponding isotopic ratios (Table XXVII), when shown on an interpretive plot of U series disequilibria ($^{234}\text{U}/^{238}\text{U}$ vs $^{230}\text{Th}/^{238}\text{U}$, Fig. 107), indicate a more complex pattern in the downflow borehole MF12 than was observed in MF10. For example, samples 12-16 (laterite cover) and 12-37 (competent, reduced phonolite) lie clearly within the U accumulation zone which can be represented by a single process, while 12-28 (border between laterite and oxidized phonolite) and 12-31 (oxidized phonolite) lie within a zone of U accumulation which is forbidden for any single process, be it short-term or continuous. The deepest sample analyzed within this core, 12-58, also a reduced phonolite, has isotopic ratios sufficiently close to 1.0 to imply attainment of secular equilibrium. One sample within this core,

TABLE XXVII

Activity ratios in core samples from borehole MF12.

Sample no	Ratio ± 1 SD		
	$^{234}\text{U}/^{238}\text{U}$	$^{230}\text{Th}/^{234}\text{U}$	$^{228}\text{Th}/^{232}\text{Th}$
12-16-1a	1.17 \pm 0.03	0.83 \pm 0.06	1.06 \pm 0.05
12-28-1a	1.06 \pm 0.02	1.13 \pm 0.08	1.03 \pm 0.05
12-31-1b	1.06 \pm 0.02	1.10 \pm 0.08	0.92 \pm 0.04
12-35-1a	0.89 \pm 0.03	1.13 \pm 0.09	1.09 \pm 0.05
12-37-1b	1.18 \pm 0.03	0.86 \pm 0.06	0.97 \pm 0.04
12-58-1a	0.98 \pm 0.02	0.96 \pm 0.07	0.97 \pm 0.04

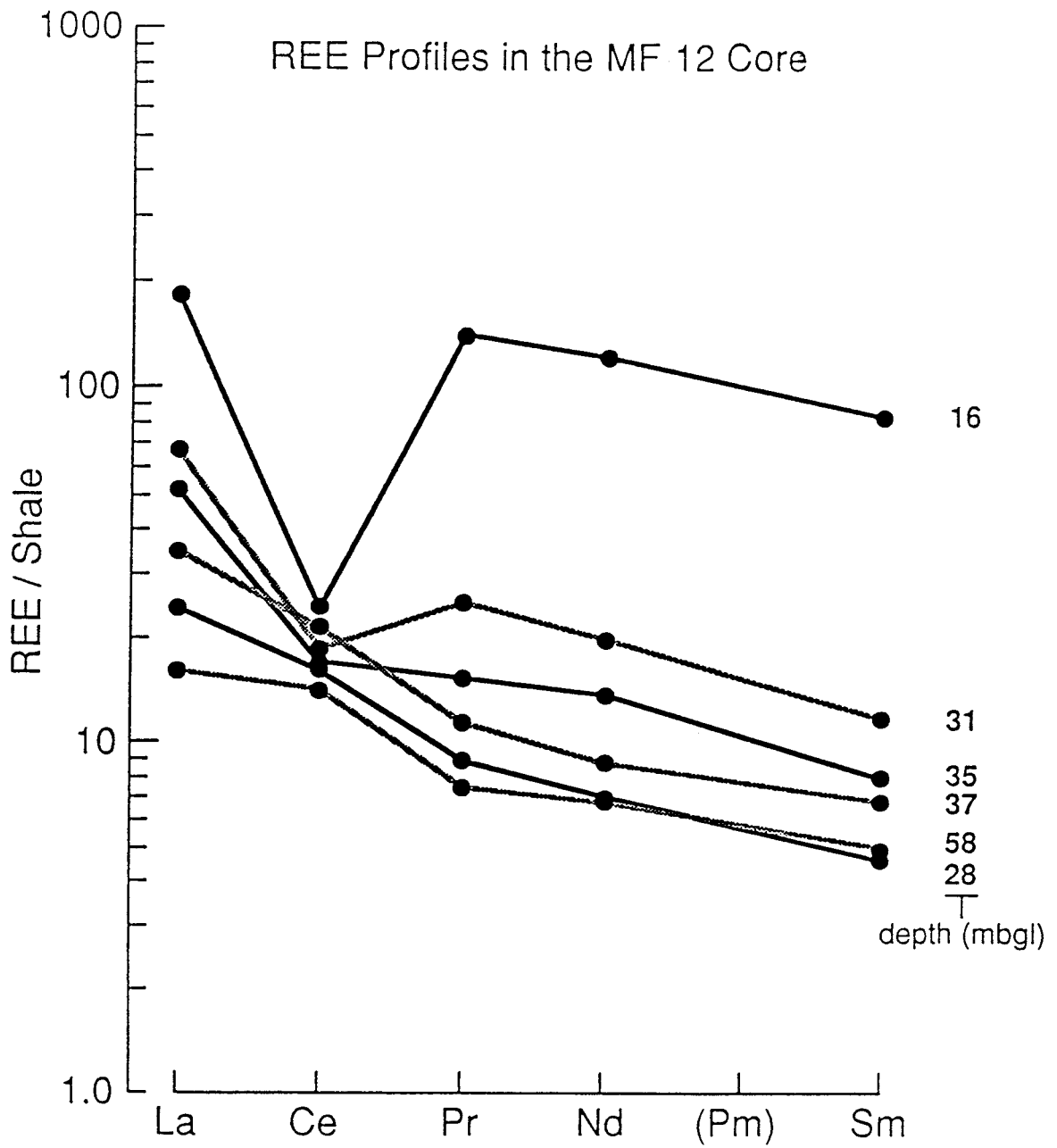


Figure 106. Shale-normalized concentration ratio diagram for eight rare-earth elements for samples from drillcore MF12.

Uranium Decay Series Analysis for the MF 12 Borehole

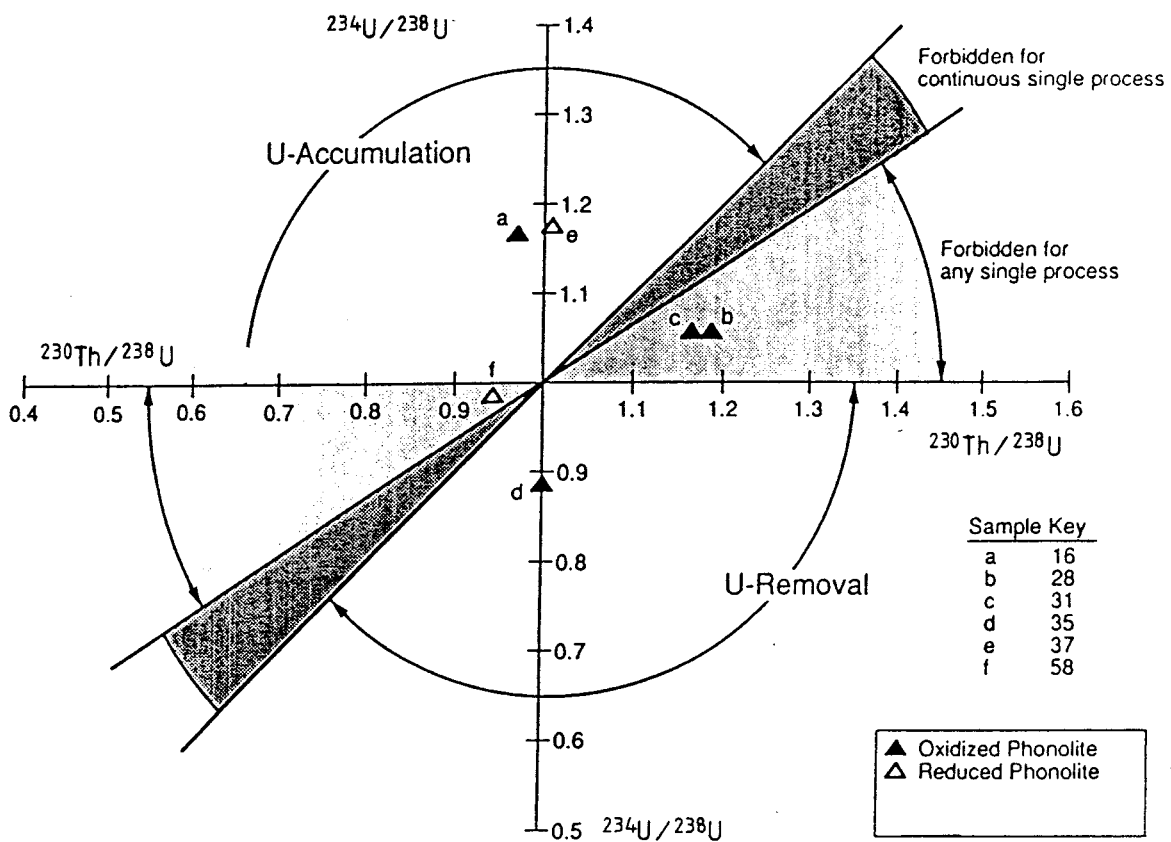


Figure 107. $^{234}\text{U}/^{238}\text{U}$ activity ratio versus $^{230}\text{Th}/^{238}\text{U}$ activity ratio diagram for samples from drillcore MF12.

12-25, an oxidized phonolite taken at the dispersed redox front, clearly lies within the zone of U removal attainable by a single process.

3.3. Discussion

The very complex clay mineralogy which constitutes the sampled material, together with preliminary findings of a random occurrence of Fe and Mn oxyhydrates (Waber, this report series; Rep. 3), has precluded any clear correlation of the observed Th or LREE patterns with either the occurrence or concentration of any particular clay minerals, original or secondary host minerals, or any potentially important surficial constituents such as oxyhydrates of Fe and Mn which are in abundance throughout the cores.

A hypothesis for the recurring positive/negative Ce anomalies observed in MF10 may be that the pattern is a relic from the earlier migration of a redox front. For example, the oxidation of Ce (III) to less soluble Ce (IV) in samples taken near the current surface, e.g. 10-3 and 10-4, would tend to retard the vertical migration of this element relative to the trivalent LREEs, resulting in an apparent Ce enrichment. The faster moving or more soluble trivalent LREEs may subsequently become more readily available for adsorptive processes or otherwise be retarded in their downward migration, resulting in an apparent negative Ce anomaly as exemplified within deeper samples such as 10-6-1A and 10-12-1B.

Samples that show the positive Ce anomaly might also be expected to have $^{230}\text{Th}/^{234}\text{U} > 1.0$ since oxidation would be expected to result in increased U mobility due to the formation of more stable soluble uranyl complexes. This is evident in samples 10-3, 10-4 and 10-18, but not in 10-25, which has the positive anomaly but a $^{230}\text{Th}/^{234}\text{U}$ ratio of 0.93 ± 0.07 . The absence of any observed positive Ce anomaly in MF12 (at least below the surface 16 m) is consistent with the contemporary upward flow path of reducing groundwaters.

4. Conclusions

The following general conclusions can be drawn from the preceding discussion.

1. The generally greater solubility of U(VI) and Ra than U(IV), Th and Pa in groundwater is confirmed.

2. The long-term (on a 10^6 a timescale) direction of groundwater flow has probably been approximately parallel with the redox fronts, i.e. downwards along the line of the fracture intersecting the F1 drillcore at 50 m.
3. There is clear evidence of preferential deposition and enrichment of uranium on the reduced side of redox fronts within the last 3×10^5 a. The deposited uranium occurs both as dispersed uranium, probably in the form of very thin precipitates on the surfaces of other minerals, and as nodules.
4. Uranium deposition also occurs on the oxidized side of the fronts, probably by incorporation in iron oxides. Thermodynamically, uranium would be predicted to be soluble in this environment, but there is clear evidence of significant enrichment and retention of uranium in the oxidized rock for times up to 7×10^5 a.
5. The probability of removal of uranium to solution in groundwater in the reduced rock of the Osamu Utsumi mine is estimated to be about $0.36 \times 10^{-6} \text{a}^{-1}$ for ^{238}U and about $0.8 \times 10^{-6} \text{a}^{-1}$ for ^{234}U . The probability of ^{238}U removal to solution in groundwater from the oxidized rock is estimated to be about $1.7 \times 10^{-6} \text{a}^{-1}$.
6. The distribution of uranium (and other elements) about the redox fronts suggests that long-term advective flow of groundwater has occurred parallel to the direction of the fronts, with dissolution at the front and diffusive movement of the dissolved species into both the oxidized and the reduced rock.
7. Dissolution of dispersed uranium occurs at the redox front at the same position as the colour change marking the Fe(II)/Fe(III) transition, indicating a sharp gradient in Eh. Deposition of dispersed uranium can occur at depths of metres into the reduced rock.
8. Some of the uranium nodules are young (on a $10^5 - 10^6$ a timescale) and exhibit growth rates of 1.8 – 2.6 cm in 10^6 a. Other nodules are old (on a $10^5 - 10^6$ a timescale) and demonstrate the chemical stability of uranium plus daughters in this form of deposit under reducing conditions for times in excess of 3×10^5 a.
9. The time required for growth of micronodules of uranium in the reduced rock close to the front is in the order of 10^5 a. Unlike dispersed uranium, nodules are not necessarily dissolved at the redox front marking the Fe(II)/Fe(III) colour change. Micronodule dissolution in the oxidized rock, following movement of the front past the nodule, takes in the order of $10^4 - 10^5$ a.

10. The natural ^{239}Pu content of a uranium nodule from the mine was measured as $2.3 \pm 0.7 \times 10^8$ atoms per gram, consistent with a state of secular equilibrium with the uranium present. The result indicates the chemical stability of co-existing uranium and plutonium in nodules in the reduced rock for at least 10^7 a.
11. The redox front at 42.0 m in the F1 drillcore has moved very little, on a cm scale, during the last 7×10^5 a. The other redox fronts have probably moved at a rate in the range 2 to 20 m in the last 10^6 a.
12. $^{234}\text{U}/^{238}\text{U}$ versus $^{230}\text{Th}/^{238}\text{U}$ diagrams are confirmed as highly useful in the interpretation of natural decay series data, with excellent agreement between observed results and theoretical models in a number of cases.
13. Some degree of dissolution and redistribution of thorium is apparent, but the degree of redistribution of thorium is about two orders of magnitude less than that of uranium.
14. Thorium is preferentially enriched on the reduced side of the redox fronts but the magnitude of this effect decreases with increasing depth in the mine, consistent with decreasing transport of thorium with increasing length of flow path of the groundwater. This is the opposite of the trend exhibited by uranium, where the extent of enrichment increases for deeper redox fronts, i.e. the greater the length of the water flow path, the greater is the degree of separation of uranium from thorium.
15. Alpha recoil effects clearly result in preferential loss of ^{234}U from the solid phase to solution in both the oxidized and the reduced rock, resulting in an enhanced mobility of the daughter isotope. The effect must clearly be considered in any far-field situation where serial decay of escaped radionuclides occurs. It is, however, significant that ^{234}U produced in situ is more mobile than ^{230}Th despite the fact that both will be susceptible to alpha recoil loss to solution.
16. ^{226}Ra is lost from the reduced rock and deposited in the oxidized rock at the deeper redox fronts but is subject to more general deposition in upper sections of the mine. These trends suggest that the ^{226}Ra concentration in solution is controlled either by the sulphide/sulphate system or by iron or manganese oxide scavenging.

17. Active redistribution of uranium and radium is apparent in the reduced phonolite well below the redox fronts, particularly in the vicinity of the conductive zone in the F1 drillcore. This may represent the incipient effects of a developing finger of oxidation around the conductive zone in response to preferential downward flow of oxidizing water at this location.
18. In addition to uranium, other elements which are subject to dissolution or deposition as a result of oxidation also show major redistribution as a consequence of the movement of the redox front through the rock e.g. Mo and Ce.
19. There is a general depletion of elements of higher solubility from the oxidized rock, but an enrichment in resistate species (such as Th) and in elements scavenged from solution by iron oxides.
20. The redox fronts represent zones of enrichment for many elements, with the distribution of elements about the front varying with their chemistry. The redox fronts thus constitute retardation zones which, in the context of far-field migration, of radionuclides would, in the first instance, be beneficial. In the longer term, however, if the redox front were to move over a sufficient distance, it could result in the breakthrough of a front containing enhanced radionuclide concentrations into the near-surface zone.

5. Acknowledgements

The authors express their thanks to the funding bodies: SKB (Sweden), NAGRA (Switzerland), The Department of the Environment (UK) and The Department of Energy (USA). Our gratitude is also extended to Nick Waber of The University of Bern, who collected, prepared and distributed most of the samples used in this study. Thanks also go to our numerous colleagues in Brazil who contributed much to the project, in particular Eduardo Penna Franca, Luis Borosso and Hans Schorscher. The members of The Project Technical Committee are thanked for their efforts throughout the course of the work, in particular John Smellie and Ian McKinley for comments and assistance in preparation of this manuscript. Finally, our thanks go to Fred Karlsson as manager of the Project.

6. References

- Alexander, W.R., Scott, R.D., MacKenzie, A.B. and McKinley, I.G., 1988. A natural analogue study of radionuclide migration in a water conducting fracture in crystalline rock. *Radiochim. Acta*, 44/45, 283-289.
- Alexander, W.R., McKinley, I.G., MacKenzie, A.B. and Scott R.D., 1989(a). Attempted verification of matrix diffusion by means of natural decay series disequilibria in a profile across a water conducting fracture in granitic rock. In: Scientific Basis for Nuclear Waste Management, XIII. *Mat. Res. Soc. Symp. Proc.*, 567 – 576.
- Alexander, W.R., MacKenzie, A.B., Scott, R.D. and McKinley, I.G., 1989(b). Natural analogue studies using the natural decay series radionuclides. *NAGRA Tech. Rep.* (NTB 87-08), Baden, Switzerland.
- Anderson, R.F., Bacon, M.P. and Brewer, P.G., 1983(a). Removal of ^{230}Th and ^{231}Pa from the open ocean. *Earth Planet. Sci. Lett.*, 62, 7-23.
- Anderson, R.F., Bacon, M.P. and Brewer, 1983(b). Removal of ^{230}Th and ^{231}Pa at ocean margins. *Earth Planet. Sci. Lett.*, 66, 73-90.
- Andrews, J.N. and Kay, L.F., 1982. $^{234}\text{U}/^{238}\text{U}$ ratios of dissolved uranium in groundwater from a jurassic aquifer in England. *Earth Planet. Sci. Lett.*, 57, 139-151.
- Briesmeister, J.F., 1986 (Ed.). MCNP – a general Monte Carlo Code for neutron and photon transport. *Los Alamos Report LA-7396-M*.
- Broecker, W.S., Kaufman, A and Trier, R.M., 1973. The residence time of thorium in surface sea water and its implications regarding the fate of reactive pollutants. *Earth Planet. Sci. Lett.*, 20, 35-44.
- Campos, M.S., Penna Franca, E., Lobas, N., Trindade, H. and Sachett, I., 1986. Migration of radium from the thorium deposit of Morro do Ferro, Poços de Caldas, Brazil. *J. Environ. Radioactivity*, 3, 145-161.
- Chapman, N.A., McKinley, I.G. and Smellie, J.A.T., 1984. The potential of natural analogues in assessing systems for deep disposal of high-level radioactive waste. *SKB Tech. Rep.* (TR 84-16), Stockholm, Sweden; *NAGRA Tech. Rep.* (NTB 84-41), Baden; Switzerland, *EIR (now PSI) Tech. Rep.* (EIR-545), Würenlingen, Switzerland.
- Colley, S., Thomson, J., Wilson, T.R.S. and Higgs, N.C., 1984. Post depositional migration of elements during diagenesis in brown clay and turbidite sequences in the North East Atlantic. *Geochim. Cosmochim. Acta*, 48, 1223-35.

- Colley, S., Thomson, J. and Toole, J., 1989. Uranium relocations and derivation of quasi isochrons for a turbidite/pelagic sequence in the Northeast Atlantic. *Geochim. Cosmochim. Acta*, 53, 1223-34.
- Cook, G.T., Baxter, M.S., Duncan, H.J., Toole, J. and Malcolmson, R., 1984. Geochemical associations of plutonium in the Caithness environment. *Nucl. Instr. Methods. Phys. Res.*, 223, 517-522.
- Cotton, F.A. and Wilkinson, G., 1968. *Advanced Inorganic Chemistry*. John Wiley and Son.
- Cowart, J.B., 1980. The relationship of uranium isotopes to oxidation/reduction in the Edwards Carbonate aquifer of Texas. *Earth Planet. Sci. Lett.*, 48, 277-283.
- Das, N., 1985. Geochemical studies of the Caithness Flags. *Ph.D. Thesis*, University of Glasgow.
- Edmond, J.M., 1970. Comments on the paper by Ku *et al.*. Radium in the Indian-Antarctic Ocean. *J. Geophys. Res.*, 75, 6878-9.
- Eisenbud, M., Krauskopf, K., Penna Franca, E., Lei, W., Ballad, R. and Linsalata, P., 1984. Natural analogues for the transuranic actinide elements. *Env. Geo. Water Sci.*, 6, 1-9.
- Fleischer, R.L., 1980. Isotopic disequilibrium of uranium: alpha recoil damage and preferential solution effects. *Science*, 207, 979-81.
- Frayha, R., 1962. Uranio o torio no planalla de Poços de Caldas. *Nat. Dept. of Mineral Production, Bull.*, 116, 75 pp.
- Friedlander, G., Kennedy, J.W., Macias, E.S. and Miller, J.M., 1981. *Nuclear and radiochemistry*, 3rd Edition. John Wiley and Sons.
- Gascoyne, M., 1986. Evidence for the stability of the potential nuclear waste host, sphene, over geological time, from uranium – lead ages and uranium series measurements. *Appl. Geochem.*, 1, 199-210.
- Gascoyne, M. and Schwarcz, H.P., 1986. Radionuclide migration over recent geologic time in a granitic pluton. *Chem. Geol.*, 59, 75-85.
- Greenwood, N.N. and Earnshaw, A., 1984. *Chemistry of the elements*. Pergamon Press.
- Guppy, R.M. and Atkinson, A., 1989. The evolution of redox conditions in a repository: preliminary investigations. *UK DOE Rep. (DOE/RW/89/103)*, London, U.K.
- Haskin, L.A. and Frey, F.A., 1966. Dispersed and not-so-rare earths. *Science*, 152, 299-152.

- Ivanovich, M. and Harmon, R.S., 1982 (Eds.). Uranium series disequilibrium: applications to environmental problems. *Oxford University Press, Oxford*.
- Kaufman, M.I., Rydell, H.S. and Osmond J.K., 1969. $^{234}\text{U}/^{238}\text{U}$ disequilibrium as an aid to the hydrologic study of the Floridan aquifer. *J. Hydrol.*, 9, 374-386.
- Kaufman, A., Trier, R.M., Broecker, W.S. and Feely, H.W., 1973. Distribution of ^{226}Ra in the world ocean. *J. Geophys. Res.*, 78, 8827-8848.
- Krauskopf, K.B., 1986. Thorium and rare-earth metals as analogues for actinide elements. *Chem. Geol.* 55, 323-335.
- Ku, T.L., Li, Y.J., Mathieu, G.G. and Wong, H.K., 1970. Radium in the Indian-Antarctic Ocean south of Australia. *J. Geophys. Res.*, 75, 5286-90.
- Latham, A.G. and Schwarcz, H.P., 1987(a). The relative mobility of U, Th and Ra isotopes in the weathered zones of the Eye-Dashwa Lakes granite pluton, northwestern Ontario, Canada. *Geochim. Cosmochim. Acta*, 51, 2787-93.
- Latham, A.G. and Schwarcz, H.P., 1987(b). On the possibility of determining rates of removal of uranium from crystalline igneous rocks using U-series disequilibria-1: a U-leach model and its applicability to whole-rock data. *Appl. Geochem.*, 2, 55-65.
- Latham, A.G. and Schwarcz, H.P., 1987(c). On the possibility of determining rates of removal of uranium from crystalline igneous rocks using U-series disequilibria-2: applicability of a U-leach model to mineral separates. *Appl. Geochem.*, 2, 67-71.
- Latham, A.G. and Schwarcz, H.P., 1989. Review of the modelling of radionuclide transport from U-series disequilibria and of its use in assessing the safe disposal of nuclear waste in crystalline rock. *Appl. Geochem.*, 4, 527-537.
- Lei, W., 1984. Thorium mobilization in a terrestrial environment. *Ph.D. Thesis*, New York University.
- Lei, W., Linsalata, P., Penna Franca, E. and Eisenbud, M., 1986. Distribution and mobilization of cerium, lanthanum and neodymium in the Morro do Ferro basin, Brazil. *Chem. Geol.*, 55, 3/4, 313-322.
- Li, Y.H., Ku, T-L., Mathieu, G.G. and Wolgemuth, K., 1973. Barium in the Antarctic Ocean and implications regarding the marine geochemistry of Ba and ^{226}Ra . *Earth Planet. Sci. Lett.*, 19, 352.

- Linsalata, P., Penna Franca, E., Sachett, I., de Castro, M.B., Lobão, N., Ballard, R., Lei, W., Ford, H., Morse, R. and Eisenbud, M., 1987. Radium, thorium and the light rare earth elements in soils and vegetables grown in an area of high natural radioactivity. In: J.E. Pinder, J.J. Alberts, K.W. McCleod and R.G. Schreckhise (Editors). *Environmental Research on Actinide Elements. CONF-841142*, 131-147.
- Linsalata, P., Morse, R., Ford, H., Eisenbud, M., Penna Franca, E., de Castro, M.B., Lobas, N., Sachett, I. and Carlos, M., 1989. An assessment of soil to plant concentration ratios for some natural analogues of the transuranic elements. *Health Phys.*, 56, 33-46.
- MacKenzie, A.B., Scott, R.D., Houston, C.M. and Hooker, P.J., 1989. Natural decay series radionuclide studies at the Needle's Eye natural analogue site, 1986-89. *British Geol. Surv. Rep.*, (WE/90/4), Keyworth, U.K.
- McKee, B.A., de Master, D.J. and Nittrouer, A., 1984. The use of $^{234}\text{U}/^{238}\text{U}$ disequilibrium to examine the fate of particle-reactive species on the Yangtze continental shelf. *Earth Planet. Sci. Lett.*, 68, 431-42
- Moore, W.S., 1969(a). Measurement of ^{228}Ra and ^{230}Th in sea water. *J. Geophys. Res.*, 74, 694.
- Moore, W.S., 1969(b). Oceanic concentrations of ^{228}Ra . *Earth Planet. Sci. Lett.*, 6, 437-446.
- Moore, W.S., 1972. Radium-228: application to thermocline mixing studies. *Earth Planet. Sci. Lett.*, 421-22.
- Moore, W.S. and Reid, D.E., 1973. Extraction of radium from natural waters using manganese impregnated acrylic fibres. *J. Geophys. Res.*, 78, 8880.
- NAGRA, 1985. Project Gewähr 1985. *NAGRA Tech. Rep.*, (NGB 85-09), Baden, Switzerland.
- Neretnieks, I., 1982. Diffusivities of some dissolved constituents in compacted wet bentonite clay – MX80 and the impact on radionuclide migration in the buffer. *KBS Tech. Rep. (TR 82-27)*, Stockholm, Sweden.
- Neretnieks, I. and Åslund, B., 1983 a. The movement of radionuclides past a redox front. *KBS Tech. Rep. (TR 83-66)*, Stockholm, Sweden.
- Neretnieks, I. and Åslund, B., 1983 b. Two dimensional movement of a redox front downstream from a repository for nuclear waste. *KBS Tech. Rep. (TR 83-68)*, Stockholm, Sweden.

- Osmond, J.K., Cowart, J.B., and Ivanovich, M., 1983. Uranium disequilibrium in groundwaters as an indicator of anomalies. *Int. J. Appl. Radiat. Isotopes*, 34, 283-308.
- Schwarcz, H.P., Gascoyne, M., and Ford, D.C., 1982. Uranium series disequilibrium studies of granitic rocks. *Chem. Geol.*, 36, 87-102.
- Scott, R.D., MacKenzie, A.B., Ben Shaban, Y.A., Hooker, P.J. and Houston, C.M., 1990. Uranium transport and retardation at the Needle's Eye natural analogue site, south west Scotland. *Radiochim. Acta*. (In press).
- Smellie, J.A.T., MacKenzie, A.B. and Scott, R.D., 1986. An analogue validation study of natural radionuclide migration in crystalline rocks using uranium series disequilibrium studies. *Chem. Geol.*, 55, 233-254.
- Thiel, K., Vorwerk, R., Saager, R. and Stupp, H.D., 1983. ^{235}U fission tracks and ^{238}U series disequilibria as a means to study recent mobilisation of uranium in Archaean pyritic conglomerates. *Earth Planet. Sci. Lett.*, 65, 249-262.
- Wedepohl, K.H., 1978 (Ed.). Handbook of Geochemistry, Vol. 11/5 Uranium. *Springer Verlag, Berlin*.
- Wedow, Jr. H., 1967. The Morro do Ferro thorium and rare earth ore deposits, Poços de Caldas District, Brazil. *U.S. Geol. Surv. Bull.*, 1185-D, Washington, pp.34.
- Wolgemuth, K., 1970. Barium analyses from the first Geosecs test cruise. *J. Geophys. Res.*, 76, 7686.
- Wolgemuth, K. and Broecker, W.S., 1970. Barium in sea water. *Earth Planet. Sci. Lett.*, 8, 372.

Appendix 1

Interlaboratory comparison of analytical methods.

Appendix 1

Interlaboratory comparison of analytical methods.

Three of the laboratories involved in the analysis of natural decay series radionuclides in the Poços de Caldas Project, namely the Scottish Universities Research and Reactor Centre (SURRC), New York University Medical Center (NYU) and the Pontifical Catholic University of Rio de Janeiro (PUC), participated in an analytical intercomparison. In this exercise, selected whole-rock samples from the F1 drillcore were analyzed for uranium and thorium isotopes by anion exchange separation and alpha spectroscopy techniques, while total uranium and thorium concentrations were also determined by a variety of additional methods.

The results for ^{238}U specific activity and $^{234}\text{U}/^{238}\text{U}$ activity ratio determinations by alpha spectrometry are shown in Table 1-I. The ^{238}U specific activity data show generally good agreement between the three laboratories with the agreement for the

TABLE 1-I

Intercomparison of results for isotopic analysis of uranium in samples from the F1 drillcore.

Sample	^{238}U specific activity (Bq kg ⁻¹)			$^{234}\text{U}/^{238}\text{U}$ activity ratio		
	SURRC	PUC	NYU	SURRC	PUC	NYU
16-1A	248	242	–	1.03	1.05	–
26-1A	198	220	–	1.10	1.16	–
33-1A	1090	1150	–	1.03	1.01	–
34-1B-A	227	215	240	1.00	1.12	0.95
34-1B-D	212	222	200	0.97	1.05	0.98
34-1B-F	582	673	530	0.98	0.95	0.96
42-1A	31300	–	35000	1.15	–	1.18
42-1B-B	345000	443000	367000	1.08	1.11	1.12
42-1B-D	110000	116000	110000	1.10	1.07	1.08
42-1B-F	52500	63000	57000	1.02	0.98	1.03
42-1B-H	2020	2150	1950	0.51	0.56	0.53
42-1B-I	335	335	310	1.02	1.03	1.07
42-1B-K	557	641	540	0.93	1.01	0.94
43-1A	603	556	600	0.99	1.04	0.97
66-1A-A	750	763	790	0.94	0.93	0.88
67-1A-B	1160	1260	1260	0.84	0.75	0.79
67-1A-D	1340	1590	1670	0.86	0.87	0.83
68-1A-A	2530	2400	2470	0.88	0.88	0.90
80-1A	560	537	–	1.01	1.00	–

majority of results being within 10%. Larger deviations, of up to 28%, are observed for a small number of samples, particularly those from the vicinity of the uranium mineralization at 42.0 m, suggesting that problems of sample heterogeneity may be more pronounced for the high concentration samples. Linear correlation plots for the three sets of ^{238}U data are shown in Figures 1-1 to 1-3 and a correlation coefficient of 0.999 was obtained in each case. Significant deviations from the ideal $y = x$ agreement are, however, apparent in the best fitting straight lines produced by the regression analysis. Exclusion of the high uranium content samples from the vicinity of the 42.0 m redox front gives rise to the linear correlation plots shown in Figures 1-4 to 1-6. Correlation coefficients of 0.99 are applicable to each of these data sets and much better agreement with the perfect $y = x$ line is obtained in each case than in the corresponding correlations which include the high uranium content samples, again indicating that sample heterogeneity probably represents a more severe problem for the mineralized samples than for those of lower uranium concentration. The agreement between the three sets of ^{238}U data is therefore generally satisfactory, despite the large range of concentrations of the samples, the heterogeneity of the original rock and the fact that independent uranium yield tracer spikes were used by the three laboratories.

The $^{234}\text{U}/^{238}\text{U}$ activity ratio data given in Table 1-I are calculated simply as the ratio of the integrals of two peaks in the alpha spectra and, provided that the sources are sufficiently thin, are not influenced by the tracer α -peak. Also, they do not require the use of information for the yield tracer spike. This reduces the scope for variation in determination of the $^{234}\text{U}/^{238}\text{U}$ activity ratio relative to determination of the ^{238}U specific activity, where data for the spike must be used. Thus the activity ratio data show significantly closer agreement between the three sets of results than do the ^{238}U data. Most of the $^{234}\text{U}/^{238}\text{U}$ activity ratio results show agreement within 5% and extremely good linear correlations are observed for the data as shown in Figures 1-7 to 1-9. Thus the problems apparent in determination of the ^{238}U specific activity for the mineralized samples do not effect the determination of the $^{234}\text{U}/^{238}\text{U}$ activity ratios.

The results for ^{232}Th specific activity and $^{230}\text{Th}/^{234}\text{U}$ activity ratio determinations by alpha spectroscopy are shown in Table 1-II. The NYU results were obtained with a ^{229}Th yield tracer while the PUC and SURRC analyses utilized independent ^{228}Th yield tracers. Both of these thorium yield tracers are subject to problems as follows. ^{229}Th has the advantage that it does not occur naturally in the samples but has the disadvantage that the alpha spectrum of ^{229}Th comes close to overlapping with that of ^{230}Th , so that any thorium sources of significant thickness will suffer from overlap of the ^{229}Th and

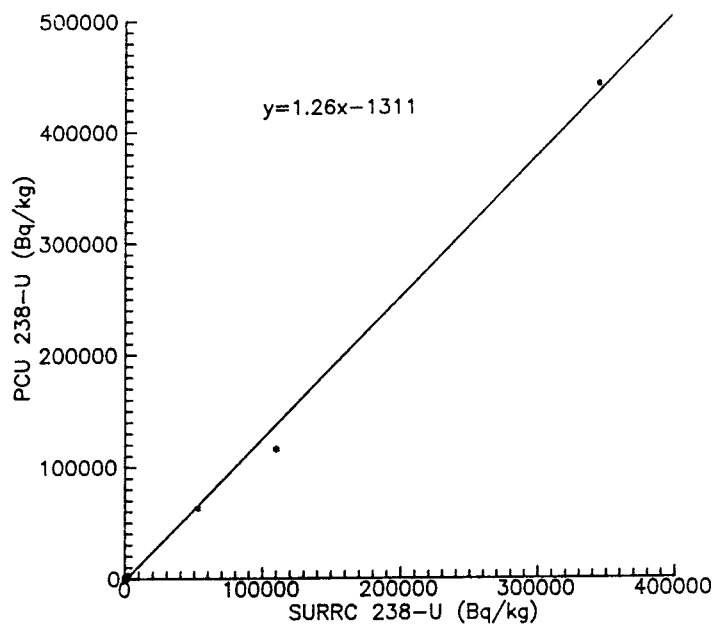


Figure 1-1. Correlation of PUC and SURRC ²³⁸U results obtained by alpha spectrometry (correlation coefficient = 0.999).

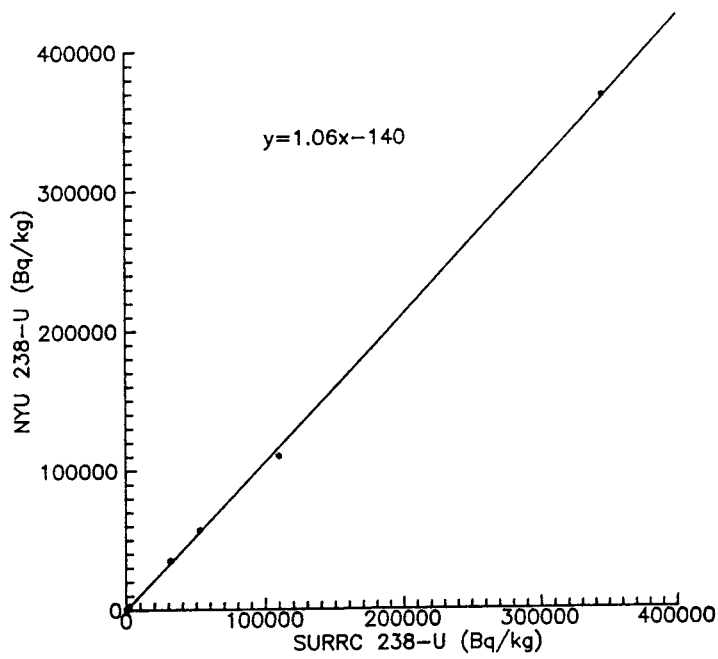


Figure 1-2. Correlation of NYU and SURRC ²³⁸U results obtained by alpha spectrometry (correlation coefficient = 0.999).

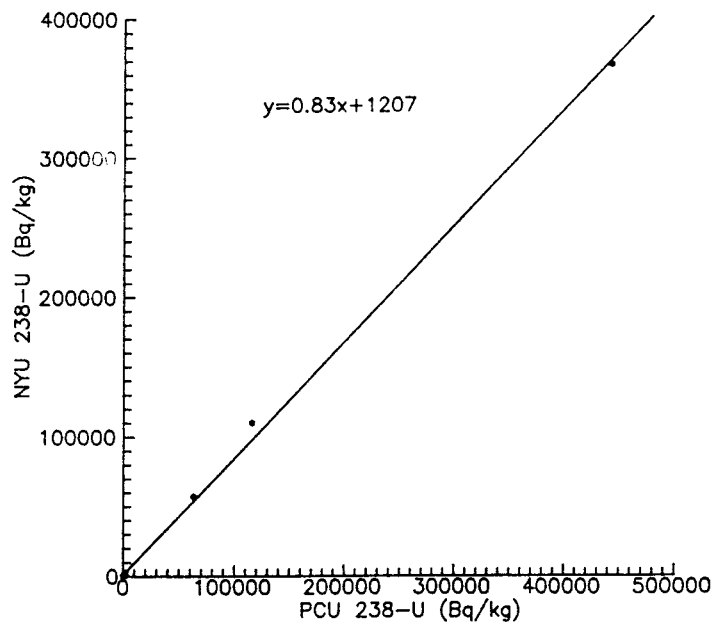


Figure 1-3. Correlation of NYU and PUC ^{238}U results obtained by alpha spectrometry (correlation coefficient = 0.999).

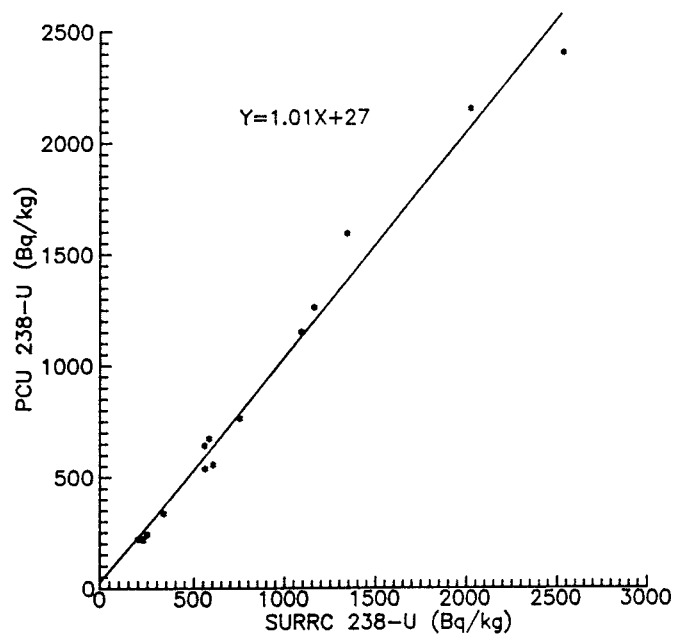


Figure 1-4. Correlation of PUC and SURRC ^{238}U results obtained by alpha spectrometry excluding samples from the uranium mineralization at 42.0 m (correlation coefficient = 0.992).

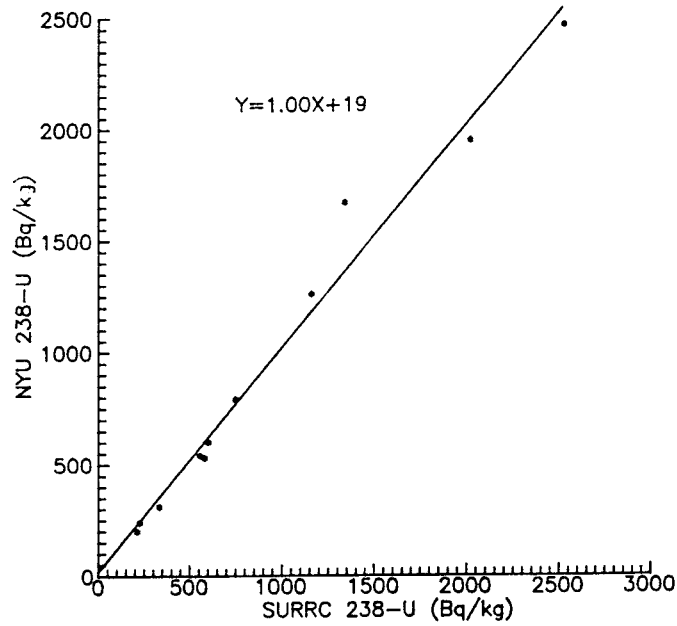


Figure 1-5. Correlation of NYU and SURRC ^{238}U results obtained by alpha spectrometry excluding samples from the uranium mineralization at 42.0 m (correlation coefficient = 0.989).

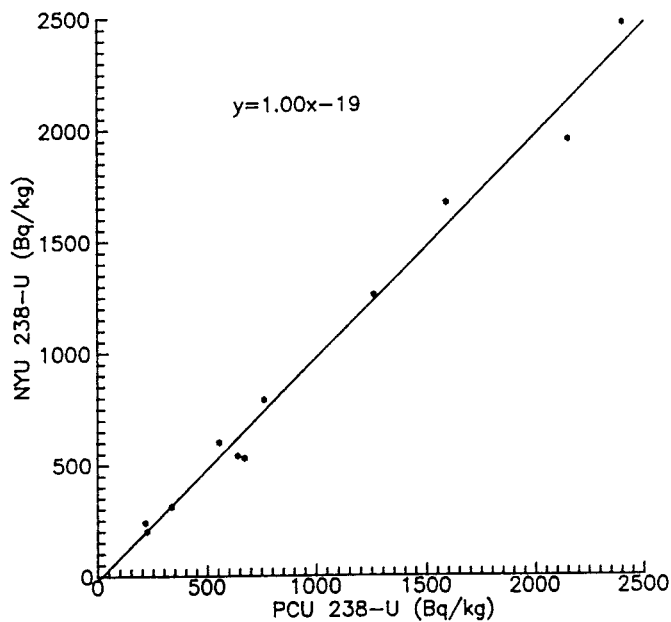


Figure 1-6. Correlation of NYU and PCU ^{238}U results obtained by alpha spectrometry excluding samples from the uranium mineralization at 42.0 m (correlation coefficient = 0.993).

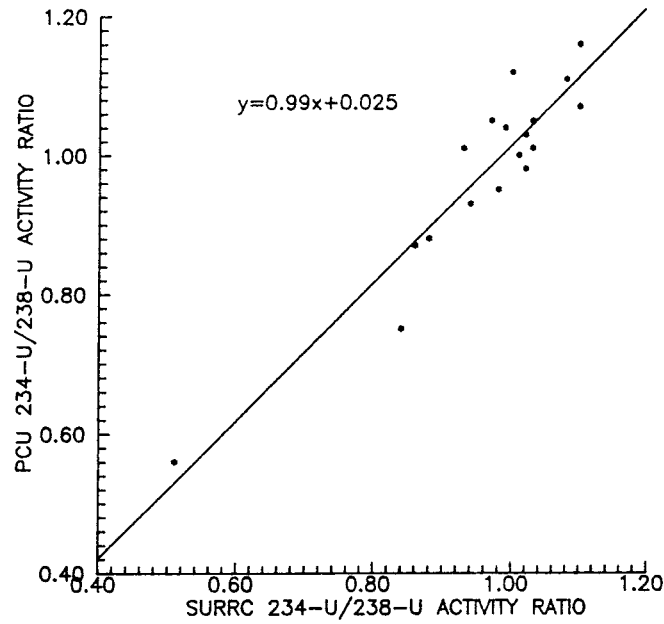


Figure 1-7. Correlation of PUC and SURRC $^{234}\text{U}/^{238}\text{U}$ activity ratio results (correlation coefficient = 0.933).

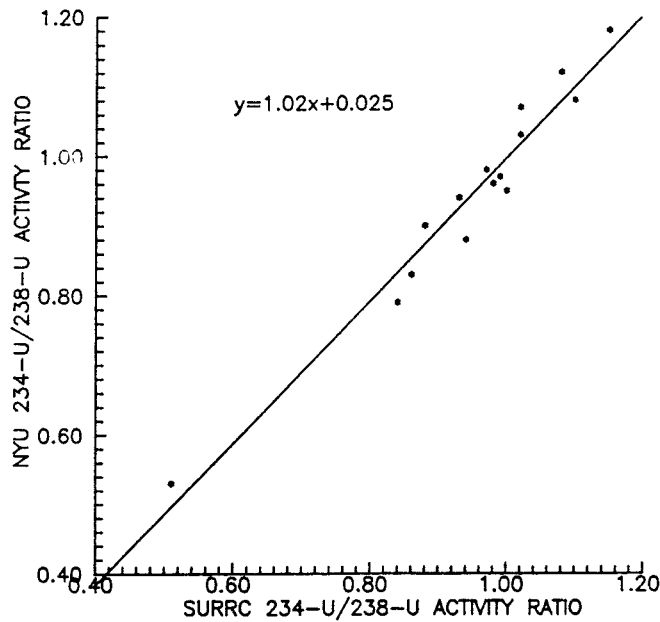


Figure 1-8. Correlation of NYU and SURRC $^{234}\text{U}/^{238}\text{U}$ activity ratio results (correlation coefficient = 0.976).

TABLE 1-II

Intercomparison of results for isotopic analysis of thorium in samples from the F1 drillcore.

Sample	^{232}U specific activity (Bq kg ⁻¹)			$^{230}\text{U}/^{234}\text{U}$ activity ratio		
	SURRC	PUC	NYU	SURRC	PUC	NYU
16-1A	103	72	–	0.99	1.02	–
26-1A	213	202	–	0.96	1.09	–
33-1A	150	154	–	1.02	1.09	–
34-1B-A	302	352	320	0.95	0.99	0.92
34-1B-D	320	327	350	1.06	0.94	1.03
34-1B-F	427	–	520	0.94	0.95	1.21
42-1A	250	–	190	0.94	–	0.91
42-1B-B	–	1570	< 2000	0.96	–	0.98
42-1B-D	250	250	–	0.97	1.05	0.90
42-1B-F	1170	1000	1180	0.88	0.99	1.03
42-1B-H	327	333	390	1.00	0.82	1.05
42-1B-I	280	318	310	1.09	1.11	1.11
42-1B-K	477	637	480	1.00	1.02	1.13
43-1A	293	262	290	1.00	1.00	1.05
66-1A-A	150	132	140	1.27	1.21	1.23
67-1A-B	197	190	230	1.69	1.46	1.71
67-1A-D	135	–	140	1.04	–	1.03
68-1A-A	88	–	90	1.04	–	1.02
80-1A	87	50	–	1.00	0.85	–

^{230}Th peaks. The use of ^{228}Th as a yield tracer is complicated by the fact that this isotope occurs naturally in the samples and the assumption of a state of secular equilibrium between the natural ^{228}Th and ^{232}Th in the sample must be made, or else the natural $^{228}\text{Th}/^{232}\text{Th}$ activity ratio of the sample must be determined. These additional difficulties in the thorium analysis result in a significantly poorer level of agreement for the ^{232}Th data (Table 1-II) from the different laboratories than was obtained for the ^{238}U analyses. Most of the ^{232}Th results agree to within 15%, but in some cases deviations of more than 30% are observed between the results obtained by different laboratories. Reasonable linear correlations are obtained between the different ^{232}Th data sets as shown in Figures 1-10 to 1-12, with correlation coefficients in each case being better than 0.96. Significant deviations from the $y = x$ line representing perfect agreement are, however, apparent indicating correspondingly significant differences between the results produced by the different laboratories. A similar situation is observed for the $^{230}\text{Th}/^{234}\text{U}$ activity ratio data shown in Table 1-II, with most of the pairs of results

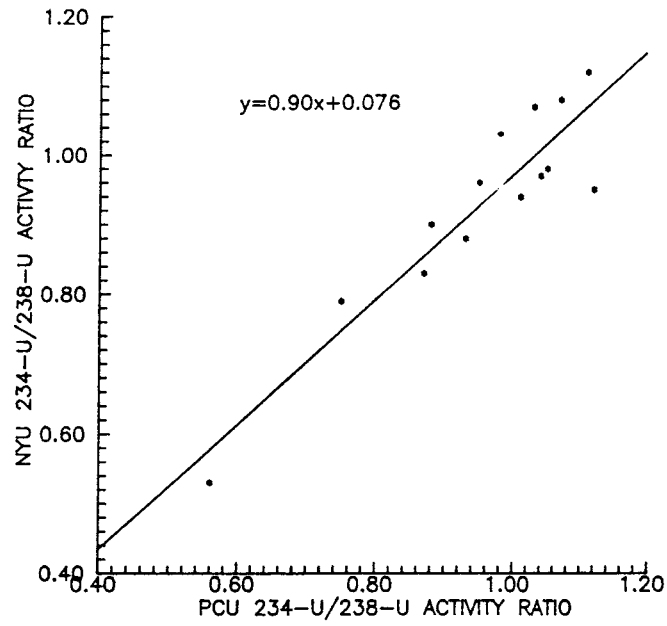


Figure 1-9. Correlation of NYU and PUC $^{234}\text{U}/^{238}\text{U}$ activity ratio results (correlation coefficient = 0.919).

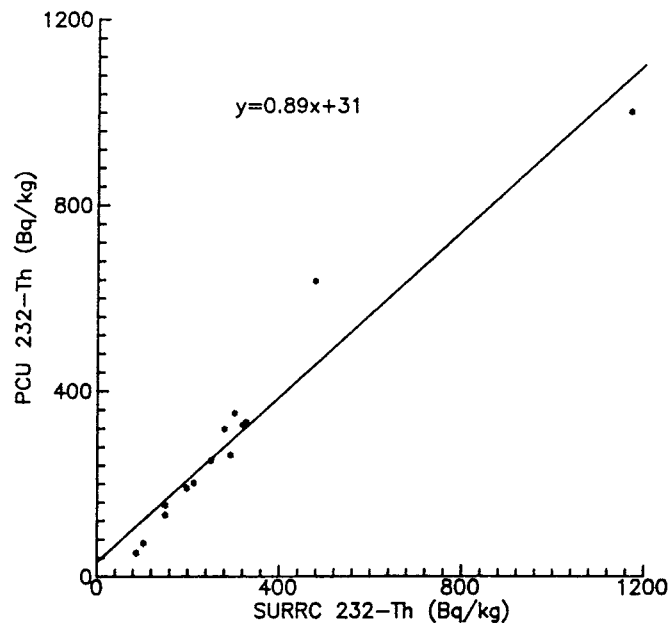


Figure 1-10. Correlation of PUC and SURRC ^{232}Th results obtained by alpha spectrometry (correlation coefficient = 0.967).

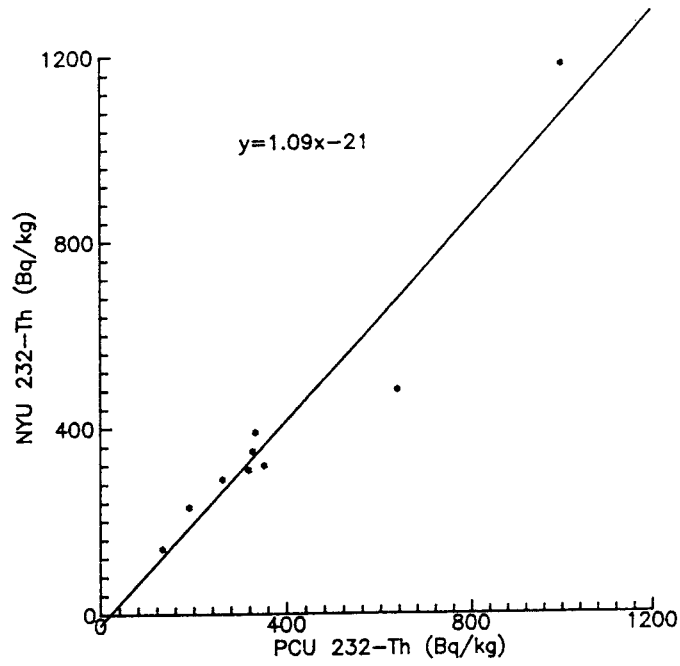


Figure 1-11. Correlation of NYU and SURRC ^{232}Th results obtained by alpha spectrometry (correlation coefficient = 0.991).

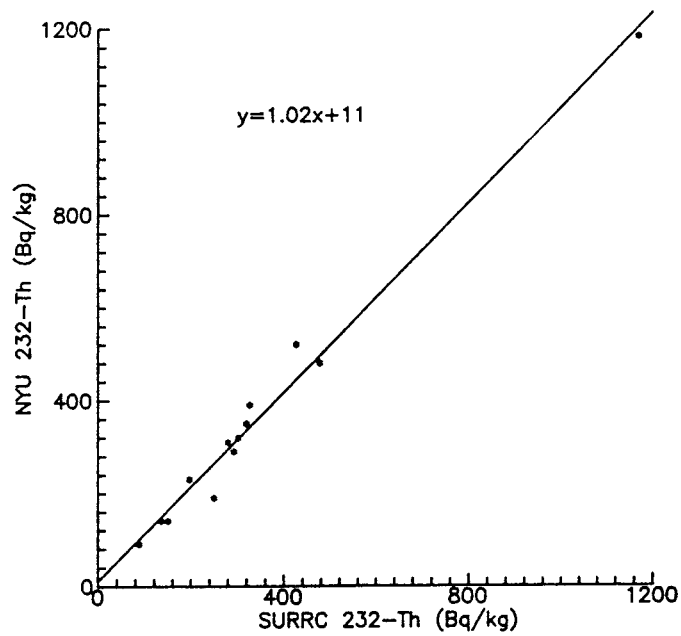


Figure 1-12. Correlation of PUC and NYU ^{232}Th results obtained by alpha spectrometry (correlation coefficient = 0.960).

agreeing within 15% but a small number exhibiting larger variations of up to 30%. The pairs of $^{230}\text{Th}/^{234}\text{U}$ data sets show distinct linear correlations (Figures 1-13 to 1-15) with correlation coefficients in each case being better than 0.9. Significant deviations from the $y = x$ case are, however, observed for the best fitting straight lines derived from the regression analyses, with the deviation being most pronounced in the correlation of the PUC and SURRC data.

Significant differences do, therefore, exist between the thorium data produced by the three laboratories, but the cause of this is not clear. Inaccuracies introduced by any $^{228}\text{Th}/^{232}\text{Th}$ disequilibrium would be unlikely to produce the observed magnitude of differences since the quantity of spike added was designed to match the ^{238}U content of the samples which was in general much larger than the ^{232}Th content. Thus the spike ^{228}Th activity was correspondingly much larger than the natural ^{228}Th content of the samples so that any small inaccuracy in estimation of the natural ^{228}Th content would have a relatively small effect on the calculation of the thorium isotope activities. The differences in results between the three laboratories, moreover, appear to be random, indicating that the observed deviations are not simply a consequence of a systematic difference in the calibration of the different spikes. The cause of the observed differences remains ill defined, with possible contributing factors being problems in analysis of the thorium alpha spectra, incomplete sample dissolution and sample heterogeneity. In the light of the observed differences in thorium results, all subsequent analyses using $^{232}\text{U}/^{228}\text{Th}$ spike included an analysis of the natural $^{228}\text{Th}/^{232}\text{Th}$ activity ratio of the sample in order to eliminate this possible source of inaccuracy.

In addition to the alpha spectroscopic analysis of uranium and thorium isotopes, total uranium concentrations were also derived by semi quantitative ICP-MS analysis, fluorometry and direct gamma spectroscopy, while total thorium analysis was also performed by semi quantitative ICP-MS analysis. The results of these additional analyses (in concentration units of ppm) are shown in Table 1-III along with the average uranium and thorium concentrations obtained by alpha spectrometry. The semi quantitative ICP-MS data for total uranium concentration agree reasonably well with the average alpha spectroscopy results for the lower concentrations of uranium but at values of greater than 10^3 ppm, the ICP-MS data are systematically lower than the alpha spectroscopy results. This effect, which is almost certainly the consequence of signal suppression in the ICP-MS at very high uranium concentrations, is clearly shown in the linear correlations for the total data set and for the data excluding the high concentration samples shown in Figures 1-16 and 1-17 respectively.

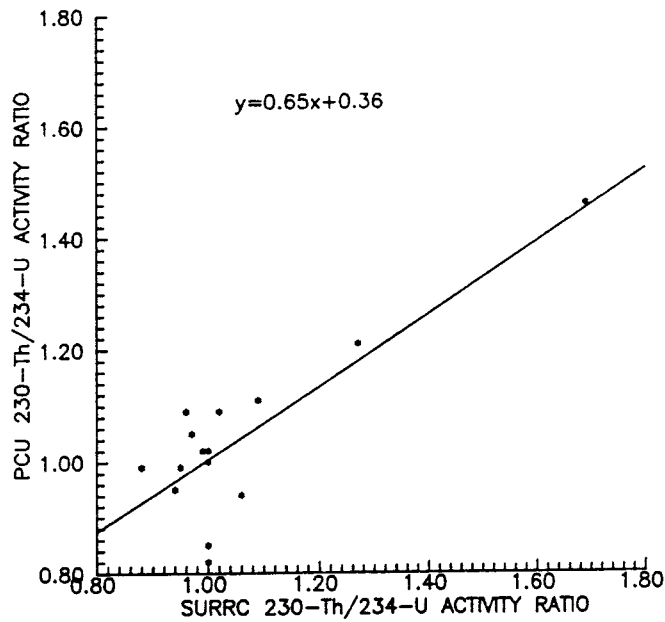


Figure 1-13. Correlation of PUC and SURRC $^{230}\text{Th}/^{234}\text{U}$ activity ratio results (correlation coefficient = 0.834).

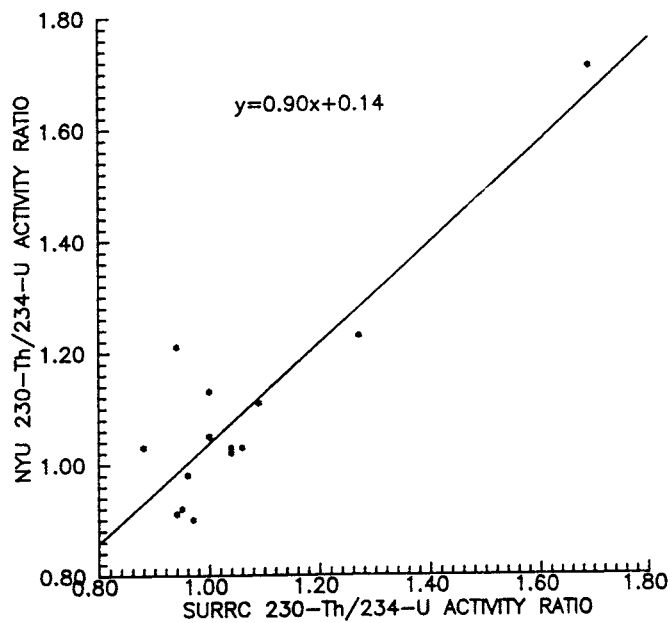


Figure 1-14. Correlation of NYU and SURRC $^{230}\text{Th}/^{234}\text{U}$ activity ratio results (correlation coefficient = 0.897).

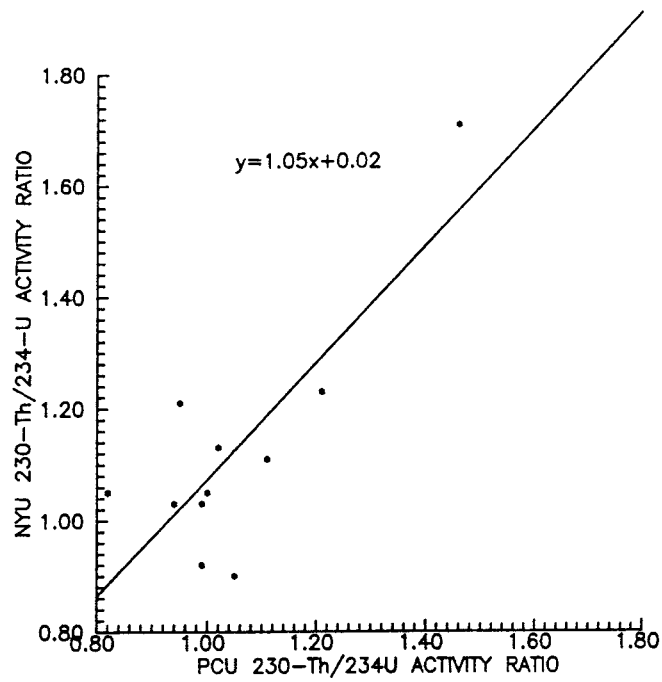


Figure 1-15. Correlation of PUC and NYU $^{230}\text{Th}/^{234}\text{U}$ activity ratio results (correlation coefficient = 0.803).

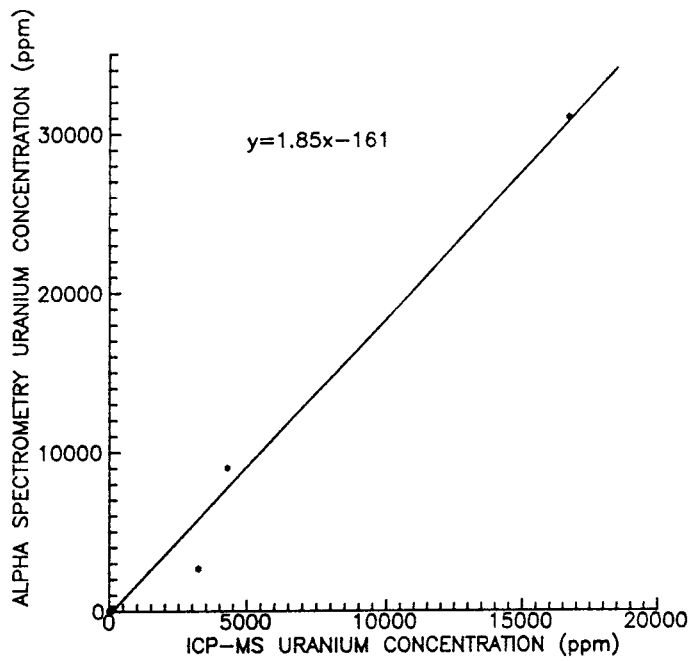


Figure 1-16. Correlation of semi quantitative ICP-MS results and average alpha spectrometry results for total uranium concentrations (correlation coefficient = 0.994).

TABLE 1-II

Intercomparison of results for isotopic analysis of thorium in samples from the F1 drillcore.

Sample	^{232}U specific activity (Bq kg ⁻¹)			$^{230}\text{U}/^{234}\text{U}$ activity ratio		
	SURRC	PUC	NYU	SURRC	PUC	NYU
16-1A	103	72	–	0.99	1.02	–
26-1A	213	202	–	0.96	1.09	–
33-1A	150	154	–	1.02	1.09	–
34-1B-A	302	352	320	0.95	0.99	0.92
34-1B-D	320	327	350	1.06	0.94	1.03
34-1B-F	427	–	520	0.94	0.95	1.21
42-1A	250	–	190	0.94	–	0.91
42-1B-B	–	1570	<2000	0.96	–	0.98
42-1B-D	250	250	–	0.97	1.05	0.90
42-1B-F	1170	1000	1180	0.88	0.99	1.03
42-1B-H	327	333	390	1.00	0.82	1.05
42-1B-I	280	318	310	1.09	1.11	1.11
42-1B-K	477	637	480	1.00	1.02	1.13
43-1A	293	262	290	1.00	1.00	1.05
66-1A-A	150	132	140	1.27	1.21	1.23
67-1A-B	197	190	230	1.69	1.46	1.71
67-1A-D	135	–	140	1.04	–	1.03
68-1A-A	88	–	90	1.04	–	1.02
80-1A	87	50	–	1.00	0.85	–

The fluorometry analysis results show excellent agreement with the average alpha spectrometry results both for the complete data set and for the samples excluding those from the mineralization, as shown in Figures 1-18 and 1-19. Finally, the gamma spectroscopy results also show a generally good agreement with the average alpha spectroscopy results as shown in Figures 1-20 and 1-21, but with an indication of systematically low results by gamma spectroscopy relative to alpha spectroscopy at uranium concentrations in excess of 10³ ppm. This effect is most likely the result of enhanced self absorption of gamma photons within the samples at higher uranium concentrations. The total thorium concentrations derived from ICP-MS, like the corresponding uranium results, agree well with the alpha spectroscopy results at low concentrations, but for the samples from the vicinity of the 42.0 m uranium mineralization the ICP-MS thorium data are significantly lower than the alpha spectrometry results (Figures 1-22 and 1-23). Thus the high concentrations of uranium in these samples suppress the ICP-MS signal not only of uranium itself but also of thorium.

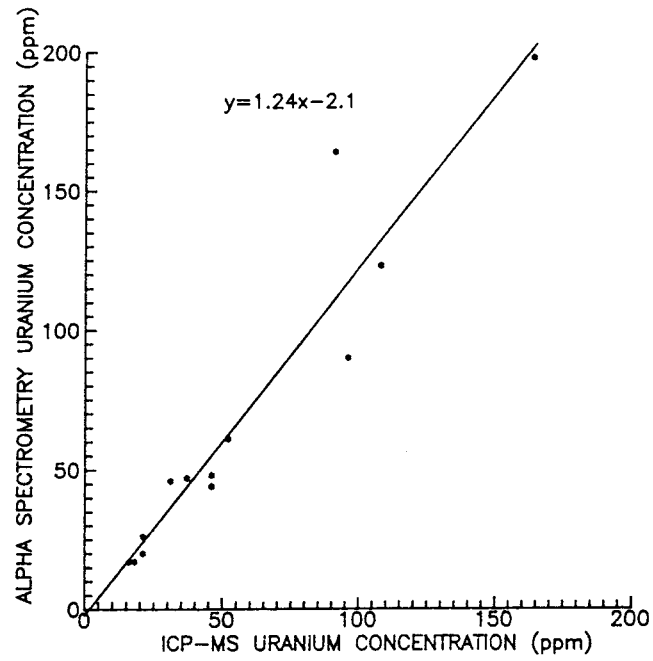


Figure 1-17. Correlation of semi quantitative ICP-MS results and average alpha spectrometry results for total uranium concentrations excluding samples from the uranium mineralization at 42.0 m (correlation coefficient = 0.950).

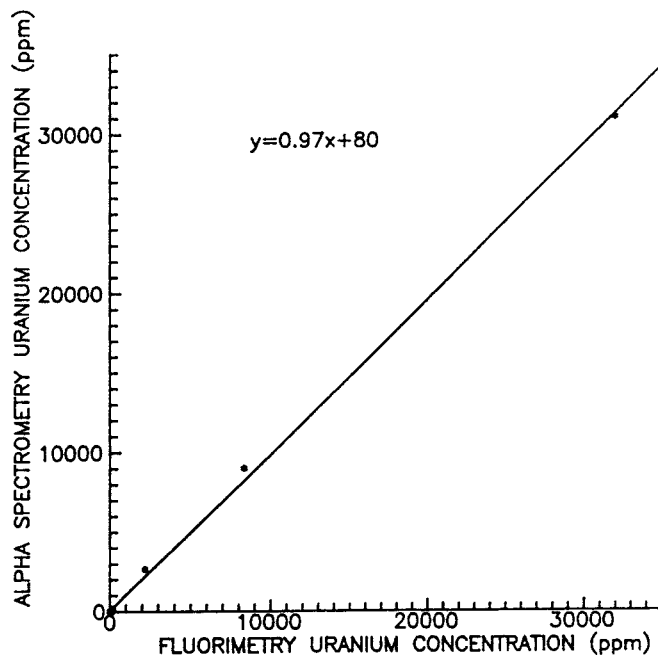


Figure 1-18. Correlation of fluorimetry results and average alpha spectrometry results for total uranium concentrations (correlation coefficient = 0.993).

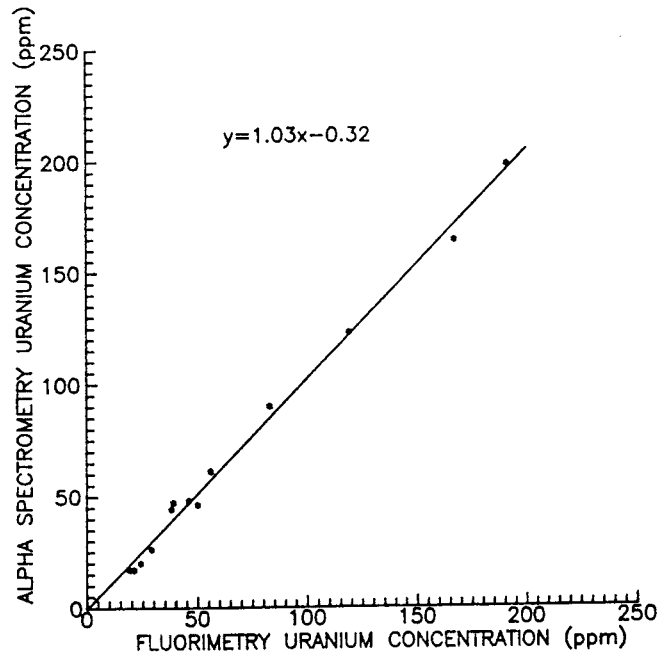


Figure 1-19. Correlation of fluorimetry results and average alpha spectrometry results for total uranium concentrations excluding samples from the uranium mineralization at 42.0 m (correlation coefficient = 0.997).

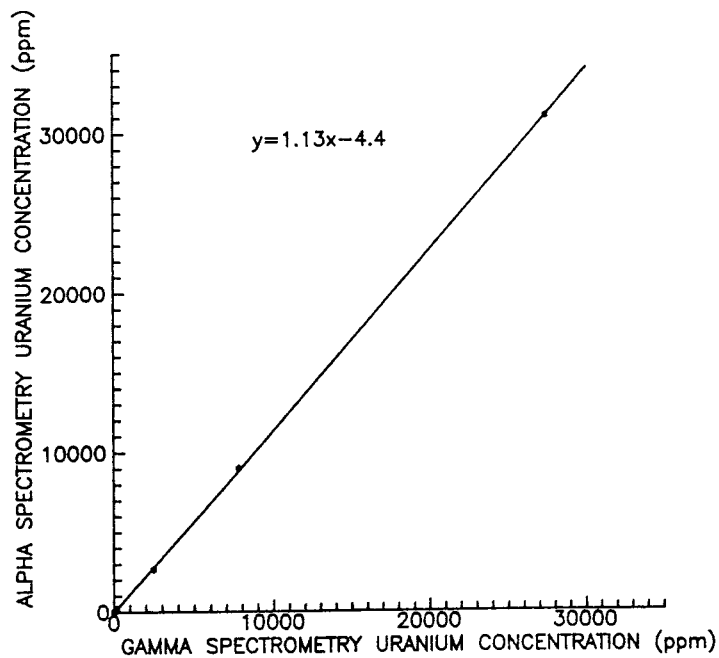


Figure 1-20. Correlation of gamma spectrometry and average alpha spectrometry results for total uranium concentrations (correlation coefficient = 0.999).

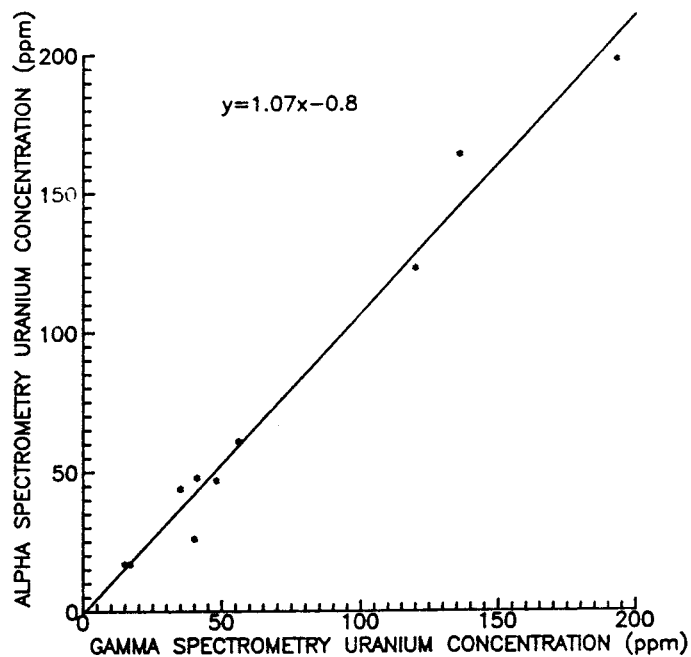


Figure 1-21. Correlation of gamma spectrometry and average alpha spectrometry results for total uranium concentrations excluding samples from the uranium mineralization at 42.0 m (correlation coefficient = 0.989).

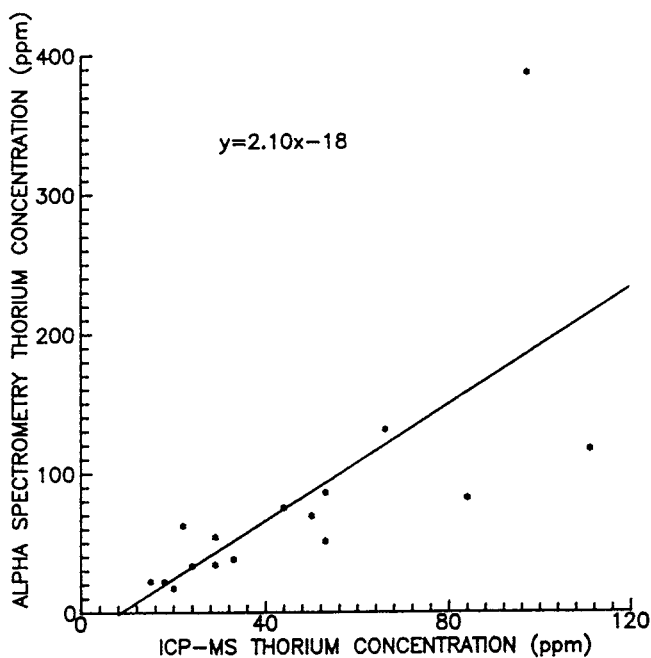


Figure 1-22. Correlation of semi quantitative ICP-MS results and average alpha spectrometry results for total thorium concentrations (correlation coefficient = 0.70).

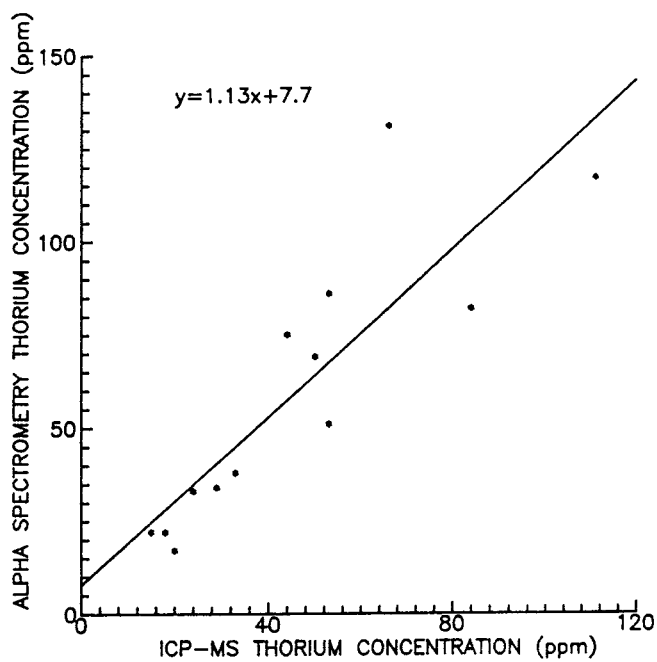


Figure 1-23. Correlation of semi quantitative ICP-MS results and average alpha spectrometry results for total thorium concentrations excluding samples from the uranium mineralization at 42.0 m (correlation coefficient = 0.859).

In addition to the above intercomparison of analytical methods, analyses of certified reference materials were performed to evaluate the accuracy of the analytical methods being used. Table 1-IV and 1-V show analytical results and reference values for analysis of the reference materials CANMET DI 1a and IAEA SOIL5 by SURRC and NYU respectively, using radiochemical separation and alpha spectrometry techniques. In both cases, satisfactory agreement is obtained with the certified reference values. Finally, Table 1-VI shows a set of results for semi quantitative ICP-MS analysis of the certified reference material IAEA SL-1. In this case, two of the four sets of results show systematically low uranium and thorium concentrations but the maximum deviations of the observed uranium and thorium results from the certified values are 13% and 29% respectively, values entirely consistent with those expected by the semi quantitative mode of operation of the ICP-MS. The average observed concentrations in fact show relatively good agreement with the reference values, with uranium and thorium deviations of 5.5% and 9.2% respectively.

TABLE 1-IV
SURRC analysis of certified reference material CANMET DI 1a.

	^{238}U (ppm)	$^{234}\text{U}/^{238}\text{U}$ (activity ratio)	$^{230}\text{Th}/^{234}\text{U}$ (activity ratio)	^{232}Th (ppm)
Observed values	114 ± 3	1.02 ± 0.02	1.00 ± 0.03	74.5 ± 3
Certified values	116 ± 3	1.00	1.00	76

TABLE 1-V
NYU analysis of certified reference material IAEA SOIL5.

Analysis no.	U (ppm)	Th (ppm)
1	3.05 ± 0.28	10.9 ± 1.8
2	2.74 ± 0.26	12.0 ± 1.8
3	2.93 ± 0.50	12.1 ± 1.0
Weighted mean	2.89 ± 0.10	11.8 ± 0.8
Certified values	3.15 ± 0.45	11.3 ± 0.7

TABLE 1-VI

Semi quantitative ICP-MS analysis of certified reference material IAEA SL1.

Analysis no.	U (ppm)	Th (ppm)
1	4.1	14
2	3.6	13
3	3.5	10
4	4.1	14
Average $\pm 1\sigma$	3.8 ± 0.3	12.8 ± 1.9
Certified values	4.02 ± 0.32	14.1 ± 1

List of SKB reports

Annual Reports

1977-78

TR 121

KBS Technical Reports 1 – 120

Summaries

Stockholm, May 1979

1979

TR 79-28

The KBS Annual Report 1979

KBS Technical Reports 79-01 – 79-27

Summaries

Stockholm, March 1980

1980

TR 80-26

The KBS Annual Report 1980

KBS Technical Reports 80-01 – 80-25

Summaries

Stockholm, March 1981

1981

TR 81-17

The KBS Annual Report 1981

KBS Technical Reports 81-01 – 81-16

Summaries

Stockholm, April 1982

1982

TR 82-28

The KBS Annual Report 1982

KBS Technical Reports 82-01 – 82-27

Summaries

Stockholm, July 1983

1983

TR 83-77

The KBS Annual Report 1983

KBS Technical Reports 83-01 – 83-76

Summaries

Stockholm, June 1984

1984

TR 85-01

Annual Research and Development Report 1984

Including Summaries of Technical Reports Issued during 1984. (Technical Reports 84-01 – 84-19)

Stockholm, June 1985

1985

TR 85-20

Annual Research and Development Report 1985

Including Summaries of Technical Reports Issued during 1985. (Technical Reports 85-01 – 85-19)

Stockholm, May 1986

1986

TR 86-31

SKB Annual Report 1986

Including Summaries of Technical Reports Issued during 1986

Stockholm, May 1987

1987

TR 87-33

SKB Annual Report 1987

Including Summaries of Technical Reports Issued during 1987

Stockholm, May 1988

1988

TR 88-32

SKB Annual Report 1988

Including Summaries of Technical Reports Issued during 1988

Stockholm, May 1989

1989

TR 89-40

SKB Annual Report 1989

Including Summaries of Technical Reports Issued during 1989

Stockholm, May 1990

Technical Reports

List of SKB Technical Reports 1990

TR 90-01

FARF31 –

A far field radionuclide migration code for use with the PROPER package

Sven Norman¹, Nils Kjellbert²

¹Starprog AB

²SKB AB

January 1990

TR 90-02

Source terms, isolation and radiological consequences of carbon-14 waste in the Swedish SFR repository

Rolf Hesböl, Ignasi Puigdomenech, Sverker Evans
Studsvik Nuclear

January 1990

TR 90-03

Uncertainties in repository performance from spatial variability of hydraulic conductivities – Statistical estimation and stochastic simulation using PROPER

Lars Lovius¹, Sven Norman¹, Nils Kjellbert²

¹Starprog AB

²SKB AB

February 1990

TR 90-04

Examination of the surface deposit on an irradiated PWR fuel specimen subjected to corrosion in deionized water

R. S. Forsyth, U-B. Eklund, O. Mattsson, D. Schrire
Studsvik Nuclear
March 1990

TR 90-05

Potential effects of bacteria on radionuclide transport from a Swedish high level nuclear waste repository

Karsten Pedersen
University of Gothenburg, Department of General and Marine Microbiology, Gothenburg
January 1990

TR 90-06

Transport of actinides and Tc through a bentonite backfill containing small quantities of iron, copper or minerals in inert atmosphere

Yngve Albinsson, Birgit Sätmark, Ingemar Engkvist, W. Johansson
Department of Nuclear Chemistry, Chalmers University of Technology, Gothenburg
April 1990

TR 90-07

Examination of reaction products on the surface of UO_2 fuel exposed to reactor coolant water during power operation

R. S. Forsyth, T. J. Jonsson, O. Mattsson
Studsvik Nuclear
March 1990

TR 90-08

Radiolytically induced oxidative dissolution of spent nuclear fuel

Lars Werme¹, Patrik Sellin¹, Roy Forsyth²
¹Swedish Nuclear Fuel and waste Management Co (SKB)
²Studsvik Nuclear
May 1990

TR 90-09

Individual radiation doses from unit releases of long lived radionuclides

Ulla Bergström, Sture Nordlinder
Studsvik Nuclear
April 1990

TR 90-10

Outline of regional geology, mineralogy and geochemistry, Poços de Caldas, Minas Gerais, Brazil

H. D. Schorscher¹, M. E. Shea²
¹University of Sao Paulo
²Battelle, Chicago
December 1990

TR 90-11

Mineralogy, petrology and geochemistry of the Poços de Caldas analogue study sites, Minas Gerais, Brazil

I: Osamu Utsumi uranium mine

N. Waber¹, H. D. Schorscher², A. B. MacKenzie³, T. Peters¹

¹University of Bern

²University of Sao Paulo

³Scottish Universities Research & Reactor Centre (SURRC), Glasgow

December 1990

TR 90-12

Mineralogy, petrology and geochemistry of the Poços de Caldas analogue study sites, Minas Gerais, Brazil

II: Morro do Ferro

N. Waber
University of Bern
December 1990

TR 90-13

Isotopic geochemical characterisation of selected nepheline syenites and phonolites from the Poços de Caldas alkaline complex, Minas Gerais, Brazil

M. E. Shea
Battelle, Chicago
December 1990

TR 90-14

Geomorphological and hydrogeological features of the Poços de Caldas caldera, and the Osamu Utsumi mine and Morro do Ferro analogue study sites, Brazil

D. C. Holmes¹, A. E. Pitty², R. Noy¹
¹British Geological Survey, Keyworth
²INTERRA/ECL, Leicestershire, UK
December 1990

TR 90-15

Chemical and isotopic composition of groundwaters and their seasonal variability at the Osamu Utsumi and Morro do Ferro analogue study sites, Poços de Caldas, Brazil

D. K. Nordstrom¹, J. A. T. Smellie², M. Wolf³
¹US Geological Survey, Menlo Park
²Conterra AB, Uppsala
³Gesellschaft für Strahlen- und Umweltforschung (GSF), Munich
December 1990